ISSN: 1715-9997

Canadian Journal of pure & applied sciences

an International Journal

SENRA
Academic Publishers
Burnaby, British Columbia

The Canadian Journal of Pure and Applied Sciences (CJPAS-ISSN 1715-9997) is a peer reviewed multi-disciplinary specialist journal aimed at promoting research worldwide in Agricultural Sciences, Biological Sciences, Chemical Sciences, Computer and Mathematical Sciences, Engineering, Environmental Sciences, Medicine and Physics (all subjects).

Editorial Office
E-mail: editor@cjpas.ca
: editor@cjps.net

SENRA Academic Publishers
7845 15th Street Burnaby
British Columbia V3N 3A3 Canada
www.cjpas.net
E-mail: senra@cjpas.ca

Print ISSN 1715-9997
Online ISSN 1920-3853

Volume 3, Number 3
Oct 2009

CANADIAN JOURNAL OF PURE AND APPLIED SCIENCES

Board of Editorial Advisors

Canadian Journal of pure & applied sciences

Volume 3, Number 3
October 2009

CONTENTS

LIFE SCIENCES

PHYSICAL SCIENCES

SENRA Academic Publishers, Burnaby, British Columbia
Vol. 3, No. 3, pp. 875-885, 2009
ISSN: 1715-9997

Canadian Journal of pure&applied sciences

CHARACTERIZATION OF THORNLESS *RUBUS GLAUCUS* IN COLOMBIA

*Marta Leonor Marulanda and Ana María López
Biodiversity and Biotechnology Group, Universidad Tecnológica de Pereira
La Julita, Pereira, Colombia

ABSTRACT

High phenotypical plasticity has been identified within the species *Rubus glaucus* Benth, commonly known as 'mora de castilla' or Castilla blackberry, in Colombia's coffee-growing area using AFLP molecular markers as well as morphological characters. Thornless plants have been observed among the blackberry materials grown. These plants present the same characteristics of productivity as thorny varieties are widely distributed. A first approximation to the genetic relationship between thorny and thornless materials indicated that thornless blackberry could possibly originate from the departments of Risaralda or Quindío. This work focuses on identifying the genetic and morpho-agronomic differences in thornless *R. glaucus* materials found in the coffee-growing region, especially in the department of Risaralda. Materials were collected from five different locations**:** two in the department of Risaralda, one in the department of Caldas, and two in the department of Quindío. For the morpho-agronomic characterization, 40 farmers were selected in the municipalities of Santa Rosa de Cabal and Guática, Risaralda, each farmer planting 50 plants from each of the five different collection sites, which had been multiplied *in vitro*, as well as 50 plants of thornless blackberry propagated by farmers, totaling 12,000 plants. Eight microsatellite (SSR) sequences were used to study 23 regional accessions of *Rubus*, including thorny and thornless *R. glaucus*, both cultivated and wild. Genetic and molecular differences were observed between thornless blackberry materials of different origins.

Keywords: *Rubus glaucus*, thornless blackberry, Castillo blackberry, genetic characterization, Colombia.

INTRODUCTION

American *Rubus* species are perennial shrubs that show a broad range of growth habits: from erect to semi-erect to creeping (Daubeny, 1996). In addition, their morphological and phenotypical characteristics are probably among the most well known. *Rubus* species of economic importance present perennial roots, foliage that produces biannual productive canes or branches with flower structures, and new branches, known as primary branches, which present vegetative growth and form tillers (Moore and Skirvin, 1990).

In temperate regions, the prolonged exposure of blackberries to the cold induces both vegetative and primary branches to develop flower buds or productive branches, also known as female branches, which die after producing fruit. Some species produce flowers without being exposed to the cold in addition to another very desirable characteristic—a productive primary branch capable of producing flower branches during the early growth cycle (López-Medina and Moore, 1999; Lopez-Medina *et al*., 2000). However, in the case of *Rubus glaucus*, the formation of female branches does not occur with the same mechanisms. According to popular belief, this formation is not a physiological phenomenon strongly controlled by environmental conditions, as described elsewhere in the world, but is determined rather by genetic factors.

Another interesting characteristic of most *Rubus* species is the absence of thorns or brambles. For example, commercial varieties 'Chester Thornless', 'Thornfree', and 'Thornless Evergreen' are thornless genotypes from the United States. This monogenic characteristic is controlled by a recessive gene that has been widely studied in Europe and the United States (Jennings and Ingram, 1983; Hall, 1990; Skirvin *et al.*, 2005; Strik *et al*., 2006). In Colombia, farmers of the department of Quindío discovered a thornless blackberry biotype, which has been multiplied by farmers throughout the country, without really understanding its agronomic and genetic characteristics. This thornless blackberry offers great potential for blackberry cultivation not only in the Quindío region but throughout the country.

Previous work carried out by Aguilar (Aguilar, SB. 2006) and Marulanda *et al*. (2007) revealed high phenotypical and molecular plasticity in *R. glaucus* in Colombia's coffee-growing region. Other wild species of *Rubus* found in the area and nearby lots planted to the Castilla blackberry were also submitted to morphological and molecular characterization, using amplified fragment length polymorphism (AFLP) and simple sequence repeat (SSR) molecular markers.

*Corresponding author email: ubioteve@utp.edu.co

Some of the cultivated thornless blackberry genotypes present the same productivity and same fruit size as thorny plants. Because of their interesting phenotypical characteristics and reduced production costs, these materials, commonly known as thornless blackberry, have been massively disseminated by farmers in the region using vegetative methods. Marulanda *et al*. (2007) found two possible sites of origin of thornless *R. glaucus* materials: one is located in the department of Risaralda and the other in the department of Quindío. There could be other sources of thornless *R. glaucus*, but further study is necessary.

Many studies using molecular markers, such random amplified polymorphic DNA (RAPD), AFLP, and SSR, have been conducted in *Rubus* (Graham and MacNicol, 1995; Graham *et al*., 2002, and 2004; Marulanda and Márquez, 2001**;** Marulanda *et al*., 2007; Amsellem *et al*., 2000 and 2001). However, the studies conducted with SSR markers are of particular interest because these markers are co-dominant, highly replicable, frequent in most eukaryotes, and reveal a high allelic diversity (Mohan *et al*., 1997).

The SSR of related species has been used in diversity and genetic variability studies (Stafne *et al*., 2005) and several have demonstrated the success of this strategy, which is based on the transferability of SSR primers between species and between genera of the Rosacea family (Ashley *et al*., 2003; Cipriani *et al*., 1999; Decroocq *et al*., 2003; Dirlewanger *et al*., 2002; Graham *et al*., 2002; Lewers *et al*., 2005; Marulanda *et al*., 2007).

For example, Stafne *et al*. (2005) used SSR developed from Glen Moy red raspberries (*R. idaeus* ssp. *idaeus*) reported by Graham *et al*. (2002, 2004). On the other hand, Amsellem *et al*. (2001) used SSR from wild blackberry (*R. alceifolius*) from Asia; Lewers et al. (2005) used SSR from strawberry (*Fragaria* × *ananassa*), Ashley *et al*. (2003) used SSR from *Fragaria virginiana*; and James *et al*. (2003) SSR from *Fragaria vesca* to evaluate parental genotypes of North American raspberry and blackberry and determine the level of polymorphism present in parental lines. Stafne *et al*. (2005) found 60 SSRs available for evaluating American blackberries and raspberries.

This study therefore aims to (1) identify the genetic and morpho-agronomic differences of thornless *R. glaucus* materials grown in the department of Risaralda and (2) characterize cultivated and wild *Rubus* materials found in Colombia's coffee-growing region both genetically and morphologically, using SSR molecular markers.

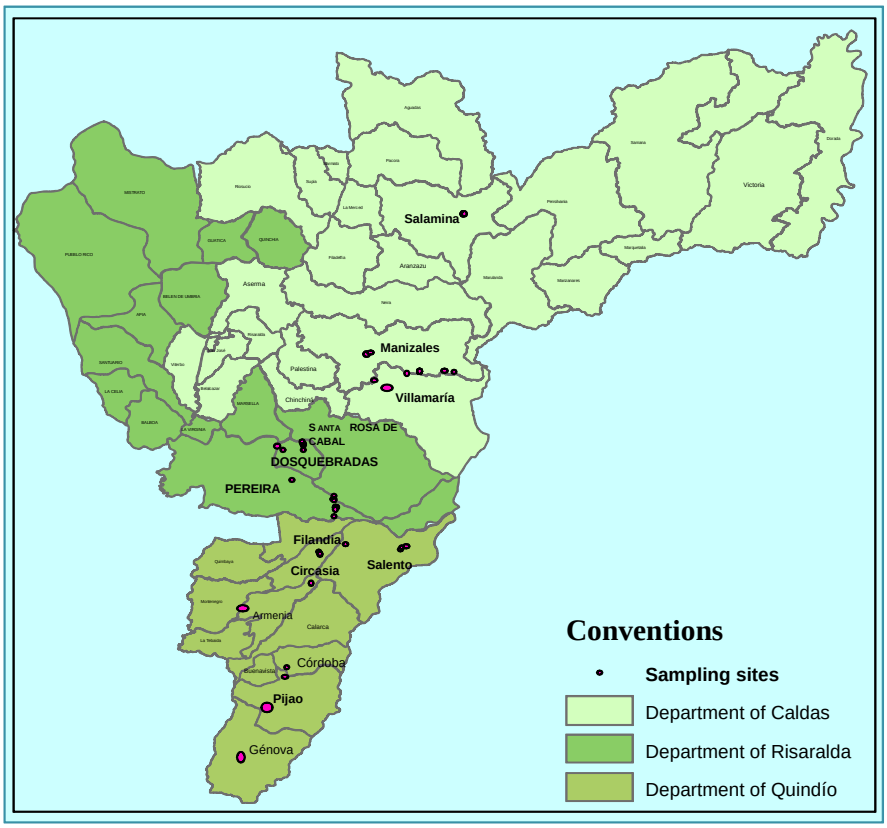

Fig. 1. Collection sites of cultivated and wild blackberries in Colombia's coffee-growing region.

MATERIALS AND METHODS

Collection of Study Materials

From 2005 to 2008, plants of cultivated and wild blackberry species were collected in several municipalities of Colombia's coffee-growing region where blackberry is grown (Fig. 1).

Morpho-agronomic Characterization

Thornless *R. glaucus* accessions were collected from five different collection sites in three different departments of Colombia (Risaralda, Caldas, and Quindío). Each accession was assigned a code beginning with the letter P and numbered 1 to 5. Table 1 lists the different sampling sites and the identification code assigned to each material**.** Blackberry plants were multiplied in vitro and, after hardening, a total of 50 plants from each of the five collection sites (P1, P2, P3, P4, P5) were delivered to 20 farmers in each of the two municipalities of Risaralda (Santa Rosa de Cabal and Guática). Thornless plants from Santa Rosa de Cabal propagated by the farmers (P6) were used as control. Overall, each farmer established 300 plants, totaling 6,000 plants per municipality and 12,000 plants for the entire experiment. Fifteen morpho-agronomic variables were evaluated as follows: number of female and male branches, number of runners, length of internodes of female and male branches, width and length of folioles on female and male branches, stem diameter on female and male branches, plant height at weeks 15 and 32 after planting, number of flower buds, and days to flowering.

STATISTICAL ANALYSIS

A multivariate analysis was performed and groups were identified by cluster analysis, using the SAS program. Information on origins and sites was compared and 12 combinations were identified for the cluster analysis (Table 2). Data were supported by the results of the multiple correspondence analysis.

Evaluating Thorny and Thornless Accessions using SSR Markers

Twenty-three microsatellite sequences developed by Amsellem (2001) and Graham *et al*. (2002 and 2004) were evaluated and, of these, eight SSRs were selected for their polymorphism and amplification quality. Twenty-three regional accessions of *Rubus*, including thorny and thornless *R. glaucus*, both cultivated and wild, were analyzed as follows.

- 9 wild and cultivated accessions of thornless *R. glaucus*
- 4 wild accessions of thorny *R. glaucus*
- 2 cultivated accessions of thornless *R. glaucus*
- 1 accession of *Rubus rosifolius*
- 6 accessions of *Rubus urticifolius*
- 1 accession of *Rubus robustus*

To determine groups of genetic diversity, the genetic similarity (GSij) was calculated based on the formulas of

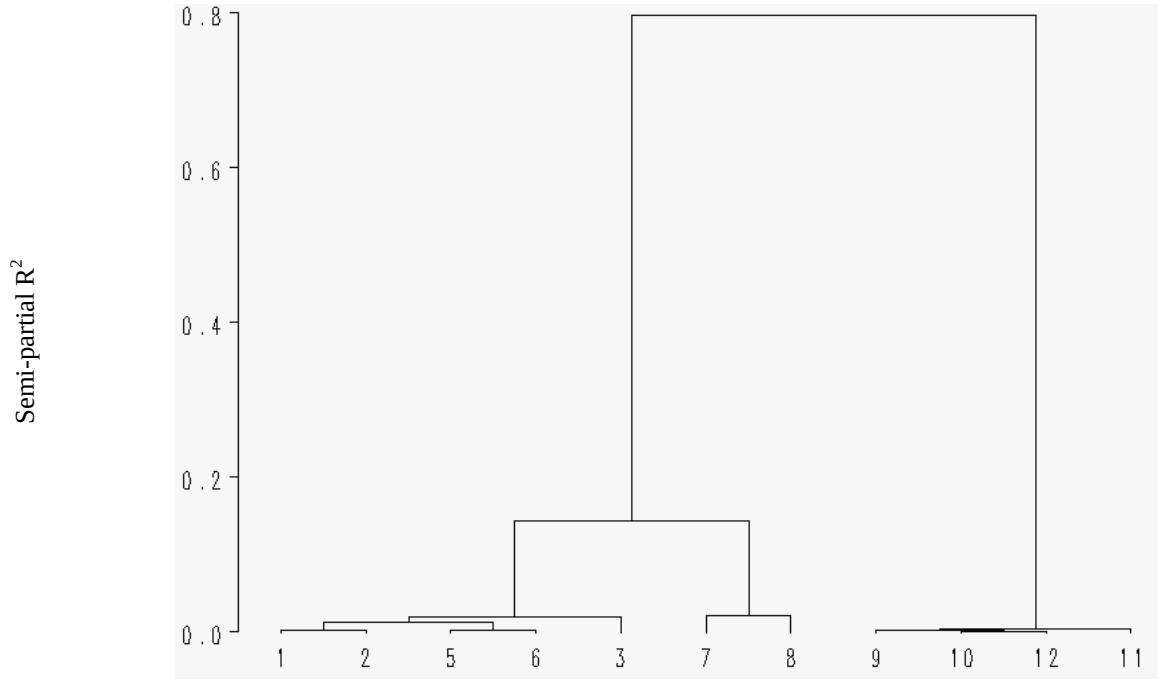

Fig. 2. Dendogram and cluster analysis based on morpho-agronomic characterization.
Treatments* see table 2

Dice (1945) and Nei and Li (1979). Genotypes were grouped based on dissimilitude values (1-GSij) between all genotype pairs (Sneath and Sokal, 1973), using the unweighted pair-group method with arithmetic average (UPGMA) with the statistical package NTSys PC version 2.02i (Rolhf, 1998).

RESULTS AND DISCUSSION

Morpho-agronomic Characterization

Table 3 presents the cluster grouping of the 12 combinations described, while table 4 presents the average, minimum, and maximum values, standard error, and coefficient of variation for each morpho-agronomic variable, regardless of the site and of the material. Data on plant height at weeks 15 and 32 after planting present coefficients of variation of 85.9% and 58.2%, respectively. This variation can be attributed to the difference in vegetative growth presented by plants, which is strongly influenced by agricultural tasks. The variable "number of runners" presents a coefficient of variation of 82.6%, with a maximum value of 3, a minimum value of 0, and an average value of 1 runner, which can be attributed to the difficulty in identifying these branches because they are easily confused with thin branches.

According to principal component analysis, the variables described are classified into six components, in such a way that those contributing the greatest variation with regard to total variation are located in the first component and those contributing the smallest variation in the sixth component (Table 5).

Variables presenting the greatest variation were, in descending order: length of foliole on the male branch, width of foliole on the male branch, stem diameter on the male branch, number of runners, and number of male branches. The number of male branches indirectly determines the productive capacity of a material because, after pruning, male branches can become female branches.

The contribution of variables related to the productive capacity, such as number of female branches and number of flower buds, to total variation was smaller, respectively ranking fifth and sixth, which indicates that these variables alone have a smaller capacity to differentiate materials. The variable "number of flower buds" is directly related to fruit production and presents the smallest contribution to total variation, meaning that it is highly unlikely that this variable can be used to differentiate materials.

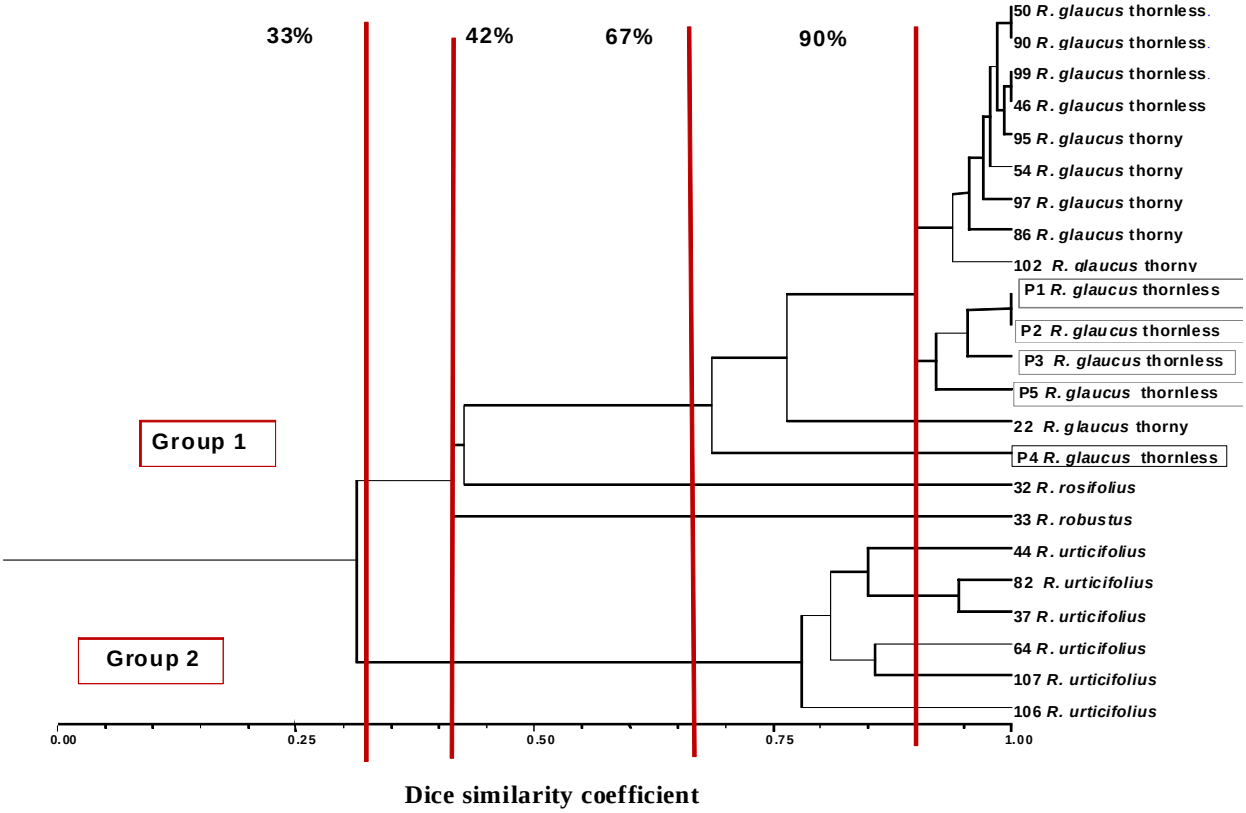

Fig. 3. Dendrogram of blackberries estimated by Dice similarity index (1945), based on SSR markers.

The dendrogram in figure 2 shows the grouping of materials depending on the combination of site of origin and planting site. Two groupings are possible: the first separates the materials originating from Villamaría (Caldas) and Génova (Quindío) and planted in Santa Rosa de Cabal and Guática from the others. The second conserves the distance from these combinations, but separates materials originating from SENA-Manizales (Caldas) and Pereira (Risaralda) and planted in Guática. Overall, the dendrogram shows that the materials originating from Villamaría (Caldas) and Génova (Quindío) are promising and different, regardless of the site where they are planted.

Based on the dendrogram, the three groups were submitted to cluster analysis (Table 3), resulting in the following combination of materials and planting sites:

Cluster 1: Material originating from Santa Rosa de Cabal and planted in Santa Rosa de Cabal; material from Santa Rosa de Cabal propagated by farmers and planted in Santa Rosa de Cabal (control); material originating from

Table 1. Collection sites of blackberry materials to be evaluated in the field and assigned code.

Collection site	Department	Assigned ID code
Santa Rosa de Cabal	Risaralda	P1
SENA-Manizales	Caldas	P2
Alto Manzano, Pereira	Risaralda	P3
Cumaral, Génova	Quindío	P4
Papayal, Villamaría	Caldas	P5
Material from Santa Rosa de Cabal propagated by farmers (control)	Risaralda	P6

Table 2. Combinations used in the cluster analysis, origin of materials and evaluation site.

Combination	Origin	Evaluation site
1	Santa Rosa de Cabal	Santa Rosa de Cabal
2	Santa Rosa de Cabal (control)	Santa Rosa de Cabal
3	Santa Rosa de Cabal	Guática
4	Santa Rosa de Cabal (control)	Guática
5	SENA-Manizales	Santa Rosa de Cabal
6	Pereira	Santa Rosa de Cabal
7	SENA-Manizales	Guática
8	Pereira	Guática
9	Génova	Santa Rosa de Cabal
10	Villamaría	Santa Rosa de Cabal
11	Génova	Guática
12	Villamaría	Guática

Table 3. Materials evaluated at two sites and group identification by cluster analysis.

Combination	Origin	Site	Cluster 1	Cluster 2
1	Santa Rosa de Cabal	Santa Rosa de Cabal	1	1
2	Santa Rosa de Cabal (control)	Santa Rosa de Cabal	1	1
3	Santa Rosa de Cabal	Guática	1	1
4	Santa Rosa de Cabal (control)	Guática	1	1
5	SENA-Manizales	Santa Rosa de Cabal	1	1
6	Pereira	Santa Rosa de Cabal	1	1
7	SENA-Manizales	Guática	3	1
8	Pereira	Guática	3	1
9	Génova	Santa Rosa de Cabal	2	2
10	Villamaría	Santa Rosa de Cabal	2	2
11	Génova	Guática	2	2
12	Villamaría	Guática	2	2

Santa Rosa de Cabal and planted in Guática; material originating in SENA-Manizales and planted in Santa Rosa de Cabal; material originating in Pereira and planted in Santa Rosa de Cabal.

Cluster 2: Material originating in Génova and planted in Santa Rosa de Cabal; material originating in Villamaría and planted in Santa Rosa de Cabal; material originating in Génova and planted in Guática, and material originating in Villamaría and planted in Guática.

Cluster 3: Material originating in SENA-Manizales and planted in Guática; material originating in Pereira and planted in Guática.

This grouping corroborates the data presented in the dendrogram—that materials originating from Villamaría and Génova can be differentiated, regardless of the planting site (Cluster 2). The cluster analysis for the three groups and Duncan's multiple comparison test at 5%, indicate that the only variable that differentiates the three clusters is "plant height at week 32". Whereas cluster analysis for any two groups and the results of the minimum difference test, at 5%, indicate that the only variable that differentiated any two groups was the number of male branches.

Based on the results obtained, materials originating from Santa Rosa de Cabal, SENA-Manizales, and Pereira

Table 4. Values obtained for morpho-agronomic variables.

Variable	Average	Minimum	Maximum	Standard error	C.V. (%)
Number of female branches	10.6	4	28	0.51	43.9
Number of male branches	2.4	0	4	0.09	35.3
Number of runners	0.98	0	3	0.09	82.6
Length of internodes of female branches	6.62	4.5	8.5	0.09	13.0
Length of internodes of male branches	7.28	3.0	10.0	0.12	14.6
Width of folioles on female branches	21.04	15.0	29.5	0.30	12.6
Length of folioles on female branches	16.35	12.0	21.0	0.21	11.5
Width of folioles on male branches	21.29	11.0	26.0	0.30	12.6
Length of folioles on male branches	16.60	8.5	19	0.22	12.2
Stem diameter on female branches	4.30	2.0	8.0	0.14	28.5
Stem diameter on male branches	4.80	2.5	8.0	0.11	21.5
Plant height at week 15	23.81	3.0	99.0	2.28	85.9
Plant height at week 32	145.30	16.0	354	9.40	58.2
Number of flower buds	32.31	11	95	1.37	37.1
Days to flowering	168.9	143	190	1.80	9.24

Table 5. Variables identified in each component.

Groups of factors	Variable
First factor	Width of folioles on male branches Length of folioles on male branches Number of runners Stem diameter of male branches Number of male branches
Second factor	Width of folioles on female branches Length of folioles on female branches
Third factor	Stem diameter on female branches Plant height at 15 weeks after planting Plant height at 32 weeks after planting Days to flowering
Fourth factor	Length of internodes on female branches (cm)
Fifth factor	Number of females branches Length of internodes on male branches (cm)
Sixth factor	Number of flower buds

differ, in general, from materials originating from Génova and Villamaría for all study variables and individually (univariate analysis) for the variables "number of male branches" and "plant height at week 32".

"Days to flowering" was another variable presenting a low coefficient of variation because flowering is closely linked to a unified physiological condition of blackberry, regardless of origin of the material or planting site. Foliole length and width on both male and female branches are variables with unique characteristics for thornless blackberry and are also important in differentiating materials. Variables presenting the highest coefficient of variation were "plant height at 15 and 32 weeks after planting", for which plants presented differences in their vegetative growth associated with fertilization and weed control, as well as the variable "number of runners" because some farmers found it difficult to identify these branches in the field, confusing them with thin branches or they want to attribute the lack of crop vigor to the presence of these branches.

Evaluating Thornless Blackberry Accessions using SSR Markers

A total of 57 alleles with eight loci were obtained as a result of the evaluation of 23 genotypes belonging to four *Rubus* species: *R. glaucus*, *R. urticifolius*, *R. robustus*, and *R. rosifolus*. The genotypes of *R. glaucus* included in the study belonged to two groups: thorny and thornless. The number of alleles per SSR marker ranged from 3 to 11 (Table 6). Polymorphic bands were obtained in thornless *R. glaucus* genotypes, evidencing that genetic variability does exist among these materials, which were considered to be very uniform because of their limited genetic origin and their massive multiplication by cuttings and widespread distribution by blackberry farmers in the region over the last five years.

The dendrogram in figure 3 shows 67% similarity for Group 1, which includes all *R. glaucus* accessions. The material differing most from the others was the P4 thornless blackberry from Génova, Quindío—an outlier from the rest of the group due to molecular differences.

At 90% similarity, two groups are formed that separate the remaining *R. glaucus* accessions. One group gathers thornless blackberry materials P1, P2, P3, and P5; P1 and P2, which are 100% similar with the SSR markers used. Both P4, originating from Génova (Quindio), and P5, originating from Villamaría (Caldas) show large differences at the molecular level. The dendrogram also shows other thornless blackberry genotypes that do not differ significantly from cultivated genotypes such as 50, 90, 99, and 46.

Analyses using SSR Molecular Markers

The SSRs used differentiated the studied genotypes by specie, producing exclusive bands for each and separating

Table 6. Description of the SSRs used for genetic characterization of *Rubus* species.

Locus[1]	SSR	Average PIC[2] value	*Rubus* species[4]					Expected band size (pb)
			Thornless *R. glaucus*	Thorny *R. glaucus*	*R. rosifolius*	*R. urticifolius*	*R. robustus*	
mRaCIRRIV2A8[1]	$(CA)_{12}$ $(CT)_{11}$	0.08678	1-3*	1-2*	1	1	1	191-237
mRaCIRRIV2F4[1]	$(CT)_8$ $(CA)_{17}$ $(CT)_{11}$	0.38143	6-11*	8-11*	2	3	3	180-242
mRaCIRRI1G3[1]	$(GA)_{28}$	0.43543	5-6*	2-6*	1	1-2*	2	195-265
Rubus 105b[2]	$(AG)_8$	0.4444	1-3	1-3	1-4	1-2*	1-2	165/173/181
Rubus 98d[2]	$(GAA)_5$ $(GA)_6$	NA[3]	1-2	1-2	1	1	1	173
Rubus 76b[2]	$(CT)_5$ $(CT)_4$	0.30215	1-3*	1-2	1	1	1-2	190-210
Rubus 16a[2]	$(AT)_8$ $(GT)_{11}$	0.31519	4	4-6*	4	2-4*	NAmp[5]	169
Rubus 116a[2]	$(CT)_{12}$ $(T)_{10}$	0.79717	2-5*	2	4	3-5*	5	299

1 1 = Derived from *Rubus alceifolius* (Amsellem *et al*., 2001); 2 = Derived from *Rubus* (red raspberry) hybrid species (Graham *et al*., 2002, 2004).
2 PIC = Polymorphism index content.
3 NA = non-available.
4 Presence of polymorphism.
5 NAmp = No amplification.

R. glaucus from other *Rubus* species, thus proving to be powerful markers for inter- and intra- specific studies.

Polymorphic bands were obtained in thornless *R. glaucus* genotypes, evidencing genetic variability within these materials traditionally considered highly homogenous because of their restricted genetic origin, their massive multiplication by stakes, and their broad distribution by farmers in the region over the past five years. The morpho-agronomic data obtained are highly consistent with those obtained with molecular data.

Badjakov (2007) characterized 48 raspberry accessions from Bulgaria, using nine SSR markers developed by the Scottish Crop Research Institute by Graham *et al*. (2002 and 2004). He obtained 59 alleles. The number of alleles per locus varied from 4 to 10, with an average of 6.5 per locus. The SSRs allowed him to calculate the genetic distance between the materials under study as well as analyze their heterozygosity, thanks to the co-dominant character of the SSRs. Of the nine SSRs used by Badjakov (2007), two of them—Rubus 76b and Rubus 98d—were also used in this study to evaluate different *Rubus* species as well as thorny and thornless accessions of *R. glaucus* collected in Colombia (Tables 6 and 7).

The species *R. urticifolius* was characterized by the presence of eight exclusive bands; *R. rosifolius* by the presence of four exclusive bands; *R. robustus* by the presence of two exclusive bands; and *R. glaucus* by the presence of nine exclusive bands. When using SSR Rubus 116a, thornless blackberry genotypes P4 and P5 were characterized by the presence of 1 exclusive band or allele and, when SSR Rubus 116a was used, thornless blackberry genotypes P1, P2, P3, P4, and P5 were characterized by the presence of 2 exclusive bands or alleles. All thornless *R. glaucus* genotypes were differentiated by the SSRs mRaCIRRIV2F4 and mRaCIRRIV2A8 (Table 7).

The highest number of single alleles was observed in *R. glaucus*, followed by *R. urticifolius*. The SSRs used allowed the *Rubus* species under study to be differentiated by their band patterns and the presence of bands exclusive to each species (Table 7). The presence of single bands for thornless *R. glaucus* genotypes (P1, P2, P3, P4, and P5) allowed the molecular characterization and differentiation of thornless blackberry genotypes. DNA profiles made it possible to clearly differentiate these materials from other *R. glaucus* genotypes (Table 7).

Of the 60 microsatellite markers described and used by Stafne *et al*. (2005) to evaluate the diversity of North American *Rubus* species, four were selected for this study: Rubus 98d, Rubus 105b, Rubus 116a, and Rubus 16a (Graham *et al*., 2002, 2004). The molecular marker mRaCIRRIV2A8 of *Rubus alceifolius* (Amsellem et al., 2001) was used also to evaluate Colombian *Rubus* species and genotypes (Tables 6 and 7).

When the results of this study were compared with those obtained by Stafne *et al*. (2005), who found Rubus 98d to be monomorphic and Rubus 105b, Rubus 116a, and mRaCIRRIV2A8 to be polymorphic, our results differed regarding the number of alleles identified per each primer. When used to analyze Colombian species and genotypes, the SSRs produced the following results: Rubus 98d (3 alleles), Rubus 105b (7 alleles), Rubus 116a (11 alleles), and Rubus 16a (7 alleles) (Tables 6 and 7).

The highest number of alleles per locus was obtained with the SSR markers Rubus 116a and mRaCIRRIV2F4, with

Table 7. Exclusiveness of markers in *Rubus* materials analyzed with SSRs.

Marker	Alleles specific to species/genotype (no.)	*Rubus* species/genotype
Rubus 105b	3	*R. urticifolius*
Rubus 105b	1	*R. rosifolius* and *R. robustus*
mRaCIRRIV2A8	2	*R. glaucus* (thornless)
mRaCIRRIV2A8	2	*R. glaucus*
mRaCIRRIV2F4	1	*R. glaucus* (thornless)
mRaCIRRIV2F4	6	*R. glaucus*
Rubus 98d	1	*R. urticifolius*
Rubus 98d	1	*R. glaucus*
Rubus 76b	4	*R. glaucus* (thornless)
mRaCIRRI1G3	3	*R. glaucus*
Rubus 16a	2	*R. urticifolius*
Rubus 116a	1	*R. glaucus* (P4 and P5)*
Rubus 116a	2	*R. glaucus* (P1, P2, P3, P4, P5)*
Rubus 116a	2	*R. rosifolius*
Rubus 116a	1	*R. urticifolius*

11 alleles each (Table 7). Markers mRaCIRRIV2F4 and Rubus 76b presented the highest number of polymorphic bands in thornless *R. glaucus* genotypes. Other markers that produced a high number of alleles per locus were Rubus 16a (9 alleles), mRACIRRI1G3 (6 alleles), Rubus 105b (7 alleles), mRaCIRRIV2A8, (5 alleles), and Rubus 76b (5 alleles).

When Colombian *Rubus* species and accessions were evaluated using with eight SSRs, a total of 57 alleles were obtained. The SSRs produced Rubus 76b (6 alleles) and Rubus 98d (3 alleles). Of the eight SSRs used, five belonged to the microsatellite series obtained in *Rubus idaeus* by Graham *et al*. (2002 and 2004) and three SSRs were obtained in *Rubus alceifolus* by Amsellem *et al*. (2001).

These results corroborate the efficient transferability and usefulness of the *R. alceifolius* markers described by Amsellem et al. (2001), as well as the markers described by Graham *et al*. (2002 and 2004) developed in red raspberries. The eight SSRs were highly polymorphic in Colombian *Rubus* species and accessions.

Furthermore, according to the results of Stafne *et al*. (2005), who evaluated eight SSR markers developed by Amsellem et al. (2001) in *R. alceifolius*, amplification was only obtained with mRaCIRRI1D3 and mRaCIRRIV2A8, which turned out to be polymorphic. In the current study, 22 alleles of a total of 57 were obtained with the SSR of *R. alceifolius.* The Colombian *Rubus* species evaluated shared 38.59% of the alleles of *R. alceifolus*; of a total of 57 alleles, 42 were obtained with markers obtained from red raspberry. Colombian *Rubus* species shared 62.68% of the alleles of *R. idaeus*.

In other studies carried out by Marulanda *et al.* (2007) that evaluate other Colombian *Rubus* genotypes and species, amplification was obtained in six of the eight SSR markers used by Amsellem (2001). These results contrast with those obtained by Stafne *et al*. (2005), who only obtained amplification with two of these markers, perhaps because of the divergent evolution of the study species and because *R. alceifolius* is an Asian type of the subgenus *Rubus*, probably more related phylogenetically with *R. glaucus*, which means that *R glaucus* shares 75% of the SSRs of *R alceifolius* (Stafne *et al*., 2005; Marulanda *et al*., 2007).

In the evaluation of 96 *Rubus* accessions of the Oregon germplasm bank, Castillo (Castillo, NRF. 2006) obtained 12 pairs of SSR primer derived from *Rubus* and several from *R. idaeus* that generated between 3 and 16 alleles per locus, for a total of 98 alleles and an average number of eight alleles per primer. These results are very similar to those obtained in the evaluation of Colombian *Rubus* species and accessions in which eight SSRs generated between 3 and 11 alleles per primer, for a total of 57 alleles and an average of 7.25 alleles per locus.

CONCLUSIONS

The analysis allows the differentiation of materials originating from Villamaría (P5) and Génova (P4) and planted in both Santa Rosa and Guática and those originating from SENA-Manizales (P2) and Pereira (P3) and planted in Guática. The most promising materials are those originating from Villamaría (P5) and Génova (P4), regardless of the planting site.

The variables with the lowest coefficient of variation were days to flowering and length and width of foliole. These variables are valuable because of their characteristics unique to thornless blackberry materials and their important contribution in the differentiation of materials.
The variables with the highest coefficient of variation were plant height at week 15 after planting, plant height at week 32 after planting, and number of runners.

The variables that contribute most to the differentiation of materials were length of folioles on the male branch, width of folioles on the male branch, stem diameter on the male branch, number of runners, and number of male branches.

The variables that contribute less to the differentiation of materials were those related to productive capacity, such as number of female branches and number of flower buds, indicating that these variables, when used independently, are less capable of differentiating materials.

The number of flower buds—a variable directly related to fruit production—contributes the least to total variation. In other words, it is highly unlikely that this variable serves to differentiate materials.

Polymorphic bands and bands exclusive to certain genotypes were obtained from thornless *R. glaucus*, indicating that genetic variability does exist within these materials.
The SSRs grouped the *Rubus* species studied, and exclusive bands were identified for genotyping each species.

The SSR markers of *R. alceifolius* and *R. idaeus* (red raspberry) were highly polymorphic in Colombian *Rubus* species and accessions.

ACKNOWLEDGEMENTS

Our special thanks to the blackberry farmers of the department of Risaralda. Our sincere appreciation to the Governor's Office of the department of Risaralda and COLCIENCIAS for co-financing this project; to Juan

Manuel Vásquez, undergraduate agronomy student for collecting field data; to Dr. César Sierra of the Colombian Agriculture and Livestock Institute (ICA) for monitoring the health of evaluation plots and accompanying the field evaluations; to Dr. Esther Cecilia Montoya for her support in experiment design and statistical analyses; to Juliana Arias Villegas, environment administrator, for planning and managing the present project. Our sincere thanks also go to the laboratory and nursery staff of the Biodiversity and Biotechnology Group, Universidad Tecnológica de Pereira.

REFERENCES

Amsellem, L., Dutech, C. and Billotte, N. 2001. Isolation and characterization of polymorphic microsatellite loci in *Rubus alceifolius* Poir (Rosaceae), an invasive weed in La Reunion island. Molecular Ecology Notes. 1:33-35.

Amsellem, L., Noyer JL., Le Bourgeois, T. and Hossaert-McKey, M. 2000. Comparison of genetic diversity of the invasive weed *Rubus alceifolius* Poir. (Rosaceae) in its native range and in areas of introduction, using amplified fragment length polymorphism (AFLP) markers. Molecular Ecology. 9:443-455.

Ashley, MV., Wilk, JA., Styan, SMN., Craft, KJ., Jones, KL., Feldheim, KA., Lewers, KS. and Ashman, TL. 2003. High variability and disomic segregation of microsatellites in the octoploid *Fragaria virginiana* Mill (Rosaceae). Theoretical and Applied Genetics. 107:1201-1207.

Badjakov, IK. 2007. Program on Euro-berry Research: from Genomics to sustainable production, Quality and Health. STSM–REPORT.

Cipriani, G., Lot, G., Huang, W-G., Marrazzo, MT., Peterlunger, E. and Testolin, R. 1999. AC/GT and AG/CT microsatellite repeats in peach [*Prunus persica* (L.) Batsch]: Isolation, characterization, and cross species amplification in *Prunus*. Theoretical and Applied Genetics. 99:65-72.

Daubeny, HA. 1996. Brambles. In: Fruit Breeding: Vine and Small Fruit Crops, Volume II. Eds. Janick, J. and Moore, JN. p. 109-190. John Wiley and Sons Inc, New York, N.Y.

Decroocq, V., Fave, MG., Hagen, L., Bordenave, L. and Decroocq, S. 2003. Development and transferability of apricot and grape EST microsatellite markers across taxa. Theoretical and Applied Genetics. 106:912-922.

Dice, LR. 1945. Measures of the amount of ecological association between species. Ecology. 26:297-302.

Dirlewanger, E., Crosson, P., Tavaud, M., Aranzana, MJ., Poizat, C., Zanetto, A., Arus, P. and Laigret, F. 2002. Development of microsatellite markers in peach (*Prunus persica*) (L. Batsch) and their use in genetic diversity analysis in peach and sweet cherry (*Prunus avium* L). Theoretical and Applied Genetics. 105:127-138.

Graham, J. and MacNicol, RJ. 1995. An examination of the ability of RAPD markers to determine the relationships within and between Rubus species. Theor. Appl Genet. 90: 1128-1132.

Graham, J., Smith, K., MacKenzie, K., Jorgenson, L., Hackett, C. and Powell, W. 2004. The construction of a genetic linkage map of red raspberry (*Rubus idaeus* subsp. *idaeus*) based on AFLPs, genomic-SSR and EST-SSR markers. Theoretical and Applied Genetics. 109:740-749.

Graham, J., Smith, K., Woodhead, M. and Russell, J. 2002. Development and use of simple sequence repeat SSR markers in *Rubus* species. Molecular Ecology Notes. 2:250-252.

Hall, HK. 1990. Blackberry breeding, Plant Breeding Reviews. 8:249-312.

James, CM., Wilson, F., Hadonou, AM. and Tobutt, KR. 2003. Isolation and characterization of polyploid microsatellites in diploid strawberry (*Fragaria vesca* L.) for mapping, diversity studies and clone identification. Molecular Ecology Notes. 3:171-173.

Jennings, DL. and Ingram, R. 1983. Hybrids of *Rubus parviflorus* (Nutt.) with raspberry and blackberry, and the inheritance of spinelessness derived from this species. Crop Research (Horticultural Research.). 23:95-101.

Lewers, KS., Styan, SM., Hokanson, SC. and Bassil, NV. 2005. Strawberry GenBank-derived and genomic simple sequence repeat (SSR) markers and their utility with strawberry, blackberry, and red and black raspberry. Journal of the American Society for Horticultural Science. 130:102-115.

Lopez-Medina, J. and Moore, JN. 1999. Chilling enhances cane elongation and flowering in primocane-fruiting blackberries. HortScience 34/44:638-640.

Lopez-Medina, J., Moore, JN. and McNew, RW. 2000. A proposed model for inheritance of primocane fruiting in tetraploid erect blackberry. Journal of the American Society for Horticultural Science. 125:217-221.

Marulanda, ML., López, AM. and Aguilar, SB. 2007. Genetic diversity of wild and cultivated *Rubus* species in Colombia using AFLP and SSR markers. Crop Breeding and Applied Biotechnology. 7:243-253.

Marulanda, MP. and Márquez, MP. 2001. Caracterización de la diversidad genética de *Rubus glaucus* Benth mediante el empleo de marcadores moleculares (RAPD). Actualidades Biológicas. 23(74):57-63.

Mohan, M., Nair, S., Bhagwat, A., Krishna, TG., Yano, M., Bhatia, CR. and Sasaki, T. 1997. Genome mapping,

molecular markers and marker assisted selection in crop plants. Molecular Breeding. 3:87-103.

Moore, JN. and Skirvin, RM. 1990. Blackberry management. In: Small Fruit Crop Management. Eds. Galletta, GJ. and Himelrick, DG. Prentice Hall, Englewood Cliffs, NJ, USA. 214-244.

Nei, M. and Li, WH. 1979. Mathematical model for studying genetic variation in terms of restriction endonuclease. Proceedings of the National Academy of Science of the USA.79:5267-5273.

Rohlf, FJ. 1998. NTSYS-pc numerical taxonomy and multivariate analysis system, Version 2.02. Exeter Publications, New York, USA.

Skirvin, RM., Motoike, S., Coyner, M. and Norton, M. 2005. *Rubus* spp. cane fruit. In: Biotechnology of Fruit and Nut Crops. Ed. Litz, RE. CABi Publishing, Cambridge, MA, USA. 566-580.

Sneath, PHA. and Sokal, RR. 1973. Numerical taxonomy. Freeman, San Francisco. pp. 573.

Stafne, E., Clark, J., Weber, C., Graham, J. and Lewers, K. 2005. Simple sequence repeat (SSR) markers for genetic mapping of raspberry and blackberry. Journal of the American Society for Horticultural Science. 130(5):722-728.

Strik, B., Finn, C., Clark, J., and Bañados, M. 2006. Worldwide production of blackberries. Department of Horticulture, Oregon State University, October 31st. Blackberry, Berry Crops, About Infonet.

Received: Nov 6, 2008, Revised: Aug 27, 2009; Accepted: Aug 29, 2009

SENRA Academic Publishers, Burnaby, British Columbia
Vol. 3, No. 3, pp. 887-895, 2009
ISSN: 1715-9997

Canadian Journal of pure&applied sciences

AMELIORATIVE EFFECT OF VOLATILE OIL FROM *CINNAMOMUM ZEYLANICUM* ON HYPERALGESIA IN ALLOXAN DIABETIC RATS

*Rajbir Bhatti[1], S Kaur[1], J Singh[2] and MPS Ishar[1]
[1]Department of Pharmaceutical Sciences, Guru Nanak Dev University, Amritsar, Punjab
[2]Department of Pharmacology, Government Medical College, Amritsar, Punjab, India

ABSTRACT

Diabetic neuropathy is generally considered to be one of the most common complications of diabetes. Neuropathic pain is the most troublesome and early symptom of diabetic neuropathy, and has been recognized as one of the most difficult types of pain to treat due to its multifactorial pathogenesis. The aim of the present study was to evaluate the antinociceptive effect of volatile oil from *Cinnamomum zeylanicum* on hyperalgesia due to alloxan induced diabetes in rats. Diabetes was induced with single intra peritoneal injection of alloxan monohydrate (150mg/kg b.w.). Animals were divided into different groups. Treatment groups received cinnamon oil from 3rd day onward upto 14th day at different doses (5, 10 and 20mg/kg b.w.; i.p.). Diabetic control animals received normal saline (0.9% NaCl; 1ml/kg). After 2 weeks, rats were tested in tail immersion and hot plate assays. Diabetic control rats exhibited significant hyperalgesia along with increased plasma glucose levels as compared with normal rats. Cinnamon oil treatment significantly decreased thermal hyperalgesia and the plasma glucose levels as compared with diabetic control rats. These results indicate the protective effect of volatile oil from the bark of *Cinnamomum zeylanicum* on hyperalgesia due to alloxan induced diabetes in rats.

Keywords: *Cinnamomum zeylanicum*, diabetic neuropathy, hyperalgesia.

INTRODUCTION

Diabetic neuropathy (DN) is generally considered to be one of the most common complications of diabetes, affecting both types of diabetes equally (Vinik *et al.,* 1992). DN affects up to 50% of patients with diabetes (Dyck *et al.,* 1993). It is generally related to the duration and severity of hyperglycaemia. However, it may also occur acutely even with hypoglycaemia (Harati, 1996). Pain is the most troublesome and early symptom of diabetic neuropathy (Vinik, 2004). Neuropathic pain is mostly characterized by pain which can occur spontaneously as a result of exposure to normally mildly painful stimuli, i.e. hyperalgesia (Brown and Asbury, 1984). Although hyperglycaemia (Green *et al.,* 1992), neuronal loss (Dyck *et al*., 1985) have been reported to be responsible for the change in pain perception, the exact aetiological factors involved are still under investigation (Anjaneyulu and Chopra, 2006). Experimentally induced diabetic rats have been used as a model of chronic pain with signs of hyperalgesia and allodynia due to diabetic neuropathy that may reflect symptoms observed in humans (Anjaneyulu and Chopra, 2006). Alloxan at a dose of 150mg/kg bw i.p., has been reported to induce reproducible and persistant hyperglycaemia in rats (Ryle *et al.,* 1984; Diniz *et al.,* 2008). Alloxan-injected diabetic rats have been reported to exhibit thermal allodynia and hyperalgesia, tested on hot-plate and tail-immersion assays (Morani and Bodhanker, 2007). Both hyperalgesia and allodynia have been reported to be established after 14 days of alloxan treatment (Aubel *et al.,* 2004).

Currently, there is growing interest in herbal remedies due to a number of side effects associated with hypoglycaemic agents used in allopathic medicine (Kim *et al.,* 2006). The effects of these plants may delay the development of diabetic complications and correct the metabolic abnormalities. It is believed that herbal medicines have lesser side effects and also have slow onset of these side effects (Habib *et al.,* 2005).

Cinnamon is one of the most common traditional folk herbs used in Korea, China and Russia for diabetes mellitus (Bailey and Day, 1989). Cinnamon bark is widely used as a spice and flavouring agent. Common cinnamon correctly refers to "true cinnamon", or its synonym Ceylon cinnamon (*Cinnamomum verum, C. zeylanicum)* (Jellin, 2006). Common and cassia cinnamon have been shown to be generally safe when ingested and to have many pharmacological properties, such as antioxidant activity (Singh *et al.,* 2007), antimicrobial activity (Tabak *et al.,* 1999; Ooi *et al.,* 2006) anti inflammatory activity (Tung *et al.,* 2008) and antifungal activity (Cheng *et al.,* 2008). Common and Cassia cinnamon are well known for their pharmacological properties in the treatment of diabetes (Khan *et al.,* 2003;

*Corresponding author email: rajbirkb@yahoo.com

Verspohl *et al.,* 2005). The analgesic and anti-inflammatory effects of *Cinnamomum zeylanicum* have been described in experimental studies (Atta and Alkofahi, 1998). Moreover, the major component found in cinnamon leaf and bark volatile oil, cinnamaldehyde (Singh *et al.,* 2007) has been studied for its inhibitory effects on pro-inflammatory mechanisms (Chao *et al.,* 2008), NF-κB activation (Liao *et al.,* 2008), nitric oxide production (Lee *et al.,* 2005) and cyclooxygenase-2 inhibitory activity (Guo *et al.,* 2006). However, the role of cinnamon in diabetic neuropathy has not been investigated so far. Therefore, the present study was designed to investigate the effect of cinnamon oil on diabetic neuropathy.

MATERIALS AND METHODS

Plant Material

C. zeylanicum (Lauraceae) was purchased from National Medicos, Amritsar, India. The species was identified and authenticated by Dr. Amarjit Singh Soodan, Guru Nanak Dev University, Amritsar. [voucher specimen (SR./Bot.Sci./0345) is deposited in the herbarium of the Department of Botanical and Environmental Sciences, Guru Nanak Dev University, Amritsar, India].

Extraction of volatile oil

Volatile oil was extracted according to the method reported by Chang and Cheng (2002) with little modification. Briefly, 500g of the dried bark was taken, broken into small pieces and hydrodistilled with a *Clavenger* apparatus for 6 h. The light yellow coloured essential oil was collected and dried over anhydrous sodium sulphate and, after filtration, stored in screw tight bottle at – 10°C.

Experimental Animals

Wistar albino rats of either sex (150-200g) were housed in 3 per cage, with food and water *ad libitum* for several days before the beginning of the experiment. The animals were kept on straw bedding in cages with a natural light: dark cycle and had free access to standard rodent food pellets and water. Animals were acclimatized to the laboratory conditions (room temperature 25±5°C) for one week before the start of experiment. All the experiments were conducted between 09.00 and 17.00 hrs.

Preparation of Drugs

Preparation of Alloxan solution (15mg/ml)

150mg of alloxan was accurately weighed and then dissolved into 10 ml of distilled water. Freshly prepared solution was used in each experiment.

Preparation of Cinnamon Oil (5, 10 & 20mg/ml)

50, 100 & 200µL of Cinnamon Oil was taken out and dissolved in 10ml of dimethyl sulfoxide (DMSO; 0.05%) to produce 5, 10 & 20 mg/ml of the cinnamon oil.

Preparation of Glipizide (10mg/ml)

50mg of Glipizide was accurately weighed and dissolved in DMSO (0.05%) and volume made upto 5ml.

Preparation of Fluoxetine (2mg/ml)

20mg of fluoxetine was accurately weighed and dissolved in 10ml of distilled water.

Experimental Protocols

In the present study, total of 42 rats were used. The rats were divided into 7 groups of 6 rats each.

Group I- Non-Diabetic group (n=6). The animals were injected with normal saline (0.9%, NaCl; 1 ml/kg) instead of the corresponding treatments.

In the rest of the groups the animals were fasted overnight prior to alloxan treatment and diabetes was induced by a single intraperitoneal injection of freshly prepared alloxan (150mg/kg bw) and the treatment with the cinnamon oil and glipizide was started on day 3. The blood glucose levels were estimated on 3rd day of alloxan treatment and the animals with fasting blood glucose levels more than 150mg/dl were considered diabetic and included in the study. The treatment with different drugs was as follows:

Group II- Diabetic control group (n = 6). The animals were administered normal saline (1 ml/kg) from 3rd day onward upto 14 days.

Group III- Diabetic vehicle group (n = 6). The diabetic animals were administered a daily dose of vehicle dimethyl sulfoxide (DMSO; 0.05%; 1ml/kg) from 3rd day onward upto 14 days.

Group IV- Glipizide treated group (n = 6). The animals were treated with glipizide at a dose of 10mg/kg; ip., from 3rd day onward upto 14 days.

Group V- Fluoxetine treated group (n = 6). The animals were treated with fluoxetine at a dose of 20mg/kg; i.p. dissolved in distilled water from 3rd day onward to 14 days. Fluoxetine was used as the standard for assessment of thermal hyperalgesia.

Group VI - Cinnamon oil (5mg/kg) group (n = 6). A daily dose of 5mg/kg of cinnamon oil was administered from 3rd day onward to 14 days.

Group VII - Cinnamon oil (10mg/kg) group (n = 6). A daily dose of 10 mg/kg was administered from 3rd day onward to 14 days.

Group VIII - Cinnamon oil (20mg/ kg) group (n = 6). A daily dose of 20mg/kg was administered from 3rd day onward upto 14 days.

Estimation of Fasting Blood Glucose (FBG)
For the estimation of blood glucose, blood samples were taken from retro orbital plexus. Blood samples were kept at room temperature for 5-10 minutes and were allowed to clot. After clotting the samples were centrifuged at 2000 rpm for 10 minutes to separate plasma. Separated plasma was used for the estimation of fasting blood glucose by GOD/POD method using commercial kit (Span Diagnostics Ltd, Surat).

Assessment of thermal hyperalgesia
Thermal hyperalgesia was assessed with tail-immersion and hot plate tests. Preliminary threshold to tail-immersion and hot-plate responses, by taking the means of two consecutive stable values which did not differ by more than 10% were determind (Chopra and Anjaneyulu, 2006). Nociceptive latency was measured at 15, 30, 60, 120 and 180 min. after the administration of drug. The nociceptive latency was expressed as mean ± S.E.M.

Tail-immersion (warm water) test
The tail was immersed in a warm water bath (52.5 ± 5^0C) until tail withdrawl (flicking response) or signs of struggle were observed, the cut-off time was 12s. The hyperalgesic response in the tail withdrawl test is generally attributed to central mechanisms (Chopra and Anjaneyulu, 2006).

Hot-Plate test
The hyperalgesic response on the hot plate is considered to result from a combination of central and peripheral mechanisms (Chopra and Anjaneyulu, 2006). In this test, animals were individually placed on a hot-plate (Eddy's Hot-Plate) with the temperature adjusted to 55 ± 1^0C. The latency to the first sign of paw licking or jump response to avoid the heat was taken as on index of the pain threshold; the cut-off time was 10 s in order to avoid damage to the paw.

STATISTICAL ANALYSIS

Results were expressed as Mean±SEM. The intergroup variation was measured by one way analysis of variance (ANOVA) followed by Tukey's test. Statistical significance was considered at $p < 0.05$. The statistical analysis was done using the Sigma Stat Statistical Software version 2.3.

RESULTS

Yield of Volatile Oil from Bark of *C. zeylanicum*
6.5ml of volatile oil was obtained from hydrodistillation of 500g of cinnamon bark. The percentage yield of the cinnamon oil was 1.3%. The density of the oil was found to be 1.059g/ml. The crude volatile oil so obtained was more than 98% pure cinnamaldehyde as evidenced the ^{1}H & ^{13}C NMR and IR spectra of the oil. In the ^{1}H NMR (400 M Hz, $CDCl_3$ solvent) the aldehydic proton showed up at δ 9.67 (1 H, doublet, J = 7.22 Hz), aromatic protons along with Cβ-olefinic H formed a 6H multiplet at δ7.76 – 7.28 and the Cα-olefinic H appeared as a double doublet at δ6.89 (1H, J = 16.00 and7.72 Hz); there was no other significant resonance signal in the proton NMR of the oil. Presence of only cinnamaldehyde is also corroborated by ^{13}C NMR through resonances at δ 192.91 (CHO), δ152.23 (olefinic Cβ), 133.85 (quaternary aromatic carbon) and other resonances at δ 1309.974 (olefinic C α), 128.873 (m-C of aromatic ring), 128.395 (o-C of aromatic ring), 128.263 (p-C of aromatic ring). The aldehyde band in the IR spectrum appeared at 1681 cm^{-1}. The determined density of the oil 1.059g/ml is also close to the value reported for pure cinnamaldehyde (1.048).

Effect of alloxan injection on Fasting Blood Glucose (FBG) in rats
The levels of fasting blood glucose were found to be significantly higher in diabetic rats than those of normal (non-diabetic) rats after 1 and 2 weeks of intraperitoneal administration of alloxan (Fig.1).

Effect of various therapeutic interventions on Fasting Blood Glucose in alloxan induced diabetic rats
The fasting blood glucose levels were estimated in different groups on 7th and 14th day of the alloxan treatment. Glipizide treatment was found to produce a significant decrease in fasting blood glucose in treated rats as compared with that of untreated control rats. The treatment with the vehicle did not alter the increase in FBG of alloxan treated animals. The treatment with cinnamon oil at 5, 10 and 20mg/kg dose was found to decrease the fasting blood glucose significantly in dose dependent manner on 7th and 14th day as compared to diabetic control group. The maximum decrease in fasting blood glucose was achieved in 20mg/kg treatment group and was similar to that of glipizide treatment (Fig. 2).

Effect of alloxan injection on tail immersion nociceptive threshold in rats
The tail immersion nociceptive threshold was observed to be significantly decreased in diabetic rats as compared with that of normal rats. Hyperalgesia was evident in tail immersion test after 1 week, the maximum decrease in pain threshold was observed at 2 weeks after alloxan injection in rats (Fig. 3).

Effect of various therapeutic interventions on tail immersion nociceptive threshold in alloxan – inducted diabetic rats
A significant increase in nociceptive threshold in tail immersion test was observed in diabetic rats treated with fluoxetine (20mg/kg) i.p. as compared with that of untreated diabetic control rats. Treatment with vehicle did

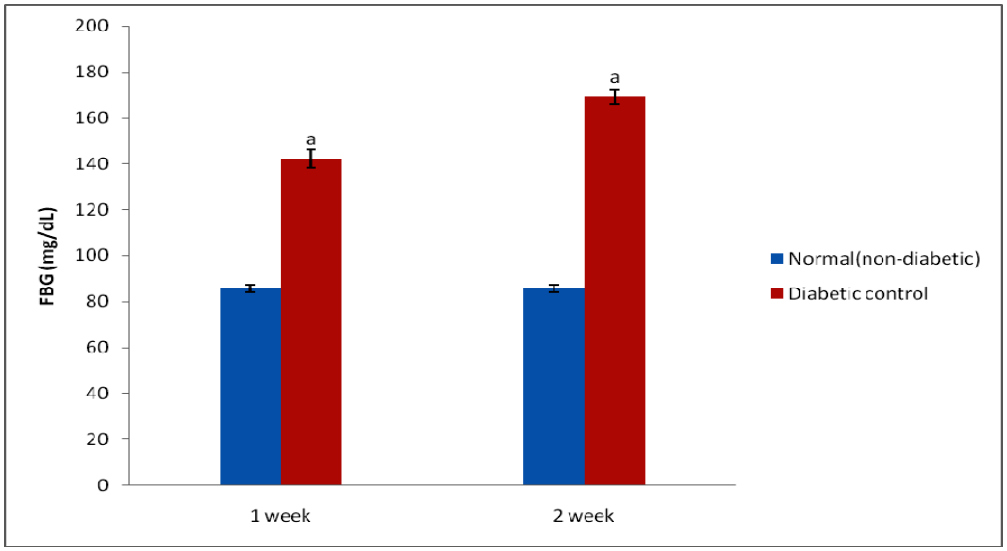

Fig. 1. Effect of alloxan-injection on Fasting Blood Glucose in Rats after 1 and 2 weeks.
$p < 0.05$; a, as compared to normal.

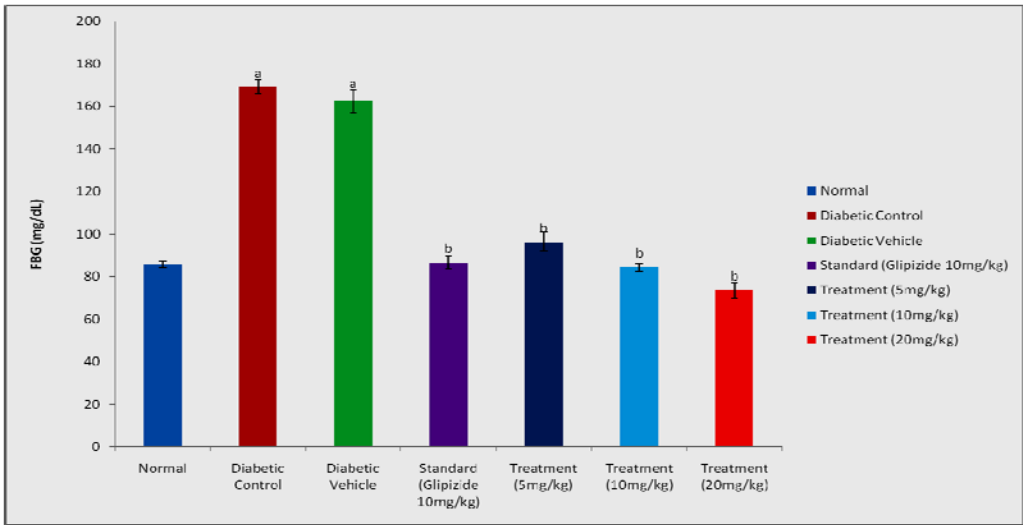

Fig. 2. Effect of various pharmacological interventions on Fasting Blood Glucose Diabetic Rats on Day 14.
$p < 0.05$; a, as compared to normal; b, as compared to Diabetic Control.

not produce any change in the nociceptive threshold in rats. Treatment with cinnamon oil at doses 5, 10 and 20 mg/kg was found to increase the nociceptive threshold in tail immersion test significantly in the treated rats as comared to that of untreated diabetic control rats. The data is expressed as mean ± S.E.M. The maximum protective effect against thermal hyperalgesia was observed at 30 min. after administration of volatile oil from *C. zeylanicum*. The protective effect produced by cinnamon oil on thermal hyperalgesia was found to be more than that of standard dug fluoxetine in tail-immersion assay. The maximum dose-dependent decrease in nociceptive threshold in tail-immersion assay was observed at the dose of 20mg/kg in alloxan-induced diabetic rats (Fig. 4).

Effect of alloxan injection on hot plate nociceptive threshold in rats

The nociceptive threshold was observed to be significantly decreased in diabetic rats as compared with that of normal rats in hot plate assay. Hyperalgesia was evident in hot plate test after 1 week, the maximum decrease in pain threshold was observed at 2 weeks after alloxan injection in rats (Fig. 5).

Effect of various therapeutic interventions on hot plate nociceptive threshold in alloxan – inducted diabetic rats

A significant increase in nociceptive threshold in hot plate test was observed in diabetic rats treated with fluoxetine (20mg/kg) i.p. as compared with that of untreated diabetic

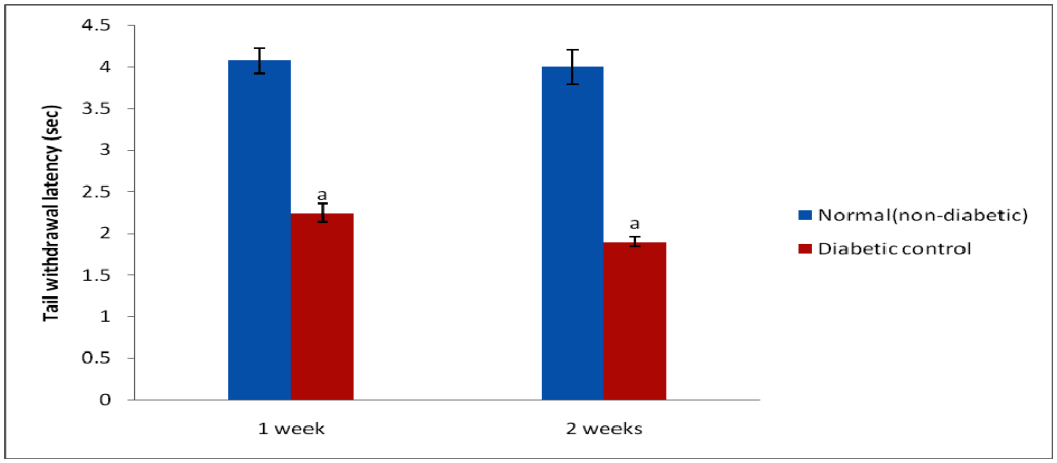

Fig. 3. Effect of alloxan-injection on tail-withdrawl latency in tail-immersion test in rats, as observed after 1 and 2 weeks.
a=p<0.05 vs normal (non-diabetic).

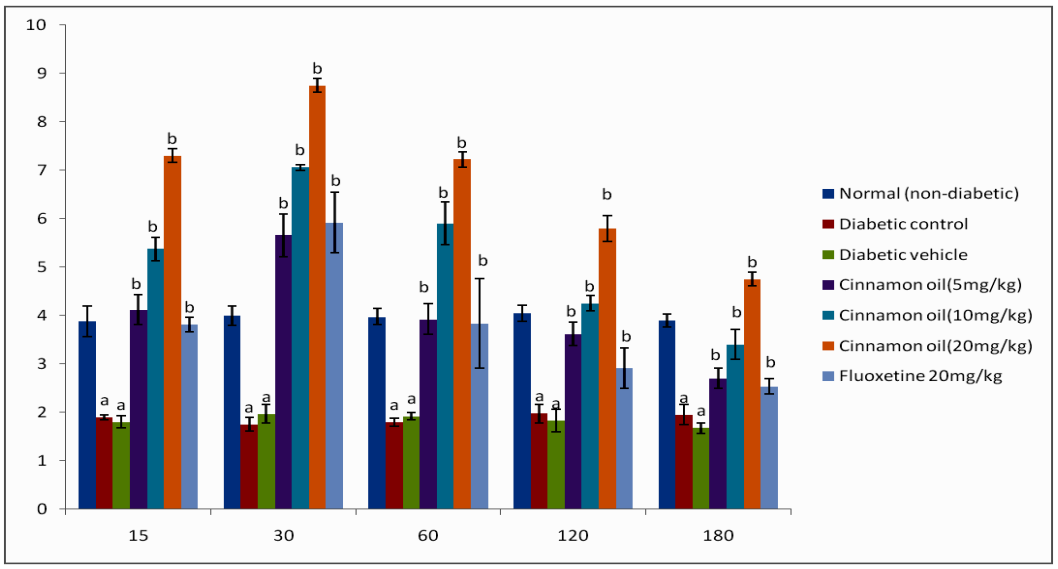

Fig. 4. Effect of various pharmacological interventions on tail-withdrawl latency (expressed as Mean ± S.E.M.) in tail-immersion test in alloxan-induced diabetic rats, as observed on day 14.
a=p<0.05 vs normal (non-diabetic); b=p<0.05 vs Diabetic control.

control rats. Treatment with vehicle did not produce any change in the nociceptive threshold in rats. Treatment with cinnamon oil at doses 5, 10 20mg/kg was found to increase the nociceptive threshold in hot plate test significantly in the treated rats as compared to that of untreated diabetic control rats. The data is expressed as mean ± S.E.M. The maximum protective effect against thermal hyperalgesia was observed at 30min. after administration of volatile oil from *C. zeylanicum*. The protective effect produced by cinnamon oil on thermal hyperalgesia was found to be more than that of standard dug fluoxetine in hot plate assay. The maximum dose-dependent decrease in nociceptive threshold in tail-immersion assay was observed at the dose of 20mg/kg in alloxan-induced diabetic rats (Fig. 6).

DISCUSSION

The aim of this study was to evaluate the protective effect of *C. zeylanicum* bark volatile oil on alloxan induced diabetic neuropathy in rats. Diabetes was induced by single intraperitoneal injection of 150mg/kg of alloxan monohydrate. Alloxan at the similar dose has been reported to induce reproducible and persistant hyperglycaemia in rats (Ryle *et al.*, 1984; Diniz *et al.*, 2008). Experimentally induced diabetic rats have been used as a model of chronic pain with signs of hyperalgesia and allodynia due to diabetic neuropathy that may reflect symptoms observed in humans (Anjaneyulu and Chopra, 2006). In the present study, the tail-immersion and hot-plate latency was observed to be significantly shorter in

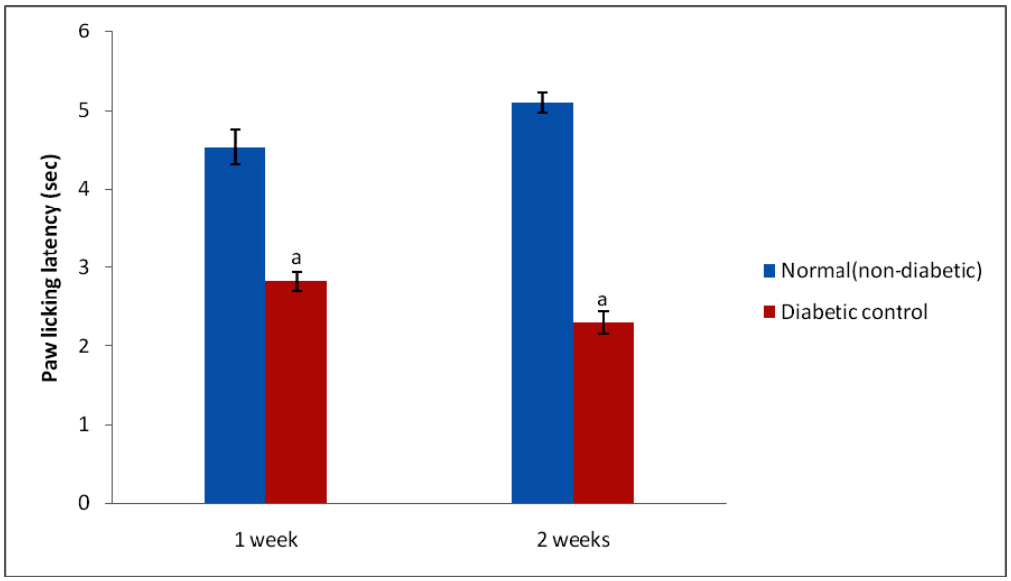

Fig. 5. Effect of alloxan-injection on paw-licking latency in hot-plate test in rats, as observed after 1 and 2 weeks.
a=p<0.05 vs normal (non-diabetic).

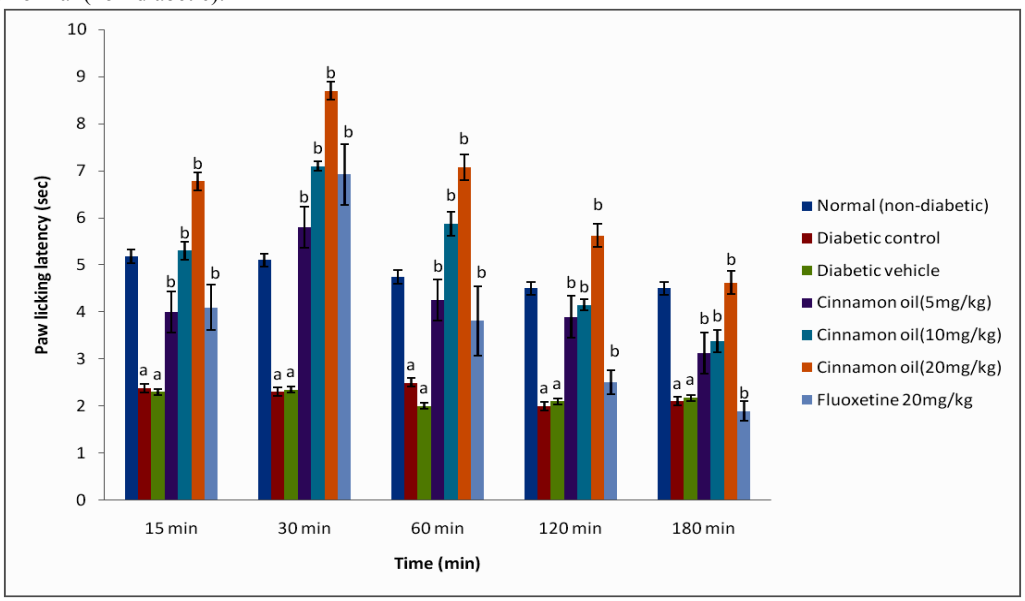

Fig. 6. Effect of various pharmacological interventions on paw licking latency (expressed as Mean ± S.E.M.) in hot plate test in alloxan-induced diabetic rats, as observed on day 14.
a=p<0.05 vs normal (non-diabetic); b=p<0.05 vs Diabetic control.

the diabetic control rats as compared to that of the normal (non-diabetic rats) indicating that alloxan-induced diabetic rats exhibit thermal hyperalgesia. It has been reported that alloxan-injected diabetic rats exhibit thermal allodynia and hyperalgesia, tested on hot-plate and tail-immersion assays (Morani and Bodhanker, 2007). Both hyperalgesia and allodynia have been reported to be established after 14 days of alloxan treatment (Aubel *et al.,* 2004), which was observed behaviorally. The hyperalgesic response in tail-withdrawal test is generally attributed to central mechanisms whereas the hyperalgesic response on hot plate is attributed to the combination of both central and peripheral mechanisms (Anjaneyulu and Chopra, 2004). The altered pattern of nociception may not be due to the inherent neurotoxicity of alloxan, but alloxan may induce various pathological alterations that can lead to altered nociceptive responses in the present study, cinnamon oil produced a marked dose-dependent antinociception in alloxan-induced diabetic rats tested in the both tail-immersion and hot-plate assays. Diabetic neuropathy develops as a result of hyperglycaemia-induced local metabolic and microvascular changes (Sharma *et al.,* 2006). Pathogenetic mechanisms underlying the progressive nerve fiber loss seem to be

multifactorial, include the polyol pathway (Finegold *et al.,* 1983), glycation (Wada and Yagihashi, 2005) and oxidative stress (Chung *et al.,* 2003; Vincent *et al.,* 2004). Oxidative stress could damage the nerves by direct toxic effects or with different biochemical changes that lead to endothelial dysfunction (Goycheva *et al.,* 2006). The volatile oil from *C. zeylanicum* has been reported to possess antioxidant activity (Shobana and Naidu, 2000; Singh *et al.,* 2007). Cinnamaldehyde which is the chief component of the cinnamon oil may be responsible for the antioxidant activity. Cinnamon has been reported to have a very high concentration of antioxidants chiefly cinnamaldehyde which make it an excellent candidate for disorders arising from oxidant stress (Su *et al.,* 2007; Jang *et al.,* 2007). Also cinnamon is documented to inhibit aldose reductase (Aida *et al.,* 1987), the latter plays a vital role in conversion of glucose to sorbitol. This sorbitol is further converted to fructose by sorbitol dehydrogenase which leads to the depletion of organic osmolites such as taurine, myoinositol etc. (Zhu *et al.,* 1999). Myoinositol depletion results in inactivation of Na^+/K^+ ATPase, Na^+ retention and cellular edema (Brownlee, 2001). Also the conversion of glucose to sorbitol depletes the cellular stores of NADPH which are required for the conversion of oxidized glutathione to reduced glutathione (Brownlee, 2001). All these factors play vital role in various complications of diabetes (Brownlee, 2001). From the above discussion it may tentatively be suggested that the protective effect of cinnamon oil may be attributed to its insulin enhancing and antioxidant effects.

Further, studies have demonstrated that even with stringent blood glucose control, the prevention of neuropathy is not successful which suggest that there may be a release of early mediators between hyperglycaemia-induced metabolic and enzymatic changes and the nerve damage (Sharma *et al.,* 2006). Once these mediators are released, it is possible that they modulate neuronal homeostasis independly of the initial metabolic stimulus (Sharma *et al.,* 2006). Previous studies have shown that chronic hyperglycaemia accelerates the production of endogenous tumor necrosis factor-α (TNF-α) in microvascular and neuronal tissues (Kuhad *et al.,* 2008).

Cinnamaldehyde has been reported to have inhibitory effects on TNF-α (Liao *et al.,* 2008). Cinnamaldehyde has been demonstrated to inhibit TNF-α-induced signaling pathways by inhibiting the expression of cell adhesion molecules in endothelial cells by suppressing nuclear factor-kappa B (NF-κB) activation (Liao *et al.,* 2008). It has been shown that clinical application of the agents that suppress the production and/or activity of TNF-α may inhibit the development and exacerbation of chronic diabetic complications (Satoh *et al.,* 2003).

Superoxide and nitric oxide have been reported as the other key mediators which combine to form peroxynitrite, which rapidly causes protein nitration or nitrosylation, lipid peroxidation, DNA damage and cell death and to have direct toxic effects on the nerve tissue leading to neuropathic pain (Kuhad *et al.,* 2008). Cinnamon has been evaluated for its NO-suppressing activity via different pathways such as the blocking of inducible nitric oxide synthase (iNOS) expression, the inactivation of iNOS catalytic function and the scavenging of NO (Tsai *et al.,* 2007).

Cinnamaldehyde has also been reported to reduce IL-1β-induced cyclooxygenase-2 (COX-2) activity in rat cerebral microvascular endothelial cells significantly (Guo *et al.,* 2006). It has been reported that COX-2 is upregulated in the peripheral nerves and dorsal root ganglia neurons in experimental diabetes and that COX-2 gene inactivation or selective COX-2 inhibition provides protection against various diabetic peripheral neuropathy defects (Kellogg *et al.,* 2008). COX-2 upregulation leads to an altered prostaglandin profile with an increased production of vasoconstricting PGH_2, thromboxane-A_2 (TXA_2) and $PGF_{2\alpha}$ and reduction of vasodilatory prostacyclin (PGI_2), thereby favouring vasoconstriction and ischemia (Kuhad *et al.,* 2008). It has also been demonstrared that COX-2 gene deficient experimental diabetic rats showed a differential protection against biochemical and functional markers of experimental neuropathy and that the extent of this protection appeared to be dependent on the degree of COX-2 gene deficiency (Kellogg and Pop-Busui, 2005).

CONCLUSION

On the basis of present results and above discussed mechanisms, the antinociceptive effect of cinnamon oil in alloxan-induced diabetic rats as observed in the present study may be attributed to its hypoglycaemic, antioxidant and pro-inflammatory inhibitory effects i.e. suppressing TNF-α signaling pathway, inhibiting NF-κB activation, suppressing NO production and activity, and reducing IL-1β-induced COX-2 activity. In conclusion, it may tentatively be stated that volatile oil from *Cinnamomum zeylanicum* could provide a novel therapeutic approach in attenuation of hyperalgesia due to diabetes.

REFERENCES

Aida, K., Shindo, H., Tawata, M. and Oaya, T. 1987. Inhibition of aldose reductase activities by kampo medicines. Pl Medica. 53:131-135.

Anjaneyulu, M. and Chopra, K. 2004. Quercetin attenuated thermal hyperalgesia and cold allodynia in STZ-induced diabetic rats. Ind J Expt. Bio. 42:766-769.

Anjaneyulu, M. and Chopra, K. 2006. Possible involvement of cholinergic and opiod receptor mechanisms in fluoxetine mediated antinociception

response in streptozotocin-induced diabetic mice. Eur J Pharmacol. 539:80-84.

Atta, A.H. and Alkofahi, A. 1998. Anti-nociceptive and anti-inflammatory effects of some Jordanian medicinal plant extracts. J Ethnopharmacology. 60:117-124.

Aubel, B., Kayser, V., Mauborgne, A., Farre, A., Hamom, M. and Bourgoin, S. 2004. Antihyperalgesic effects of cizolirtine in diabetic rats: behavioral and biochemical. B74-B77.

Bailey, CJ. and Day, C. 1989. Traditional plant medicines as treatments for diabetes. Diabetes Care. 12:553-564.

Brown, MJ. and Asbury, AK. 1984. Diabetic neuropathy. An. Neurol. 15(1):2-12.

Brownlee, M. 2001. Biochemistry and molecular cell biology of diabetic complications. Nature. 414**:**813-820.

Chang, ST. and Cheng, SS. 2002. Antitermitic Activity of Leaf Essential Oils and Components from Cinnamomum osmophleum. J. Agric. Food Chem. 50:1389-1392.

Chao, LK., Hua, KF., Hsu, HY., Cheng, SS., Lin, IF., Chen, CJ., Chen, ST. and Chang, ST. 2008. Cinnamaldehyde inhibits pro-inflammatory cytokines secretion from monocytes/macrophages through suppression of intracellular signaling. Food and Chem Toxicol. 46:220-231.

Cheng, SS., Liu, JY. Ed-Haun, Chang, EH. and Chang, ST. 2008. Antifungal activity of cinnamaldehyde and eugenol congeners against wood-rot fungi. Bioresource Technology. 99:5145-5149.

Chung, SSM., Ho, ECM., Lam, KSL. and Chung, SK. 2003. Contribution of polyol pathway to diabetes induced oxidative stress. J Am Soc Nephrol. 14:S233-S236.

Diniz, SF., Amorim, PLG., Cavalcante-Neto, FF., Bocca, AL., Batista, AC., Simm, GEPM. and Silva, TA. 2008. Alloxan-induced diabetes delays repair in a rat model of closed tibial fracture. Brazil J Med Bio Res. 41:373-379.

Dyck, I., Hansen, S., Karnes, J., O'Brien, P., Yasuda, M., Windebank, A. and Simmerman, B. 1985. Capillary number and percentage closed in human diabetic neuronal nerve. Nat. Acad Sci USA. 82:2513-2517.

Dyck, PJ., Katz, KM., Karnes, JL., Litchy, WJ., Klein, R., Pach, JM., Wilson, DM., Brein, PC., Melton, LJ. and Service, FJ. 1993. The prevalence by staged severity of various tupes of diabetic neuropathy,retinopathy and nephropathy in population-based cohort: the Rochester Diabetic neuropathy study. Neurology. 43:817-824.

Finegold, D., Lattimer, SA., Nolle, S., Bernstein, M. and Greene, DA. 1983. Polyol pathway activity and myo-inositol metabolism. A suggested relationship in the pathogenesis of diabetic neuropathy. Diabetes. 32:988-992.

Goycheva, P., Gadjeva, V. and Popov, B. 2006. Oxidative stress and its complications in diabetes mellitus. Trakia J Sci. 4(1):1-8.

Greene, DA., Sims, AA., Stevens, MJ., Feldman, EL. and Lattimer, SA. 1992. Complications:neuropathy, pathogenetic conciderations. Diabetes Care. 15(12):1902-1925.

Guo, JY., Huo, HR., Zhao, BS., Liu, HB., Li, LF., Ma, YY., Guo, SY. and Jiang, TL. 2006. Cinnamaldehyde reduces IL-1β-induced cyclooxygenase-2 activity in rat cerebral microvascular endothelial cells. Eur J Pharmacol. 537:174-180.

Habib, M.Y., Islam, M.S. and Khan, M.A. (2005) Herbal products: a novel approach for diabetic patients. *Pak J Nutrition*, 4(1):17-21.

Harati, Y. 1996. Diabetes and the nervous system. Endocrinol metab Clin North Am. 25(2): 325-359.

Jang, HD., Chang, KS., Huang, YS., Hsu, CL., Lee, SH. and Su, MS. 2007. Principal phenolic phytochemicals and antioxidant activities of three Chinese medicinal plants. Food Chemistry. 103:749-756.

Jellin, JM. 2006. Cinnamon bark- Monograph [online]. Available at www.naturaldatabase.com.

Kellogg, AP., Cheng, HT. and Pop-Busui, R. 2008. Cyclooxygenase-2 pathway as apotential therapeutic target diabetic peripheral neuropathy. Curr Drug Targets. 9(1):68-76.

Kellogg, AP. and Pop-Busui, R. 2005. Peripheral nerve dysfunction in experimental diabetes is mediated by cyclooxygenase-2 and oxidative stress. Antioxd Redox Signal. 7:1521-1529.

Khan, A., Safdar, M., Khan, MMA., Khattak, KN. and Anderson, RA. 2003. Cinnamon improves glucose and lipids of people with type II diabetes. Diabetes Care. 26:3215-3218.

Kim, SH., Hyun, SH. and Choung, SY. 2006. Antidiabetic effect of cinnamon extract on blood glucose I db/db mice. J Ethnopharmacology. 104**:**119-123.

Kuhad, A., Sharma, S. and Chopra, K. 2008. Lycopene attenuates thermal hyperalgesia in a diabetic mouse model of neuropathic pain. Eur J Pain. 12:624-632.

Lee, SH., Lee, SY., Son, DJ., Lee, H., Yoo, HS., Song, S., Oh, KW., Han, DS., Kwon, BM. and Hong, JT. 2005. Inhibitory effect of 2'-hydroxycinnamaldehyde on nitric oxide production through inhibition of NF-kappa B activation in RAW 264.7 cells. Biochem Pharmacol. 69(5):791-799.

Liao, BC., Hsieh, CW., Liu, YC., Tzeng, TT., Sun, YW. and Wung, BS. 2008. 'Cinnamaldehyde inhibits the tumor necrosis factor-α-induced expression of cell adhesion

molecules in endothelial cells by suppressing NF-κB activation: Effects upon IκB and Nrf2. Toxicology and Applied Pharmacology. 229:161-171.

Morani, AS. and Bodhankar, SL. 2007**.** Neuroprotective effect of early treatment with pioglitazone and pyridoxine hydrochloride in alloxan induced diabetes in rats. Pharmacologyonline. 2:418-428.

Ooi, LS., Li, Y., Kam, SL., Wang, H., Wong, EY. and Ooi, VE. 2006. Antimicrobial activities of cinnamon oil and cinnamaldehyde from the Chinese medicinal herb Cinnamomum cassia Blume. Am J Med. 34(3):511-522.

Ryle, PR., Barker, J., Gaines, PA., Thomson, AD. and Chakraborty, J. 1984. Alloxan-induced diabetes in the rat - protective action of (-) epicatechin? Life Sci. 34:591-595.

Satoh, J., Yagihashi, S. and Toyota, T. 2003. The possible role of tumor necrosis factor-a in diabetic polyneuropathy. Expt. Diab. Res. 4:65-71.

Sharma, S., Kulkarni, SK., Agrewala. and J.N., Chopra, K. 2006. Curcumin attenuates thermal hyperalgesia in a diabetic mouse model of neuropathic pain. Eur J Pharmacol. 536:256-261.

Shobana, S. and Naidu, KA. 2000. Antioxidant activity of selected Indian species. Prostaglandins, Leukotrienes and Essential Fatty Acids: 62:107-110.

Singh, G., Maurya, S., Delampasona, M.P. and Catalan, CAN. 2007. A comparison of chemical, antioxidant and antimicrobial studies of cinnamon leaf and bark volatile oils, oleoresins and their constituents. Food and Chem Toxicol. 45:1650-1661.

Su, L., yin, JJ., Charles, D., Zhou, K., Moore, J. and Yu, L. 2007. Total phenolic contents, chelating capacities, and radical-scavenging properties of black peppercorn, nutmeg, rosehip, cinnamon and oregano leaf. Food Chemistry. 100:990-997.

Tabak, M., Armon,R. and Neeman, I. 1999. Cinnamon extracts' inhibitory effect on *Helicobacter pylori*. J Ethnopharmacology. 67:269-277.

Tsai, PJ., Tsai, TH., Yu, CH. and Ho, SC. 2007. Evaluation of NO-suppressing activity of several Mediterranean culinary spices. Food Chem Toxicol. 45:440-447.

Tung, YT., Chua, MT., Wang, SY. and Chang, ST. 2008. Anti-inflammation activities of essential oil and its constituents from indigenous cinnamon (Cinnamomum osmophioem) twings. Biores Techn. 99:3908-3913.

Verspohl, EJ., Bauer, K. and Neddermann, E. 2005. Antidiabetic Effect of Cinnamomum cassia and Cinnamomum zeylanicum In vivo and In vitro. Phytother Res. 19:203-206.

Vincent, AM., Russel, JW., Low, P. and Feldman, EL. 2004. Oxidative stress in the pathogenesis of diabetic neuropathy. Endocrine Rev. 25(4):612-628.

Vinik, AI. 2004. Advances in diabetes for the millennium: new treatments for diabetic neuropathies**.** Med Gen Med. 6(3):13.

Vinik, AI., Holland, MT., LeBeau, JM., Liuzzi, FJ., Stansberry, KS. and Colen, LB. 1992. Diabetic neuropathies. Diabetes Care. 15:1926-1975.

Wada, R. and Yagihashi, S. 2005. Role of advanced glycation end products and their receptors in development of diabetic neuropathy. Ann N Y Acadm Sci. 1043:598-604.

Zhu, XL. and Eichberg, J. 1999. A myo-inositol pool utilized for phosphotidyl inositol synthesis is depleted in sciatic nerve from streptozotocin- induced diabetic rats**.** Proc. Natl. Acad. Sci. USA. 87:9818-9822.

Received: April 4, 2009; Accepted: July 8, 2009

SENRA Academic Publishers, Burnaby, British Columbia
Vol. 3, No. 3, pp. 897-902, 2009
ISSN: 1715-9997

Canadian Journal of pure&applied sciences

RESPONSE OF COWPEA (*VIGNA SINENSIS* L.) TO ARSENIC

*SM Imamul Huq, Kanta Parvin, Sylvia Rahman and JC Joardar
Bangladesh-Australia Centre for Environmental Research
Department of Soil, Water and Environment
University of Dhaka, Dhaka-1000, Bangladesh

ABSTRACT

Responses of cowpea (*Vigna sinensis* L.) to different levels of spiked arsenic in pots with two soil series *viz.*, Sonargaon and Dhamrai were investigated. Arsenic (As) content in plant increased with increasing As application to soil. Arsenic treated plants of cowpea were shorter in heights and at 50 mg As/L treatment, all leaves were shed after 60 days of growth. The number and size of nodules showed gradual decrease with increasing As application. The plant N decreased while plant P increased with increasing As concentration. The nodule nitrogen content showed a decreasing tendency with increasing As accumulation in plant, thus demonstrating a negative impact on Rhizobium-legume symbiotic association.

Keywords: Arsenic, Cowpea, *Vigna sinensis*, nodulation, mineral nutrition, accumulation.

INTRODUCTION

Arsenic (As) contamination of ground water in Bangladesh has emerged as the largest water pollution event of all time where millions of people are exposed to As concentrations, the Bangladesh and WHO drinking water standards being far above. Another possible potential exposure pathway is through the food chain where As contaminated ground water is used for irrigation and there is report of increased concentrations of the element in soil and many food materials (Huq and Naidu, 2005).

Food crops such as vegetables and cereals are potential sources from which As may enter the food chain, and these can reflect the levels of As that exist in the environment in which they are grown. Leguminous plant, such as cowpea is rich in vital nutritive value protein. Any adverse effect on protein production due to use of As contaminated irrigation water may, therefore, have a negative impact on the nutritive quality of grain legume. Moreover, the presence of As at elevated levels in the growth media might adversely affect the symbiotic system, leading to a crop failure. The present study aims at understanding the risk associated with As contaminated soils for the cowpea- Rhizobium symbiotic association.

MATERIALS AND METHODS

The experiment was carried out with two soils *viz*., Sonargaon (collected from Narayanganj) and Dhamrai (collected from Dhamrai, Dhaka) soil series being spiked with different levels of As concentrations to investigate its transfer to and effect on the growth of cowpea. Arsenic levels of the Sonargaon and Dhamrai soils were 0.46 mg/kg and 0.31 mg/kg soil, respectively. These were taken as control and As at the rates of 20, 30 and 50mg /L in water were applied as solution of sodium meta arsenite ($NaAsO_2$). There were three replications for each treatment. The As solution was added to the treated soils from seed sowing to plant maturity. The total amount of solution added was recorded. Plastic pots of equal sizes (2.5L) were used. Two kg soil was put in each pot. The soil in each pot was mixed with triple super phosphate and muriate of potash according to the need of the soils as calculated from Fertilizer Recommendation Guide (BARC, 1997). Before sowing, seeds were mixed with Rhizobium biofertilizer procured from Bangladesh Institute of Nuclear Agriculture (BINA). Rhizobium biofertilizer is known to increase soil nitrogen by 50-300 kg/ha in optimum condition (BINA, 1999). The cowpea seeds were collected from BARI, Gazipur. About 10-12 cowpea seeds were sown in each of the plastic pots and then they were allowed to grow. The pots were arranged in a completely randomized way. There were a total of 24 (2×4×3) pots. In Dhamrai soil at 50 mg As/L treatment, no cowpea seeds germinated. Treatment plants received watering with As solution and control plants with tap water twice a week. Plant protection measures were taken for both sets of plants. During the whole growth period, all visible symptoms were noted. In the cowpea plants on Sonargaon soil at 50mg As/L treatment, leaves shed gradually after eight weeks of germination. The plants were harvested after 90 days of seed sowing. The harvested roots were washed with deionized distilled water several times to remove ion from the ion free space

*Corresponding author email: imamhuq@hotmail.com
[1]Present address: University of Development Alternative, Dhaka

as well as to dislodge any adhering particles on the root surface. The numbers of plants were counted and the heights of plants were measured separately. The total number of root nodules of each plant was counted and isolated with the help of forceps. In Dhamrai soil, the nodules formed were very small in size, more particularly in the treated soils. The fresh weight of roots, shoots, leaves and nodules were taken separately. The collected plant samples were air dried and then oven dried at $70^0 \pm 5^0$C for 48 hours and the dry weights of plant samples were noted. The dried plant samples were then ground into fine powder and preserved in small plastic vials for further analysis. After harvest, the soil samples in each pot were thoroughly air dried and homogenized and were sieved to pass through a 0.5 mm sieve for chemical analysis.

For determination of As, soil was digested in aqua regia and the As in the extracts was estimated by Hydride Generated Atomic Absorption Spectrometer (HG-AAS) as described by (Portman and Riley 1964). The water soluble soil As was extracted by shaking samples of soil at a 1:5 soil-water ratios for 24 hours. Plant samples were digested with HNO_3 on a digestion block. Samples were normally predigested overnight over a temperature range of about 40-100^0 C before increasing the temperature to 140^0 C for the final dissolution of the organic material. This extract was used for the determination of As and other elements of plant (Portman and Riley, 1964). The experimental data were statistically analyzed using MINITAB Package.

The various physical, chemical and physiochemical properties of the soils were determined following procedures as described in the book by Huq and Alam (2005). Certified reference materials were carried through the digestion and analyzed as part of the quality assurance/quality control protocol. Reagent blanks and internal standards were used where appropriate to ensure accuracy and precision in the analysis of arsenic. Each batch of 20 samples was accompanied with reference standard samples to ensure strict QA/QC procedures.

Some basic properties of the selected soils are given in table 1.

RESULTS AND DISCUSSIONS

Morphological change

Symptoms due to As application were observed. The

Table 1. Some basic properties of the selected soils.

Soil	Sand (%)	Silt (%)	Clay (%)	Textural Class	pH	OM (%)	Total N (%)	Av. N (ppm)	Av. P (ppm)	As (ppm)	
										Total	Av.
Sonargaon	2.33	59.58	38.08	Silty Clay Loam	7.0	3.45	0.005	31.50	8.41	0.46	0.10
Dhamrai	9.26	49.68	41.06	Silty Clay	5.9	1.30	0.020	47.25	3.02	0.31	0.15

Table 2. Mean height and fresh weight (g/10 plants) of cowpea (*Vigna sinensis* L.) plants.

Treatment (mg As/L)	Sonargaon Soil		Dhamrai Soil	
	Height (m)	Fresh weight (g)	Height (m)	Fresh weight (g)
0	1.067	38.9	1.621	116.2
20	1.247	22.5	1.643	86.3
30	1.016	30.2	1.328	56.1
50	0.889	44.6	-	-

LSD at 1% level, 1.075 and 0.814 for height and 4.51 and 1.83 for fresh weight in Sonargaon and Dhamrai soil, respectively.

Table 3. Number, fresh and dry weights of root nodules.

Treatment (mg As/L)	Sonargaon Soil			Dhamrai Soil		
	Number per plant	F.W.	D.W.	Number per plants	F.W.	D.W.
		(mg/plant)			(mg/plant)	
0	5.5	12	5	1.2	6	2
20	2.1	6	2	0.6	4	1
30	1.0	4	1	0.4	2	1
50	0.6	2	1	-	-	-

LSD at 1% level, 0.38 and 0.036 for number and 0.03 and 0.04 for fresh weight of root nodule in Sonargaon and Dhamrai soil, respectively.

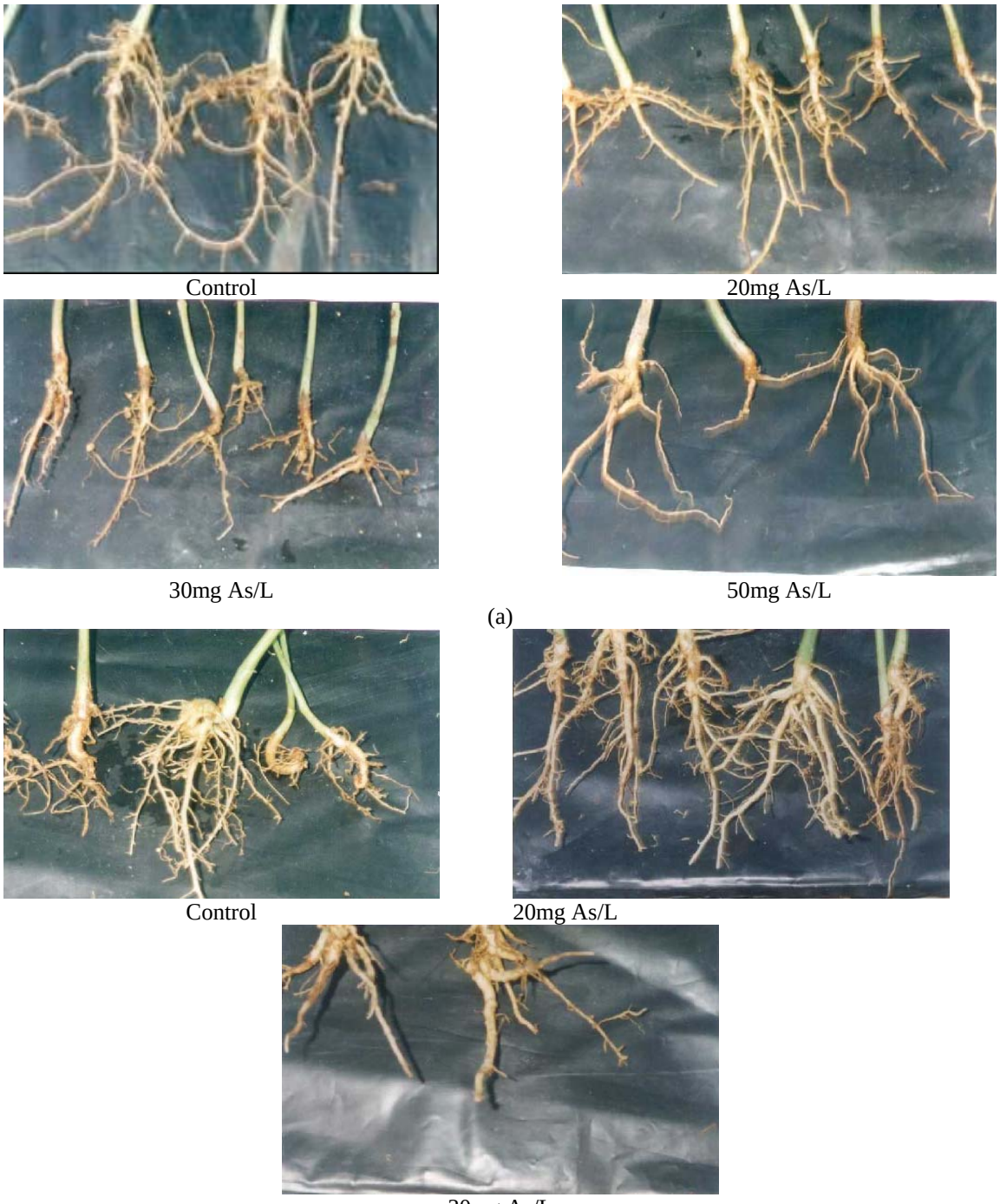

Fig. 1. Root nodules of cowpea: (a) Sonargaon soil; (b) Dhamrai soil.

seeds did not germinate on Dhamrai soil at 50mg As/L treatment. The plants showed severe symptoms at higher As concentration and the symptoms became pronounced with time of exposure to arsenic stress. The symptoms were shading of leaves, reduced plant growth, and brown necrotic spots on the leaves. The brown necrotic spots were observed on old leaves at 30 and 50mg As/L treatment. Red-brown necrotic spots on old leaves, tips and margins due to arsenic toxicity have also been reported by Aller *et al.* (1990) and Marin *et al.* (1992). Reduced chlorophyll content due to As toxicity and resulting chlorosis were reported in garden pea by Paivoke (1983). The plants grew vigorously up to approximately 45 days and then growth of treated plants

declined and caused a reduction in plant heights over control plants. The mean values of heights (m) and fresh weights (g/10 plants) of the plants were recorded after harvest of the plants at 90 days and are presented in Table 2. The plants on both soils at 20mg As/L treatment grew taller than control plants and had the maximum height (1.247 m and 1.643 m for Sonargaon and Dhamrai soil, respectively). It could be so because of the fact that the presence of As in soil might have induced the release of phosphorus and P requirement of legumes is high. The height of the plants for other treatments decreased significantly with increasing As treatment in both the soils ($p = 0.000$ for both the soils). Fresh weight of plants also decreased with increasing As treatment in both the soils; however, in Sonargaon soil, the trend of decrease was not uniform; a significantly higher fresh weight was observed for 30 and 50mg As/L As treatment over 20mg As/L treatment (Table 2). The effect of As on fresh weight was statistically significant ($p = 0.000$ for both the soils). Sizes (Fig. 1) and numbers and weights (Table 3) of the root nodules were reduced with increasing As treatment ($p = 0.000$ for Sonargaon soil and $p = 0.005$ and 0.025 for number and weight respectively for Dhamrai soil).

Arsenic accumulation in plants

The mean values of arsenic concentration (mg/kg) in root, shoot, and leaf of Sonargaon and Dhamrai soils are presented in figure 2. Corresponding soil As concentrations (mg/kg) after harvest are also presented in figure 2. It is important to note that in control plants As concentrations increased slightly through the uptake of water extractable As present (Table 1) in both the soils.

Arsenic concentrations in root, shoot and leaf increased with increasing arsenic treatment more in the Sonargaon than in the Dhamrai soil. The reasons could be attributed to the differences in clay contents of the two soils and soil reaction. Dhamrai soil contained higher clay and the pH was lower than the Sonargaon soil. Higher clay content in soil is known to retain As more tenaciously and make it less phytoavailable (Joardar *et al*., 2005) while higher pH make the As more phytoavailable (Huq and Naidu, 2003). Arsenic treatment in soil had a significant ($p = 0.000$ in all the cases and in both the soils) increase in As accumulation in all parts of cowpea. Arsenic accumulation was found to be higher in root followed by shoot and leaf.

The consequence might be due to the fact that the upward transport of As from roots was inhibited by its high toxicity to the membranes of radicle (Wauchope, 1983; Barrachina *et al*., 1995). Higher accumulations of arsenic in roots in many plants have also been reported by many investigators *e.g.* in arum (Parvin *et al*., 2006), in marigold and ornamental arum (Huq *et al*., 2005), in rice (Huq and Naidu, 2005; Odanka *et al*., 1985) in lodgepole pines (Frans *et al*., 1988; Yamare, 1989), in alfalfa (Maclauchlan *et al*., 1988), and in lettuce and wheat (Kapustka *et al*., 1995). Accumulation of arsenic in some aquatic plants like duckweed (*Spirodela polyrhiza* Dh 116) and water fern (*Azolla pinnata* var. pinnata Dh 113) is also in report (Aziz, 2002). After harvest, the soil As was also found higher in Dhamrai soil than in Sonargaon soil and it might be due to the fact that the high clay content in Dhamrai soil retained high amount of As (Huq *et al*., 2006).

A mass balance of arsenic was calculated between the amount of As added to soil and the amount of As in plant and in soil. A substantial fraction of the total As applied remained unaccounted for. This fraction, however, varied between the two soils. The unaccounted As was higher except at 50 mg As/L treatment in Sonargoan soil. The uncounted fraction was 39%, 27% and 25% in Sonargaon soil for 20, 30 and 50mg As/L treatment respectively and it was 36.4% and 28.3% in Dhamrai soil at 20 and 30mg As/L treatment respectively. It needs to be mentioned again that in Dhamrai soil the seeds treated with 50mg

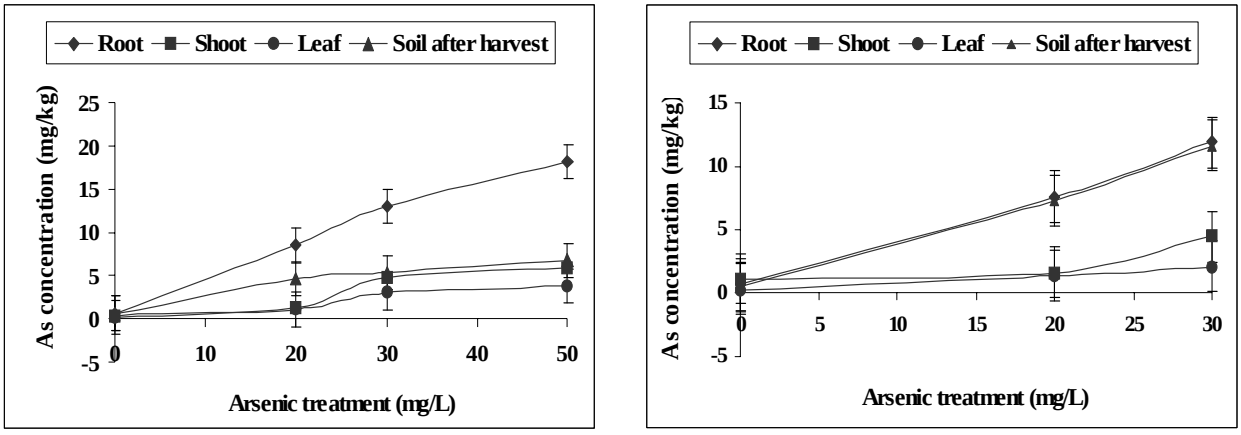

Fig. 2. Arsenic concentrations in different parts of cowpea: (a) Sonargaon soil (b) Dhamrai soil.

Table 4. Nitrogen and Phosphorus contents in plant parts and in soils after harvest.

Soil	Treatment (mg As/L)	Root (%)		Shoot (%)		Leaf (%)		Soil (%)	
		N	P	N	P	N	P	N	P (total)
Sonargaon	0	7.7	0.1	1.7	0.2	3.9	0.2	0.08	0.06
	20	5.0	0.2	2.1	0.2	4.8	0.4	0.11	0.08
	30	4.5	0.5	2.0	0.2	3.5	0.4	0.07	0.08
	50	4.3	0.4	2.2	0.2	3.7	0.4	0.05	0.09
Dhamrai	0	7.9	0.3	2.8	0.2	3.4	0.2	0.10	0.08
	20	4.7	0.3	2.7	0.2	3.4	0.4	0.12	0.08
	30	4.9	0.4	2.7	0.2	3.5	0.4	0.10	0.07

As/L did cause no germination. The possible reason for the unaccounted fraction might be that the method used for extraction was not able to bring most of the As into solution from soil, or there was a loss of arsenic through volatilization by biomethylation process active in soil.

Mineral nutrition as affected by arsenic toxicity

Increasing levels of As had a pronounced effect on the nutrient uptake as well as its transport in plants. To evaluate the effect of As on N and P concentrations in root, shoot and leaf both N and P were analyzed.

Nitrogen content

Mean values of the nitrogen content in soil after harvest and in different parts of cowpea are presented in table 4. Nitrogen content significantly decreased in plant roots with increased As concentration ($p = 0.000$ for both the soils) whereas there has been an increase in the shoot N content of cowpea grown on Sonargaon soil ($p = 0.043$). There was no significant reduction of leaf nitrogen. Decreased nitrogen content in different plant parts might be due to reduced growth and reduced number of root nodules.

It needs to be mentioned here that the nodules formed on Dhamrai soil were not sufficient enough to be analyzed separately. These were analyzed with the roots. The poor growth of nodules, even in the control plants on Dhmarai soil could be due to the fact that the Dhamrai soil does not contain indigenous cowpea Rhizobium; the nodulation that occurred could have been due to inoculation with biofertilizer. In Sonargaon soil, however, the nodule nitrogen concentrations were 6.1%, 3.6%, 3.1% and 2.8%, in 0, 20, 30 and 50 mg As/L treated plants respectively. The corresponding nodule As concentrations were 0.5, 5.6, 7.9, and 10.3 mg/kg respectively. This shows that with increasing As accumulation in nodules, the nodule nitrogen also decreased. From this observation, it is realized that *Rhizobium*-legume symbiotic association is affected by high level of As in the growth medium. It has been observed that high concentration of As has a depressing effect on the *in vitro* growth of *Rhizobium* (data not shown in this paper) Similar effects might have occurred *in vivo* too.

Root nodules of control plants in Sonargaon soil contained the highest amount of nitrogen (6.1%) among all other plant parts. Nodule nitrogen concentrations significantly differed among control and all treated plants and decreased with increased As concentrations. Paivoke (1983) reported that the nodulation and nitrogen fixation were depressed and plant nitrogen content decreased at As treatments in garden pea. The antagonistic effects between As and nitrogen have also been reported in rice (Yamare, 1989) and in silver beet (Merry *et al*., 1986).

Phosphorus content

Phosphorus content in different plant parts are shown in Table 4. Phosphorus content increased with As treatment compared to the control in roots but there was no difference among the treatments. Leaves contained comparatively higher amount of phosphorus than root and shoot. But the increased phosphorous content in root and leaf was highly significant ($p = 0.000$ for root and leaf in both the soils) whereas in shoot it was insignificant in both the soils. Increased uptake of P in presence of As might be due to the fact that arsenate and phosphate are taken up by the same plasma membrane transport system (Meharg and Macnair, 1990) in plants. Increased P accumulation in presence of As in the growth medium has also been observed in hydroponically grown rice by Shaibur *et al*. (2006).

CONCLUSION

It is apparent from the present study that As in the growth medium of leguminous plants could adversely affect the symbiotic system and cause a negative effect on the nutritive quality of the legumes. Further studies with more comestible grain legumes are emphasized.

REFERENCES

Aller, AJ., Bernal, JL., Del Nozal, MJ. and Deban, L. 1990. Effect of selected trace elements on plant growth. J. Sci. Food and Agric. 51:447-472.

Aziz, A. 2002. Arsenic problems: Integrated approach for solution by floating plants. In: Bangladesh Environment. vol. 1. Eds. Ahmed, MF., Saleh, AT. and Badruzzaman,

ABM. Bangladesh Paribesh Andolon, Dhaka, Bangladesh. pp. 186-191.

BARC (Bangladesh Agricultural Research Council). 1997. Fertilizer Recommendation Guide 1997. Eds. Rashid, MM., Idris, A., M., Bhuiyan, NI., Hossain, AKM., Huq, F., Talukder, AB., Panaullah, GM., Nuruzzaman, M. and Miah, MU. BARC, Dhaka, Bangladesh. pp. 196.

Barrachina, AC., Carbonell, FB. and Beneyto, JM. 1995. Arsenic uptake, distribution and accumulation in tomato plants: Effects of arsenic on plant growth and yield. J. Plant Nutr. 18(6):1237-1250.

BINA (Bangladesh Institute of Nuclear Agriculture). 1999. Zibanu Sar O Amader Krishi. Eds. Podder, AK., Md. Zahurul Islam, Md. Harun-or-Rashid, Saiyera C. and Md. Niaz Uddin Pasha). Bangladesh Institute of Nuclear Agriculture, Mymensingh, Bangladesh. pp. 9.

Frans, R., D. Horton and L. Burdette. 1988. Influence of MSMA on straight head, arsenic uptake and growth response in rice *(Oryza sativa)*. Report series, Arkansas Agric. Expt. Stn. 302(12):10.

Huq, SMI. and Alam, MD. 2005. A handbook on analyses of Soil, Plant and Water. BACER-DU, University of Dhaka, Bangladesh. xxii+246pp.

Huq, SMI. and Naidu, R. 2003. Arsenic in groundwater of Bangladesh: Contamination in the food chain. In: Arsenic Contamination: Bangladesh Perspective. Eds. Ahmed, MF. pp. 203-226. ITN-Centre, BUET, Dhaka, Bangladesh.

Huq, SMI. and Naidu, R. 2005. Arsenic in ground water and contamination of the food chain: Bangladesh Scenario. In: Natural arsenic in ground water: occurrence, remediation and management. Eds. Bundschuh, B. and Chandrasekharam. A.A. Balkema Publishers, New York. pp. 95-101.

Huq, SMI., Joardar, JC. and Parvin, S. 2005. Marigold (*Tagetes patula*) and ornamental arum (*Syngonia sp.*) as phytoremediators for arsenic in pot soil. Bangladesh J. Bot. 34(2):65-70.

Huq, SMI., MS., Joardar, JC. and Khan, TH. 2006. Retention of some environmental pollutants (As, Pb and Cd) in soil and subsequent uptake of these by plant (*Ipomoea aquatica*). Bangladesh J. Agric. & Environ. 2(1):61-68.

Joardar, J.C., Rashid, MH. and Huq, SMI. 2005. Adsorption of arsenic (As) in soils and in their clay fraction. Dhaka Univ. J. Biol. Sci. 14(1):51-61.

Kapustka, LA., Lipton, J., Galbraith, H., Cacela, D. and Lejeune, K. 1995. Metal and arsenic impacts to soils, vegetation communities and wildlife habitat in south west Montana uplands contaminated by smelter emissions. II Laboratory phytotoxicity studies. Environment toxicity and chemistry. 14(2):1905-1212.

Maclauchlan, LE., Borden. JH. and Auria, JM. 1988. Distribution of As in lodgepole pines treated with MSMA. Western J. Appl. Forestry. 3(2):37-40.

Marin, AR., Masscheleyn, PH. and Patrick, WH. Jr. 1992. The influence of chemical form and concentration of arsenic on rice growth and tissue arsenic concentration. Plant Soil. 139:175-183.

Meharg, AA. and Macnair, MR. 1990. An altered phosphate uptake system in arsenate tolerant *Holcus lanatus*. New Phytol. 116:29-35.

Merry, RH., Tiller, KG. and Alsten, AM. 1986. The effect of contamination of soil with copper, lead and arsenic on the growth and composition of plants II. Effect of source of contamination, varying soil pH and prior water logging. Plant Soil. 95:225-268.

Odanka, Y., Tsuchi, N., Matano, O. and Goto, S. 1985. Characterization of arsenic metabolites in rice plant treated with DSMA. J. Agric. Food Chem. 33**(**4):757.

Paivoke, A. 1983. The term effect of lead and arsenate on the growth and development, chlorophyll content and nitrogen fixation of the garden pea. Annals - Botanici - Fennici. 20(3):297-306.

Parvin, S., Rashid, MH., Joardar, JC. and Huq, SMI. 2006. Response of arum (*Colocasia antiquorum*) to different levels of arsenic (As) treatments. Dhaka Univ. J. Biol. Sci. 15(1):11-20.

Portman, JE. and Riley, JP. 1964. Determination of arsenic in seawater, marine plants and silicate and carbonate sediments. Anal. Chem. Acta. 31:509-519.

Shaibur, MR, N. Kitajima, N., Sugawara, R., Kondo, T., Huq, SMI. and Kawai, S. 2006. Physiological and mineralogical properties of arsenic-induced chlorosis in rice seedlings grown hydroponically. Soil Sci. Plant Nutr. 52:691-700.

Wauchope, RD. 1983. Uptake, translocation and phytotoxicity of arsenic in plants. *In*: Industrial, biomedical, environmental perspectives. Eds. Lederer and Fensterheim. Arsenic Symp. Gaiothersburg. MD, USA. pp. 348-374

Yamare, T. 1989. Mechanism and counter measures of arsenic toxicity to rice plant. Bull. Shimane Agric. Expt. Stn. 24:104.

Received: May 10, 2009; Revised: July 10, 2009; Accepted: July 11, 2009.

SENRA Academic Publishers, Burnaby, British Columbia
Vol. 3, No. 3, pp. 903-910, 2009
ISSN: 1715-9997

Canadian Journal of pure&applied sciences

THE INFLUENCE OF MONO-DISPERSED TIN – DOPED INDIUM OXIDE NANOPOWDERS ON ITS DIELECTRIC PROPERTIES

FF Hammad[1] and *AH Salama[2]
[1]Department of Inorganic Chemistry, National Research Center, Dokki, Giza
[2]Department Physical Chemistry, National Research Center, Dokki, Giza

ABSTRACT

Mono-dispersed tin doped indium oxide (ITO) nanopowders were prepared by wet chemical co-precipitation method at 300^0C for 3h with maintaining the In/Sn atomic ratio 90:10, 70:30 and 50: 50 wt.%. The grain size of the prepared samples was determined by TEM technique. Structural characterization of the prepared samples was studied by X-ray diffraction analysis. It is found that the samples were a mixture of cubic and rhombohedra crystals with sharp diffraction peaks except for the sample with atomic ratio 50:50 shows very poor crystalline and no peaks ascribed to the phase of the compounds are observed which confirms the amorphicity of this sample. The dielectric properties including dielectric constant, έ and dielectric loss, ε`` of the prepared samples were evaluated from the observed capacitance values in the frequency range 100 Hz to 5 MHz and in the temperature range of 25 ^{0}C to 160^0C. Further, from the dielectric properties studies AC- conductivity was evaluated. The activation enthalpy ΔH and the entropy change ΔS of the prepared samples were calculated. The obtained data were correlated to the structure of the prepared samples.

Keywords: Indium Tin Oxide nanopowder, XRD- spectroscopy, dielectric constant έ, dielectric loss ε``, ac-conductivity.

INTRODUCTION

Indium tin oxide is a colorless in thin layers solid solution of In_2O_3 and SnO_2 (typically 90% In_2O_3 and 10% SnO_2 by weight). In_2O_3 is an important transparent conducting oxide (TCO) material, passing over 90% of visible light. Increased interest to In_2O_3, which is one of the wide band gap semi conducting materials (3.6 or ~3.7eV) (Korotcenkov, *et al*., 2007; Zhu *et al*., 2005; Rey *et al*., 2005) and crystallizes with C-type rare earth sesquioxide structure. Due to the wide band gap, it is transparent to the visible radiation. It is an insulator in its stoichiometric form and becomes conducting in the oxygen deficient nonstoichiometric form. Each oxygen vacancy can act like a doubly or singly ionized donor. Therefore, nonstoichiometric In_2O_3 exhibits high electrical conductivity similar to that of a heavily doped degenerate n-type semiconductor (Malar *et al*., 2005; Zhan *et al*., 2004). The interest in nonstoichiometric In_2O_3 is mainly due to the possibility of varying the electrical resistivity by more than 10 orders of magnitude by changing the oxygen content alone (Malar *et al*., 2005).

Indium tin oxide (ITO) is an advanced ceramic material with many electronic and optical applications due to its excellent properties of high conductivity ($\approx 10^4$ $\Omega^{-1}cm^{-1}$) and high transparency (85-90%) to visible light, high infrared reflectivity for wavelengths higher than 1 μm (Lee and Choi, 2005).

Up till now, tin-doped indium oxide (ITO) yields the lowest resistivity of about 1.10^{-4} Ω cm. This, together with its very good stability, are the reasons why ITO is presently used exclusively as transparent electrode material for flat panel displays, based on liquid crystals, micro plasmas or organic light emitting diodes (OLED) and sensors (Ellmer and Mientus, 2008). High conductivity of ITO is achieved by doping with Sn and thereby increasing the oxygen vacancies in the In_2O_3 lattice. An improvement of conductivity can also be achieved by stabilizing the cubic In_2O_3 phase instead of the hexagonal modification (Pujilaksono *et al*., 2005).

To increase the conductivity up to the metallic conductivity (10^3-10^4 $\Omega^{-1}cm^{-1}$), a solid solution of indium-tin oxide (ITO) with a few percent of Sn is used (Cho *et al*., 2006).

ITO thin films of nanoparticles have been reported by Sung *et al*., 1996. In recent years, great attention has been paid to nanometresized materials in studies of their fundamental mechanism, such as the size effect and the quantum effect, and in applications of these materials. In particular, nanocrystalline indium-doped tin dioxide powders are widely applied by a screen-printing technique (Yang *et al*., 1998).

The present work aims to study the effect of different additives ratio of Sn on the crystallographic structure properties and dielectric properties of In_2O_3 using X-ray diffraction analysis, dielectric constant ε`, dielectric loss ε`` and ac- conductivity in order to select the best composition of In / Sn having cubic structure with higher dielectric properties.

*Corresponding author email: alia2005salama@yahoo.com

MATERIALS AND METHODS

Preparation of nano-grain ITO

Indium tin oxide (ITO) nano powders of different compositions (In: Sn = 90: 10, 70: 30 and 50: 50 wt.%) were prepared from the starting materials, aqueous indium nitrate and $SnCl_4.5H_2O$. The resulting solution was stirred genetically for 2h at 65^oC and the pH of the above solution was maintained in the range 7.0-7.5. White powder solid was obtained. The samples were heated at 300 ^oC at 3h (Jagadish *et al*., 2003).

TEM

TEM images were taken with a JEDL model 1230 Transimation Electron Microscope.

X-ray diffraction study

A computer controlled X-ray diffraction (Diano- 8000, USA) was used with a filtered Co K_α radiation (λ= 1.7903$\mathring{}$A). The scanning range was 20$\mathring{}$ -80$\mathring{}$ (2θ).

Dielectric properties

The dielectric properties (dielectric constant $\varepsilon`$ and dielectric loss $\varepsilon``$) were measured as disc of 12 mm diameter, in the temperature range (298 K – 483 K) and frequency range (0.1KHz – 5 MHz) using HIOKI 3532 LCR Hi – Tester.

RESULTS AND DISCUSSION

TEM

Figure 1, shows TEM images of pure In_2O_3 and ITO nanopowder of different compositions namely (90: 10, 70: 30 and 50: 50 wt.%). It is clear that the particle was in spherical shape with size range from 10 nm to 70 nm.

X-ray diffraction for ITO nanopowder

Figure 2a and 2b, Shows XRD patterns of pure In_2O_3 and indium tin oxide (ITO) nanopowder of different composition namely (In: Sn = 90:10, 70:30 and 50:50 wt.%). It is clear that there is no any diffraction line for separate In_2O_3 or SnO_2. It is found that the samples were a mixture of cubic and rhombohedra In_2O_3 and SnO_2 with sharp diffraction peaks. The deconvoluted X-ray peaks of (222) and (104) corresponding to cubic and rhombohedra In_2O_3 respectively in confirmed with the result obtained by Kim *et al*. (1999).

Dielectric properties of ITO samples

Variation of dielectric constant $\varepsilon`$ and dielectric loss $\varepsilon``$ of ITO with frequency and temperatures

Figure 3, shows variation of dielectric constant $\varepsilon`$ with frequency at different temperatures for ITO samples containing different Sn^{4+} ion concentrations. The measurement was carried out in the frequency range from 100 Hz to 5 MHz and in the temperature range from room temperature to 160^oC. From this figure, as the frequency increases the following can be noticed:

The dielectric constant ($\varepsilon`$) is the frequency dependent within the range used. It is clear that it decreases with the increase of frequency at lower frequency range. This decrease can be attributed to the dielectric dispersion originated from the lag of the molecules behind the alternations of the applied electric field. At the higher

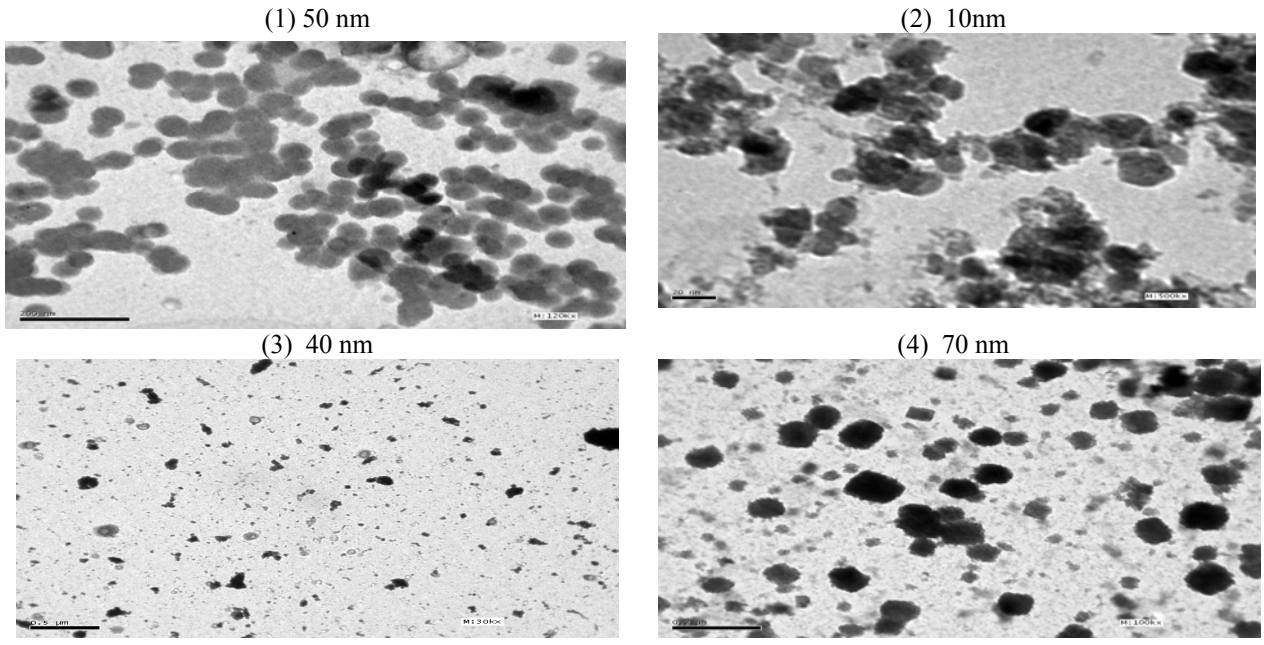

Fig. 1. TEM image of structure ITO particles: (1) Pure In_2O_3, (2) (In: Sn = 90:10), (3) (In: Sn = 70:30) and (4) (In: Sn = 50:50).

frequency range almost at 1 KHz, the dielectric constant becomes frequency independent. This phenomenon can be attributed to the decrease of the apparent carrier mobility. When the ceramic was heated in air, oxygen diffuses into the specimen and this is followed by the formation of a non-conducting oxide layer at the inter-granular spacing. On the oxide layer, space charges easily accumulate to form a high resistance barrier layer for the conduction electrons (Richerson, 1992).

On the other hand, from the measured dielectric loss (ε``) shown in figure 4, increasing frequency is accompanied by a decrease in the dielectric loss with formation of a peak that shifts to higher frequency as the temperature increased. Generally, the values of the dielectric losses varied from 0.9 to 0.1. It can be noticed that, there are

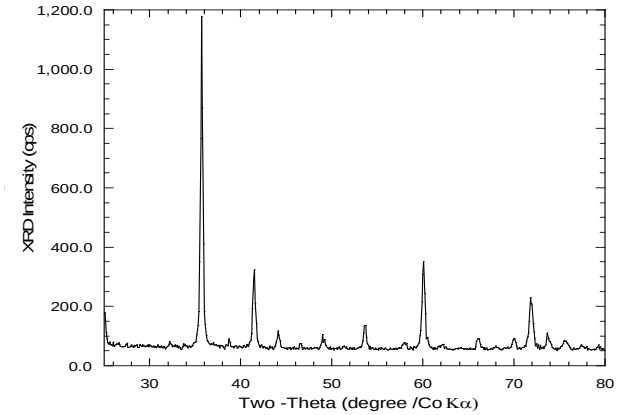

Fig. 2a. X-ray Diffraction pattern for pure In_2O_3.

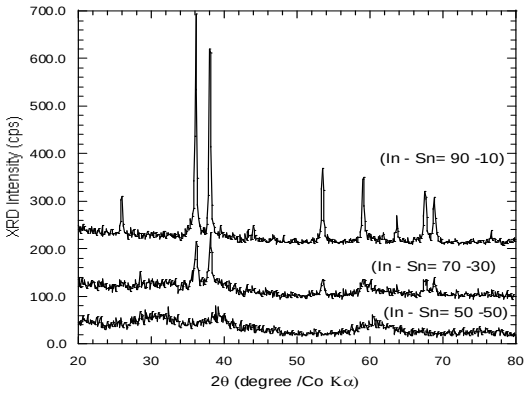

Fig. 2b. X-ray Different Patterns of the samples of different In: Sn ratio heated at 300 ̊C.

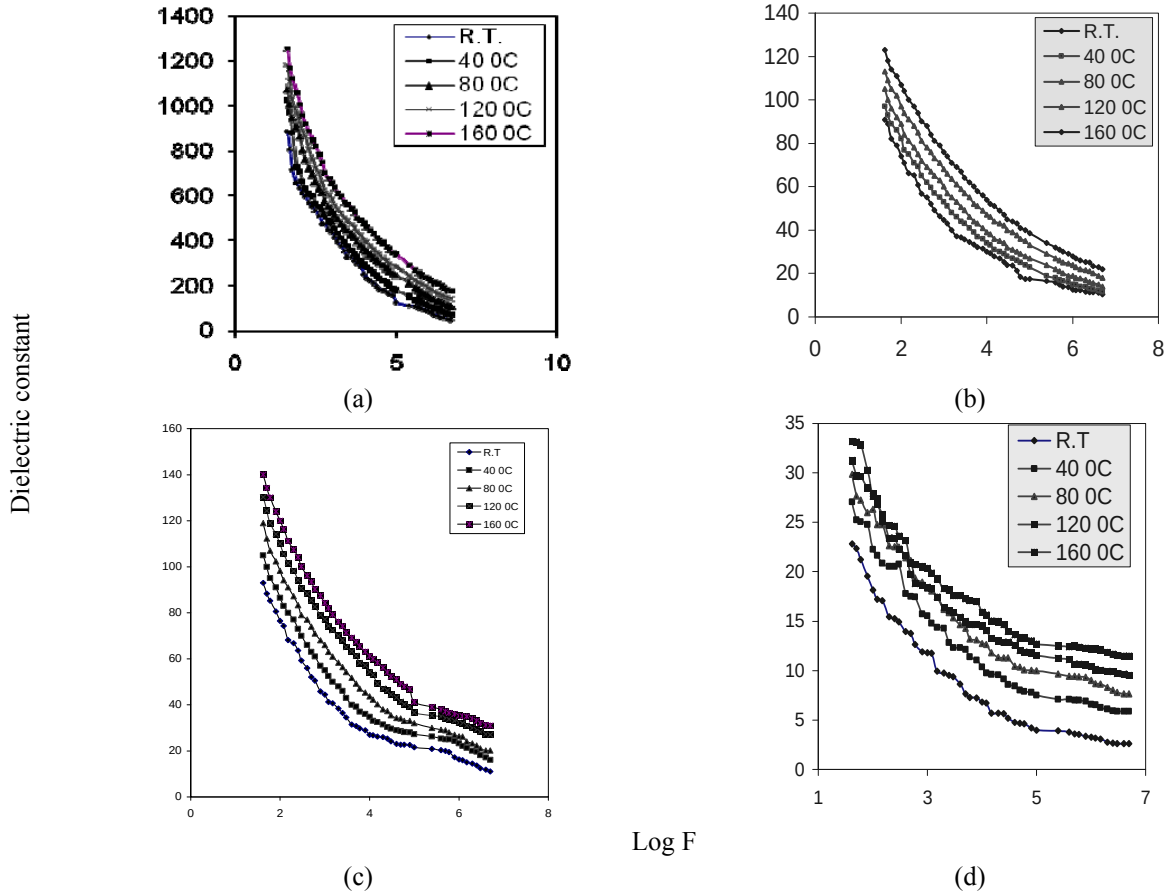

Fig. 3. The frequency dependent of dielectric constant □`a) Pure In_2O_3, (b) (In: Sn = 90:10) , (c) (In: Sn = 70:30) and (d) (In: Sn = 50:50).

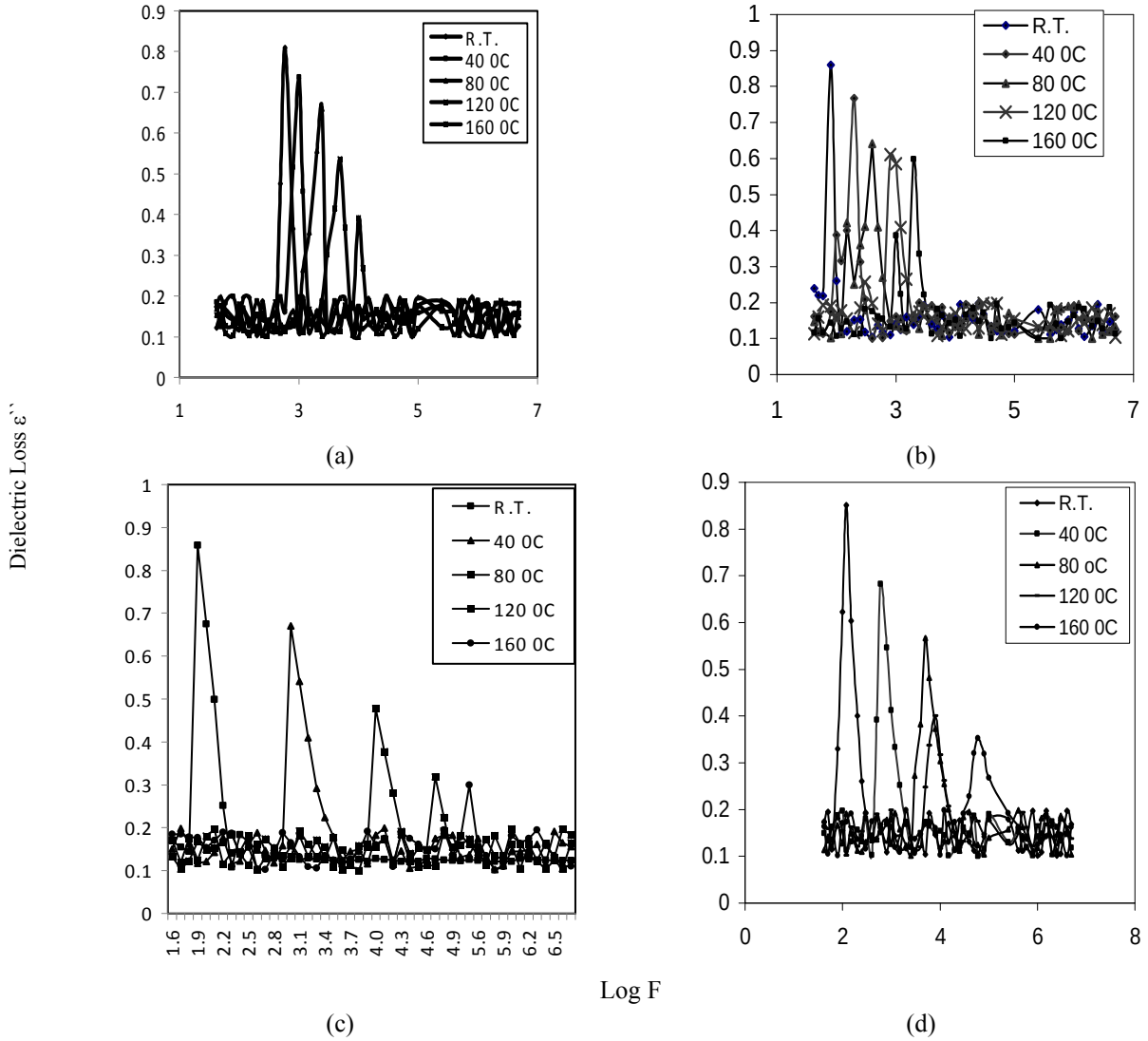

Fig. 4. The frequency dependent of dielectric loss e`` for (a) pure In_2O_3, (b) (In: Sn = 90:10), (c) (In: Sn = 70:30) and (d) (In: Sn = 50:50).

different types of electric energy losses in the presence of alternating electric field. The d.c loss is due to the transitional motion of free charges and it's trapping in holes. The Debye type loss is due to orientation polarization of polar groups, which are able to orient or to polarize in the electric field. The two types of losses are always present, but sometimes one of them is predominant (El-Anwar and El-Sayed, 1997). The loss absorption bands recorded in curves of ε`` vs. log F, show shift towards a higher temperature as the frequency is increased. This shift can be attributed to the increased mobility of free electrons with temperature. The position of F_m, the maxima of the loss absorption bands, for the prepared samples is listed in table 1. The apparent relaxation times for these samples are calculated from the equ.

$$\tau = 1/ 2\pi F_m$$

Where, τ is the apparent relaxation time and F_m is the critical frequency corresponding to maximum energy loss $\varepsilon``_m$. the values obtained are listed in table 1. The activation enthalpy ΔH and the entropy change ΔS of the dielectric relaxation are calculated from the usual rate equation. The calculated values of ΔH and ΔS are also listed in table 1.

The observed low values of activation enthalpy ΔH of the ITO samples with different Sn^{4+} ratio compared to pure In_2O_3, may be attributed to lower orientation polarization as a result of solid nature of the ceramics, which acquires semi-crystalline nature, polarization is partially occur in the molecule through electrons and some ions, that need low activation energy. Otherwise, the entropy change is negative indicating that the rate determining factor is the displacement of the dipoles, which possess a particular

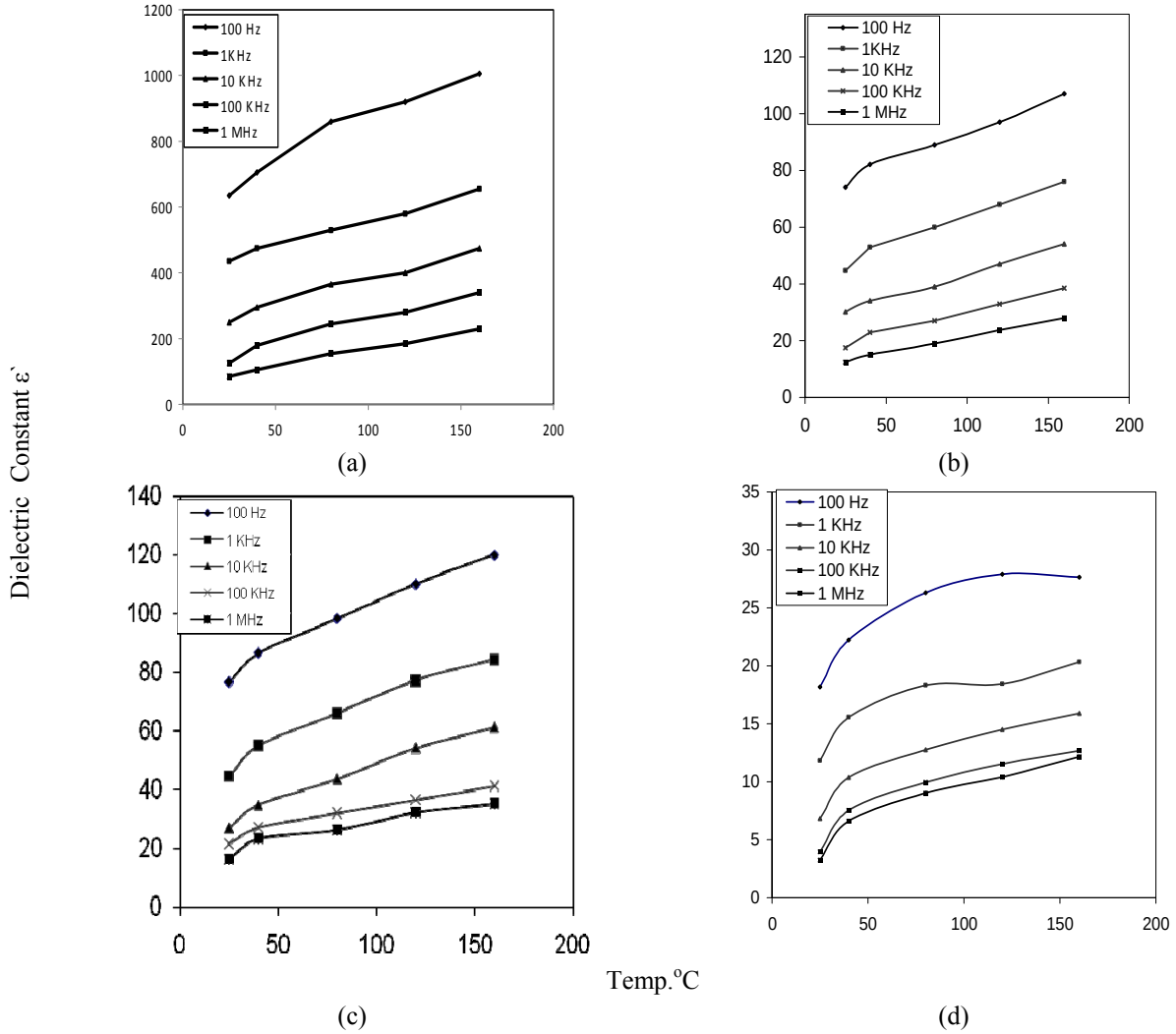

Fig. 5. The variation of dielectric constant as a function of temperature for (a) pure In_2O_3, (b) (In: Sn = 90:10), (c) (In: Sn = 70:30) and (d) (In: Sn = 50:50).

vibration configuration. The negative value of entropy change indicates presence of oscillation polarization and least orientation, i.e., activated molecules is in a state of low order. The relatively stable entropy change values are also indicating that the main chain and the polarization are stables. Accordingly changes that may occur are very low which make these materials good candidates to be used as substrate because of its independent on their constituents.

Figure 6, shows the variation of dielectric constant ε` as a function of $Sn^{4+}$ ion concentration as a doping for $In_2O_3$. The dielectric constant ε` of pure In_2O_3 oxide is very high ranged from 1200 to 100 where as dielectric constant ε` recorded for the ITO samples with different ratio of is very low ranged from 123 to 10.4 for ITO (90:10), from 96 to 10.3 for ITO (70:30) and finally from 33.175 to 2.625 for ITO (50:50). It is clear that as the ratio of Sn^{4+} ion increased the dielectric constant decreased. This behavior may be referred to the fact that, Sn^{4+} with its small ionic radius (0.62 Å) replace In^{3+} ion wits high ionic radius (0.92 Å), leading to shrinkage of the unit cell of the crystal structure. In addition, the very low values of dielectric constant recorded for 50:50 samples may be referred to the amorphicity of this sample and the very grain size of it. The temperature has a strong effect on the crystal structure and polarization characteristics of ITO. Figure 5, shows variation of dielectric constant ε` of ITO samples with different concentrations of $Sn^{4+}$ ion with temperature at different frequencies (100Hz, 1 KHz, 10 KHz, 100 KHz and 1 MHz). The initial increase of ε` can be attributed to the expected decrease in density, which decreases the effect of the environment. Consequently, atomic/ionic polarization tends to increase with temperature.

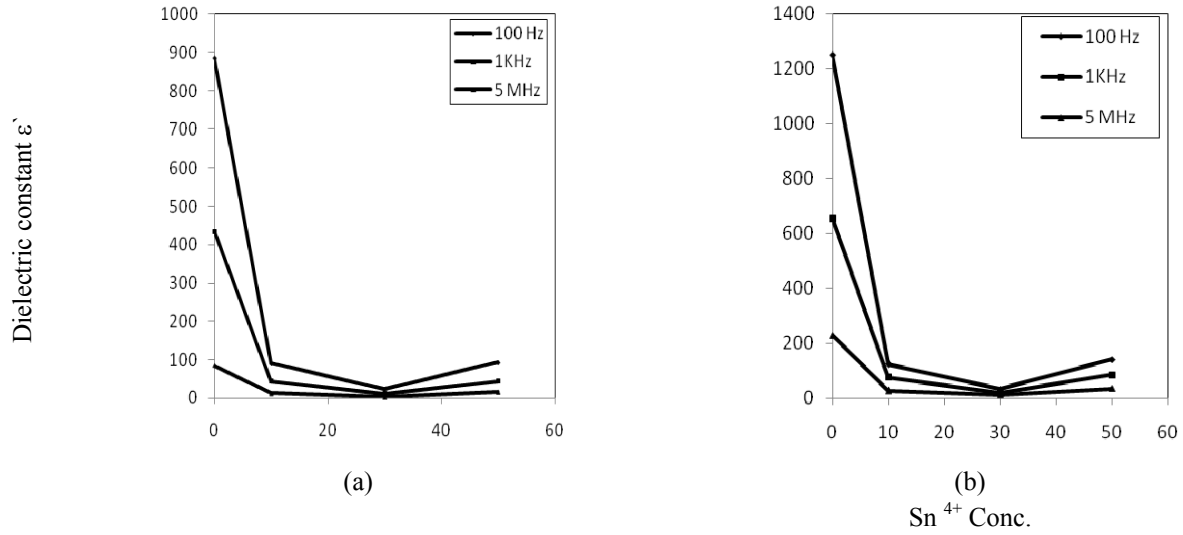

Fig. 6. The variation of dielectric constant ε` with different concentration of Sn $^{+4}$ at (a) room temperature and (b) 160^{o}C .

Table 1. The apparent relaxation time τ (Sec.), the activation enthalpy ΔH and entropy change ΔS for ITO samples with different Sn^{+4} ratio.

Sample	τ(Sec.)					ΔH	ΔS
	R.T	40 ^{0}C	80 ^{0}C	120 ^{0}C	160 ^{0}C	KJ/mole	J/deg/mole
Pure In_2O_3	$2.65x10^{-4}$	$1.59x10^{-4}$	$6.36x10^{-5}$	$3.18x10^{-5}$	$1.59x10^{-5}$	$5.011x10^{3}$	$2.88x10^{-2}$
ITO (90:10)	$1.99x10^{-3}$	$7.96x10^{-4}$	$3.98x10^{-4}$	$1.99x10^{-4}$	$7.96x10^{-5}$	$3.80x10^{-3}$	$-2.817x10^{-2}$
ITO (70:30)	$1.99x10^{-3}$	$1.59x10^{-4}$	$1.59x10^{-5}$	$3.18x10^{-6}$	$6.37x10^{-7}$	$1.48x10^{-3}$	$1.46x10^{-4}$
ITO (50:50)	$1.32x10^{-3}$	$2.65x10^{-4}$	$3.19x10^{-5}$	$1.99x10^{-5}$	$2.65x10^{-6}$	$1.94x10^{-3}$	$4.89x10^{-2}$

Table 2. The data of ac- conductivity for pure In_2O_3 and ITO with different ratio at room temperature and 160^{0}C.

Sample	100 Hz		1KHz		1 MHz	
	Log σ_{ac} (ohm^{-1}cm^{-1})		Log σ_{ac} (ohm^{-1}cm^{-1})		Log σ_{ac} □ (ohm^{-1}cm^{-1})	
	R.T	160 ^{0}C	R.T	160 ^{0}C	R.T	160 ^{0}C
Pure In_2O_3	-9.187	-8.999	-8.214	-7.958	-5.121	-5.040
ITO (90:10)	-9.839	-10.226	-9.103	-8.668	-6.014	-6.037
ITO (70:30)	-8.426	-8.067	-8.059	-7.037	-5.172	-3.995
ITO (50:50)	-7.460	-8.022	-7.002	-7.045	-4.251	-4.162

Moreover, it can be assumed that, the dependence of dielectric constant on the ratio of the Sn^{4+} and consequently on the grain size of the prepared samples figure 6, corresponds to the transfer of water molecules from the surface adsorbed state to the volume adsorbed state under condition of ultra – small pore volume of the nano-sized ITO samples. As ultra-fine volume applies restrictions on evaporation and diffusion.

Variation of ac-conductivity of ITO with frequency

To obtain conductivity (σ_{ac}) due to the dielectric loss ε`` taking 0.9 x 10^{12} as the ratio of the farad to the electrostatic unit of capacitance and of the mho to the electrostatic unit of conductance, and using the expression for the capacitance C_0 in farads of the empty condenser.

$$C_o \frac{A}{4\pi d \times 0.9 \times 10^{12}}$$

The following equation is used,

$$\sigma = \frac{\varepsilon'' \omega}{4\pi d \times 0.9 \times 10^{12}} = \frac{\varepsilon'' F}{1.8 \times 10^{12}} \text{ohm}^{-1}\ \text{cm}^{-1}$$

The dielectric conductivity sums over all dissipation effects and may represent as well as an actual conductivity caused by migrating charge carriers as refer to an energy loss associated with a frequency dependence (dispersion of ε`) for example to the friction accompanying the orientation of the dipoles. The values of ac-conductivity are listed in table 2.

As the measurement was carried out in air, oxygen is absorbed from the environment and since the temperature was raised from room temperature to 160^0C, H_2O molecules were desorbed from the crystal structure. Because of the large value of the specific surface area, we assumed that adsorption from the gas phase has a significant influence on the conductivity.

It is known that, H_2O molecules possess electron – donor properties under adsorption:

$$H_2O + S = H2O_{(ads)} + e^-$$

Adsorbed oxygen possess electron acceptor properties

$$½\ O2_{(g)} + V^{**}_o + 2e = O^*_o$$

We can explain the temperature dependence of the conductivity in the following way, changes in conductivity are related to the desorption and adsorption of water and oxygen molecules. Under heating, electron – donor H_2O molecules desorbed and the concentration of charge carriers decreased. In addition, the electron acceptor oxygen molecules occupying the adsorption sites of desorbed H_2O molecules. Molecular oxygen desorbs under heating more than H_2O molecules, Since ITO is oxygen deficit compound and oxygen molecules can become embedded in the crystal lattice.

CONCLUSION

The crystal structures of the samples were found to be a mixture of cubic and rhombohedra structures as determined from the XRD- analysis. The dielectric constant ε` of pure In_2O_3 is high compared with the samples containing different Tin ion concentrations which can be attributed to the change of crystal structure from cubic to a mixture of cubic and rhombohedra. The dielectric loss ε`` was found to be frequency dependent and ranged from 0.9 to 0.1. The ac-conductivity of the dielectric loss was calculated and found to be ranged from Log σ_{ac} = -9.839 (ohm^{-1} cm^{-1}) at room temperature to Log σ_{ac} = -4.162 (ohm^{-1} cm^{-1}) at 160 ^{0}C. The activation enthalpy and the entropy change of the prepared samples were calculated, it is found that the changes in the values are very low which make these materials good candidate to be used as substrate because of its independent on their constituents.

REFERENCES

Cho, Y-S., Gi-Ra Yi, Hong, JJ., Jang, SH. and Yang, SM. 2006. Colloidal Indium Tin Oxide nanoparticles for transparent and conductive films. Thin Solid Films. 515(4):1864- 1871.

El–Anwar, IM. and El-Sayed, AM. 1997. Some Electrical and Dielectric Properties of Titanium Substituted Li -Zn Ferrites. Egypt. J. Chem. 40 (4): 305-315.

Ellmer, K. and Mientus, R. 2008. Carrier transport in polycrystalline transparent conductive oxide: A comparative study of Zinc oxide and indium oxide. Thin solid films. 516 (14):4620-4627.

Jagadish, C., Ray, C., Saha, R. and Pramanik. 2003. Chemical Synethesis of Nanocrystalline Tin doped Cubic ZrO_2 Powders. Mater. Letts. 57(13-14): 2140-2144.

Kim, SS., Choi, SY., Park, CG. and Jin, HW. 1999. Transparent conductive ITO thin films through the sol – gel process using metal salts. Thin Solid Films. 347:155-160.

Korotcenkov, G., Nazarov, M., Zamoryanskaya, MV. and Ivanov, M. 2007. Cathod-luminescence emission study of nanocrystalline indium oxide films deposited by spray pyrolysis. Thin Solid Films. 515(20-21):8065-8071.

Lee, JS. and Choi, SC. 2005. Solvent effect on synthesis of indium tin oxide nanopowders by a solvothermal process. Journal of the European Ceramic Society. 25(14):3307-3314.

Malar, P., Mohanty, BC. and Kasiviswanathan, S. 2005. Growth and Rutherford backscattering spectrometry study of direct current sputtered indium oxide films. Thin Solid Films. 488 (1-2):26-33.

Pujilaksono, B., Klement, U., Nyborg, L., Jelvestam, U., Hill, S. and Burgard, D. 2005. X-ray Photoelectron Spectroscopy Studies of Indium Tin Oxide Nanocrystalline Powder. Materials Characterization. 54:1-7.

Rey, JFQ., Plivelic, TS., Rocha, RA., Tadokoro, RA., Torriani, I. and Muccillo, ENS. 2005. Synthesis of In_2O_3 Nanoparticles by Thermal Decomposition of a Citrate Gel Precursor. Journal of Nanoparticle Research. 7(2-3):203.

Richerson, DW. 1992. Modern Ceramic Engineering, Properties, Processing and Use in Design, Marcel Dekker, Inc. New York, Bassal, Hong Kong.

Sung, XW., Huang, HC. and Kwok, HS. 1996. On the initial growth of Indium Tin Oxide on Glass. Appl. Phys. Lett. 68:2663-2665.

Yang, H., Han, S., Wang, L., Kim, IlJ. and Son, YM. 1998. Preparation and Characterization of Indium-doped

tin dioxide Nanocrystalline powders. Materials Chemistry and Physics. 56:153.

Zhan, Z., Song, W. and Jiang, D. 2004. Preparation and property control of nanosized indium tin oxide particle. Journal of Colloid and Interface Science. 271, 366.

Zhu, H., Wang, N., Wang, L., Yao, K. and Shen, X. 2005. In Situ X-ray Diffraction Study of the Phase Transition of Nanocrystalline $In(OH)_3$ to In_2O_3. Inorganic Materials. 41 (6):609-612.

Received: Jan 23, 2009 Revised: May 16, 2009 Accepted: June 9, 2009

SENRA Academic Publishers, Burnaby, British Columbia
Vol. 3, No. 3, pp. 911-915, 2009
ISSN: 1715-9997

Canadian Journal of pure&applied sciences

THE MICROWAVE-ASSISTED SOLVENT EXTRACTION OF PROPRANOLOL FROM TABLETS

*JR Williams, F Al-Nabhani and A Al-Hamdi
Department of Chemistry, College of Science, Sultan Qaboos University
PO Box 36, Al-Khod 123, Sultanate of Oman

ABSTRACT

A rapid alternative technique for the extraction of propranolol from tablets is reported. Traditionally, propranolol has been extracted using sonication, but this has proved to be significantly solvent consuming. In this study, propranolol has been extracted successfully from tablets using an optimised microwave-assisted solvent extraction (MASE) method. The optimum conditions for MASE for this application were: extraction solvent, methanol; extraction time, 45 s (5 s heat and 40 s cool); and extraction solvent volume, 5.00 mL. The recovery of propranolol from tablets by the optimised MASE method was 89.8% with a RSD of 3.7%. This performance was acceptable and comparable with sonication. The determination and identification of the extracts was performed using high-performance liquid chromatography with ultraviolet detection at 290nm. A domestic microwave oven was used for the study, because an industrial MASE apparatus was uncompetitive with sonication with respect to extraction time due to the amount of time required to cool the sample following microwave heating. Safety considerations for domestic microwave ovens are discussed, including the use of a novel two-vial sample cell.

Keywords: High-performance liquid chromatography, microwave-assisted solvent extraction, propranolol, sonication, tablets.

INTRODUCTION

One use of microwaves presently being studied is as a rapid heat source for the solvent extraction of soluble organic substances from insoluble matrices. The sample and solvent are contained together in a closed, non-metallic extraction vessel housed inside the microwave oven. Polar solvent molecules become excited by the microwave radiation and rotate faster, generating heat (Chang, 1998). Consequently, the solvent warms up much more quickly than in conventional heating. Furthermore, a higher temperature liquid has more solvating power, so accelerating the desorption of solute molecules from the sample surface, and lower viscosity, so improving solvent penetration into matrix pores. The resultant higher pressure also facilitates solvent penetration, and keeps the solvent safely below its boiling point. Consequently, less solvent may be required to extract the same amount of material and extraction can be faster. Solute recovery can also be improved compared to conventional solvent extraction.

Conventional solvent extraction methods can have major disadvantages, such as the use of significant amounts of toxic and corrosive organic solvents. Many organic solvents are expensive to buy and dispose of, as well as posing an environmental health hazard. Consequently, microwave-assisted solvent extraction (MASE) is proposed as an alternative with the potential advantage of the reduced use of hazardous solvents. For such exploitation in chemical analysis, the extraction should ideally be quantitative, reproducible, efficient, and compare favourably with existing extraction methods.

Medicinal drugs in tablets are routinely extracted as part of quality control programmes in the pharmaceutical industry. Pharmaceutical companies prepare tablets dosed with drug at a known concentration. Dosed drugs are then extracted to confirm the level of inclusion. In this regulated environment, a recovery of greater than 90% and a relative standard deviation (RSD) of less than 5% is required.

Microwave-assisted solvent extraction has already seen some use for pharmaceutical applications. As an illustration, Labbozzetta *et al.* (2005) extracted naproxen from suppositories and found advantages over conventional methods. Woźniakiewicz *et al.* (2008) extracted tricyclic antidepressants from human serum quantitatively and reproducibly. There have only been a few reports in the chemical literature of the MASE of drugs from tablets. Eskilsson *et al.* (1999) reported the MASE of felodipine and its degradation product from tablets. Average recoveries were just below 100% and competitive with a validated ultrasonication method. Interestingly, the MASE method could be used successfully without the need for reducing the tablet to a powder. This was achieved by using a 5% methanol in

*Corresponding author email: jrwtranmere@yahoo.co.uk

acetonitrile extraction solvent. Methanol dissolved the outer covering layer and acetonitrile made the inner matrix swell, fragmenting the tablet into small pieces, and releasing the analytes. Eight years later, Hoang *et al.* (2007) applied MASE to the extraction of active pharmaceutical ingredients from solid dosage forms including tablets. They found that MASE gave results comparable with validated mechanical extraction procedures. In the same year, Lee *et al.* (2007) compared MASE, accelerated solvent extraction, and Caliper Life Sciences Tablet Processing Workstation II with a conventional manual extraction method for the extraction of a compound from spray dried dispersion tablet formulations. They found that all three modern extraction methods were faster than the traditional method. More specifically, MASE was slower than the Tablet Processing Workstation II, but gave a higher recovery than accelerated solvent extraction. A year later, Nickerson *et al.* (2008) also found that these same three modern extraction methods gave significantly reduced sample preparation times compared to the standard method for the extraction of active pharmaceutical ingredients from controlled release tablet formulations.

This study describes a MASE method to recover the well-known beta-blocker propranolol (as the hydrochloride) from tablets quantitatively and reproducibly. Propranolol is used to treat hypertension (Windholz, 1976). Sonication, the existing extraction method, uses significant amounts of methanol, a toxic organic solvent. It is anticipated that MASE may consume less solvent and complete the extraction faster. Quantitation was by high-performance liquid chromatography (HPLC) with ultraviolet detection at 290nm**.**

MATERIALS AND METHODS

Instrumentation, reagents and standards

The industrial microwave apparatus was purchased from Milestone, Sorisole, Italy. The domestic microwave oven was manufactured by Bosch, England, UK. An ultrasonic bath was obtained from JAC, Kodo, Japan. The HPLC instrument was procured from Dionex, Germering, Germany. The propranolol hydrochloride tablets (40 mg per 200 mg tablet) were produced by AstraZeneca, Macclesfield, UK and obtained from Sultan Qaboos University Hospital Pharmacy. Pure propranolol hydrochloride (99%), methanol (HPLC grade), and ethanol (HPLC grade) were obtained from Sigma Aldrich, Steinheim, Germany. The ammonium formate (99.995%+) was procured from Sigma Aldrich, St. Louis, MO and trifluoroacetic acid (TFA) (99.9%) was purchased from Panreac, Barcelona, Spain. The deionised water used in some of the extraction solvents and HPLC mobile phase was produced in-house by passing tap water through a TKA DI 800 mixed-bed water demineraliser (Niederelbert, Germany).

Sample preparation

Twenty pink tablets of propranolol hydrochloride were weighed and ground using a pestle and mortar to give a pinkish powder. The powdered tablets were cone and quartered until an appropriate amount was left for use as a sub-sample.

Microwave-assisted solvent extraction with an industrial microwave apparatus

About 100mg of sample were weighed accurately (±0.1mg) into a Teflon extraction vessel, followed by 15.00mL of methanol and a magnetic stir bar. A reference vessel, used for temperature control, was also assembled. The vessels were put inside the microwave irradiation chamber. The power was set to 1000W and the heating cycle was 5 min at 80^{o}C and 1 bar. Once the extraction programme was completed, high temperature and pressure were reached inside the vessels, so it was necessary to cool them down for 30 min before opening them. Once the vessels had cooled to room temperature, the extract was filtered through Whatman paper #1 and diluted to 25.00mL with methanol. Then, 5.00mL of that solution was diluted to 10.00mL with methanol ready for analysis by HPLC. The extractions were performed in triplicate.

Microwave-assisted solvent extraction with a domestic microwave oven

Sample (33.3mg) was weighed directly and accurately (±0.1mg) into a tared 9.50mL hinged-lid vial (EP290 Polyvial®, LA Packaging, Yorba Linda, CA). Using a micropipette, 2.50, 3.75, or 5.00mL of extraction solvent were added to the sample. The lid was snapped shut and the vial shaken and placed inside a 50mL polypropylene centrifuge tube from Bibby Sterilin, Stone, UK. The cap was screwed on to the centrifuge tube. The two-vial system was then put inside the microwave oven and heated at 600W for 5 s. Then, it was removed from the oven, the screw cap of the outer tube removed, the tube inverted and the smaller, inner vial removed and placed upright in an ice-salt bath for 40 s. For a 90 s extraction time, this heating and cooling procedure was repeated once more. The resulting extract was filtered by pouring into a 5mL plastic syringe (Terumo, Leuven, Belgium) attached to a 13 mm diameter, 0.2-µm pore size filter unit (Schleicher and Schuell, Dassel, Germany) with a small glass sample tube underneath. The plunger of the syringe was pressed down. The filtered extracts were then ready for analysis by HPLC. The extractions were performed in triplicate.

Safety considerations for the domestic microwave oven

The industrial microwave apparatus has built-in safety features, such as sensors for monitoring temperature and pressure, and for the detection of solvent leaks. The domestic microwave oven, however, does not.

Consequently, a careful and considered approach needs to be adopted when using the latter apparatus for extraction purposes with flammable organic solvents.

One safety measure used in this study was to place a 9.50mL vial containing the tablet sample and extraction solvent inside a 50-mL tube. This step exploits Boyle's law (Zumdahl and Zumdahl, 2007). If the pressure inside the smaller, inner vial becomes dangerously high during microwave heating, the hinged lid pops open. The larger volume of the screw-capped outer tube causes a decrease in the pressure, allowing the analyst time to switch off the oven before the pressure rises again to dangerous levels. This two-vessel arrangement also prevents vapours of flammable organic solvents entering the heating chamber.

Another precaution taken in this study was the use of a weighted clear plastic safety shield in front of the oven during the extractions. The shield was obtained from Aldrich, Steinheim, Germany.

Sonication

The sonication extraction method was that used by Shinde *et al.* (1993). About 200 mg of the powdered propranolol tablets were weighed accurately (±0.1mg) and transferred to a 50.00 mL volumetric flask. Then, 30.00 mL of methanol was added and the flask kept in an ultrasonic water bath at 22ºC for 5 min and finally diluted to the mark with methanol. The solution was filtered through Whatman paper #1 ready for analysis by HPLC. The extractions were performed in triplicate.

High-performance liquid chromatography

Quantitation was by isocratic HPLC using a method developed by Law and Appleby, (1996). A 15cm × 4.6mm i.d. strong cation-exchange column (Hichrom, Reading, UK) was employed to separate the components in the extracts. The mobile phase was 0.02 *M* ammonium formate in methanol-water (80:20, v/v). The pH of the mobile phase was adjusted to 2.45 by the addition of TFA. The mobile phase was pumped at a flow rate of 1 mL/min by a Dionex P580 pump. In order to facilitate the introduction of sample solutions into the HPLC system, a Rheodyne 8125 injection valve (Cotati, CA) fitted with a 20µL loop was needed. The loop was flushed with 100µL of sample solution immediately prior to injection. A Dionex UVD170S ultraviolet detector was used to quantify and confirm the presence of propranolol in the extracts and was set at 290nm. A DTK Pentium III computer loaded with the Dionex Chromeleon Chromatography Information Management System Software was used to observe the detector response and provide quantitative data. The peak for propranolol appeared at about 8.3 min.

RESULTS AND DISCUSSION

An industrial MASE apparatus was considered first for the extraction of propranolol from tablets. The initial experiment gave the following promising result: 84.0 ± 3.6% (n = 3). Its use was, however, curtailed because of the long cooling stage required (30 min) that made the process uncompetitive with sonication with respect to extraction time. Consequently, attention was switched to a domestic microwave oven, and the subsequent reduction in scale, where cooling time was much faster (40 s).

In this study with the domestic microwave oven, three different variables were optimised: extraction solvent, extraction solvent volume, and extraction time.

Optimisation of extraction solvent

Four different extraction solvents were used: methanol, ethanol, ethanol-aqueous 1 *M* TFA (96.2:3.8, v/v), and 0.02 *M* ammonium formate in ethanol-water (80:20, v/v). This final extraction solvent was adjusted to pH 2.45 by the addition of TFA. Ethanol and ethanol-based extraction solvents were tried as less hazardous alternatives to methanol and methanol-based ones. Methanol-aqueous 1 *M* TFA (96.2:3.8, v/v) has been used to extract propranolol successfully from rodent food (Williams *et al.*, 1996). A solution of 0.02 *M* ammonium formate in methanol-water (80:20, v/v) at pH 2.45 is a successful HPLC mobile phase for the separation of propranolol (Law and Appleby, 1996).

The average recoveries of propranolol from tablets were very close to 90% for each of the four extraction solvents (Table 1). Analysis of variance (Morgan, 1991) showed that there was no significant difference at the 5% probability level between recoveries of propranolol using the four different extraction solvents. Methanol was chosen as the optimum extraction solvent of the four, because it gave the best precision (lowest RSD). In addition, it was the cheapest of the four extraction solvents. Furthermore, it did not require any time-consuming preparation, unlike ethanol-aqueous 1 *M* TFA (96.2:3.8, v/v) and 0.02 *M* ammonium formate in ethanol-water (80:20, v/v).

Table 1. Recoveries by MASE of propranolol from tablets using different extraction solvents. Solvent volume, 5.00 mL; extraction time, 90 s; number of replicates, 3.

Extraction solvent	Recovery ± RSD (%)
Methanol	88.5 ± 1.2
Ethanol	89.3 ± 5.6
Ethanol-aqueous 1 *M* TFA (96.2:3.8, v/v)	87.9 ± 7.1
0.02 *M* ammonium formate in ethanol-water (80:20, v/v) at pH 2.45	89.3 ± 4.8

Optimisation of extraction solvent volume

Three volumes of methanol were studied: 2.50mL, 3.75mL, and 5.00mL. It was found that 5.00mL gave the highest average recovery of the three volumes tried (Table 2). Furthermore, average recovery increased steadily with increasing extraction solvent volume. This inferred that the highest volume of the solvent gave the greatest solubility of the drug. Volumes of extraction solvent greater than 5.00mL may have given higher recoveries, but solvent volume was limited to 5.00mL by the equipment used. Larger volumes of solvent increased the frequency of the inner vial popping open.

Table 2. Recoveries by MASE of propranolol from tablets using different volumes of extraction solvent. Solvent, methanol; extraction time, 90 s; number of replicates, 3.

Extraction solvent volume (mL)	Recovery ± RSD (%)
2.50	74.8 ± 1.6
3.75	78.9 ± 2.7
5.00	82.7 ± 1.8

Optimisation of extraction time

The last variable to be investigated was extraction time. Two times were tried: 45 and 90 s. It was found that the average recovery of propranolol was greater when extracting for 45 s (91.3 ± 3.6%) than for 90 s (88.7 ± 3.6%). The *t*-test (Morgan, 1991) at $P = 0.05$ showed that there was no significant difference between the recovery of propranolol at the two different times. In both cases, recoveries were about 90% and the RSDs were an acceptable 3.6%. Consequently, 45 s was chosen as the optimum extraction time.

In summary, the optimum extraction conditions for MASE were extraction solvent, methanol; solvent volume, 5.00mL; and extraction time, 45 s.

There was some variation of recovery by MASE from experiment to experiment given the same extraction conditions. As an illustration, the following recoveries and RSDs were obtained when methanol was the extraction solvent, extraction time was 90 s, and extraction solvent volume was 5.00mL: 88.5 ± 1.2% (Table 1), 82.7 ± 1.8% (Table 2), and 88.7 ± 3.6% (Optimisation of extraction time). The 82.7% result is significantly lower than the 88.5 and 88.7% recoveries at the 5% probability level. This was presumably because an external standard was used during the study. The use of an internal standard, such as atenolol, may have given better reproducibility from experiment to experiment.

Comparison of MASE with sonication

The optimised MASE method was compared with the literature technique, sonication, for the extraction of propranolol from tablets. It was found that sonication gave significantly higher recovery of the drug from the tablets at the 5% probability level and better precision (as measured by RSD), but recovery by MASE and its associated precision were acceptable (Table 3). Furthermore, MASE gave a faster extraction and used less extraction solvent and sample.

Table 3. Comparison of MASE with sonication for the extraction of propranolol from tablets. Number of replicates, 3.

Variable	MASE	Sonication
Recovery (%)	89.8	99.5
RSD (%)	3.7	0.5
Solvent volume (mL)	5.00	30.0
Extraction time (s)	45	300
Sample size (mg)	33.3	200.0

CONCLUSIONS

It can be concluded that MASE is a viable alternative to the conventional extraction method for the recovery of propranolol from tablets. It has been shown that MASE recovery and precision data were acceptable. In addition, MASE was significantly faster and used less solvent than sonication. Propranolol recovery by MASE was significantly lower than by sonication. To improve recovery by MASE, it is suggested for the future that the volume of extraction solvent be increased. To overcome the problem of vial popping when using larger volumes of solvent with the present sample cell arrangement, larger volume inner vials can be purchased. Another suggestion is to increase microwave power from the present 600 W to, for example, 1000 W. The use of greater power should heat the extraction solvent faster, producing a higher temperature solvent in the sample vial for the same extraction time. Since solubility is usually greater at higher temperature, one might reasonably expect greater recovery of propranolol from the tablet. In addition to use as a sample pre-treatment step in pharmaceutical industry quality control programmes, the MASE method described in this study could also be applied successfully to student laboratory classes. The use of a novel two-vial sample cell has allowed safe use of the domestic microwave oven. Furthermore, the domestic microwave oven has been demonstrated to be advantageous compared to an industrial extractor for applications where the extraction time is relatively short. A univariate approach was taken in this study. This cautious approach was adopted, because it was unknown in advance whether the results would be reproducible since sample size was modest and the experiments were performed on a small scale. It was found that recoveries were generally reproducible despite the small scale used. Armed with this knowledge, it can be proposed that a full- or fractional-factorial approach

could also be applied to the MASE of propranolol from tablets successfully. Chemometrics is not a panacea though. Poor reproducibility with an experimental design approach can lead to anomalous results and wrong conclusions being made.

ACKNOWLEDGEMENTS

The authors thank Sultan Qaboos University for funding this study.

REFERENCES

Chang, R. 1998. Chemistry. p. 382-383. McGraw-Hill, New York, N.Y.

Eskilsson, CS., Bjorklund, E., Mathiasson, L., Karlsson, L. and Torstensson, A. 1999. Microwave-assisted extraction of felodipine tablets. Journal of Chromatography A. 840:59-70.

Hoang, TH., Sharma, R., Susanto, D., Di Maso, M. and Kwong, E. 2007. Microwave-assisted extraction of active pharmaceutical ingredient from solid dosage forms. Journal of Chromatography A. 1156:149-153.

Labbozzetta, S., Valvo, L., Bertocchi, P. and Manna, L. 2005. Focused microwave-assisted extraction and LC determination of the active ingredient in naproxen-based suppositories. Journal of Pharmaceutical and Biomedical Analysis. 39:463-468.

Law, B. and Appleby, JRG. 1996. Re-evaluation of strong cation-exchange high-performance liquid chromatography for the analysis of basic drugs. Journal of Chromatography A. 725:335-341.

Lee, C., Gallo, J., Arikpo, W. and Bobin, V. 2007. Comparison of extraction techniques for spray dried dispersion tablet formulations. Journal of Pharmaceutical and Biomedical Analysis. 45:565-571.

Morgan, E. 1991. Chemometrics: Experimental Design. Wiley, Chichester, UK.

Nickerson, B., Arikpo, WB., Berry, MR., Bobin, VJ., Houck, TL., Mansour, HL. and Warzeka, J. 2008. Leveraging elevated temperature and particle size reduction to extract API from various tablet formulations. Journal of Pharmaceutical and Biomedical Analysis. 47:268-278.

Shinde, VM., Desai, BS. and Tendolkar, NM. 1993. Simultaneous determination of propranolol hydrochloride and hydrochlorothiazide in tablets by quantitative TLC. Indian Drugs. 31:192-196.

Williams, JR., Morgan, ED. and Law, B. 1996. Comparison of supercritical, subcritical, hot, pressurized and cold solvent extraction of four drugs from rodent food. Analytical Communications. 33:15-17.

Windholz, M. 1976. The Merck Index. Merck, New Jersey, USA. pp 1016.

Woźniakiewicz, M., Wietecha-Posłuszny, R., Garbacik, A. and Kościelniak, P. 2008. Microwave-assisted extraction of tricyclic antidepressants from human serum followed by high performance liquid chromatography determination. Journal of Chromatography A. 1190:52-56.

Zumdahl, SS. and Zumdahl, SA. 2007. Chemistry. Houghton Mifflin, New York, USA. 181-184.

Received: July 27, 2009; Revised: Aug 27, 2009; Accepted: Aug 29, 2009

SENRA Academic Publishers, Burnaby, British Columbia
Vol. 3, No. 3, pp. 917-924, 2009
ISSN: 1715-9997

Canadian Journal of pure&applied sciences

EFFECT OF GREEN TEA ON CYTOGENETIC CHANGES INDUCED BY GIBBERELLIN A_3 IN HUMAN LYMPHOCYTE CULTURE

*Saber A Sakr, Sobhy E Hassab-Elnabi and Dalia A El-Ghonaimy
Department of Zoology, Faculty of Science, Menoufia University, Shebin El-kom, Egypt

ABSTRACT

Gibberllin A_3 is a plant growth regulator hormone used to increase the growth and flowering of fruits and vegetables. In the present work, the cytogenetic effect of different concentrations of gibberellin A_3 (0.1, 0.5, 1 and 2 mg) was studied in human lymphocyte culture. Treating cultures with gibberellin A_3 induced chromosomal aberrations, sister chromatid exchanges and DNA damage. The chromosomal aberrations include gap, break, deletion and centromeric attenuation. DNA damage was detected by comet assay and by total genomic damage method using gel electrophoresis. By increasing the concentration of gibberellin A_3, the number of damage cells and the damage DNA spots increase. Moreover, the gel electrophoresis method showed that there was an increase of released DNA and RNA as the concentration of gibberellin A_3 increase. Green tea (*Camellia sinensis*) is one of the most popular bervages consumed. Green tea and its constituents were found to have a variety of therapeutic effects. The results obtained in the present investigation showed that when green tea and gibberellin A_3 were simultaneously applied in the culture media, the mutagenic changes induced by gibberellin A_3 were significantly reduced.

Keywords: Gibberellin A_3, cytogenesis, green tea, human lymphocytes.

INTRODUCTION

Gibberellic acids are a group of plant growth regulators that have been identified in different plants (Jones and MacMillan, 1984) and they are used in agriculture as plant regulators to stimulate both cell division and cell elongation that affect leaves as well as stems (Liu and Loy, 1976). Gibberellic acid or one of its metabolites if applied to dwarf varieties of peas, broad beans or maize, growth is greatly accelerated (Carpita *et al*., 1979). On the other hand, GA_3 was found to have carcinogenic effect in experimental animals. Feeding toads *Bufo regularis* with gibberellin A_3 induced hepatocellular carcinomas in 16% of the animals (El-Mofty and Sakr 1988). Moreover, El-Mofty *et al*. (1994) showed that gibberellin A_3 induced breast and lung adenocarcinomas in mice. Gibberellic acid was found to induce chromosomal aberrations in human lymphocytes (Arutiunian and Zalinian, 1987) and mice (Bakr *et al*., 1999).

Green tea (*Camellia sinensis*) is one of the most popular beverages consumed. A number of studies have shown that traditional beverages, as represented by teas, are beneficial to human health, suggesting that these beverages might warrant investigation from the viewpoint of nutrition. Green tea or its constituents were found to possess a variety of effects, including antimutation (Kada *et al*., 1985), antibiotic action (Toda *et al*., 1989), antihypercholesterolemia (Muramatsu *et al*., 1986), antihypertension (Hara and Tonooka, 1990), antihyperglycemia (Shimizu *et al*., 1988) and anti-inflammatory action (Sagesaka *et al*., 1996). Various systems were used to confirm anticancer activities of green tea. These included experimental animals in which cancer was induced chemically. Green tea was found to inhibit hepatocarcinogenesis induced in rats by diethylnitrosamine (Klaunig, 1992) and suppresses the growth of urinary bladder tumor in rats induced by N-butyl-N (4-hydroxybutyl) nitrosamine (Sato, 1999). Epidemiological studies revealed that the incidences of stomach cancers all over the world are the lowest among a population that consumes green tea on a regular basis (Fujiki *et al*., 1996). Gibberellic acid is used in Egypt to increase the size of some fruits and vegetables such as strawberries, grapes, tomatoes and cabbages. On the other hand, the exposure to such chemicals, increase the risk of many diseases including cancer in farmers and other agricultural uses. This stimulated us to study the side cytogenetic effect of gibberellic acid in human lymphocytes culture and an attempt to reduce its hazardous effects by green tea.

*Corresponding author email: Sabsak@yahoo.com

MATERIALS AND METHODS

Tested compounds

a. Gibberellic acid (GA_3) was dissolved in the tissue culture media and was applied at doses of 0.1, 0.5, 1 and 2mg/ 5ml culture medium.

b. Green tea aqueous extract was prepared according to Han (1997). It was applied at dose of 0.5mg/5ml culture medium.

Media

Human lymphocytes are easy to culture, and readily available. They do not divide and grow unless artificially

stimulated this is usually activated by adding phytohaemagglutinin (PHA) to the cultures and results in a high mitotic yield. These lymphocyte cultures were used according to the method adopted by **(**Moorhead *et al.*, 1960**)**. The culture medium consists of RPMI 1640 culture medium with L-glutamine (sigma) supplemented with 20% fetal calf serum; 1% peincillin (5000 IU/ml), streptomycin (5000mg/ml); and 0.005g% phytohaemagglutinine (PHA) (Biochrome).

Applied techniques

a. Chromosomal aberrations

One ml heparinized whole blood from healthy non-smoking donor was mixed with 5 ml culture medium and incubated at 37°C. Gibberellic acid and green tea was added at 72 hours of incubation. Colcimed (10mg/ml; Biochrome) was used to inhibit spindle formation at a final concentration of 0.2µg/ml. Two hours before harvesting and fixation, cells were arrested in metaphase by addition of colcimed. After 72 hrs, cells were centrifuged (1000rpm; 10 min) and the supernatants were discarded. The cell pellets were then resuspended in approximately 5 ml of prewarmed hypotonic solution (KCl) and incubated for 15 min. Tubes were then centrifuged at 1000 rpm for 10 min. The supernatant was removed and the pellets were thoroughly mixed with 5ml of cold fixative (1 part acetic acid to 3 parts methanol) added drop by drop; this step was repeated twice. The tubes were spanned at 900 rpm for 10 min. The cells pellets were resuspended in equal small volumes of fresh fixative to form a milky suspension. Slides were prepared by pipetting 4 drops of cells suspension on to clean, grease free slides and air dried. The slides were then stained with 10% Giemsa for 12 min; immersed in distilled water for washing; air dried for 3 days and mounted in DPX. For each treatment, at least 250 well spread metaphases were examined for chromosomal aberrations. For the mitotic index, minimum of 1000 cells per dose were counted.

b. Sister chromatid exchanges (SCEs)

In this experiment SCE's technique was used, which based on the fact that after two rounds of replication in the presence of Bromodeoxyuridine (BrdU), the chromosomes contain one chromatid in which the DNA is unifilarly substituted with BrdU and one chromatid in which the DNA is bifilarly substituted. These two chromatids are stained differently with Giemsa. For this purpose, cultures were used as previously described in the detection of chromosomal aberrations.

Staining technique of SCE's

Slides from BrdU-treated cultures were air-dried and kept in the dark. Three days old slides were stained using the fluorescence plus giemsa technique according to Pery and Wolff (1974). With this technique a light-dark contrast between sister chromatids can be presented giving the chromosomes a "harlequin-like" appearance (unifiliarly BrdU substituted chromatid: dark: bifilarly substituted chromatid: light).

Fluorescence-plus Giemsa Staining

A stock solution of Hoechst 33258 (bisbenzimide) was prepared at a concentration of 0.5mg/ml in sterile H_2O. This can be stored for up to 1 month in the dark at 4°C. The stock Hoechst solution was diluted 1:200 with distilled water immediately prior to use. The slides were immersed in diluted Hoechst for 10 min, washed one time with distilled water (Immersing). This was followed by exposure of the slides to UV rays (254 nm) at a distance of approximately 15 cm for 60 min, covered with 2 × SSC (sodium salt citrate) – solution (pH 7.0). After that the slides remained in a solution of 2 × SSC (pH 7.0) at 60°C for 90 min. The cells were stained with 10% Giemsa in phosphate buffer solution (pH 6.8) for 15 min, left to air dry and mounted in DPX.The SCE frequency was scored of 50 metaphases (2N = 46) in the second cycle of division (MII) per dose.

c. Total damage of DNA (double strand breaks)

Double strand breaks of DNA were detected according to Wlodek *et al*. (1991). Human lymphocytes were isolated according to Boyum (1968) from whole blood by ficoll separating solution (Sigma). The cells were washed in a medium of TGD of DNA. The isolated lymphocytes were incubated with the tested agents for 2 hr. The viability of the cells was determined by trypan blue. From the stock of lymphocytes, 0.5ml (1×10^6 lymphocytes) to 0.2 ml (4×10^5) were transferred to 1.5 ml ependorf tube and completed to 1 ml with medium, then treated with tested substances. Viability of treated cells was measured. Treated cells were centrifuged for 1 min by Ependorf microcentrifuge. The pellets were suspended in 15 micro-liter medium and loaded directly in the well of gel.

Gel preparation

Gels were prepared with 1.5% electrophoretic grade agarose (BRL) and 0.2% polyvinylpyrolidine (PVP; Sigma). The agarose and PVP were boiled with tris borate EDTA buffer (1 × TBE buffer; 89mM Tris, 89mM boric acid, 2mM EDTA, pH 8.8). 0.5 micro-gram/ml ethidium bromide was added to gel at 40°C. then gels were poured and allowed to solidify at room temperature for 1hr. before the samples were loaded. Treated human lymphocytes from 0.5 ml blood were loaded in wells. 15 micro-liter of lysing buffer (50mM NaCl, 1 mM Na_2 EDTA, 1% SDS, pH 8.3) was added on the cells for 15min. 5 µl from 6X loading buffer was added on the lysis cells. Electrophoresis was performed for 2hrs at 50 volt using 1X TBE buffer as running buffer. Gel was photographed using a Polaroid camera while the DNA

was visualized using a 312 nm UV light under a transilluminator.

Damage scoring

The intensity of intact, fragmented (released DNA) and RNA were measured as optical density by gel pro analyzer program.

d. Comet assay (single strand breaks of DNA)

DNA stranded breaks were measured in the alkaline comet assay using the method described by and Singh *et al*. (1988).The isolation and treatment of human lymphocytes with GA_3 and green tea in this technique are similar to the steps of total genomic technique. Viability of the cells was determined by trypan-blue exclusion before using the cells for studies (Boyum, 1968). Scoring was performed according to Hassab El-Nabi and Sallam (2002). Examinations were done with a fluorescent microscope equipped with an excitation filter of 510 nm and barrier filter of 590 nm. The migration was evaluated by observing and measuring the nuclear DNA, where the rounded spot of DNA was considered as a normal DNA spot, while the nuclear DNA, migrating towards the anode, appeared as comet spot and considered as damaged DNA spot. Five hundred spots of DNA were examined and classified into three types: (1) normal spots; round shape, (2) damaged spots; in which the length of the migrated fragments is less than or equal to the diameter of the basal nuclear DNA, and (3) strongly damaged spots; where the length of the comet was greater than the diameter of the basal nuclear DNA.

e. Statistical Analysis

In the present work, the chromosomal aberrations and the number of damaged cells (single cell gel electrophoresis assay) are represented in tables as percentage (%) while, SCE's are represented as mean ± standard deviation. The significance of difference between the treated and control were calculated according to χ^2 test and Student's t-test.

RESULTS

1. Chromosomal aberrations

Different types of chromosomal aberrations were observed in human lymphocyte cultures treated with gibberellic acid. These aberrations included chromatid gap, dicentric, chromatid break, chromatid deletion, fragment, and centromeric attenuation (Figures 1-3). An increase in the percentage of these aberrations was observed with the increase of the dose. The percentage of total chromosomal aberrations showed significant increase at doses 0.5, 1 and 2 mg of GA_3 and the percentages were 5.6, 9.2 and 11.6, respectively (Table 1). Conversely, cultures treated with GA_3 and green tea showed a decrease in the percentage of the chromosomal aberrations when compared with those treated with GA_3 alone. Green tea induced no chromosomal abnormality.

2. Sister chromatide exchange

Data in table 2 showed the frequencies of sister chromatid exchanges in human lymphocyte cultures treated with different doses of GA_3 and green tea. The data showed that there was highly significant ($p<0.01$) increase in SCE's frequencies in cultures treated with different doses of GA_3. Simultaneous application of GA_3 at the used doses and green tea caused reduction of the high SCE values induced by GA_3. This reduction did not reach the SCE's frequencies of control.

3. DNA damage

DNA detection by comet assay showed that strong damage spots of DNA (migration towards the anode) were observed in human lymphocyte cultures treated with different doses of GA_3 (Fig. 4). The tested doses of GA_3 induced a significant increase in the percentage of total damaged spots with values of 24.7, 34.8, 47.4 and 58.6 % when compared with control (5.1%). Simultaneous treatments with green tea and GA_3 decrease the percentage of total damage spots (Table 3).

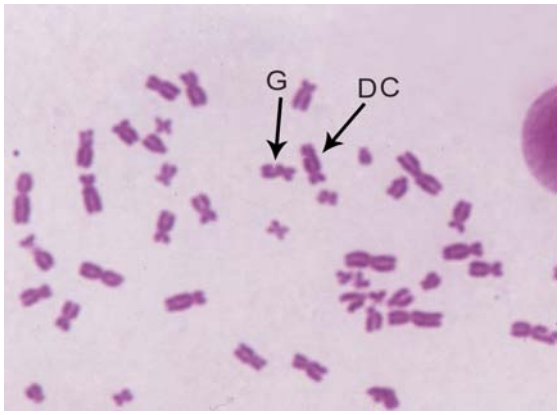

Fig. 1. Chromosomes with gab (G), dicentric chromosome (DC) in human lymphocyte cultures treated with gibberellic acid. (X 1000).

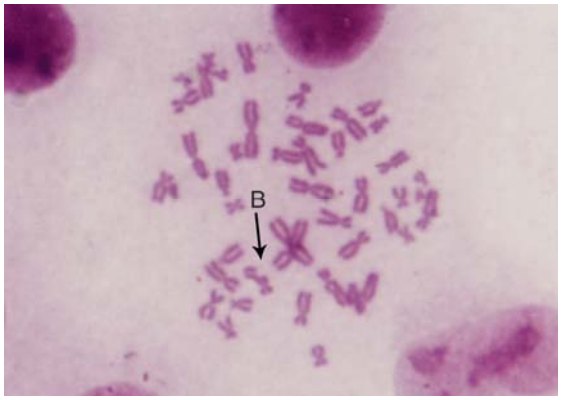

Fig. 2. Chromosomes with break (B) in human lymphocyte cultures treated with gibberellic acid. (X1000).

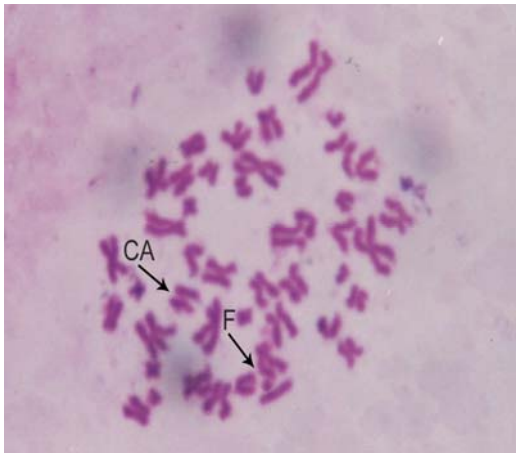

Fig. 3. Chromosomes with centromeric attenuation (CA) and fragment (F) in human lymphocyte cultures treated with gibberellic acid. (X 1000).

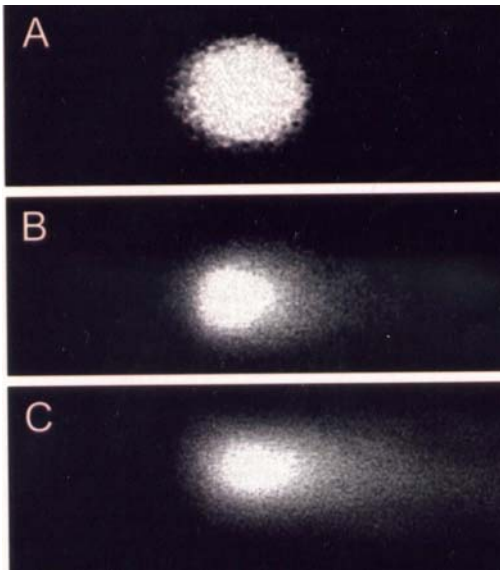

Fig. 4. Photomicrograph showing single strand breaks (comet assay) of DNA of human lymphocyte cultures treated with gibberellic acid. (A) Normal DNA spots (no migration). (B) Damaged DNA spots (migration towards the anode). (C) Strong damaged DNA spots (more migration towards the anode).

Electrophoretic pattern of nucleic acids of lymphocytes appeared as three main bands in gel. RNA area located at up 150 bp, nucleoprotein area located at 300-350 bp and DNA area located near the wells of gel to nucleoprotein area (Fig. 5). The DNA and RNA have orange color with ethidium bromide, while nucleoprotein has a purple color. When the gel was exposed to UV by UV transilluminator for 5 min. the color of nucleoprotein changed from purple to white. After staining the gel with commassi blue the DNA and RNA not stained while, nucleoprotein stained darkly with blue color (Hassab El-Nabi and Elhassaneen, 2008). Figure 5 revealed that the intensity of DNA fragmentation increased in GA_3-treated cultures. GA_3 induced strong and obvious damage at concentrations of 1 and 2mg as represented in lanes 4 and 5. On the other hand, treatment with GA_3 and green tea decreased the amount of fragmented DNA. Similarly, GA_3 increased the intensity of total RNA in a dose dependent manner. The optical density of released DNA is shown in figure 6. There was an increase in the intensity of released (fragmented) DNA in human lymphocyte cultures treated with GA_3. The values of the optical density of released DNA were increased with values of 36.242, 50.028, 65.003, and 126.44 at the dose levels of 0.1, 0.5, 1 and 2 mg GA_3 respectively, when compared with control. Simultaneous treatment with gibberellic acid at the previous doses, and green tea decreased the amount of fragmented DNA and the optical density values were 33.28, 38.494, 45.908, and 125.03. The optical density of total RNA was increased with values of 51.992, 55.243, 57.986, and 74.091 when compared with control value of 45.496. Treatment with GA_3 and green tea decreased the intensity of total RNA with values of 49.196, 54.42, 55.337, and 58.702 when compared with that treated with GA_3 (Fig. 7).

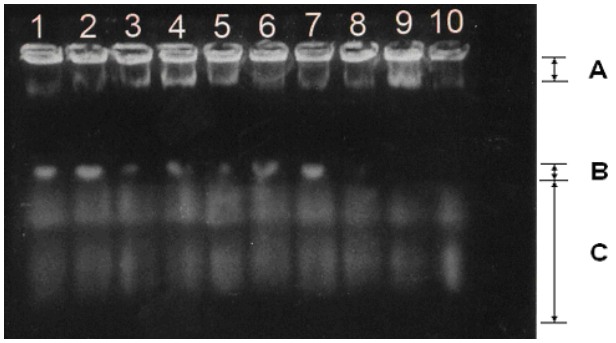

Fig. 5. Gel electrophoresis showing the effect of GA_3 and green tea on total DNA (section A), nucleoprotein (section B), and RNA pattern (section C) in human lymphocyte cultures; lane 1 control; lanes 2, 3, 4, 5 represent human lymphocyte cultures treated with 0.1, 0.5, 1, and 2 mg/ml respectively; lanes 6, 7, 8, 9 represent human lymphocyte cultures treated with the same doses of GA_3 and green tea .Lane 10 : green tea .

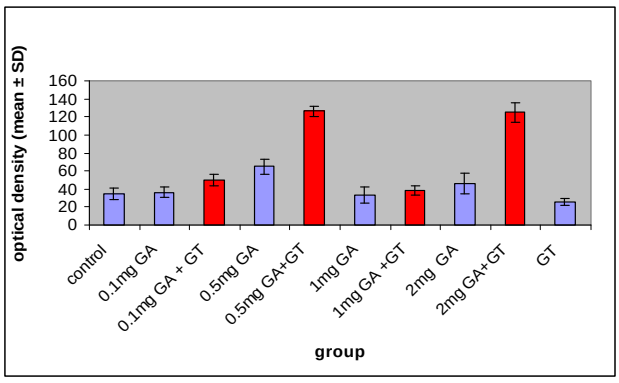

Fig. 6. Optical density of released fragments of DNA.

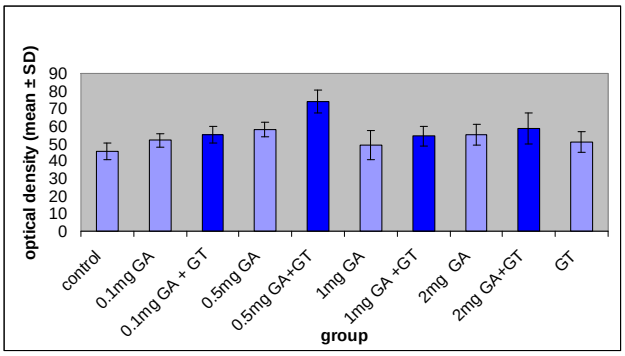

Fig. 7. Optical density of released RNA.

DISCUSSION

The present results showed that gibberellin A_3 induced chromosomal aberrations in human lymphocyte culture.Similar result was obtained by Zalinian *et al.* (1990). Gibberellic acid caused highly significant increase ($p<0.001$) in the percentage of total damage spots at all tested doses when detected with comet assay. Using total genomic damage of DNA method, gel pro analyzer charts have shown that there was an increase in the intensity of released DNA and that of RNA as the dose of gibberellic acid increased. In this concern, Hassab-Elnabi and Sallam (2002) reported that gibberellic acid induced total genomic damage of DNA especially at high doses.

The effect of growth hormones, especially gibberellins on plants was studied by many investigators Fath *et al.* (1999) reported that endogenous barley aleuronic nucleases degraded aleuronic DNA to 180 base pairs. When the aleuronic cells were incubated with gibberellic acid, nucleases enzymes were accumulated in the cells causing DNA fragmentation or damage. So, the DNA damage may results from direct attack of DNA by gibberellic acid causing alkali labile and single strand breaks and total genomic damage and this may be due to accumulation of nucleases. Jacqmard (1968) has proposed that one of the effects of GA_3 is to promote the onset of DNA synthesis in cells which are arrested in the G1 phase of the cell cycle. This notion is supported by the data of Liu and Loy (1976) on the effect of GA_3 on the cell cycle of watermelon seedlings. GA_3 reduces the duration of the cell cycle by nearly 30% and it does so primarily by reducing the length of G1 by 30% and that of S by 36%. It was well established that plant hormones and growth regulators affect the synthesis of RNA and protein (Jacobsen 1977; Bewley and Black, 1978).

Chemical carcinogens - by themselves or after activation - interact with cellular macromolecules such as DNA, RNA, and proteins, and these interactions result in the development of neoplasia (Williams and Weisburger, 1991). It has also been reported that replication of DNA with carcinogen-induced lesions is an essential step in the initiation of carcinogenesis. Gibberellin A_3 was found to have carcinogenic effects in amphibians (El-Mofty and Sakr, 1988) and mammals (El-Mofty *et al*., 1994). Thus, the present results may explain some of the events led to carcinogenicity of GA_3.

The present results indicated that green tea has a curative effect against mutagenicity of gibberellic acid. Green tea was found to reduce chromosomal aberrations induced by gibberellic acid. Similar effects of green tea or its constituents were studied by different investigators. Sasaki *et al*. (1993) reported that green tea decreased the frequency of chromosome aberrations induced by benzo[a]pyrene or mitomycin C in cultured Chinese Hamster Ovary (CHO) cells and mice. They suggested

Table 1. Frequency of chromosomal abnormalities observed in 250 metaphase spreads of human lymphocyte cultures treated with gibberellic acid (0.1, 0.5, 1 & 2mg) and green tea (0.5mg).

Dose	% of chromosomal abnormalities						% of TCA
	Gap	Break	Deletion	Fragment	Dicentric	Centromeric Attenuation	
Control	0.8	0	0	0.4	0	0	1.2
0.1mg GA	0.8	0.4	0.4	0.8	0	0	2.4
0.1mg GA +GT	0.8	0	0.4	0.4	0	0	1.6
0.5mg GA	1.6	0.8	0.8	1.6	0.4	0.4	5.6*
0.5mg GA +GT	1.2	0.4	0.4	1.2	0	0	3.2
1mg GA	2.4	1.2	1.2	2.8	0.8	0.8	9.2**
1mg GA +GT	1.6	0.4	0.8	1.6	0.4	0.4	5.2
2mg GA	2.8	1.6	1.6	3.2	1.2	1.2	11.6**
2mg GA +GT	2.4	0.8	1.2	2.4	0.4	0.4	7.6

GA: gibberellic acid; GT: green tea; TCA: Total chromosomal aberrations
* Statistically significant ($p<0.01$) , ** highly significant ($p<0.001$)

that catechins, well-known antimutagens in tea samples, might account for the observed inhibitory effect green tea extract. Ito *et al*. (1989) recorded the suppression of chromosomal aberrations induced by aflatoxin-B_1 in rat bone marrow cells *in vivo* by green tea.

Table 2. Sister Chromatid exchanges (SCE's) of human lymphocyte cultures treated with gibberellic acid and green tea.

Treatment	SCE's (mean +/- SD)
Control	3.4 +/- 2.12
0.1 mg GA	4.84 +/- 2.49
0.1 mg GA+GT	3.68 +/- 1.93
0.5 mg GA	5.56 +/- 3.02**
0.5 mg GA+GT	3.84 +/- 2.13
1mg GA	6.28 +/- 2.6**
1mg GA+GT	4.2 +/- 1.68
2mg GA	6.56 +/- 2.88**
2mg GA+GT	4.72 +/- 1.49

** Statistically highly significant ($p<0.01$)

Simultaneous treatment with gibberellic acid and green tea revealed a reduction in the frequency of sister chromatid exchange. Cheng (1989) reported that green tea decreased the frequency of sister chromatid exchanges induced by oxygen radical in IAR 20 liver cells treated with hypoxanthine and xanthine oxidase.Wang *et al*. (1989**)** reported that water extracts of green tea and their major constituents, green tea polyphenols , have antimutagenic activity. They found that green tea polyphenols inhibited gene forward mutation in V79 cells treated with benzo[alpha]pyrene (BP)and aflatoxin-B_1 and also decreased the frequency of sister-chromatid exchanges and chromosomal aberrations in V79 cells treated with AFB_1. Fujie *et al*. (1993) reported that crude catechin extracted from green tea suppressed sister-chromatid exchanges induced by trihalomethanes in rat erythroblastic cells *In vitro*. Tanaka (2000) observed that epigallocatechin gallate, the major constituent of green tea and catechin a minor constituent, equivalently decreased the frequencies of sister-chromatid exchanges induced by paraquat which is a generator of reactive oxygen species. Green tea strongly inhibited the increase in sister chromatid exchanges and micronuclei induced by Fried fish in V79 and IAR20 cells (Liu, 1990).

The present work revealed that human lymphocyte cultures treated with gibberellic acid showed strong damage cells using comet assay. After treating with green tea the percentage of the total damage spots decreased. Similarly, Roy *et al*. (2003) reported that the green tea extract, polyphenol epigallocatechin gallate had a curative effect on the cytogenetic change and DNA damage induced by toxicants $H_{(2)}O_{(2)}$ and carcinogen N-methyl-N'-nitro-N-nitrosoguanidine in Chinese hamster V-79 cells in culture. Zhang *et al*. (2002) recorded modification of lung cancer susceptibility by green tea extract as measured by the comet assay. Lin *et al.* (2003) studied the induction of apoptosis in HL-60 cells by tea extracts: green tea, oolong tea, black tea, and pu-erh using DNA fragmentation ladder and flow cytometry. The results showed that the ability of tea extracts to induce apoptosis was in the order green tea > oolong > black tea > pu-erh tea. Chen *et al*. (2004) reported that epigallocatechin gallate, a major constituent of green tea polyphenols, induced a GO/G1 arrest and apoptosis in NBT-II bladder tumor cells.

Parshad *et al*. (1998) found that addition of green or black tea extracts, their polyphenols or curcumin to cultures of human skin fibroblasts or PHA-stimulated blood lymphocytes significantly reduced the frequencies of radiation-induced chromatid breaks. The protective action of these plant polyphenols seems to result from their

Table 3. The percentage of DNA damage detected by comet assay in human lymphocyte cultures treated with gibberellic acid and green tea.

Treatment	% of Normal Spots	% of Damage Spots	% of Strong damage spots	% of total damage spots
Control	94.9	4	1.1	5.1
GT	93.8	5	1.2	6.2
0.1 mg GA.	75.3	14.3	10.4	24.7**
0.1 mg GA.+GT	90.8	5	4.2	9.2
0..5 mg GA.	65.2	18.4	16.4	34.8**
0..5 mg GA. +GT	86.3	8.2	5.5	13.7
1 mg GA.	52.6	19.1	28.3	47.4**
1 mg GA. +GT	81.4	10.3	8.3	18.6*
2 mg GA.	41.4	21.2	37.4	58.6**
2 mg GA. +GT	77.8	15	7.2	22.2**

* Statistically significant ($p<0.01$); ** Statistically highly significant ($p<0.001$)

known antioxidant properties, particularly the scavenging of hydroxyl free radicals. Feng *et al*. (2002) reported that black tea polyphenols, theaflavins, prevent cellular DNA damage using the comet assay by inhibiting oxidative stress and suppressing cytochrome P450 1A1 in cell cultures.

The present results proved that green tea had a curative effect against cytogenicity of GA_3. A growing body of research has demonstrated green tea polyphenols to be powerful components with anticarcinogenic and antimutagenic properties. The mechanism of these green tea components is attributed to: 1- Antioxidant and free radical scavenging activity, 2- Stimulation of detoxification systems, especially selective induction or modification of phase I and phase II metabolic enzymes with increasing the formation and excretion of detoxified metabolites of carcinogens, 3- Inhibition of biochemical markers of tumor initiation and promotion, including lowering the rate of cell replication and thus the growth and development of neoplasm, and 4- Prevention of mutagenicity and genotoxcity (Weisburger,1999). Thus in the present work, it is speculated that one or more constituents of green tea may be responsible for prevention of mutagenic effects of gibberellic acid through one or more of these mechanisms.

REFERENCES

Arutiunian, RM. and Zalinian, GG. 1987. Cytogenetic effect of natural mutagenesis modifiers in a human lymphocyte culture. The action of caffeine during the induction of chromosome aberrations by gibberellic acid. Tsitol. Genet. 21(2):101-105.

Bakr, SM., Moussa, EM. and Khater, E. Sh. 1999. Cytogenetic evaluation of gibberellin A_3 in Swiss albino mice. J Union Arab Biol. 11(A):345-351.

Bewley, JD. and Black, M. 1978. Physiology and Biochemistry of Seeds in Relation to Germination, Vol. 1. Development, Germination, and Growth. Springer-Verlag, Berlin. 1:306.

Boyum, A. 1968. Separation of leukocytes from blood and Bone marrow. Scand. J. Clin. Lab. Invest. 21 (Suppl. 97):77-89.

Carpita, NC., Nabors, MW., Ross, CW. and Petrie, NL. 1979. The growth physics and water relations of red-light induced germination in lettuce seeds. III. Changes in the osmotic and pressure potential in the embryonic axes of red- and far-red-treated seeds. Planta. 144:217-224.

Chen, JH., Tipoe, GL., Long, EC., SH So, H., Ka-Man Leung., Wai-Ming Tom, Fung, CW. and Nanji, AA. 2004. Green tea polyphenols prevent toxin- induced hepatotoxicity in mice by down-regulating inducible nitric oxide-derived prooxidants. American J Clin Nutrition. 80(3):742-751.

Cheng, SJ. 1989. Inhibitory effect of green tea extract on promotion and related action of TPA. Zhongguo Yi Xue Ke Xue Yuan Xue Bao. 11(4):259-264.

El-Mofty, MM. and Sakr, SA. 1988. Induction of neoplasm in the Egyptian toad *Bufo regularis* By gibberellin-A_3.Oncology. 45:61-64.

El-Mofty, MM., Sakr, SA., Rizk, AM. and Moussa, EA. 1994. Carcinogenic effect of gibberellin A_3 in Swiss albino mice. Nutr Cancer. 21:183-190.

Fath, A., Bethke, PC. and Jones, RL. 1999. Barley aleurone cell death is not apoptotic: characterization of nuclease activities and DNA degradation. Plant J. 20(3): 305-315.

Feng, Q., Torii, Y., Uchida, K. Nakamura, Y. and Osawa, T. 2002. Black tea polyphenols, theaflavins, prevent cellular DNA damage by inhibiting oxidative stress and suppressing cytochrome P450 1A1 in cell cultures. J. Agric. Food. Chem. 50(1): 213-220.

Fujie, K., Aoki, T., Ito, Y. and Maeda, S. 1993.Sister-chromatid exchanges induced by trihalomethanes in rat erythroblastic cells and their suppression by crude catechin extracted from green tea. Mutat. Res. 300(3-4):241-246.

Fujiki, H., Suganuma, M., Okabe, S., Komori, A., Sueoka, E., Sueoka, N., Kozu, T. and Sasaki, Y. 1996. Japanese green tea as a cancer preventive in humans. Nutr. Rev. 54:S67-S70.

Han, C. 1997. Screening of anticarcinogenic ingredients in tea polyphenols. Cancer letters. 114:153-158.

Hara, Y. and Tonooka, F.1990. Hypotensive effect of tea catechin on blood pressure of rats. Nippon Eiyo Shokuryo Gakkaishi. 43:345-348.

Hassab El-Nabi, SE. and Sallam, FA. 2002. The protective effect of ellagic acid against the mutagenic potential of berelex in human lymphocyte cultures. J. Egypt. Ger. Soc. Zool. 37(C):77-98.

Hassab El-Nabi, SE. and Elhassaneen, YA. 2008. Detection of DNA damage, molecular apoptosis and production of home-made ladder by using simple techniques. Biotechnology. 7(3):514-522.

Ito, Y. Ohnishi, S and Fujie, K. 1989.Chromosome aberrations induced by aflatoxin B1 in rat bone marrow cells *in vivo* and their suppression by green tea. Mutat. Res. 222(3):253-261.

Jacobsen, JV. 1977. Regulation of ribonucleic acid metabolism by plant hormones. Ann. Rev. Plant Physiol. 28:537-564.

Jacqmard, A. 1968. Early effects of gibberellic acid on mitotic activity and DNA synthesis in the apical bud of *Rudbeckia bicolor*. Physiol. Veg. 6: 409-416.

Jones, RL. and MacMillan, M. 1984. Gibberellins. In: Advanced Plant Physiology. Ed. Wilkins, MB. Pitman, London. pp.21-52.

Kada, T., Kaneo, K., Matsuzaki, S., Matsuzaki, T. and Hara, Y. 1985. Detection and chemical identification of natural bioantimutagens. Mutat. Res. 150:127-132

Klaunig, JE. 1992. Chemopreventive effects of green tea components on hepatic carcinogenesis Prev. Med. 21(4):510-519.

Lin, YS., Tsai, YJ., Tsay, JS. and Lin, JK. 2003. Factors affecting the levels of tea polyphenols and caffeine in tea leaves. J. Agric. Food Chem. 51(7):1864-1873.

Liu, PB. and Loy, JB. 1976. Action of gibberellic acid on cell proliferation in the subapical shoot meristem of watermelon seedlings. Am. J. Botany. 63:700-704.

Liu, XL. 1990. Genotoxicity of fried fish extract, MelQ and inhibition by green tea antioxidant. Zhonghua Zhong Liu Za Zhi. 12(3):170-173.

Moorhead, PS., Nowell, PC., Mellraan, WJ., Battips, DM. and Hungerford, DA. 1960. Chromosome preparations of leukocytes cultured from human peripheral blood. Exp. Cell Res. 20:613-616.

Muramatsu, K. Fukuyo, M. and Hara, Y. 1986. Effect of green tea catechins on plasma cholesterol level in cholesterol-fed rats. J. Nutr. Sci. Vitaminol. 32:613-622.

Parshad, R., Sanford, KK., Price, FM., Steele, VE., Tarone, RE., Kelloff, GJ. and Boone, CW. 1998. Protective action of plant polyphenols on radiation-induced chromatid breaks in cultured human cells., J.Anticancer Res. 18(5A):3263-3266.

Perry, P. and Wolff, S. 1974. New Giemsa method for the differential staining of sister chromatids. Nature (London). 251:156-158.

Roy, M., Chakrabarty, S., Sinha, D., Bhattacharya, RK. and Siddiqi, M. 2003. Anticlastogenic, antigenotoxic and apoptotic activity of epigallocatechin gallate: a green tea polyphenol. Mutat. Res. (523-524):33-41.

Sagesaka, YM., Uemura, T., Suzuki, Y., Sugiura, T., Yoshida, M., Yamaguchi, K. and Kyuki, K. 1996. Antimicrobial and anti-inflammatory actions of tea-leaf saponin. Yakugaku Zasshi. 116:238-243.

Sasaki, YF., Yamada, H., Shimoi, K., Kator, K. and Kinae, N. 1993. The clastogen-suppressing effects of green tea, Po-lei tea and Rooibos tea in CHO cells and mice. Mutat. Res. 286(2):221-232.

Sato, D. 1999. Inhibition of urinary bladder tumours induced by N-butyl-N-(4-hydroxybutyl)-nitrosamine in rats by green tea. Int. J. Urol. 6:93-99.

Shimizu, M., Wada, S., Hayashi, T., Arisawa, M., Ikegaya, K., Ogaku, S., Yano, S. and Morita, N. 1988. Studies on hypoglycemic constituents of Japanese tea. Yakugaku Zasshi. 108:964-970

Singh, NP., McCoy, MT., Tice, RR. and Schneider, EL. 1988. A simple technique for quantitation of low levels of DNA damage in individual cells. Exp. Cell Res. 175: 184-191.

Tanaka, R. 2000. Protective effects of (-)-epigallocatechin gallate and (+)-catechin on paraquat-induced genotoxicity in cultured cells. J. Toxicol. Sci. 25(3):199-204.

Toda, M., Okubo, S., Ohnishi, R. and Shimamura, T. 1989. Antibacterial and bactericidal activities of Japanese green tea. Jpn. J. Bacteriol. 44:669-672.

Wang, ZY., Cheng, SJ., Zhou, ZC., Athar, M., Khan, WA., Bickers, DR. and Mukhtar, H. 1989. Antimutagenic activity of green tea polyphenols. Mutat. Res. 223(3):273-285.

Weisburger, JH.1999. Tea and health: the underlying mechanisms. Proc Soc Exp Biol Med. 220:271-275.

Williams, GM. and Weisburger, JH. 1991. Chemical Carcinogenesis. In: Casarett and Doull's Toxicology: the basic science of poisons. Eds. Klaassen, CD., Amdur, MO. and Doull, J. (4th ed.). Pergamon Press, New York, pp. 127-200.

Wlodek, D., Banath, J. and Olive, PL. 1991. Comparison between pulsed-field and constant-field gel electrophoresis for measurement of DNA double-strand breaks in irradiated Chinese hamster ovary cells. Int. J. Radiat. Biol. 60(5):779-790.

Zalinian, GG. , Arutiumian, RM. and Sarkisian, GG. 1990. The cytogenetic effect of natural mutagenesis modifiers in a human lymphocyte culture. The action of amino benzamide during the gibberellic acid induction of chromosome aberrations. Tsitol Genet. 24(3):31-34.

Zhang, H., Spitz, MR., Tomlinson, GE., Schabath, MB., Minna, JD. and Wu, X. 2002. Modification of lung cancer susceptibility by green tea extract as measured by the comet assay. Cancer. Detect. Prev. 26(6):411-418.

Received: May 14, 2009; Revised: August 2, 2009;
Accepted: August 5, 2009

SENRA Academic Publishers, Burnaby, British Columbia
Vol. 3, No. 3, pp. 925-928, 2009
ISSN: 1715-9997

Canadian Journal of pure&applied sciences

PHYTOCHEMICAL SCREENING AND EVALUATION OF STEM BARK EXTRACT OF *KHAYA SENEGALENSIS* (MELIACEAE) ON METHICILLIN RESISTANT *STAPHYLOCCOCUS AREUS*

*Abiodun Falodun[1] and Osahon Obasuyi[2]
[1]Department of Pharmaceutical Chemistry, [2]Department of Pharmaceutical Microbiology, Faculty of Pharmacy
University of Benin, Benin City, Nigeria

ABSTRACT

Khaya senegalensis is an herbal medicinal plant, used locally in Nigeria and South Africa for the treatment of cough and sexually transmitted diseases. This antibacterial activity prompted the phytochemical and antibacterial investigation of this herbal plant. The stem bark of *K. senegalensis* was subjected to phytochemical studies using standard experimental procedures testing for secondary metabolites. The crude extract was evaluated for its antimicrobial activity using methicillin resistant strains of *Staphyloccocus aureus* MRSA. The result of the study revealed the presence of alkaloids, saponins, tannins and flavonoids in the plant extract. The extract exhibited significant antibacterial and MRSA activities against the tested organisms. The study therefore provides natural source for drugs used for the treatment of methicillin resistant strains (MRSA) infections.

Keywords: *K. senegalensis*, stem bark extract, MRSA, bacterial infections.

INTRODUCTI ION

Natural Products are an important source of new structures leading to drugs discovery in all major disease areas. In order to find new drugs in plants, it is necessary to screen plant extracts for biological activities, with the aim of obtaining novel compounds. Once novel compounds are suspected, they are generally isolated in order to have material available for further biological and toxicological testing (Newman and Cragg, 2007). The demands of traditional medicine from the public and the growing economic importance of traditional medicine have led to the increased interest on the part of academic communities and the government. The need to study a local medicinal plant *Khaya senegalensis* cannot be over emphasized.

Khaya senegalensis belongs to the family Meliaceae, and is commonly called African Mahogany and it is endemic in many African countries. *K. senegalensis* is a deciduous evergreen tree, 15-30 m high, up to 1 m in diameter, with a clean bole to 8-16 m. The plant is used in ethnomedicine for the treatment of various disease conditions such as rheumatoid arthritis, diarrhea and cough (Dalziel, 1948; Brian and Stanfield, 1966; Egwim *et al*., 2002). It has also been used as an anthelmintic, emetic, emmenagogue and in jaundice treatment (Gill, 1992). The effect of the extract on the rat kidney has also been reported (Joseph *et al*., 2003). The aqueous extract of stem bark has been reported to reduce anemia (Sanni *et al*., 2005), and inflammation (Lompo *et al*., 1998). Some limonoids have been isolated from the stems, barks, leaves and flowers of *K. senegalensis* (Nakatani *et al*., 2001; Adesida *et al*., 1971). They include phragmalin limonoids named khayanolides D and E, khayanosides, 2, 6-dihydrofissinolide and two mexicanolides named khayanone and 2-hydro- xyseneganolide. Traditional herbalists in many parts of Africa (especially northern part of Nigeria) have achieved success with the use of this plant for the treatment of tuberculosis and bacterial infections.

Methicillin resistant strains have assumed increasing importance both as a cause of nosocomial and community acquired infections (Jevons, 1961; Knox, 1961). Infections caused by MRSA resulted in increased lengths of hospital stay, health care cost, morbidity and mortality (Niclaes *et al.*, 1999). The infusion of the plant extract is used by herbal healers for the treatment of cough and wounds and boils. This biological activity necessitated the scientific validation and justification of its use as herbal remedy. This study was therefore aimed at searching for natural products that could be used to combat the effect of MRSA infections among the natives since these herbal medicinal products are cheap and readily available in the tropical forest.

MATERIALS AND METHODS

Plant material

The plant (stem bark) was collected around January 2008 in Otukpo Local Government, Benue State, Nigeria. Botanical identification and authentication was done by a staff of the Department of Pharmacognosy, University of

*Corresponding author email: faloabi25@yahoo.com

Benin. [Voucher specimen was deposited, no. AF 2008KS].

Extraction and preparation

The stem bark of *K. senegalensis* was dried and reduced to a fine powder with the aid of a mechanical blender. The powdered sample (600g) was extracted with 700ml of distilled water by maceration for 48 hours. The residue (54.28g) was stored in a refrigerator at -4^{o}C until use.

Phytochemical Screening

The crude plant sample was subjected to phytochemical screening testing for alkaloids, saponins, tannins, flavonoid and irridoids using standard experimental procedures of Trease and Evans (2002).

Biological assay

MRSA organisms isolated from clinical specimens obtained from patients visiting the University of Teaching Hospital, Benin City, were used for the study.

Drugs and Microbial Media

The antimicrobial agents used include amoxicillin (Smithkline Becham Pharmaceuticals UK), ciprofloxacin (Ranbaxy Pharmaceuticals, India), nutrient broth and Mannitol Salt agar (MSA) Oxoid, England.

Susceptibility Testing

The agar diffusion method was used to determine the antimicrobial activity of the extract (NCCLS, 1999; Barry and Thornsberry, 1985; Cruickshank *et al*., 1975). The susceptibility of isolates to methicillin using the E-test strips (AB Biodisk) was carried out by the disk diffusion method. Each isolate was grown in the nutrient broth for 18 hours. 2ml of the culture was aseptically used to seed molten mannitol salt agar which has been cooled to 45^{o}C, mixed gently and poured into sterile Petri dishes and allowed to solidify. The extract dissolved in dist. water was tested at 40mg/ml concentration. 2ml was delivered into wells (8mm diameter) bored into the surface of the already seeded MSA plates. Standard antibiotics concentration of ciprofloxacin (10mg/l) and amoxicillin (25mg/l) were assayed along using the agar well diffusion technique. The plates were incubated at 37^{o}C for 24 hours and zones of inhibition measured in mm diameter and recorded.

Determination of Minimum Inhibitory Concentration (MIC)

The modified agar well diffusion technique (Okeke *et al*., 2001) was used to determine the MIC of the extract. Two fold serial dilutions were prepared by first reconstituting in sterile distilled water, diluting to achieve a decreasing concentration range of 50 – 0.78 mg/ml. 0.1ml of each dilution was introduced into MSA plates seeded with standard inoculum (approx. 10^5 cfu/ml) of the test bacterial cells. All test plates were incubated at 37^{o}C for 24 hours. The test concentration of extract showing a clear zone of inhibition was taken as the MIC.

Statistical Analysis

The Student's *t*-test was used for the analysis of data (Dixon and Massey, 1969).

RESULTS AND DISCUSSION

The phytochemical testing (Table 1) showed that the plant contained flavonoids, saponins tannins and alkaloids in agreement with the result of Gbile (1986). The results of the antibacterial activity of the extract (inhibition zone diameter in mm) at 40mg/ml concentration, ciprofloxacin 10mg/ml and amoxicillin 25mg/ml against ten strains of are given in table 2. The dissolution solvent used for the extract did not show any activity at the volume used. The crude extract showed significant activity against all MRSA isolates whereas the standard antibiotics showed absence of activity against one and two isolates for ciprofloxacin and amoxicillin respectively.

Table 1. Phytochemical components of aqueous extract of *K. senegalensis.*

Phytochemical compositions	Presence of components
Alkaloids	+
Tannins	+++
Saponins	+++
Flavonoids	++++

+; presence of low amount of component
+++; presence of moderate amount of component
++++; indicates presence of high amount of component
-; indicates absence of components

The result further showed that the extract exhibited similar activity (zone diameter) as amoxicillin against the bacterial strains. The MIC of the extract (Table 3) is between 1.56mg/ml to 6.25mg/ml against all isolates used in this evaluation.

The observation of zones of inhibition against MRSA isolates indicates the presence of antibacterial activity which confirmed its ethnomedicinal use as anti-infective agent in bacterial infections. Further study on the prefractionation and isolation of the bioactive chemical constituents when carried out will lead to new compound which could be added to the potential list of antibacterial agents against MRSA. The work reveals for the first time marked activity of *K. senegalensis* against different isolates of MRSA at the concentration tested.

ACKNOWLEDGEMENTS

The authors are grateful to the University of Benin Teaching Hospital (UBTH) and Faculty of Pharmacy, UNIBEN for the facilities provided in executing the research.

Table 2. *In vitro* antibacterial activity of aqueous extract and standard antimicrobial agents.

Micro organisms	Extract (40mg/mL)	CP (10 mg/mL)	AMX (25 mg/mL)	DW (0.2mL)
a	18.5 ± 0.70	29.0 ± 0.00	-	-
b	15.5 ± 0.70	28.5 ± 4.9	25.5 ± 74	-
c	19.5 ± 0.70	27.0 ± 0.01	22.0 ± 0.02	-
d	19.0 ± 1.40	30.5 ± 0.70	16.5 ± 2.10	-
e	17.0 ± 1.40	27.0 ± 1.40	22.0 ± 0.00	-
f	20.5 ± 3.50	24.5 ± 0.71	19.5 ± 3.51	-
g	20.0 ± 1.40	31.5 ± 0.72	17.5 ± 0.72	-
h	20.0 ± 0.05	26.0 ± 0.01	14.5 ± 0.71	-
I	21.5 ± 4.90	-	-	-
J	17.5 ± 0.70	25.5 ± 0.70	20.0 ± 0.01	-

Key: a – j, isolates of MRSA; CP, Ciprofloxacin; AMX, Amoxicillin; DW, distilled water; #, mean of two replicates determinations; -, absence of zone of inhibition

Table 3. Minimum Inhibitory concentration of MIC aqueous extract of *K.senegalensis.*

Organisms	MIC (mg/mL)
a	3.13
b	6.25
c	3.13
d	3.13
e	3.13
f	1.56
g	3.13
h	3.13
I	1.56
J	3.13

REFERENCES

Adesida, GA., Adesogan, EK., Okorie, DA., Taylor, DAH. and Styles, BT. 1971. The limonoid chemistry of the genus *Khaya* (Meliaceae). Phytochemistry 10:1845-1853.

Barry, A. and Thornsberry, C. 1985. Susceptibility Test. Diffusion Test Procedure. J. Clin. Pathol. 19:492.

Brian, H. and Stanfield, D. 1966. Field Key to the Savanna Trees of Nigeria, pp. 2-4.

Cruickshank, R., Duguid, J, Marmion, P. and Swain, R. 1975. Test for sensitivity of antimicrobial agent. vol. 1. Medical Microbiology. (12th ed.). Churchill Livingstone, London. pp. 190.

Dalziel, JM. 1948. The useful Plants of West Tropical Africa. Crown Agents for the colonies, London. pp. 612.

Dixon, W. and Massey, F. 1969. Introduction to Statistical Analysis, (3rd ed.). McGraw-Hill, New York.

Egwim, E., Badru, A. and Ajiboye, K. 2002. Testing pawpaw (*Carica papaya*) leaves and African Mahogany (*Khaya senegalensis*) bark for antimalarial activities. Nigerian Society Experimental Biology. 2:37-39.

Gbile, Z. 1986. Ethnobotany, taxonomy and conservation of medicinal plants. In: The State of Medicinal Plants Research in Nigeria. Ed. Sofowora, A. University of Ibadan Press, Ibadan, Nigeria. pp 13-29.

Gill, LS. 1992. In: Ethnomedical Uses of Plants in Nigeria. Eds. Gills, LS. Uniben Press. pp. 143.

Jevons, MP. 1961. Celbenin – resistant *Staphylococci*. British Med. J. I :124-5

Knox, R. 1961. Celbenin – resistant *Staphylococci*. British Med. J. I :124-6

Joseph, OA., Musa, TY, Evans, CE, Victor, OB. and Bernard, UE. 2003. Effect of ethanolic extract of *Khaya senegalensis* on some biochemical parameters of rat kidney. J. Ethnopharmacol. 88:69-72.

Lompo, M., Nikiema, JB, Guissou, IP, Moes, AJ. and Fotaine, J. 1998. Topical Anti inflammatory effect of chloroform extract from *Khaya senegalensis* stem bark. Phytother. Res.12:448-450.

Nakatani, M., Abdelgaleil., SA, Kurawaki, J., Okamura, H., Iwagawa, T. and Doe, M. 2001. Antifeedant rings B and D opened limonoids from *Khaya senegalensis*. J. Nat. Prod. 64:1261-1265.

NCCLS, 1999. Performance Standards for Antimicrobial susceptibility Testing 9th Information Supplement. NCCLS document M100 - S9. Wayne PA: National Committee for Clinical Laboratory Standards.

Newman, D. and Cragg, G. 2007. Natural Products as Sources of New Drugs over the Last 25 Years Nat. Prod. 70:461.

Niclaes, L, Buntinx, F, Banuro, E. and Lesaffre, A. 1999. Consequences of MRSA Carriage in nursing home residents. Epidermiol Infect.122:235-239.

Okeke, M., Iroegbu, C, Eze, E, Okoli, A. and Esimone, C. 2001. Evaluation of extracts of the root of *Landolphia Owerrience* for antibacterial activity. J. Ethnopharmacol. 78:119 - 127.

Sanni, FS., Ibrahim, S, Esievo, KAN. and Sanni, S. 2005. Effect of Oral Administration of Aqueous extract of *Kaya senegalensis* stem bark on Phenyl hydrazine induced anaemia in rats. Pak. J. Bio. Sci. 8 (2):255-258.

Trease, GE. and Evans, WC. 2002. Pharmacognosy. (15th ed.) Ed. Evans Harcourt, WC. Publishers Ltd London. pp 3-48.

Received: July 1, 2008; Revised: July 13, 2009; Accepted: July 14, 2009

SENRA Academic Publishers, Burnaby, British Columbia
Vol. 3, No. 3, pp. 929-935, 2009
ISSN: 1715-9997

Canadian Journal of pure&applied sciences

JUGULAR VEIN CANNULATION IN RATS – A MINI REVIEW

*Nasim Karim[1] and Syed Sanowar Ali[2]
[1]Department of Pharmacology, Sindh Medical College, Dow University of Health Sciences, Karachi
[2]Department of Community Medicine, Jinnah Medical and Dental College, Karachi, Pakistan

ABSTRACT

Blood is removed from animals for a variety of scientific purposes. As suffering and distress in animals can result in physiological changes which are likely to add another variable to experimental results care should be taken to minimize stress in these laboratory animals as much as possible so that appropriate experimental results could be obtained. Various methods are in use for blood sampling in rodents like tail-clipping, retro-orbital puncture, tail puncture, jugular vein puncture, cardiac puncture, decapitation etc. Vascular cannulations are among the most widely used surgeries in research labs around the world. Cannulation for the repeated blood samples are suitable for use in all strains of rats and can be used to take blood from the femoral artery and vein, carotid artery, jugular vein, vena cava and dorsal aorta. Venous cannulation is said to have advantages which outweigh the arterial cannulation as the former is easier to implant, easier to fill, more likely to maintain patency than the latter. In this respect in addition blood sampling through the jugular catheter offers the advantage that, lost volume can easily be replaced. Thus it is possible to collect sequential samples to evaluate the time course of a response or the acquisition of a larger volume for measurement of hormones which are present at low concentrations in the circulation. Present article is a review with an attempt to provide an elaborate piece of information regarding jugular vein cannulation with precise focus in rats.

Keywords: Cannulation, jugular vein, rats.

INTRODUCTION

Jugular vein and carotid artery cannulations are among the most widely used surgeries in research labs around the world. These cannulations are extremely important for confirmed intravenous delivery of test substances and arterial blood collections. Cannulation reduces the stress of multiple sampling as observed in association with tail vein or orbital sinus technique. Very few adverse effects including a possible rise of corticosteroids and a decrease in platelets are associated with indwelling catheters except under chronic conditions Angela (2007). A cannula (from latin word little reed) is a flexible tube which when inserted into the body is used either to withdraw fluid or insert medication Cannulation (2008). Whereas cannulation is defined as a surgical procedure involving insertion of a flexible catheter into one of the large blood vessels Cannulation (2008). Synonyms used for cannulation are canulation, cannulization, cannulisation, intubation Word Net Search (2008).

Blood vessel cannulation allows repeated blood sampling from conscious, unrestrained rats while avoiding the stress due to handling, restraint and anesthesia (Yoburn *et al*., 1984; Suzuki *et al*., 1997; Reilly, 1998). Surgery may cause changes in hormonal and hemodynamic responses (Weissman, 1990). Catheter infection, while uncommon in rats is known to stimulate a stress response and is a potential consequence of long term catheterization (Popp and Brennan, 1981; Bradfield *et al*., 1992). An adequate recovery time from surgery and aseptic surgical technique may minimize these effects but the precise time for full recovery is uncertain (Fagin, 1983). An adequate recovery time is therefore required to minimize the effects of surgery on a subsequent stressor (Garcia *et al*., 2000). It would be advantageous to use a cannula within days of insertion. Besides the risk of infection in a chronic catheter and the challenge of keeping the cannula patent for more than a week other physiological changes have also been observed (Terao and Shen, 1983).

Blood sampling through the jugular catheter offers the advantage that lost volume can easily be replaced. Thus it is possible to collect sequential samples to evaluate the time course of a response or the acquisition of a larger volume for measurement of hormones at low concentrations in the circulation (Darlington *et al*., 1986; Torner *et al*., 2000) without critically affecting the hemodynamic variables. Chronic cannulation of the jugular vein in freely moving rats and the other larger laboratory animals is an established method for studying drug pharmacokinetics and effects (Popovic *et al*., 1963; Nicolaidis *et al*., 1974; Torres-Molina *et al*., 1992). It allows serial blood sampling with minimal disturbance of the animal without the need for anaesthesia. Commonly used methods for obtaining blood samples such as cardiac puncture or decapitation yield only one blood sample per animal since the animal is killed by the procedure. When

*Corresponding author email: nsm_karim@yahoo.com

using techniques like orbital sinus puncture and cutting of the tail serial blood sampling is possible however the sample volume that can be obtained is very small and the procedure is stressful for the animal. Drawing of blood from peripheral sites such as the tail may result in a different pharmacokinetic outcome than using blood taken from central sites (Chiou, 1989[a]; Chiou, 1989[b]).

Need of Cannulation

Frequent sampling increases the stress for the animal and if this is necessary the scientist should consider cannulation. Even in the short term, this technique is a favorable alternative to repeated venepuncture. Cannula (Cann.) can be implanted and used in place of multiple needle entries at any one site, or indeed in place of single sampling from several sites within a relatively short time period.

Short Term and Long Term Cannulation

If sampling over a few hours is required a temporary cann. (short term) such as a butterfly needle or a plastic cann. held in place with tape or some form of bandage could be used. Long term cannulation as indwelling jugular cann. is very suitable for repeated shorterm multiple sampling. Whatever the method employed, surgical skills are essential to position and fix the cann (Gellai and Valtin, 1979; Desjardins, 1986; Dennis *et al*., 1986; Van Dongen *et al*., 1990).

Maintaining Position bf Cannula

In both short term (upto 1 day) and long term (2 days or more) cannulation it may be necessary to restrain the animal in some way to stop it removing the cann. but this depends very much on the species. Smaller mammals like rats are often restrained by some form of harness, swivel and tether along which the cann. runs. Cannulae can be maintained in dogs, pigs, rats and rabbits without the use of harnesses or jackets for example by using simple skin buttons and tygon tubings.

Site of Cannulation

Cannulation is suitable for use in all strains of rats and can be used to take blood from the femoral artery and vein, carotid artery, jugular vein, vena cava and dorsal aorta Blood Sampling Microsite Rat (2007).

Patency of Cannula

In small animals cannulae remain patent for at least 2 to 3 days and some workers have achieved patency for 3 to 4 weeks or longer. Different techniques are available to maintain the patency of the catheter Kohn *et al*. (1997) and Luo *et al.* (2000). Patency can be maintained by using suitable anticoagulant solution as heparin. It is also necessary when considering cannulation to differentiate between infusion and the administration of substances and the removal of blood. It is easier to administer compounds than to remove blood long term, as thrombi attached to the end of a cann. can act as a one way value permitting infusion but restricting withdrawal.

Material of Cannula

Polypropylene polyethylene, nylon and rubber cannulae have been used but silicone rubber or silastic and TygonTM cannulae appears to be the most biocompatible and can be obtained in a sufficient range of sizes. Non-silastic materials tend to cause fibrotic reactions with time whereas silastic types seem to cause little reaction, even after 18 months. The problem with silastic is that it is too flexible arid, therefore predisposed to kinking. It is also easy to obstruct the lumen by over-tightening anchoring ligatures and care should be taken to check patency at the time of operation. To avoid the problem of a small cann. kinking, a polypropylene cann. inside a larger silastic cann. can be used, or a polypropylene cann. can be coated with silastic paint. This will have the effect of combining the greater rigidity of polypropylene with the biocompatibility of silastic. This type of cann. is less easily kinked, easier to flush and will also give accurate pressure measurements than silastic alone.

Placement of Jugular Cannula

Two main mechanisms exist for securing a cann. First by placing it in the lumen of the vein and tying it in place to the vein itself. This is what we have done. Second the cann. can be inserted into a tributary of the target vein with the tip in the lumen of the major vein. The former method involves tying off a vein and destroying its patency but usually this has little effect on the animal. With a jugular cann. the tip may be left very close to the right atrium in the cranial or caudal vena cava. Care should be taken not to place it within the right atrium since cardiac arrhythmias may be induced and this may lead to death by atrial fibrillation.

Sealing the Cannula

The cann. can end in a multiple entry point for example, a silicone rubber stopper can be attached to the end of the cann. and this can be pierced several times. This has the advantage that it is self sealing and will better protect against microbial contamination of the fluid column within the cann. These can be found on a saline drip bag or the plunger seal from a 1 ml disposable syringe and can be inserted into a luer mount of a needle which in turn is inserted into the end of cann. Alternatives are filling the mount with silastic glue, plugging the end with a spigot of solid plastic or metal, heat sealing of the tube ending (Morton *et al*., 1993).

Exit Site of Cannula

Two common sites are there to make the exit of the cann. first at the back of neck and second between the shoulder blades, other exit sites are also possible but over the back is safe as animal cannot interfere with it specially rats cannot chew them in this position usually. Care should be

taken to ensure that cann. should not kink when the animal moves moreover correct length of cann. is very important because if it is too short the cann. may be pulled out or if the length of tubing is too much then it may lead to flexion or kinking. Thus when the rat grows the relative position of the catheter will be shifted which may affect its patency (Thrivikraman *et al*., 2002).

Keeping Cannula Patent after Use

When collecting blood from a cann. the anticoagulant mixture in the cann. should first be removed by drawing it into a syringe until fresh blood appears. The blood sample can then be taken. The "dead space" in the cann. then should be replaced by a fresh anticoagulant to prevent thrombosis. Appropriate anticoagulants include heparin saline (10- 1000 IU/ml) or sodium citrate (0.05% w/v) or either of these in a dense solution such as 25-50% glucose, 5-40% polyvinylpyrrolidine to maintain cann. patency, the cann. should be flushed with saline at least twice a week, if not daily.

Complications with Cannulae

Various complications can occur with cannulae like blockage, infection, accidental removal, gastric ulcers. Rats may develop gastric ulcers because of long term restraint and tethering (Brodie and Hanson, 1966). Appropriate use of anticoagulants & proper flushing of cann. can avoid most of these complications.

Volume of Blood to be Removed

Removal of around 10% of the circulating blood volume will initiate homeostatic cholinergic mechanisms. Cardiac output and blood pressure will be reduced if 15-20% of blood volume is removed. Removal of 30-40% can induce haemorrhagic shock and 40% loss can cause 50% mortality in rats (McGuill and Rowan, 1989). Circulating blood volume in rats is 50-70ml/kg assuming the animal is mature, healthy and on an adequate diet. Circulating blood volume is lower about 15% in obese and older animals. Upto 10% of the circulating blood volume can be taken on a single occasion. For repeat bleeds at shorter intervals a maximum of 1% of an animal's circulating blood volume can be removed every 24 hours.

0.01 X circulating blood volume (ml/day) roughly = 0.6 ml/kg/day.

Care should be taken to replace the blood by infusing equal volume of saline or equal volume of blood from a donor animal. Blood withdrawal and fluid replacement must be performed slowly over 1-2 minutes and at a steady rate. Fluid replacement should be done with sterile, warm physiologic saline equal to the volume of blood collected Mcgill University (2005).

Anaesthesia for Jugular Vein Cannulation

An injectable balanced anaesthetic mixture which is preferred for use is prepared by mixing 1.0ml acepromazine maleate (10mg/ml), 4ml sterile water, 2.5ml ketamine HCl and 2.5ml xylazine HCl in a sealed vial Thrivikraman *et al*. (2000). The older technique of using pentobarbital (nembutol) is also followed. These can be given subcutaneously or intraperitoneally with a 25-G needle. For surgical anaesthesia the mixture is administered at a dose of 125-150µl/100gm body weight and for pentobarbital the dose is 30-50 mg/kg body weight Anesthesia and Analgesia of Mice and Rats (2003). Inhalation (gas) anaesthetics have been used successfully Wotjak *et al*. (1996) and Liebsch *et al.* (1998) for catheterization surgery, however these agents must be used with appropriate gas scavenging systems. Charles River Laboratories in USA are using injectable anesthetics for majority of procedures performed on rodents. Intraperitoneal route of administration is principally used to reduce potential tissue damage from intramuscular and subcutaneous injections. This is accomplished with a one inch needle ranging in size from 20-23gauge. Using a larger gauge needle prevents the inadvertent introduction of anesthetics into the lumen of the abdominal viscera. Smaller gauge needles are more likely to penetrate the lumen of organs due to a high total entry force on the needle tip coupled with the small lumen size of the needle. Typically injections are administered in the lower left or lower right abdominal quadrant with the animal in the head down position. The combination of anesthetics being preferred by them for surgery is Ketamine: Xylazine:sterile water = 2:1:10, administered at the rate of 3.0ml/kg.

Use of Analgesics

The standard default analgesic used by North American Research Models Surgical Services is an opioid, buprenorphine hydrochloride. An alternative non-steroidal anti-inflammatory agent (NSAID), flunixin meglumine is available for substitution. The dosages for Buprenorphine are 0.02mg/kg when under anesthesia and 0.05mg/kg when awake, administered subcutaneously. The dosage for latter is 1.1mg/kg subcutaneously every 12 hours if necessary Surgical Capabilities (2005). The same analgesic was dissolved in Nutella chocolate & provided to rats at a dose of 0.4mg/kg body weight every day, as a means of postoperative pain relief Flecknell (1998).

Heat Loss

Because the ratio of body surface area to mass is greater in small rodents than in large domestic animals, heat dissipation during surgery & post-surgical recovery is common with general anesthesia. This can cause significant variations in the metabolism of anesthetics and hence the rate of recovery. This heat loss also affects cardiovascular performance, as well as the urinary excretion of anesthetics, thereby prolonging anesthesia. For this reason during the surgical period, as well as postoperatively, supplemental heat is provided to the

animals via heated surfaces. The temperature of the heating devices should be closely monitored to avoid harmful elevation in temperature on the skin's surface that could result in burns. Generally the animals are removed from the heated surface when their righting reflexes are regained and they can maintain normal posture Surgical Capabilities (2005).

Surgical Technique

Precautions

A. Surgical gloves, eye protection, long-sleeved gown, closed in shoes.
B. All instruments and materials (including catheter) must be sterilized before use.
C. Surgery must be performed under aseptic conditions

Equipments

A. Anaesthetic
B. 70% Alcohol
C. Heparinized saline
D. Scalpel (No 22), scissors, forceps, haemostats
E. Silk ligatures
F. Suture material or staples
G. Sterile Cannula (Cann) O.D 1.05mm x I.D 0.5mm

Procedure

1. Anaesthetize rat (specify dose, route and volume).
2. Lay the rat on its back with the head away from the surgeon.
3. Measure the distance required by the cann. (around 3-4cms or ~20 cm if exteriorizing via stainless steel spring at the back of neck).
4. Shave hair on the ventral neck from midline to 1cm past jugular groove and swab the skin with alcohol.
5. Make a 1.5-2.0mm incision in the neck to one side of the midline. Blunt dissect away the fat and connective tissue.
6. Pass a pair of haemostats under the vein and place 2 ligatures around the vein.
7. Using blunt dissection, clear the area of connective tissue and fat until the bifurcation of the internal and external jugular veins is exposed.
8. Loosely position ties around the internal and external branches and the common jugular vein (i.e., one tie on each of the three branches of vein).
9. Raise the posterior ligatures and hemi-transect the vein between the two ligatures.
10. Introduce a heparinized saline filled cann. into the vein and advance it towards the heart. Verify the patency of the catheter by withdrawing blood. Flush with heparinized saline.
11. Tie the anterior ligature firmly around the catheter once inside the common jugular vein. Tie the posterior ligatures around the cann. and vein.
12. Grasp the cann. and create a "stress loop"
13. Secure the catheter loop with the posterior ligatures
14. Shave the dorsal neck and swab with alcohol.
15. Make a 0.5-1.0ml incision and create a s/c tunnel using a straight pair of haemostats.
16. Cut the cann. leaving 2.5-3.0cm exterior to the skin.
17. Suture the skin or pass the catheter through a stainless steel spring and suture the base of the spring into the subcutaneous pocket at the back of the neck The University of Queensland (2004).

In fact it would not have been possible to evaluate temporal pattern of hypothalamic pituitary adrenal (HPA) axis responses to stressors in conscious rats without the use of repeated blood sampling technique Plotsky *et al*. (1992) Engelmann *et al.* (1996), Thrivikraman *et al*. (1997), Thrivikraman *et al*. (1999), Ladd *et al.* (2000), Arborelius *et al*. (2000) and Huot *et al*. (2001). Vascular access techniques have been employed to collect blood samples since 1960's Cocchetto and Bjornsson (1983) and Lestage *et al.* (1985) in many neuroendocrinological Pich *et al*. (1993), Bohus (1998) and Lightman *et al*. (2000) and pharmacological studies Rawlings *et al*. (1994), Booze *et al*. (1997) and Rivier *et al.* (1999).

As most of our present knowledge in animal physiology comes from experiments performed on anesthetized animals or from in vitro studies the utility of these preparations is often curtailed when highly complex neural or hormonal regulatory mechanisms are investigated. Basal secretion rates and plasma levels of most hormones are drastically influenced by anesthesia and surgical trauma (Pettinger, 1975; Depocas and Behrens, 1977; Carruba *et al*., 1981) and even simple handling of animals may have profound effects. Thus from an ethical perspective, there is a moral mandate to strive to reduce stress in laboratory animals during normal husbandry as well as during and after experimental procedures. From a scientific point of view, stress is a well known and unwanted source of experimental error, because the natural response of an animal to stressors includes alterations in the normal physiology and metabolism. This may add between animal variation in responses to experimental procedures Hau *et al*. (2001) and Morton and Hau (2002).

In conclusion stress in animals is a recognized cause of experimental errors. Use of vascular access in small laboratory animals is a delicate and very good tool for the scientists and researchers to avoid stress and carry out the time course studies. In addition it is helpful in determining the cytokine and hormonal levels using less number of animals at a time. Jugular vein cannulation being a surgical procedure, is also associated with disadvantages but these are few and minor like it requires skill and time consuming, it is not very easy in comparison to tail puncture or tail clipping and if jugular vein happens to be ruptured it can be dangerous for the animal but all these can be easily overcome by carefully practicing the surgical skill. Thus Jugular vein

cannulation is a better method of cannulation in comparison to other vascular access ports in rats as it provides the overwhelming advantage of replacing the lost volume in the animal besides giving an opportunity to get larger blood volume for measurement of hormones which are present in circulation in low concentrations.

ACKNOWLEDGEMENT

The authors are thankful to Professor Joshua R. Berlin, Department of Physiology & Pharmacology, University of Medicine & Dentistry, New Jersey (UMDNJ), USA with whose help the work on vascular cannulation in rats was done by the authors as a part of postdoctoral fellowship in 2006.

REFERENCES

Anesthesia and Analgesia of Mice and Rats. 2003. Newark Research Animal Facility Standard Operating Procedures. University of Medicine and Dentistry New Jersey, USA.

Angela, Heiser. 2007. Rat jugular vein and carotid artery catheterization for acute survival studies. A Practical Guide. Springer.com.

Arborelius, L., Skelton, KH., Thrivikraman, KV., Plotsky, PM., Schulz, DW. and Owens, MJ. 2000. Chronic administration of the selective cotricotropin releasing factor I receptor antagonist CP-154, 526:Behavioral, endocrine and neurochemical effects in the rat. J Pharmacol Exp Ther. 294:588-597.

Blood sampling Microsite Rat: Blood vessel cannulation (surgical). 2007. http://www.nc3rs.org.uk/bloodsamplingmicrosite/page 1-2.

Bohus, BGJ. 1998. Neuroendocrinology of stress, behavioral and neurobiological considerations. In: Methods in Neuroendocrinology, Ed. VandeKar, LD. CRC Press, Boca Raton FL.163-180.

Booze, RM., Lehner, AF., Wallace, DR., Welch, MA. and Mactutus, CF. 1997. Dose response cocaine pharmacokinetics and metabolite profile following intravenous administration and arterial sampling in unanesthetized freely moving male rats. Neurotoxicol Teratol. 19:7-15.

Bradfield, JF., Schachtman, TR., McLaughlin, RM. and Steffen, EK. 1992. Behavioral and physiologic effects of inapparent wound infection in rats. Lab Anim Sci. 42:572-578.

Brodie, DA. and Hanson, HM. 1966. Restraint induced gastric lesions. J Industrial Med. 12:5601-5606.

Cannulation. 2008. en.Wikipedia.org/wiki/cannulation.

Cannulation. 2008. www.chop.edu/consumer/jsp/division/generic.jsp.

Carruba, MO., Picotti, GB., Miodini, P., Lotz, W. and Prada, DA. 1981. Blood sampling by chronic cannulation technique for reliable measurements of catecholamines and other hormones in plasma of conscious rats. J Pharmacol Methods. 5:293-303.

Chiou, WL. 1989[a]. The phenomenon and rationale of marked dependence of drug concentration on blood sampling site. Implications in pharmacokinetics, pharmacodynamics, toxicology and therapeutics (Part I). Clinical Pharmacokinetics.17:75-199.

Chiou, WL. 1989[b]. The phenomenon and rationale of marked dependence of drug concentration on blood sampling site. Implications in pharmacokinetics, pharmacodynamics, toxicology and therapeutics (Part II). Clinical Pharmacokinetics.17:275-290.

Cocchetto, DM., Bjornsson, TD. 1983. Methods for vascular access and collection of body fluids from the laboraotory rat. J Pharm Sci. 72:465-492.

Darlington, DN., Shinsako, J. and Dallman, MF. 1986. Responses of ACTH, epinephrine, norepinephrine and cardiovascular system to hemorrhage. Am J Physiol. 251:H612-H618.

Dennis, MB Jr., Cole, JJ. and Scribner, BH. 1986. Vascular Access in large laboratory animals. In methods of Animal Experimentation. Research Surgery and Care of the Research Animal, part-A – Patient care, Vascular Access and Telemetry. Eds. Gay, WI. and JE Heavner, JE. (Vol. VII). Academic Press.143-194.

Depocas, F. and Behrens, WA. 1977. Effects of handling, decapitation, anesthesia and surgery on plasma noradrenaline levels in the white rat. Can J Physiol Pharmacol. 55:212-219.

Desjardins, C. 1986. Indwelling vascular cannulas. In: Methods of Animal Experimentation. Vol VII: Research Surgery and Care of the Research Animal Part-A – Patient care, Vascular Access and Telemetry. Eds. WI Gay and JE Heavner. Academic Press. 143-194.

Engelmann, M., Thrivikraman, KV., Su, Y., Nemeroff, CB., Montkowski, A., Landgraf, R., Holsboer, F. and Plotsky, PM. 1996. Endocrine and behavioral effects of airpuff - startle in rats. Psychoneuro-endocrinology. 21:391-400.

Fagin, KD., Shinsako, J. and Dallman, MF. 1983. Effects of housing and chronic cannulation on plasma ACTH and corticosterone in the rat. Am J Physiol. 245. Endocrinol Metab 8. E515-E520.

Flecknell, PA., Roughan, JV. and Stewart, R. 1998. Use of oral burprenorphine (buprenorphine jello) for

postoperative analgesia in rats – a clinical trial Laboratory Animals. 33:169-174.

Garcia, A., Marti, O., Valles, A., Dal-Zotto, S. and Armario, A. 2000. Recovery of the hypothalamic pituitary adrenal response to stress. Neuroendocrinology. 72:114-125.

Gellai, M. and Valtin, H. 1979. Chronic vascular constrictions and measurements of renal function in conscious rats. Kidney International. 15:419-426.

Hau, J., Anderson, E. and Carlssen, HE. 2001. Development and validation of a sensitive ELISA for quantification of secretory IgA in rat saliva and faeces. Laboratory Animals. 35:301-306.

Huot, RL., Thrivikraman, KV., Meaney, MJ. and Plotsky, PM. 2001. Development of adult ethanol preference and anxiety as a consequence of neonatal maternal separation in long evan rats and reversal with antidepressant treatment. Psychopharmacology (Berl). 158:366-373.

Kohn, Df., Wixson, SK., White, WJ. and Benson GJ, (Eds.) 1997. Anesthesia and analgesia in laboratory animals. Academic Press, San-Diego, CA, USA.

Ladd, CO., Huot, Rl., Thrivikraman, KV., Nemeroff, CB., Meahey, MJ. and Plotsky, PM. 2000. Long term behavioral and neuroendocrine adaptations to adverse early experience. Prog Brain Res. 122:81-103.

Lestage, P., Vitte, PA., Rolinat, JP., Minot, R., Broussolle, E. and Bobillier, P. 1985. A chronic arterial and venous cannulation method for freely moving rats. J Neurosci Methods. 13:213-222.

Liebsch, G., Linthorst, ACE., Neumann, ID., Reul, JMHM., Holsboer, F. and Landgraf, R. 1998. Behavioral, physiological and neuroendocrine stress responses and differential sensitivity to diazepam in two Wistar rat lines selectively bred for high and low anxiety related behavior. Neuropsychopharmacology. 19:381-396.

Lightman, SL., Windle, RJ., Julian, MD., Harbuz, MS., Shanks, N., Wood, SA., Kershan, YM. and Ingram, CD. 2000. Significance of pulsatility in the HPA axis. Novartis Found Symp. 227:244-257.

Luo, YS., Luo, YL., Ashford, EB., Morin, RR., White, WJ. and Fisher, TF. 2000. Comparison of catheter lock solutions in rats. http://www.criver.com/products/surgery/resources.html.

Mcgill University. 2005. University Animal Care Committee. UACC Standard Operating Procedure No. 1. Blood Collection- Rodents (Rats, mice and guinea pigs). October version.

McGuill, MW. and Rowan, AN. 1989. Biological effects of blood loss: implications for sampling volumes and techniques. ILAR News. 31:5-18.

Morton, DB. and Hau, J. 2002. Welfare assessment and humane endpoints. In Handbook of Laboratory Animal Science. Vol 1. Eds. Hau, J. and LVan Hoosier Jr. and Boca Raton, FL. CRC Press.457-486.

Morton, DB., Abbot, D., Barclay, R., Close, BS., Ewbank, R., Gask, D., Heath, M., Mattic, S., Poole, T., Seamer, J., Southee, J., Thompson, A., Trussell, B., West, C. and Jennings, M. 1993. Removal of blood from laboratory mammals and birds. First report of the BVA/FRAME/RSPCA/UFAW Joint Working Group on Refinement. Laboratory Animals. 27:1-22.

Nicolaidis, S., Rowland, N., Meile, MJ., Marfaing-Jallat, P. and Pesez, A. 1974. A flexible technique for long term infusions in unrestrained rats. Pharmacology, Biochemistry Behaviour. 2:131-136.

Pettinger, WA., Tanaka, K., Keeton, K., Campbell, WB. and Brooks, SN. 1975. Renin release, an artifact of anesthesia and its implications in rats. Proc Soc Exp Biol Med. 148:625-630.

Pich, EM., Heinrichs, SC., Rivier, C., Miczek, KA., Fisher, DA. and Koob, GF. 1993. Blockade of pituitary adrenal axis activation induced by peripheral immunoneutralization of corticotrophin releasing factor does not affect the behavioral response to social defeat stress in rats. Psychoneuroendocrinology. 18:495-507.

Plotsky, PM., Thrivikraman, KV., Watts, AG. and Hauger RL. 1992. Hypothalamic pituitary adrenal axis function in the Zucker obese rat. Endocrinology. 130:1931-1941.

Popovic, VP., Kent, KM. and Popovic, P. 1963. Technique of permanent cannulation of the right ventricle in rats and ground squirrels. Proceedings of the Society for Experimental Biology and Medicine. 113:599-602.

Popp, MB. and Brennan, MF. 1981. Long term vascular access in the rat: Importance of asepsis. Am J Physiol. 241:H606-612.

Rawlings, JM., Provan, WM., Wilks, MF. and Batten, PL. 1994. Comparison of two methods for determining the toxicokinetics of flazifop butyl after intravenous dosing in rats. Hum Exp Toxicol. 13:123-129.

Reilly, J. 1998. Variables in animal based research part 2. Variability associated with experimental conditions and techniques. ANZCCART News. 11:1-12.

Rivier, JE, Kirby, DA., Lahrichi, SL., Corrigan, A., Vale, WW. and Rivier, CL. 1999. Constrained corticotrophin releasing factor antagonists (astressin analogues with long duration of action in the rat. J Med Chem. 42:3175-3182.

Surgical Capabilities. 2005. Charles River Laboratories. Reference paper (volume 13). Eds. Flecknell, PA., Roughan, JV. and Stewart, R. Use of oral buprenorphine (buprenorphine jello) for postoperative analgesia in rats- a clinical trial. Laboratory Animals. 33: 169-174.

Suzuki, K., Koizumi, N., Hirose, H., Hokao, R., Takemura, N. and Motoyoshi, S. 1997. Blood sampling technique for measurement of plasma arginine vasopressin concentration in conscious and unrestrained rats. Lab Anim Sci. 47:190-193.

Terao, N. and Shen, DD. 1983. Alterations in serum protein binding and pharmacokinetics of 1-propranolol in the rat elicited by the presence of an indwelling venous catheter. J Pharmacol Exp Ther. 227:369-375.

The University of Queensland. 2004. Standard operating procedures. Laboratory Animal Research. SOP No. AHT 52.

Thrivikraman, KV., Ladd, CO. and Plotsky, PM. 1999. HPA axis responses to stressors modulated by feedback sensitive and resistant neurocircuitry. Soc Neurosci Abst. 25:707.

Thrivikraman, KV., Nemeroff, CB. and Plotsky, PM. 2000. Sensitivity to glucocorticoid mediated fast feed back regulation of the hypothalamic pituitary adrenal axis is dependent upon stressor specific neurocircuitry. Brain Res. 870:87-101.

Thrivikraman, KV., Rebecca, L., Huot, P. and Plotsky, M. 2002. Jugular vein catheterization for repeated blood sampling in the unrestrained conscious rat. Brain Research Protocols. 10:84-94.

Thrivikraman, KV., Su, Y. and Plotsky. PM. 1997. Patterns of Fos-immunoreactivity in the CNS induced by repeated hemorrhage in conscious rats: correlations with pituitary adrenal axis activity. Stress. 2:145-158.

Torner, L., Thrivikraman, KV., Toschi, NN., Holsboer, F., Plotsky, PM. and Neumann, LD. 2000. Effect of adrenalectomy and corticosterone on hypothalamic and peripheral release of oxytocin and behavioral stress coping in male rats. Soc Neurosci Abstr. 26:422.

Torres-Molina, F., Aristorena, JC., Garcia, CC., Granero L., Chesa-Jimenez, J., Pla-Delfina, J. and Peris-Ribera, JE. 1992. Influence of permanent cannulation of the jugular vein on pharmacokinetics of amoxicillin and antipyrine in the rat. Pharmaceutical Research. 9:1578-1591.

Van Dongen, JJ., Remie, R., Rensema, JW. and VanWunnik, GHJ (Eds.). 1990. (Microsurgery on the laboratory rat, Part 1 Elsevier. 159-169.

Weissman, C. 1990. The metabolic response to stress: an overview and update. Anesthesiology. 73:308-327.

Word Net Search for: Cannulation. 2008. available at http://wordnet.princeton. edu/perl/webwns-cannulation.

Wotjak, CT., Kubota, M., Liebsch, G., Montkowski, A., Holsboer, F., Neumann, I. and Landgraf, R. 1996. Release of vasopressin within the rat paraventricular nucleus in response to emotional stress: a novel mechanism of regulating adrenocorticotropic hormone secretion? J Neurosci Methods. 16:7725-7732.

Yoburn, BC., Morales, R. and Inturrisi, CE. 1984. Chronic vascular catheterization in the rat: Comparison of three techniques. Physiol Behav. 33:89-94.

Received: July 3, 2008; Revised: August 5, 2009; Accepted: August 21, 2009

SENRA Academic Publishers, Burnaby, British Columbia
Vol. 3, No. 3, pp. 937-941, 2009
ISSN: 1715-9997

Canadian Journal of pure&applied sciences

Short Communication

A STUDY ON THE INDUCED EFFECT OF β-CYPERMETHRIN ON SKIN OF *EUPHLYCTIS CYANOPHLYCTIS*

Ghazala Yasmeen, Zaheer M Khan and Adil Akbar
Department of Zoology – Wildlife and Fisheries
University of Karachi, Karachi-75270

INTRODUCTION

The pollution of lakes and rivers with chemicals of anthropogenic origin may have adverse consequences the waters become unsuitable for drinking, irrigation, fish cultivation, household purposes, and the animal communities living in them may suffer seriously (Clickman and Lech, 1982). The amphibians are important part due to their value as indicators of environmental stress (Blaustein, 1994; Blaustein and Wake, 1995). They are in close contact with water as larvae and mostly have some contact with land as adults. Therefore, they experience both aquatic and terrestrial stressors. They have moist, permeable skin and unshelled eggs that are directly exposed to soil, water and sunlight, more sensitive to environmental toxins or to changes in patterns of temperature or rainfall than are other terrestrial vertebrate groups (Blaustein and Wake, 1990; Vitt, *et al*., 1990). The most obvious factors contributing to amphibian population decline are habitat destruction and alteration (Alford and Richards, 1999). A variety of pathogens affect wild amphibian populations. These include viruses, bacteria, parasites, protozoans, oomycetes, and fungi (Blaustein *et al.,* 1994; Jancovich *et al.,* 1997; Kiesecker and Blaustein, 1997; Longcore *et al.*, 1999; Johnson *et al*., 2002). These pathogens can be the proximate causes of mortality or they can cause sublethal damage such as severe developmental and physiological deformities. Pathogens may infect amphibians at various life stages. There are some observations of pathogens causing massive die-offs of amphibians. Of particular concern to a number of investigators is whether the diseases of amphibians are novel or if they are being triggered by an environmental change. A wide array of contaminants may affect amphibian populations which include pesticides, herbicides, fungicides, fertilizers and numerous pollutants (Sparling *et al.,* 2000). A diversity of pesticides and their residues are present in a wide variety of aquatic habitats (Harris *et al*., 1998; McConnell *et al*., 1998; Le Noir *et al*., 1999; Kolpin *et al*., 2002).

Many pyrethroids have emerged as an important class of agricultural pesticides due to their high bio-efficacy and relatively low toxicity in comparison to several organochlorine (OC) and organophosphorous (OP) pesticides (Casida *et al*., 1983) and are used in households, cereals, vegetable, cotton, tobacco, and other crops (Clickman and Lech, 1982; Smith and Stratton, 1986). During last 50 years, the application of pesticides and chemical fertilizers has increased rapidly in Pakistan, and the volume of pesticides has been used from 665 tons in 1980 to 70,000 tons in year 2002 (Iftikhar, 2003). Several studies already have been reported that some pesticides reduced cholinesterase (ChE) in frog *Rana tigrina* (Khan *et al.*, 2002[a,b] and 2003[a]) and in *Rana cyanophlyctis* (Khan *et al.*, 2003[b,c,d] ; Khan and Yasmeen, 2005; Khan *et al.*, 2006; Khan *et al.*, 2007[a]). There is some indication that field application of these pesticides may be deleterious to amphibians (Jolly *et al.*, 1978; Thybaud, 1990; Berril *et al.*, 1993; Materna *et al*., 1995). Pyrethroids appear to affect voltage-dependent neuromuscular sodium channels producing tremors, hyperexcitation and convulsions (Van den Bercken, 1977; Vijverberg *et al.,* 1982; Ruigt and Van den Bercken, 1986).

The histology of the normal amphibian skin has been described by Patt and Patt (1969) and Green (1999). The present study was aimed to determine the induced effects of pesticide β-Cypermethrin (pyrethroid) on skin of *E. cyanophlyctis*.

MATERIALS AND METHODS

The experimental work was carried out on adults of skittering frog *E. cyanophlyctis,* collected from selected areas of Sindh Province. Collected frogs were brought in laboratory and kept in glass aquarium in Wildlife and Fisheries Lab, Department of Zoology, University of Karachi. Frogs were fed with prawns and insects. For the treatment of β-Cypermethrin, 0.08ml was injected in the sub-cutaneous abdominal region of frog by using insulin syringe. Weight of each frog was measured before and after treatment. The effects of pesticide were observed on

*Corresponding author email: ghazala_yasmin@live.com

the skin during 90 days after the treatment. Histological study of skin cells was carried out by sectioning of fixed tissue by Paraffin Section Technique. The tissue was fixed, dehydrated in graded series of alcohols, cleared in xylene and finally embedded in paraffin wax. Hematoxylin & Eosin (HE) and periodic acid-schiff stain (PAS) were used for staining. Mounted in a synthetic resin DPX (Kiernan, 1990).

RESULTS AND DISCUSSION

The amphibian's skin plays important role in survival and their ability to exploit a wide range of habitats and ecological conditions (Clarke, 1997). Frog does not drink like higher animals but absorbs the required water through its skin. In the present study, after 90 days of post treatment of β-Cypermethrin, the induced effects were observed on the skin of *E. cyanophlyctis*, samples were examined, and it was found that the skin was covered with fibrocollagenous tissue and skeletal muscle tissue. Mild chronic inflammatory cells were also identified in the fibrocollagenous tissue with focal areas of necrosis.

The microscopic studies of skin cells of treated *E. cyanophlyctis* showed complete necrosis of the skin, with loss of the glands and even necrosis of the underlying cutis or possibly musculature. The subcutaneous lymph sac has also disappeared (see Fig.1). The skin section shows distinctly accumulation of inflammatory material in the subcutaneous lymph sac (see Fig. 2), this most probably is a bacterial infection. The Hematoxylin and eosin (HE) stained slide (see Fig. 3) elucidates the same elements as the periodic acid-schiff (PAS) stained slide (see Fig. 4) which shows the details of figure 3 (near the upper right corner). This again explains the presence of cellular exudates in the subcutaneous lymph sac. The PAS stained slide (see Fig. 4) exhibits the normal epidermis, normal cutis and glands. The open space lined with a very delicate endothelium (slender nucleus at the epidermal side) is a lymph space. The dark violet irregular strands are normal constituent of the frog skin, and this layer is related to water management. In the right lower corner, the dense connective tissue of normal sub-cutis is visible, and no any alterations were recognized.

Little is known about the diseases of wild amphibians. Many disease agents are present in healthy animals and disease occurs when immune system is compromised (Crawshaw, 1992; Alford and Richards, 1999). The observations that amphibians are dying in large numbers due to infectious disease raise the critical question concerning why amphibian immune systems are not successful in combating these pathogens? Amphibian immune defenses involve both innate and adaptive components that together lack only a few elements of mammalian immune systems (Carey *et al.,* 1999; Du Pasquier *et al.,* 1989) some information exists on the influence of environmental factors on the effectiveness of these defenses (Carey *et al.,* 1999**)**, this phenomenon could be due to a pesticide as well. However, the interaction of amphibian immune systems with viruses and the defenses against fungal skin infections have not been examined in detail.

The components of the innate immune system, such as macrophages, neutrophils, and antimicrobial peptides, provide the primary protection against fungal skin infections (Carey *et al.,* 1999). Histological examinations of the epidermis of amphibians suffering from fungal skin infections reveal relatively few immune responses. Fungal penetrations into the outer layer of epidermis caused little or no inflammation of the epidermis, besides few neutrophils, lymphocytes and macrophages were observed in infected skin (Pessier *et al.,* 1999; Taylor *et al.,* 1999). This sort of inflammation has been described to be caused by cytokines produced by macrophages and neutrophils in response to a foreign invader (Janeway and Travers, 1996). Therefore, inflammation is an important component of immune defense because it results in increased permeability of blood vessels. Since the pesticide could exert effects on blood properties, membrane permeability and other physiological parameters (Khan *et al.*, 2002[a,b]; Khan and Yasmeen, 2005 and 2008; Khan *et al.*, 2006, 2007[a] and 2008), thus it is conceivable, though it has not been proved that pesticide could affect on blood vessels permeability.

The change in permeability fosters the release of soluble mediators, such as immunoglobulins and complement, and also assists in recruitment of circulating leucocytes to the site of infection. While the lack of an inflammatory response could result from a number of factors. However, the fungi could produce compounds that inhibit the inflammatory response whereas macrophages and neutrophils may not recognize these fungi as pathogens, and consequently these fungi cause insufficient tissue necrosis to stimulate the inflammatory response, or other factors. This type of relatively low involvement of macrophages in mycotic epidermal infections suggests that formation of memory T and B cells and antibodies would be limited. Few amphibians appear to survive chytrid infections (Berger *et al.,* 1999), but if some do, they would likely face a repeat attack with little improvement in their resistance. Another study Khan *et al.* (2007[b]) observed the induced effect of pesticide Chlorpyrifos (organophosphate) on skin of *E. cyanophlyctis*, and reported that skin covered with fibrocollagenous tissue exhibiting areas of necrosis and aggregates of mild chronic inflammation.

In the present study, some sections examined revealed skin is covered with fibrocollagenous tissue and skeletal

muscle tissue. Mild chronic inflammatory cells were identified in the fibrocollagenous tissue with focal area of necrosis. In a case complete necrosis of the skin, with loss of the glands and even necrosis of the underlying cutis or possibly musculature was recorded, where it seems subcutaneous lymph sac has disappeared. However, it could be that the mass of cellular exudates in the subcutaneous lymph sac. Though, in this respect inflammatory material might have appeared as a result of other factors, therefore, it could not be a sole consequence of pesticide effect, hence, it remained for confirmations. The purpose of the study was to investigate the effect of β-Cypermethrin (pyrethroid) on skittering frog *E. cyanophlyctis* though histopathology conclusion indicated no strong treatment-related findings. Further study is necessary to evaluate the relative susceptibility of adult frog to key pesticides in order to utilize these species as sentinels of pesticide toxicity.

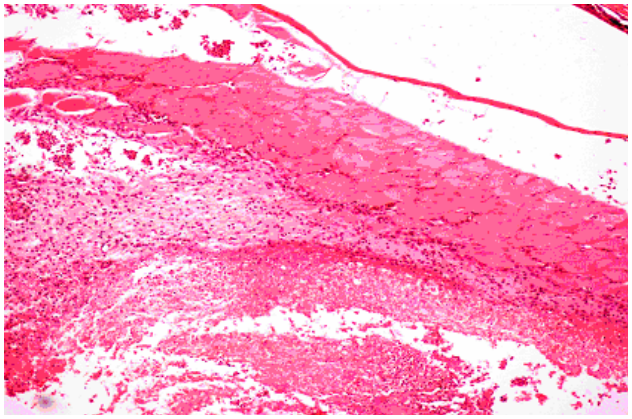

Fig. 1. Skin section of treated *E. cyanophlyctis* showing complete necrosis of the skin.

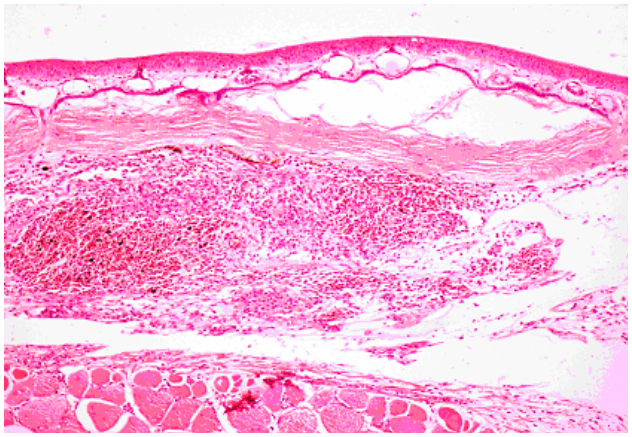

Fig. 2. Skin section of treated *E. cyanophlyctis* showing accumulation of inflammatory material in the subcutaneous lymph sac.

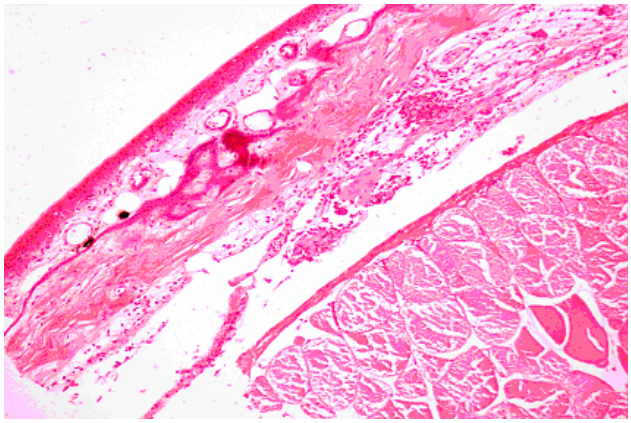

Fig. 3. Skin section of treated *E. cyanophlyctis* showing the presence of cellular exudates in the subcutaneous lymph sac.

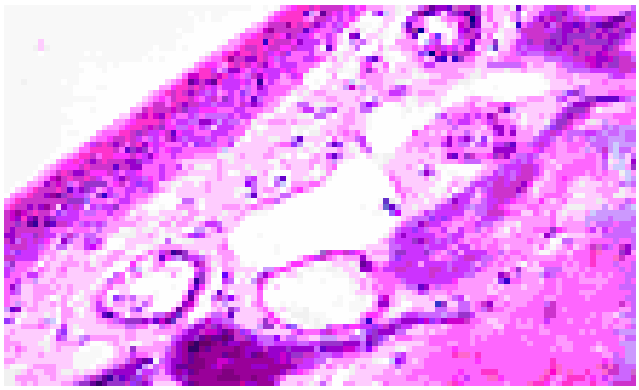

Fig. 4. Skin section of treated *E. cyanophlyctis* showing the normal epidermis, glands and dense connective tissue of normal sub-cutis.

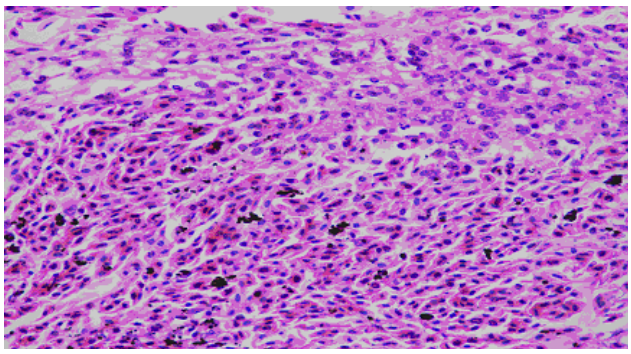

Fig. 5. Skin section of lab standard of *E. cyanophlyctis* showing normal structure of skin cells.

ACKNOWLEDGEMENT

For diagnosis we are thankful to Professor P. Zwart, Pathologist of amphibians, reptiles and invertebrates, Utrecht University, The Netherlands.

REFERENCES

Alford, RA. and Richards, SJ. 1999. Global amphibian declines: a problem in applied ecology. Ann. Rev. Ecol. Syst. 30:133-165.

Berger L, Speare, R and Hyatt, A. 1999. Chytrid fungi and amphibian declines: overview, implications and future directions. In: Declines and Disappearances of Australian Frogs. Ed. Campbell, A. Canberra Environment Australia. 21-31.

Blaustein, AR. and Wake, DB. 1990. Declining amphibian populations: a global phenomenon? Trends Ecol. Evol. 5:203-4.

Blaustein, AR. 1994. Chicken Little or Nero's fiddle? A perspective on declining amphibian populations. Herpetologica. 50:85-97.

Blaustein, AR. Hokit, DG., O'Hara, RK. and Holt, RA. 1994. Pathogenic fungus contributes to amphibian losses in the Pacific Northwest. Biol. Conserv. 67:251-254.

Blaustein, AR. and Wake, DB. 1995. The puzzle of declining amphibian populations. Sci. Am. 272:52-57.

Berril, M., Bertram, S., Wilson, A., Louis, S,, Brigham, D. and Stromberg, C. 1993. Lethal and sub-lethal impacts of pyrethroid insecticides on amphibian embryos and tadpoles. Environ. Toxicol. Chem. 12:525-539.

Carey, C., Cohen, N. and Rollins-Smith, L. 1999. Amphibian declines: an immunological perspective. Devel. Comp. Immunol. 23:459-472.

Casida, JE., Gamnion, DW., Glickman, AH. and Lawrence, LJ. 1983. Mechanism of selective action of pyrethroid insecticides, Annu. Rev. Pharmacol. Toxicol. 23:413-418.

Clarke, BT. 1997. The natural history of amphibian skin secretions, their normal functioning and potential medical applications. Biol. Rev. 72:365-379.

Clickman, AH. and Lech, JJ. 1982. Differential toxicity of transper-methrin in rainbow trout and mice. II. Role of target organ sensitivity. Toxicol. Appl. Pharmacol. 66:162-171.

Crawshaw, GJ. 1992. The role of disease in amphibian decline. In: Declines in Canadian Amphibian Populations: Designing a National Monitoring Strategy. Eds. Bishop, CA. and Pettit, KE. Can. Wildlife Serv. Occas. pap. 76:67-70.

Du Pasquier, L., Schwager, J. and Flajnik, MF. 1989. The immune system of *Xenopus*. Ann. Rev. Immunol. 7:251-275.

Green, DE. 1999. Amphibian Medicine and Husbandry, Krieger publishing.

Harris, ML., Bishop, CA., Struger, J., Ripley, B. and Bogart, JP. 1998. The functional integrity of northern leopard frog (*Rana pipiens*) and green frog (*Rana clamitans*) populations in orchard wetlands. II. Genetics, physiology, and biochemistry of breeding adults and young of the year. Environ. Toxicol. and Chemistry. 17:1338-1350.

Iftikhar, A. 2003. The Integrated Pest Management Program. PARC Newsletter 23.

Jancovich, JK., Davidson, EW., Morado, JF., Jacobs, BL. and Collins, JP. 1997. Isolation of a lethal virus from the endangered tiger salamander *Ambystoma tigrinum stebbinsi.* Dis. Aquat. Organ. 31:161-167.

Janeway, CA. and Travers, P. 1996. Immunobiology. Current Biology Ltd. London.

Johnson, PT., Lunde, JKB., Thurman, EM., Ritchie, EG, Wray, SN., Sutherland, DR., Kapfer, JM., Frest TJ., Bowerman, J. and Blaustein, AR. 2002. Parasite (*Ribeiroia ondatrae*) infection linked to amphibian malformations in the western United States. Ecol. Monogr. 72:151-168.

Jolly, AL. Jr., Avault, JW. Jr., Koonce, KL. and Graves, JB. 1978. Acute toxicity of Permethrin to several aquatic animals. Trans. Am. Fish Soc. 107: 825-827.

Jr, Koonce KL. and Graves, JB. 1978. Acute toxicity of permethrin to several aquatic animals. Trans. Am. Fish Soc. 107:825-827.

Khan, MZ., Fatima, F. and Ahmad, I. 2002[a]. Effect of Cypermethrin on Protein Contents in Lizard *Calotes versicolor* in comparison to that in Frog *Rana tigrina.* Online Journal of Biological Sciences. 2(12):780-781.

Khan, MZ., Shah, EZ., Ahmed, I. and Fatima, F. 2002[b]. Effects of agricultural pesticides permethrin (pyrethroid) on protein contents in kidney and liver of lizard species *Calotes versicolor* in comparison to that in frog *Rana tigrina*. Bull. of Pure & App. Sc. 21A (2):93-97.

Khan, MZ., Tabassum, R., Naqvi, SNH., Shah, EZ., Tabassum, F., Ahmad, I., Fatima, F. and Khan, MF. 2003[a]. Effect of Cypermethrin and Permethrin on Cholinesterase Activity and Protein Contents in *Rana tigrina* (Amphibia).Turk. J. Zool. 27: 243-246.

Khan, MZ., Nazia, M., Fatima, F., Rahila, T. and Gabol, K. 2003[b]. Comparison of the effect of Lamda cyhalothrin with permethrin on cholinesterase activity in *Rana cyanophlyctis* and *Rana tigrina (Ranidae:* amphibian). Bull. of Pure & App. Sc. 22A (1): 43-49.

Khan, MZ., Maria, Z. and Fatima, F. 2003[c]. Effect of Lamda Cyhalothrin (Pyrethroid) and Monocrotophos (Organophosphate) on Cholinesterase activity in liver, kidney and brain of *Rana cyanophlyctis.* Korean J. Biol. Sci. 7: 165-168.

Khan, MZ., Fatima, F., Mahmood, N. and Yasmeen, G. 2003[d]. Comparison of Cholinesterase activity in the brain tissue of lizard *Calotes versicolor* with that of frog *Rana cyanophlyctis* under the effect of Cypermethrin, Lamda Cyhalothrin, Malathion and Monocrotophos. Bulletin of Pure and Applied Sciences. 22 A (2):105-112.

Khan, MZ. and Yasmeen, G. 2005. Pesticide dependent cholinesterase activity in brain of *Rana cyanophlyctis* (amphibian) J. Exp. Zool. India. 8 (1):135-140.

Khan, MZ., Yasmeen, G. and Hamid, S. 2006. Effect of Sundaphos (Organophosphate) and b-Cypermethrin (Synthetic Pyrethroid) on Cholinesterase activity in liver and kidney of *Euphlyctis cyanophlyctis.* Hamadryad. 30(1&2):176-180.

Khan, MZ., Rais, M. and Yasmeen, G. 2007[a]. Inhibitory effects on cholinesterase activity produced by the two different pesticides on brain, liver and kidney of *Euphlyctis cyanophlyctis.* J. Exp. Zool. India.10(1):89-93.

Khan, MZ., Yasmeen, G., Akbar, A. and Khan, MF. 2007[b]. Determination of induced effect of pesticide chlorpyrifos (organophosphate) on skin of *Euphlyctis cyanophlyctis*. J. Basic Appl. Sci. 3(2): 101-105.

Khan, MZ., Yasmeen, G., Naqvi, SNH. and Perveen, A. 2008. The activity of Cholinesterase and Alkaline Phosphatase in liver, kidney and brain of *Euphlyctis cyanophlyctis* under the effect of Chlorpyrifos and Dathrin. Canadian J. of Pure & Applied Sci. 2(2):349-356.

Khan, MZ. and Yasmeen, G. 2008. Effect of Sandaphos and ß-Cypermethrin exposure on cholinesterase and alkaline phosphatase activity in liver, kidney and brain of *Euphlyctis cyanophlyctis*. Canadian J. of Pure & Applied Sci. 2(3):511-519.

Kiernan, JA. 1990. Histological and Histochemical Methods: Theory and Practice, (2nd ed.). Pergamon Press, Oxford.

Kiesecker, JM. and Blaustein, AR. 1997. Egg laying behavior influences pathogenic infection of amphibian embryos. Conserv. Biol. 11:214-220.

Kolpin, DW., Furlong, ET., Meyer, MT., Thurman, EM., Zaugg, SD., Barber, LB. and Buxton, HT. 2002. Pharmaceuticals, hormones, and other organic wastewater contaminants in US. streams, 1999-2000: a national reconnaissance. Environmental Science and Technology. 36:1202-1211.

LeNoir, JS., McConnell, LL., Fellers, GM., Cahill, TM. and Seiber, JN. 1999. Summertime transport of current-use pesticides from California's central valley to the Sierra Nevada mountain range. US Environ. Toxicol. Chem. 18:2715-2722.

Longcore, JE., Pessier, AP. and Nichols, DK. 1999. *Batrachochytrium dendrobatidis* gen. and sp. nov., a chytrid pathogenic to amphibians. Mycologia 91:219-227.

Materna, EJ., Rabeni, CF. and La Point, TW. 1995. Effects of synthetic pyrethroid insecticides, esfenvalerate, on larval leopard frogs (*Rana spp*.) Environ. Toxicol. Chem. 14:613-622.

McConnell, LL., LeNoir, JS., Datta, S. and Seiber, JN. 1998. Wet deposition of current-use pesticides in the Sierra Nevada Mountain range, California, USA. Environ. Toxicol. Chem. 17:1908-1916.

Patt, DI. and Patt, GR. 1969. Comparative Vertebrate Histology, Harper and Row, New York. 117-121.

Pessier, AP., Nichols, DK., Longcore, JE. and Fuller, MS. 1999. Cutaneous chytridiomycosis in poison dart frogs (*Dendrobates spp*.) and White's tree frogs (*Litoria caerulea*). J. Vet. Diagn. Invest. 11:194-199.

Ruigt, GSF. and Van den Bercken, J. 1986. Action of pyrethroids on a nerve muscle preparation of the clawed frog *Xenopus leavis.* Pestic. Biochem Physiol. 25:176-187.

Smith, TM. and Stratton, GW. 1986. Effect of synthetic pyrethroid insecticides on non target organisms. Residue Rev. 97:93-120.

Sparling, DW., Linder, G. and Bishop, CA. 2000. Ecotoxicology of amphibians and Reptiles. SETAC. Pensacola, FL, USA.

Taylor, SK., Williams, ES. and Mills, KW. 1999. Effects of malathion on disease susceptibility in Woodhouse's toads. J. Wildl. Dis. 35:436-541.

Thybaud, E. 1990. Acute toxicity and bioconcentration of lindane and deltamethrin in tadpoles of *Rana temporaria* and the mosquito fish *Gambusia affinis.* Hydrobiologia. 190:137-146.

Van den Bercken, J. 1977. The action of allethrin on the peripheral nervous system of the frog. Pestic. Sci. 8: 692-699.

Vijverberg, HPM., Zalm, JM. and Bercken, JVD. 1982. Similar mode of action of pyrethroids and DDT on sodium channel gating in myelinated nerves. Nature. 259:601-603.

Vitt, LJ., Caldwell, JP., Wilbur, HM. and Smith, DC. 1990. Amphibians as harbingers of decay. Bio Sci. 40:418-18.

Received: May 4, 2009; Revised: Sept 26, 2009; Accepted: Sept 30, 2009

SENRA Academic Publishers, Burnaby, British Columbia
Vol. 3, No. 3, pp. 943-951, 2009
ISSN: 1715-9997

Canadian Journal of pure&applied sciences

GLOBAL STUDY OF GEOMAGNETIC INDUCED CURRENT USING TIME DERIVATIVES OF GEOMAGNETIC FIELDS

Falayi EO and Beloff N
Space Science Centre, University of Sussex, Falmer, BN1 9QJ, UK

ABSTRACT

This report investigates variations in time derivatives of the geomagnetic field observed during great storms known to have caused disruption and to have had other adverse effects on power grids. The geomagnetic storms considered were those of 24th November 2004, 30th October 2003 and 28th October 2004, which occurred during the Autumnal event, and also 7th April 2000 and 31st March 2001 which occurred during the Spring events. Geomagnetic field variations are associated with geoelectric field variation at the surface of the Earth which is influenced by the conductivities of different structures of the Earth's interior. The induced electric field is proportional to the rate of change of the geomagnetic field, which explains why many researchers have used time derivatives of the geomagnetic field as a measure of GIC strength. Koen and Gaunt (2002) established that variation exceeding 30nT/min of the time derivatives of the geomagnetic field component appears to be significant, causing undesirable consequences in power grids.

Keywords: Time derivatives of geomagnetic fields, GIC (Geomagnetic induced current), higher latitudes.

INTRODUCTION

The Sun is the primary driver of space weather and most of the events have their origin in the corona. When intense surges of solar wind reach the Earth, many changes occur in the Earth's magnetosphere. On the dayside the solar wind dynamic pressure acts on the magnetosphere, forcing the magnetosphere current to become compressed closer to the surface of the Earth and the geomagnetic field to fluctuate. This is refers to as a geomagnetic storm. During geomagnetic storms the current in the higher latitudes changes as a result of the solar wind. These currents produce their own magnetic field and, combined with the Earth's magnetic field, are called geomagnetically induced currents (GICs). GICs are the ground end, space weather effect which are driven in technology systems such as electrical power transmission grids, oil and gas pipelines, phone cables and railway systems by the geoelectric field induced by geomagnetic storms at the Earth's surface.

It should also be noted that space weather-related spacecraft anomalies can occur even when there is no CME (coronal mass ejection) driven storm or high-speed stream. Energy transferred from the solar wind to the magnetosphere through the merging of the interplanetary and terrestrial magnetic field builds up in the magnetotail until it is explosively released in episodic events known as magnetospheric substorms. Substorms which occur during non-storm times as well as storm times inject energetic plasma into the inner magnetosphere and can cause an electrical charge to build up on spacecraft surfaces. The electrostatic discharge that occurs subsequently is one of the major causes of spacecraft anomalies.

GIC creates problems for all technological systems leading to economic losses and social disruption. Systems in the high magnetic latitudes, such as the northern United States, Canada, Scandinavia and Russia, are at particular risk because Earth's magnetic fields converge near the geographic poles. Oil and gas pipelines can be damaged by corrosion when buried in the ground. The voltage between a pipeline and the Earth strongly influence the electrochemical environment at the pipeline surface, which leads to corrosion occurrence (Trichtenko and Boteler, 2002; Boteler, 2000; Boteler *et al*., 1998; Gummow, 2002; Pirjola, 2002).

GIC is a function of many parameters including time derivatives of the horizontal geomagnetic field, the electric resistance of the Earth, and the geometry and resistance of the power grid. Recently, Poppe and Jordan (2006) established that GIC also occurs at mid and low latitudes even at Africa and South Africa (Baker and Skinner, 1980; Ogunade, 1986; Osella and Favetto, 2000). In South Africa, saturation of a transformer led to serious problems followed by the collapse of the whole system during the famous Halloween storm in October-November 2003. For large storms (or increasing dB/dt levels) both observations and simulations indicate that as the intensity of the disturbance increases, the relative levels of GIC and related power system impact will also increase proportionately. In these scenarios, the scale and

*Corresponding author email: olukayodefalayi@yahoo.com

speed of the problems that could occur on exposed power grids have the potential to impact power system operators in ways they have not previously experienced. Therefore, as storm environments reach higher intensity levels, it becomes more likely that these events will precipitate widespread blackouts in exposed power grid infrastructures.

GICs are driven by rapid variations in ionospheric current at high latitudes. Here the most intense GIC are experienced. These variations are thought to be related to the intensification of the electrojet during enhanced ionospheric convection conditions and to the development of the substorm current wedge during geomagnetic storms (Pulkkinen *et al*., 2003).

The objective of this paper is to study the effect of geomagnetic storm on power grids. The geomagnetic storm considered were those of 24th November 2004, 30th October 2003 and 28th October 2004, which occurred during the Autumn, and those of 7th April 2000 and 31st March 2001 which occurred during the spring. Data obtained from www.spaceweather.gc.ca/effect_e.php have been used to determine the rate of disturbance to magnetic storms occurring in different region; auroral region (Thule, 77.4^0), subauroral (Iqaluit, 63.7^0), mid (Boulder 40.1^0) and lower region (Tucson, 32.2^0).

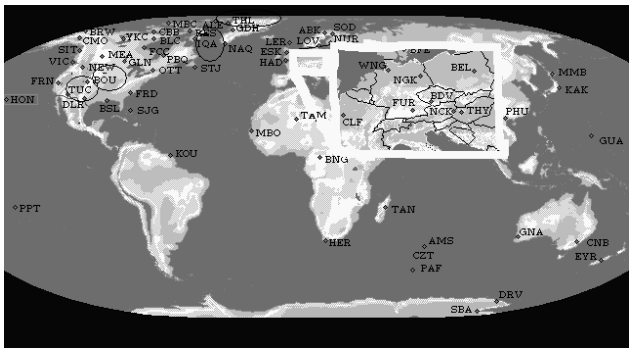

Fig. 1. Geographic location of the observatories.

OBSERVATIONS

24th November 2001

The event of November 24th 2001 was a severe magnetic storm which was characterized by a pronounced SSC (sudden storm commencement) that started at 5: 50UT in the auroral region. The disturbance lasted for about 10 hours with enhancement in the auroral electrojet index 3242nT exceeding 3000nT with a maximum value of rate of change of disturbance of dBx/dt 150nT/min, dBy/dt 150nT/min and dBz/dt 100nT/min at higher latitudes (geographic latitude Thule 77.5^o).

In the subauroral region large enhancements of the geomagnetic field were observed at 6:00UT with large geomagnetic variation (dBx/dt 350nT/min, dBy/dt 2000nT/min and dBz/dt 200nT/min) measured at Iqaluit (63.7^o). The time of occurrence of the substorm at mid latitude (Boulder 40.1^o) coincided with the onset in the subauroral region and its amplitude was not big enough for it to be considered active storm in the mid latitude region (dBx/dt 60nT/min, dBy/dt 30nT/min and dBz/dt 15nT/min). It is also clear that the rate of change of disturbance from the auroral latitude reached the lower latitude at Tucson, 32.2^o (dBx/dt 60nT/min, dBy/dt 20nT/min and dBz/dt 4nT/min). The large geomagnetic variation with a significant geoelectric field and high GIC magnitude took place during the geomagnetic storm in the auroral region.

Leonard *et al*. (2000) suggested that the electric currents in the ionosphere are the major factor in geomagnetic disturbance in the auroral region and also that the geoelectric field and other parameters are essential in computing GIC in a power system. It is also known that GIC are a proxy for the rate of change of the geomagnetic field (Trivedi *et al*., 2007). Less geomagnetic field variation is associated with low GIC value and geoelectric fields, which implies that GIC values were less active at Tucson (geographic latitude 32.2^o) and also that minimum values of time derivatives of the geomagnetic field were not big enough to drive the transformers at the power stations into saturation (see Fig. 2).

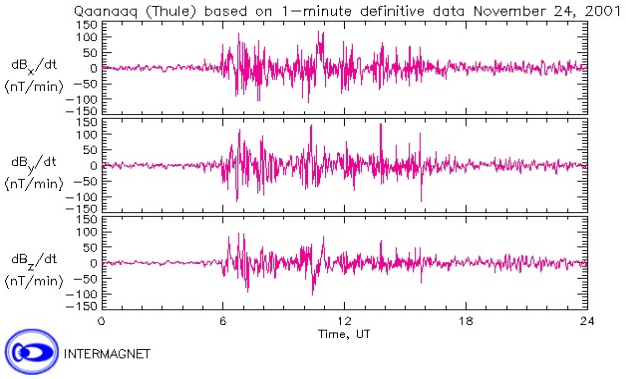

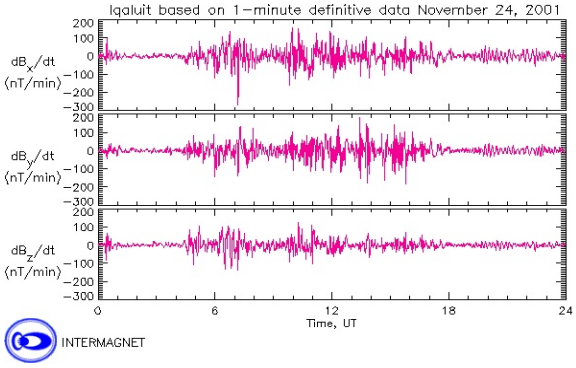

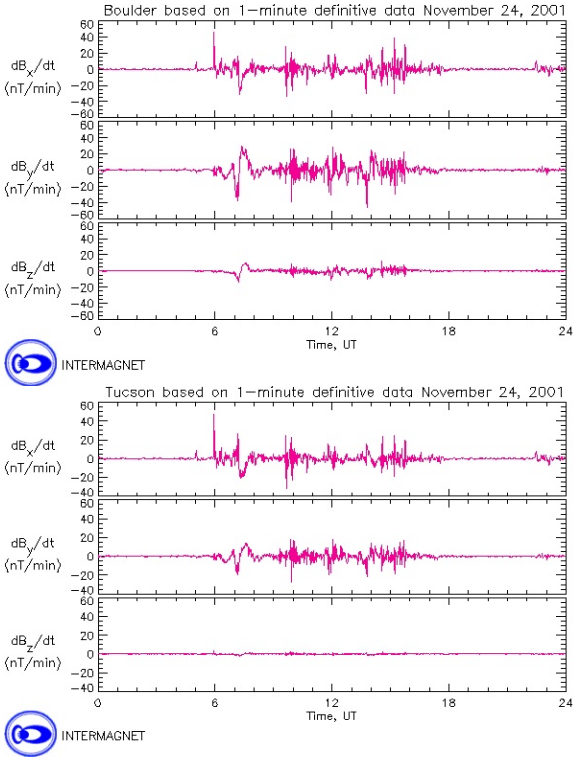

Fig. 2. Variation of the time derivatives on 24th November 2001 (a) auroral region at Qaanaaq. (b) subauroral region at Iqaluit. (c) mid latitude at Boulder (d) lower region at Tucson.

30th October 2003

The 30th October 2003 storm, known as the Halloween storm, attracted wide attention from scientists and industrial communities. On 30th October the IMF (Interplanetary Magnetic Field) reached the Earth with a southward orientation due to the magnetic reconnection between the IMF and Earth's magnetic field. As a result of this, the magnetic field was able to connect to the IMF directly so that energetic particles in the solar wind were free to enter the Earth's magnetosphere along the magnetic lines. The energetic particles entered the Earth's magnetosphere, causing the largest geomagnetic storm of 2003, as measured by the low latitude Dst index, and were also associated with ionospheric intensification.

The time derivatives signatures represent a characteristic scenario in the evolution of the geomagnetic field from a quiet period to a highly fluctuating one, and extended to the next day. In Figure 3, the first time derivatives signatures was seen in the early morning and another signature was observed at 16:20UT at the auroral region which was associated with increasing energy input from solar wind and dynamic reconfiguration in the magnetotail, as suggested by Pulkkinen *et al*. (2003). Enhancement of time derivatives of geomagnetic disturbance was also observed in the subauroral region (Iqaluit 63.7^0) in the early morning (1:50UT), with dBx/dt 120nT/min, dBy/dt 220nT/min and dBz/dt 150nT/min and at 11:00UT with dBx/dt 200nT/min, dBy/dt 300nT/min and dBz/dt 100nT/min. Another signature was also noticed between the hours of 1700UT and 1800UT with dBx/dt 300nT/min, dBy/dt 300nT/min and dBz/dt 50nT/min. In the mid latitudes, during the 30th October storm the rate of disturbance was noticed pre-midnight, with dBx/dt 40nT/min, dBy/dt 70nT/min and dBz/dt 50nT/min. Strong driving magnetospheric activity can cause auroral oval to expand towards the mid latitudes. In view of this, variations in ionospheric current can also cause large GICs at latitude where GIC is not typically experienced (Pulkkinen *et al*., 2000). In low latitude regions the effects of this substorm were noticed in the north and east components of the rate of change of geomagnetic disturbance dBx/dt 50nT/min, dBy/dt 30nT/min and dBz/dt 9nT/min.

The magnetic field measurements are very important in determining the intensity, location and orientation of the auroral electrojet which are the major causes of the geomagnetic disturbance. The enhancement of the auroral electrojet index on 30th October was 3375nT with a Dst index of -383nT. Leonard *et al*. (2000) emphasised that variations in the time derivatives of the magnetic field are due to changing intensity and movement of the electrojet. When the magnetic field increases, the resulting electric fields are found to be anti-parallel to the electrojet, while it is parallel to the electrojet, the magnetic field is found to be decreasing.

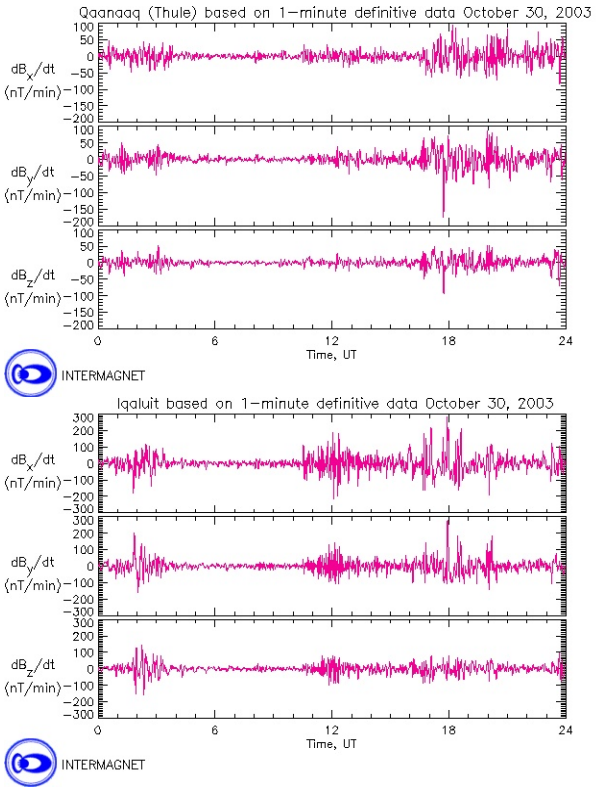

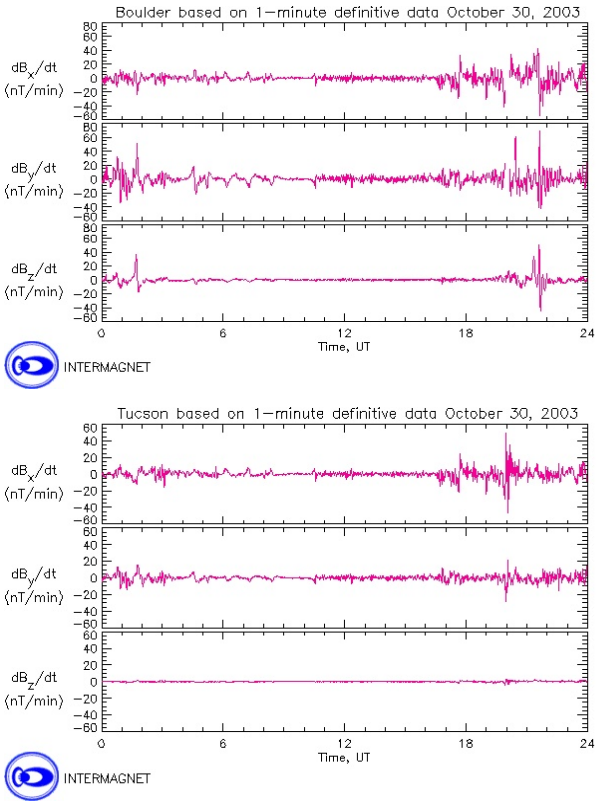

Fig. 3. Variation of the time derivatives on 30th October 2003 (a) auroral region at Qaanaaq. (b) subauroral region at Iqaluit. (c) mid latitude at Boulder (d) lower region at Tucson.

28th October 2004

We observed that dBx/dt is larger in comparison with dBy/dt and dBz/dt. The burst in time derivatives occurred at practically the same time 3:30UT (see Figure 4) in different region. The Subauroral region substorm was observed at 3:30UT in the early morning sector with high values of rate of change of disturbance of dBx/dt 130 nT/min, dBy/dt 100nT/min and dBz/dt 100nT/min. At mid latitude it was noticed that the time derivatives responded to the disturbance signature which occurred in the early morning with low value time derivatives of the geomagnetic field. The time derivatives of the north and east components at low latitude responded to the disturbance with low values of time derivatives of the geomagnetic field but the southward component of the time derivatives of the geomagnetic field did not respond to the disturbance. From our analysis we discovered that variation of the geomagnetic field during large magnetic storm induces electric current in high voltage transmission lines. GIC are a problem to higher latitudes, like the auroral and subauroral, also during large geomagnetic storms GIC can appear at all latitudes.

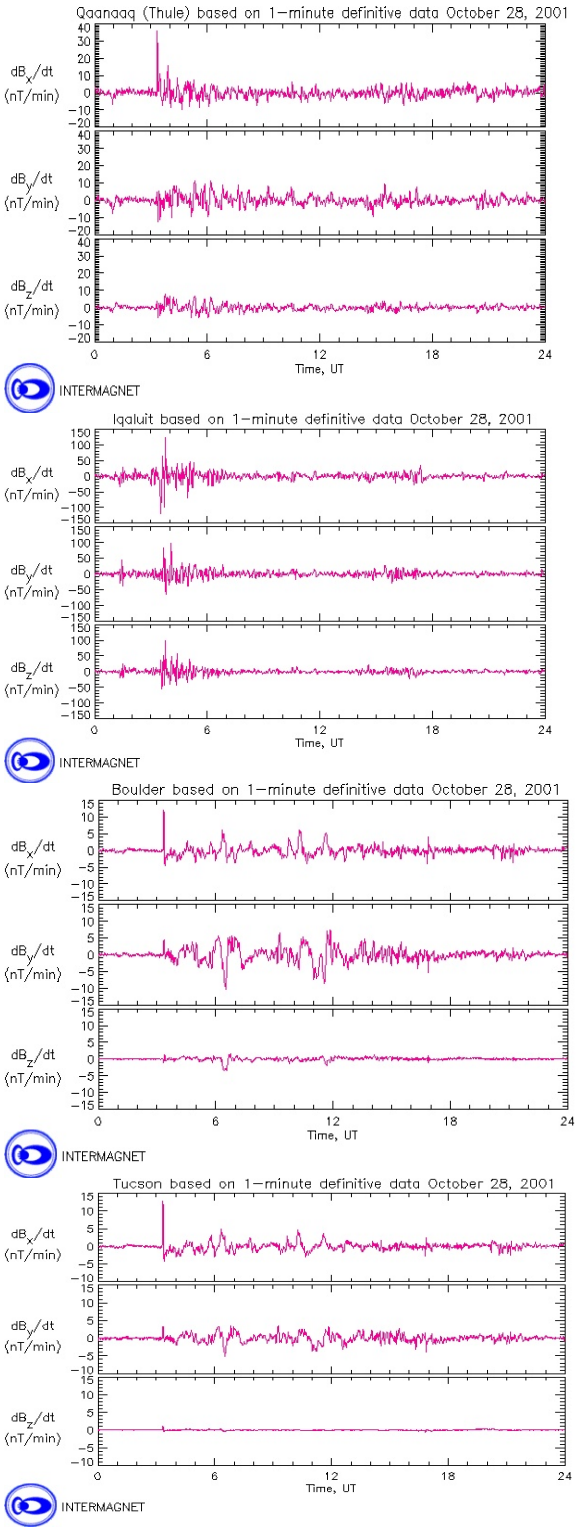

Fig. 4. Variation of the time derivatives on 28th October 2001 (a) auroral region at Qaanaaq. (b) subauroral region at Iqaluit. (c) mid latitude at Boulder (d) lower region at Tucson.

7th April 2000

From Figure 5, the magnetospheric shock associated with sudden impulse or storm sudden commencement was noticed pre-midnight on 6th April 2000 and main phase events occurred on the 7th April 2000, during a strong geomagnetic storm triggered by a complex interplanetary structure passing near the Earth. The first, second and third signatures of disturbance were observed at 00:00UT, 7:00UT and 17:00UT. In the auroral region the first signature values were dBx/dt 20nT/min dBy/dt 25nT/min and dBz/dt 17nT/min at 0:00UT. The second signature was noticed at the hour of 7:00UT with values of dBx/dt 30nT/min, dBy/dt 10nT/min and dBz/dt 10nT/min and the third signature was noticed at 17:00UT. Also in the subauroral region the geomagnetic field signature was observed at 00:00UT with dBx/dt 60nT/min, dBy/dt 20nT/min and dBz/dt 21nT/min, another was noticed at 7:00UT with values of dBx/dt 50nT/min, dBy/dt 42nT/min and dBz/dt 30nT/min while the third signature with the highest rate of disturbance occured at 17:00UT

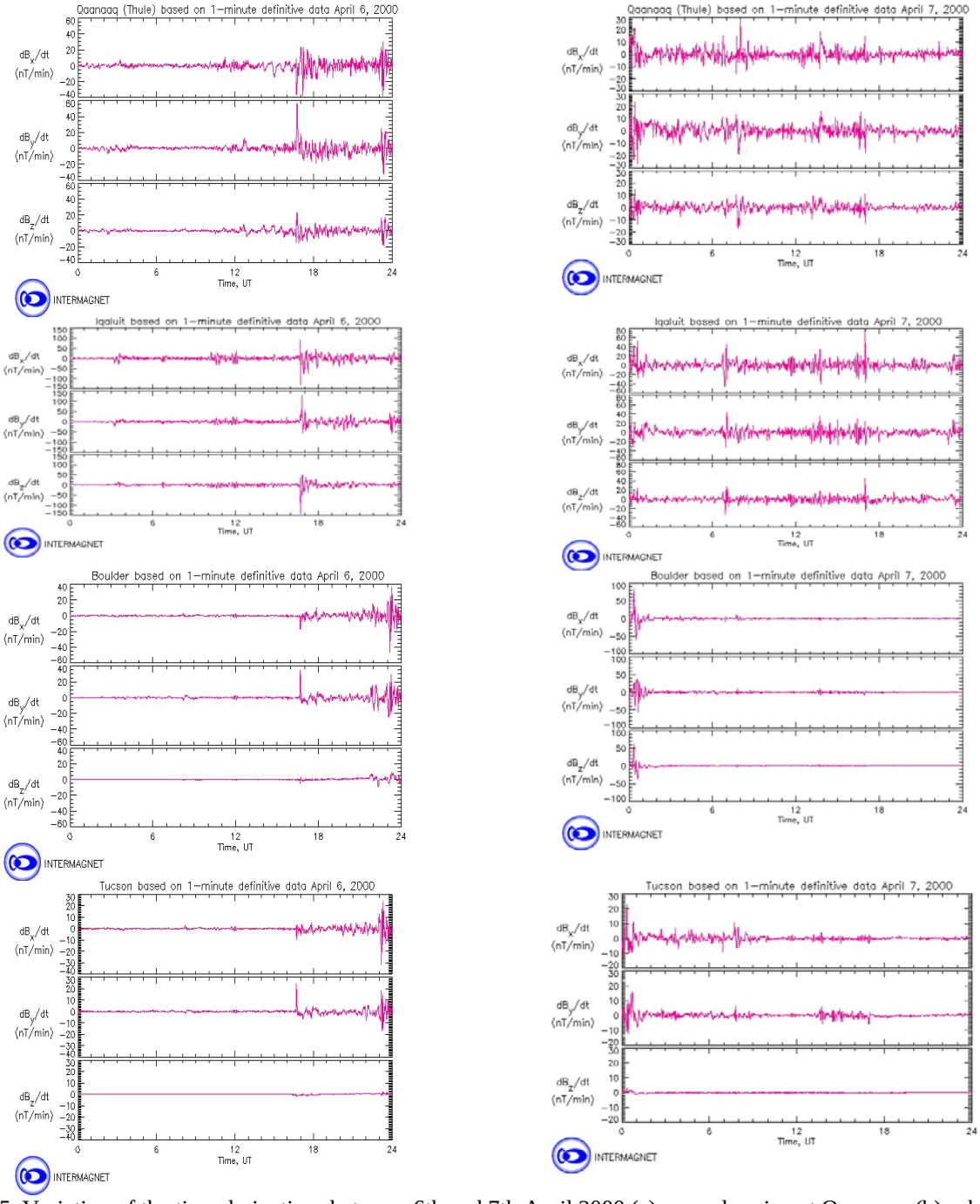

Fig. 5. Variation of the time derivatives between 6th and 7th April 2000 (a) auroral region at Qaanaaq. (b) subauroral region at Iqaluit. (c) mid latitude at Boulder (d) lower region at Tucson.

with dBx/dt 80nT/min, dBy/dt 20nT/min and dBz/dt 45nT/min.

When an increased dB/dt occurs at this location, the increases may be due to enhancement in the spectral content of the disturbance. An interesting result was also observed at mid latitude with a high value of disturbance in the early morning after 00:00UT with dBx/dt 100nT/min, dBy/dt 40nT/min and dBz/dt 60nT/min. At low latitude, the disturbances also occurred in the early morning after 00:00UT with dBx/dt 25nT/min, dBy/dt 16nT/min and dBz/dt 3nT/min.

31st March 2001

In the early hours of 31st March 2001, a sudden burst in the geomagnetic field occurred after 00:00UT (dB/dt 90nT/min dBy/dt 80nT/min and dBz/dt 90nT/min) in the auroral region under the enhanced westward electrojet; the rate of change of disturbance lasted for several hours (see Fig. 6). In the subauroral region, we noticed a high value of the rate of disturbance, dB/dt 300nT/min, dBy/dt 200nT/min and dBz/dt 200nT/min at 1:00UT. At mid latitude, the rate of disturbance at 6:20UT was dBx/dt 80nT/min, dBy/dt 190nT/min and dBz/dt 30nT/min. At low latitude, the rate of change of disturbance noticed in the early morning at 1:00UT was dBx/dt 70nT/min, dBy/dt 15nT/min and dBz/dt 6nT/min**.** Kappenman (2003) established that the risk of GIC is plausible. It may become apparent on power grids at very low latitude locations that are typically not concerned about or seldom in the proximity of large electrojet intensification.

The sudden burst of disturbance can extend to mid and low latitudes while large electrojet disturbances are generally confined to high latitudes. At low latitudes large GIC flow in power grids due to SSC. For example Fukumitsu is a substation in Japan (geographic latitude ~34^0, geomagnetic latitude ~ 26^0) where a peak GIC of 40A was observed during a moderate storm event on 6th November 2001. It was also reported that New Zealand experienced failure in a large power transformer due to an SSC event (Small, 2003).

6th November 2001

Another chain was observed on 6th November, 2001 at Qeqertarsuaq (GDH 69.2^0, 306.5) in the auroral region with dBx/dt 190nT/min, Narsarsuaq (NAQ 61.2^0 , 314.6) in the subauroral region with dBx/dt 200nT/min, St John (STJ 47.6^0, 307.3) at mid latitude with dBx/dt 120nT/min and Korou (KOU 5.2^0, 307.3) in the low latitude region with dBx/dt 40nT/min**.** Geomagnetic storms can cause serious problems for the operation of power systems, disrupting the functioning of transformers. Obviously, the amplitude of the time derivatives of the geomagnetic field, on this occasion, was big enough to drive the transformer into saturation. One can infer from the result that GIC do

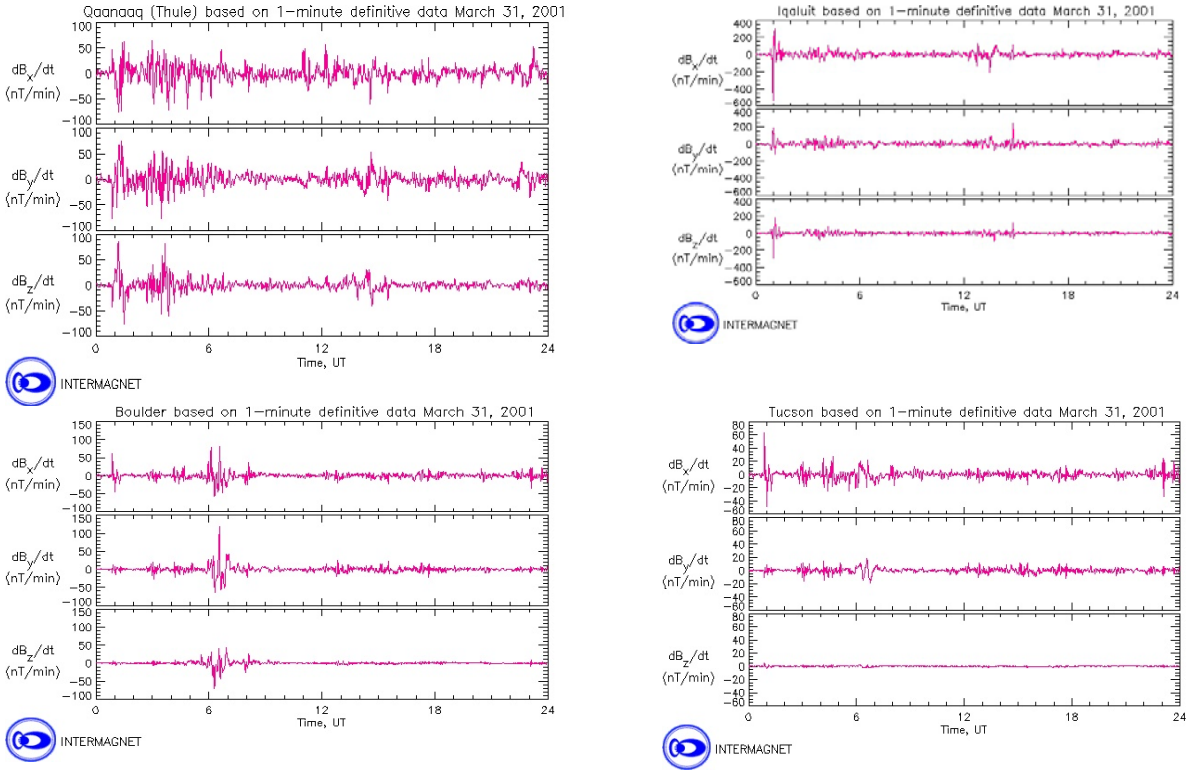

Fig. 6. Variation of the time derivatives at 31 March 2001 (a) auroral region at Qaanaaq. (b) subauroral region at Iqaluit. (c) mid latitude at Boulder (d) lower region at Tucson.

appear at low and mid latitudes. Meanwhile, even low latitudes confirm the presence of SSC events and large GIC flow (see Fig. 7).

DISCUSSION

The effects of space weather on power grids are caused by fluctuation of the Earth's magnetic field caused by high energy particles that stream out from the Sun, creating voltages between grounding points in the grid, which induce currents that flow along electric power lines and into transformers. The greater the power line, the greater the current flow will be for a given change in magnetic field (Kappenman *et al*., 1997).

Normally these GICs are small enough that the electric power system can adjust to them, but when space weather occurs GICs can grow larger, damage transformers and disrupt the power supply to consumers. Very large GICs damage the transformer beyond repair leading to large scale electrical blackout. The time derivatives of the geomagnetic field are caused by geomagnetic field variation, by a sudden pulse noticed at the beginning of the geomagnetic disturbance, pulsation of the magnetic field at recovery phase and casual disturbance of the magnetic field during geomagnetic disturbance.

During the disturbance the GIC causes the saturation of transformers, which leads to failure in power transmission grids. The low and mid latitudes are far from the magnetic poles; therefore one may propose that they do not experience such serious geomagnetic disturbance as high latitudes (auroral and subauroral regions). However, this report demonstrates (see Fig. 4) that even mid and low latitudes are considerably affected by electromagnetic disturbances. The magnitude of time derivatives of the geomagnetic field determines the geoelectric field which drives the GICs. Variation exceeding 30nT/min of the X or Y component appears to be significant causing undesirable consequences in power grids (Koen and Gaunt, 2002; Vodjanikov *et al*., 2007). Also large scale auroral ionospheric electric currents flow mostly following the east-west direction thus mostly affecting X-Z components. Horizontal currents of small scale and amplitude and field aligned currents also contribute to the Y component (Viljanen, 1997). Trichtchenko and Boteler (2006) have also confirmed that dBx/dt components represent the driving electric field and characterize GIC.

GIC causes a great deal of damage to power systems at high latitudes due to their proximity to the dynamic auroral electrojet. Ionospheric response is a good measure of magnetic field that can be used to monitor the strength of geomagnetic disturbance associated with auroral activity. The ionospheric wind dynamo may be considered as one of the major factors that contribute to the generation of ionospheric electric current during geomagnetic disturbance. The magnetospheric electric

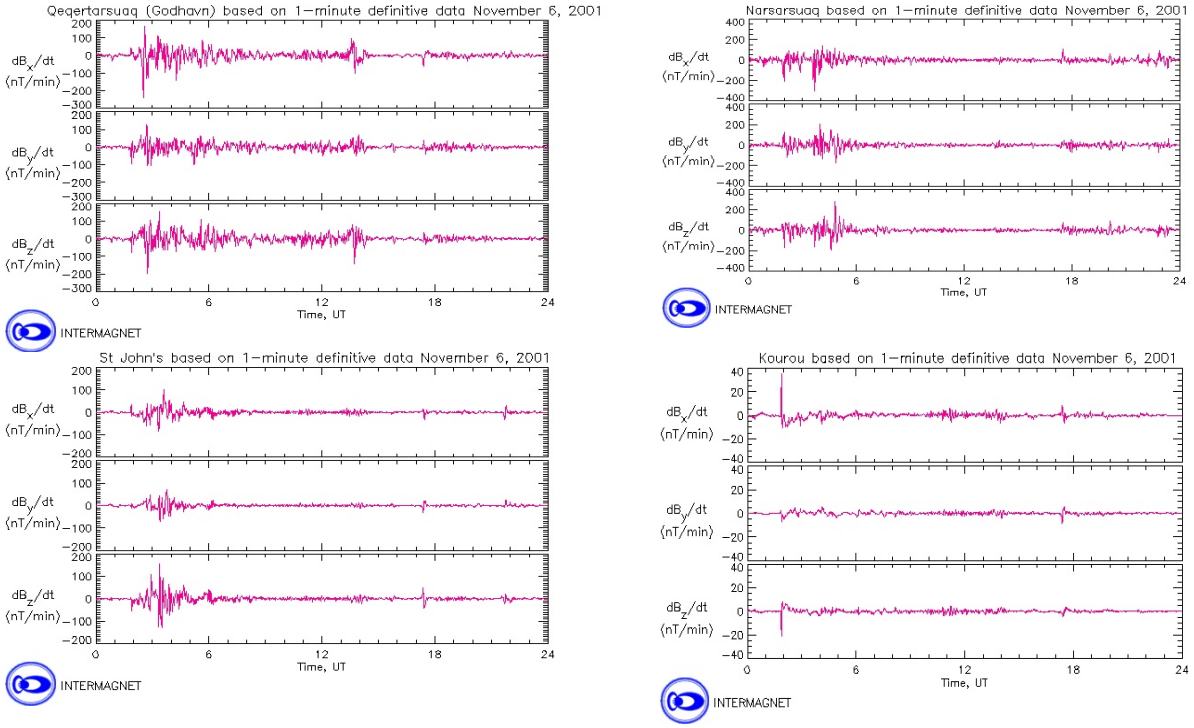

Fig. 7. Variation of the time derivatives on 6th November, 2001(a) auroral region at Qeqertarsuaq. (b) subauroral region at Narsarsuaq. (c) mid latitude at St John's (d) lower region at Kourou.

field penetrates into the low latitude ionosphere which can be another source for the electric field.

During space weather effects, the magnetospheric electric field disturbs the auroral ionosphere forming an auroral electrojet and the high latitude electric field penetrates into the equator. The electric field of the field aligned current can penetrate through the mid latitude ionosphere to the equator and may serve as a coupling agent between the auroral and equatorial ionosphere. Geomagnetic disturbance is significant at mid which poses a serious threat for high voltage power line circuits, when the rate of disturbance exceeds 30nT/min (see Figures 2, 3, 5, 6, and 7).

CONCLUSION

Space weather information and forecasts are beneficial to those who maintain electric power transmission lines, which are vulnerable to space weather effects. These arise from rapid changes in the Earth's magnetic field, caused by highly energetic particles from CMEs (Coronal Mass Ejections), creating voltage between grounding points in the grid, which in turn induce a small, irregular dc current that flows along electric power lines into the transformer. The highest rates of disturbance occur in auroral and subauroral regions. The mid and low latitudes are far from the magnetic poles and they do not experience the same severity of geomagnetic storm. From our analysis, it was clearly shown that geomagnetic disturbance can also occur at mid and low altitudes with values exceeding 30nT/min of the X or Y component; these appear to be significant, leading to failure in power transmission grids. Space weather parameters and the GIC measured by magnetometers under power grids have to be monitored. GIC values for regions both close to the auroral zones and at mid and low latitudes, should be calculated whenever major or minor changes occur and should be recorded and used to improved current knowledge

ACKNOWLEDGEMENT

We would like to acknowledge INTERMAGNET for providing geomagnetic field data.

REFERENCES

Baker, RH. and Skinner, NJ. 1980. Flow of electric current of telluric origin in a long metal pipeline and their effect in relation to corrosion. Materials performance. 19(2):25-28.

Boteler, DH., Pirjola, RJ. and Nevanlinna, 1998. The effect of geomagnetic disturbance on electrical systems at the Earth's surface. Advance Space Research. 22: 17-27.

Boteler, D. 2000. Geomagnetic effects on the pipeline-to-soil potentials of a continental pipeline. Adv. Space Res. 26:15-20.

Gummow, RA. 2002. GIC effect on pipeline corrosion and corrosion control systems. J. Atmos. Sol. Terr. Phys. 64(16):1755-1764.

Kappenman, JG., Zanetti, J. and Radasky, WA. 1997. Space weather from user's perspectives: Geomagnetic storm forecast and the power industry, Eos Trans. AGU. 78(4):37-45.

Kappenman, JG. 2003. Storm sudden commencement events and associated geomagnetically induced current risks to ground based system at low latitude and mid latitude locations. Space weather. 1, 3, 1016, doi: 1029/2003SW000009.

Koen, J. and Gaunt, CT. 2002. Geomagnetically induced current at mid latitude, Abs. The 27 general Assembly of URSI, 17-24 August, Netherlands, Maastrich, 177.

Lehtinen, M. and Pirjola, R. 1985. Current produced in the Earthed conductor networks by geomagnetically-induced electric fields. Ann. Geophys. 3(4):479-484.

Leonard, B., Langlois P., Boteler, D. and Risto P. 2000. A study of geoelectromagnetic disturbance in Quebec, 2: Detailed analysis of a large event. IEE transaction on power delivery. 15:272-278.

Ogunade, SO. 1986. Induced electromagnetic field in oil pipeline under electrojet current sources. Phys, Earth planet. Int. 307.

Osella, A. and Favetto, A. 2000. Effect of soil resistivity on currents induced on pipelines. J. Appl. Geophys. 44:303-312.

Pirjola, R. 2002. Fundamental about the flow of GIC in a power system applicable to estimating to space weather risks and designing remedies. Journal of Atmospheric and Solar Terrestrial Physics. 64:1967-1972.

Pulkkinen, A., Amm, O., Viljanen, A. and BEAR Working Group. 2000. Large geomagnetically induced current in the Finish high voltage power system. Finish Meteorological Institute Report. 2002:2, p.99.

Poppe, BB. and Jordan, KP. 2006. Sentinels of the Sun: Forecasting space weather, Johnson, Boulder, Colorado. pp 196.

Pulkkinen, A., Thomas, A., Clarke, E. and McKay, A. 2003. April 2000 geomagnetic storm: ionosphere drivers of large geomagnetically induced currents. Annales of geophysicae. 21:709-717.

Small, K. 2001. Electric power system in New Zealand caused by geomagnetically induced current on November 6, 2001, paper presented at NATO-ESPRIT Conference, NATO-ESPRIT, Rhodes, Greece.

Trichtchenko, L. and Boteler, DH. 2002. Modelling of geomagnetic induction in pipelines. Annales of geophysicae. 20:1063-1072.

Trichtchenko, L. and Boteler, DH. 2006. Response of power systems to the temporal characteristic of geomagnetic storms. IEE, CCECE/CCGEI, Ottawa, Canada.

Trivedi, NB., Vitrello I., kabata, W., Dutra , LGS., Padilha, AL., Bolongna MS., De Padua, MB, Soares, AP., Luz GS., Pinto FA., Pirjola, R. and Viljanen, A. 2007. Geomagnetically induced current in an electric power transmission system at low latitude in Brazil: A case study. Space weather. 5:S04004, diol:1029/2006SW000282.

Viljanen, A. 1997. The relation between geomagnetic variation and their time derivatives and implication for estimation of induction risks. Journal of geophysical research letter. 24:631-634.

Vodjanikov, VV., Gordienko, GI., Nechaev, SA., Sokolova, OI., Homutov, SJ. and Yakovets, AF. 2007. Study of geomagnetically induced current from time derivatives of the Earth's magnetic field. Publs. Inst. Geophys. Pol. Acad.Sc. 99(398).

Received: May 3, 2009; Accepted: Sept 22, 2009

SENRA Academic Publishers, Burnaby, British Columbia
Vol. 3, No. 3, pp. 953-957, 2009
ISSN: 1715-9997

Canadian Journal of pure&applied sciences

DIELECTRIC PROPERTIES OF SOME EDIBLE AND MEDICINAL OILS AT MICROWAVE FREQUENCY

Thomas Mathew, AD Vyas and *Deepti Tripathi
Department of Physics, Gujarat University, Ahmedabad

ABSTRACT

Dielectric properties of some edible and medicinal oils have been studied at 455 KHz, 9.1 GHz and optical frequency for the temperature range of 293^0K to 323^OK. It has been observed that the dielectric constant at optical frequency (ϵ_∞) is almost same for all oil samples where as variation in dielectric permittivity (ϵ') is more prominent at lower frequencies for pure oils. The static dielectric constant (ϵ_0) and dielectric constant at optical frequency (ϵ_∞) decrease slightly with increase in temperature for all the oil samples. Dielectric permittivity (ϵ') and loss tangent (tan δ) of different oil samples at 9.1 GHz show some interesting behaviour at particular temperature. The macroscopic relaxation time (τ_m) and molar free energy of activation (ΔF_C) is also determined which show systematic variation with temperature for most of the oil samples under consideration.

Keywords: Dielectric constant, relaxation time, molecular interaction, gas chromatography.

INTRODUCTION

Dielectric studies of biological substances and agrifood materials in microwave region of electromagnetic (e-m) spectrum are one of the areas of increasing importance. The dependence of dielectric properties of agrifood material on its density, packing fraction, moisture content and frequency of e-m wave has been studied for different grains and food materials (Nelson, 1982; Nelson, 1983[a]; Venkatesh *et al*., 1996). It is important to investigate dielectric properties of agrifood materials to develop microwave based process controls. Further, the dielectric relaxation studies have been widely utilized to investigate the molecular structure and related phenomenon of various liquids in pure and mixture form. However, very less information is available for many agrifood materials. Recently dielectric properties of grains of various packing densities, Tylose [TM] (a complex food material) and edible oils (Canola, Soya, Sunflower, coconut, groundnut ,linseed and mustard oil) were studied at some microwave frequencies (Venkatesh *et al*., 1996; Bansal *et al*., 2001; Agrawal and Bhatnagar, 2005). Edible oils are one of the agrifood materials which are highly consumed and the possibility of adulteration is also very high as most of the oils are odorless and colorless. Dielectric studies of pure oils are of importance as any variation from these standard values can be attributed to adultration or blending with other oils. The dielectric properties of Canola, Soya and Sunflower oils are studied at different temperatures and it was found that all three oils exhibit similar responses at 2.45 GHz, whereas at 915 MHz the values of dielectric permittivity (ϵ') and dielectric loss (ϵ'') responded differently (Venkatesh *et al*., 1996). Dielectric properties of different varieties of rapeseed-mustard oil and its mixing with common adultrant (argemone oil) at 8.93 GHz have been studied and the effect of adultrant is also reported (Bansal *et al*., 2001). Recently the dielectric studies of binary mixture of some edible oils have also been done at microwave frequency (Agrawal and Bhatnagar, 2005).

In the present study, dielectric properties of some oils, under edible and medicinal category were studied at microwave frequency with temperature. The macroscopic relaxation time (τ_m) and the molar free energy of activation (ΔF_ε) have been determined for all the oil samples and their variation with temperature is studied. Gas chromatography of various oils (both edible and medicinal) has been done to study the possible correlation of dielectric properties with the different fatty acid compositions present in oil samples. The effect of mixing of various oils on their dielectric constant has also been studied to see the adultration (or blending) effect. The oils studied are groundnut oil, sunflower oil, sesame oil, cottonseed oil, Soyabean oil (in edible oil category) and Almond oil, Olive Oil, Neem Oil (in medicinal oil category).

MATERIALS AND METHODS

Commercially available double filtered oil samples are used for present investigation. The gas chromatography of oils (both edible and medicinal) is done at Gujarat laboratories, Ahmedabad using Chemito Model No. 1000. The dielectric permittivity (ε') and dielectric loss (ε'') are determined at microwave frequency of 9.1 GHz with temperature, using the method suggested by Heston *et al*. (1950) adopted for short circuit termination and described elsewhere (Vashishth, 1990). Static permittivity (ϵ_o) of

*Corresponding author email: jha_deepti@hotmail.com

oils is measured at 455 KHz for different temperatures by resonance method which uses a tuned oscillator circuit and standard variable capacitor. The permittivity at optical frequency ($Є_\infty$) is taken as square of refractive indices for sodium D-line measured by Abbe's refractometer. All the measurements were done for a temperature range of 293-323^{o}K. The temperature was electronically controlled within ± 0.5^{O}C using a constant temperature water bath system. The loss tangent (tanδ) is determined for various oils at different temperatures. The macroscopic relaxation time is determined for various oils using Debye equation (Frohlich, 1958) and molar free energy of activation ($\Delta F_Є$) is calculated using Eyring's rate equation (Glastone *et al*., 1941).

RESULTS AND DISCUSSION

The measurements of dielectric permittivity (Є') at microwave frequency of 9.1 GHz, static dielectric constant ($Є_o$) and dielectric constant at optical frequency of sodium light ($Є_\infty$) for different oils at temperature of 293K is done and tabulated in table 1. It has been observed that the dielectric constant at optical frequency ($Є_\infty$) is almost same for all oil samples where as more variation is seen at lower frequency. The gas chromatography (GC) of edible and medicinal oils is done and two typical chromatograms (one for edible and other for medicinal oil) are shown in figures 1 and 2. The fatty acid composition of these oils has been tabulated in table 2. The peak corresponds to different retention time related to various fatty acids present in the oils. Four types of fatty acids are found to be present in almost all the oil samples except the olive oil sample where Linoleic acid is totally absent but none of the oils are showing exactly same fatty acid composition. Tables 1 and 2 shows that the dielectric constant of sunflower and sesame oil comes out to be same although their fatty acid compositions are different. Similar is the case for almond oil and olive oil. So it is observed that although the fatty acids present in oils are in different proportion but their dielectric constant lie very nearby. Similar results are obtained by Bansal *et al*. (2001) for rapeseed mustard oil of different variety having varying proportion of Erucic acid. The Fatty acids contain molecules made up of varying number of carbon, oxygen and hydrogen atoms with very long chain and most of them in the range of 12 to 22 atoms of carbon. These are molecules of complex nature and hence dielectric behaviour of oil samples will be governed by how the fatty acids present in the samples contribute to dielectric properties according to their own molecular structure individually and also collectively in the presence of other fatty acids .We observe no peculiarity in the value of Є' for olive oil where Linoleic acid is totally absent. This suggests that the variation in Є' is due to combined effect of the molecular rotations of all the fatty acids present in the triglyceride molecule of oils and the presence or absence of any single fatty acid does not make much difference. So, even if the percentage of a certain fatty acids present in two oils are different, they can show same dielectric properties or vice versa.

Table 1. Values of $\in_o$, $\in_\infty$, and $\in'$(at 9.1GHz) for various oils at temperature of 293^{0}K.

Oils	$\in_o$	$\in'$ (9.1GHz)	$\in_\infty$
Groundnut oil	3.09	2.40	2.16
Sunflower oil	3.11	2.42	2.16
Sesame oil	3.11	2.42	2.17
Cottonseed oil	3.15	2.45	2.17
Soyabean oil	3.13	2.46	2.17
Almond oil	3.03	2.40	2.17
Olive oil	3.08	2.40	2.16
Neem oil	3.89	2.57	2.18

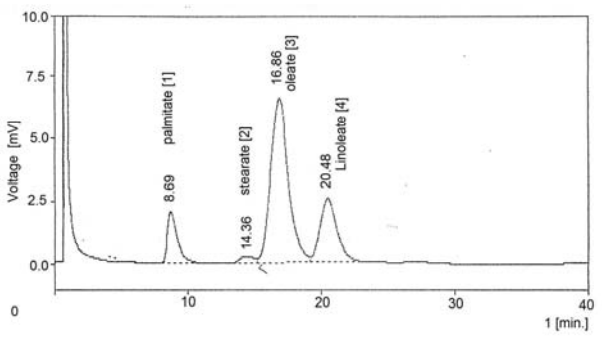

Fig. 1. Gas Chromatogram of Groundnut oil.

Table 3 shows the temperature dependence of static dielectric constant ($Є_o$), dielectric constant at optical frequency of sodium light ($Є_\infty$), dielectric permittivity

Table 2. Fatty acid composition (%) in different varieties of edible and medicinal oils.

Oils	Palmitic	Stearic	Oleic	Linoleic
Groundnut Oil	10.967	2.005	63.673	23.355
Sunflower Oil	5.480	1.279	42.626	50.615
Sesame Oil	10.116	1.993	32.355	55.536
Olive Oil	12.693	1.079	86.228	-
Almond Oil	7.359	0.635	63.913	28.093

(Є') and dielectric loss (Є") at 9.1GHz along with macroscopic relaxation time (τ_m), loss tangent (tan δ) and molar free energy of activation ($\Delta F_Є$) for various oils (edible and medicinal) in the temperature range of 293 to 313K.It is clear from table 3 that $Є_o$ and $Є_\infty$ has got similar type of variation with temperature for different oils i.e. both decrease slightly with increase in temperature for all oil samples under consideration. However the variation of Є,' Є" and tanδ for these oils show little irregularity with temperature except for cottonseed and olive oil where Є' increases with temperature in this range. The values of Є' and Є" for groundnut oil and sesame oil show a maxima at 313K whereas sunflower oil and neem oil show a minima at this temperature and other oils show still complex behaviour giving maxima and minima both. Similar results were reported by Bansal *et al*. (2001) for different variety of rapeseed-mustard oil. However, Venkatesh *et al*. (1996) reported systematic variation of Є' and Є" with temperature in the range of –30°C to 60°C for tylose (a complex food material) and oils (soya and canola) at 2.45 GHz. They observed that frozen Tylose behaved as low loss material whereas at higher temperatures (above 20°C) the reverse effect was observed. Bansal *et al*. (2001) have also observed maxima and minima type of behaviour of Є' and Є" at a temperature about 313K and attributed it to molecular resonance/anti resonance occurring between triglyceride molecules of the oil sample used. They suggested that the intermolecular association between two triglyceride molecules is present through their resonating structure which can break up due to thermal motion leading to alignment of molecular dipoles in parallel from anti parallel or vice versa at certain temperature. This will give rise to molecular resonance or anti-resonance giving maxima or minima type behaviour of ε' and ε" with temperature. Our results for most of the oils are also in confirmation with what observed by Bansal *et al*. (2001) for rapeseed-mustard oil. As shown in table 3, the macroscopic relaxation time (τ_m) of oils in general decreases with increasing temperature in the range of 293 to 323 K except in the case of sunflower oil. This is general behaviour of organic substances which show the decrement in relaxation time with the increasing temperature due to change in effective dipole length .The molecules are more closely clustered at low temperature and hence take more time to change their orientation giving large relaxation time at low temperatures. A typical plot of relaxation time with temperature for cottonseed oil is shown in figure 3. It is also evident from table 3 that molar free energy of activation ($\Delta F_Є$) for each oil sample increases in the temperature range of 293°K to 323°K. This can be understood in terms of increased thermal agitation which makes molecules to require more energy to reach activated state.

The effect of mixing of edible oils on their dielectric properties is also studied at 9.1 GHz. Since at 9.1 GHz, the dielectric constant of all oils lie very nearby, the mixing is done at 1:1 ratio (i e 50-50% by volume) but no significant change is observed in the value of Є' and Є". Recently the dielectric studies of binary mixture of some commercially available edible oils (mustard with coconut, groundnut and linseed) done by Agrawal and Bhatnagar (2005) at 9.42GHz show that the dielectric constant of the oil mixtures takes an average value of the two oils used. They suggested that by dielectric constant measurement, the adulteration in pure oils can be detected if the dielectric constant of pure oil is known. This can only be true when the dielectric constant of the pure oil and the adultrant oil is quiet different. In our present study the oils mixed with each other have dielectric constant lying very nearby. Hence the change in dielectric constant at microwave frequency of 9.1GHz is not significantly seen by us. So for detection of adulteration, the dielectric constants of pure oil and the adultrant oil should be quiet different giving noticeable change in the dielectric constant when mixed.

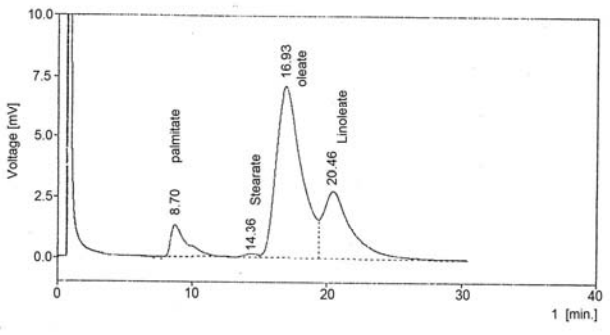

Fig. 2. Gas Chromatogram of Almond oil.

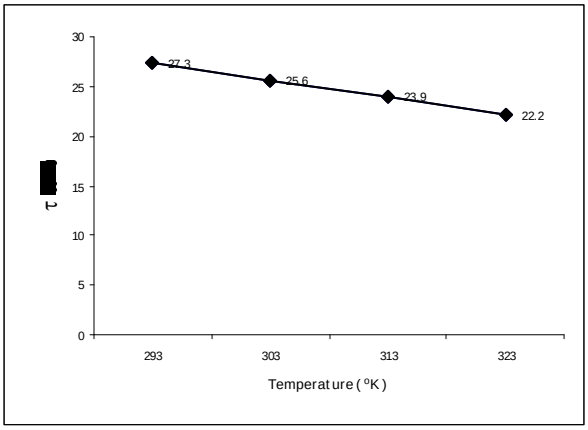

Fig. 3. Plot of Temperature Vs Relaxation time (τ_m) for Cottonseed oil.

CONCLUSION

The variation in the dielectric properties of various oils is understood as the combined effect of the molecular rotations of all the fatty acids present in the triglyceride

Table 3. Values of ϵ_o, ϵ', ϵ'', ϵ_∞, tan δ, τ_m and ΔF_ϵ for oils at different temperatures.

Temp.	ϵ_o	ϵ'	ϵ''	ϵ_∞	tan δ	τ_m	ΔF_ϵ
(^oK)	(f =455KHz)	(f=9.1GHz)		(f=optical)		(pS)	(kCal/mol)
Edible Oils:							
Groundnut Oil							
293	3.09	2.40	0.09	2.16	0.04	30.0	3031.98
303	3.09	2.41	0.09	2.16	0.04	28.3	3120.55
313	2.95	2.42	0.14	2.15	0.06	24.6	3156.61
323	2.90	2.40	0.12	2.14	0.05	24.8	3282.83
Sunflower Oil							
293	3.11	2.42	0.11	2.16	0.04	28.6	3004.16
303	3.10	2.47	0.11	2.15	0.04	24.9	3043.52
313	3.07	2.43	0.11	2.14	0.05	26.0	3191.02
323	3.03	2.47	0.14	2.12	0.06	28.6	3374.30
Sesame Oil							
293	3.11	2.42	0.08	2.17	0.03	29.0	3012.25
303	3.11	2.44	0.08	2.16	0.03	26.8	3087.77
313	3.08	2.49	0.11	2.14	0.05	23.0	3114.80
323	3.04	2.46	0.13	2.13	0.05	23.1	3237.28
Cottonseed Oil							
293	3.15	2.45	0.07	2.17	0.03	27.3	2977.09
303	3.13	2.46	0.10	2.15	0.04	25.6	3060.20
313	3.12	2.48	0.06	2.13	0.02	23.9	3138.67
323	3.09	2.49	0.15	2.12	0.06	22.2	3211.78
Soyabean Oil							
293	3.13	2.46	0.08	2.17	0.03	26.5	2959.78
303	3.12	2.44	0.12	2.16	0.05	26.9	3090.01
313	3.08	2.45	0.15	2.14	0.06	25.3	3174.06
323	3.04	2.50	0.16	2.13	0.06	21.4	3188.24
Medicinal Oils:							
Almond Oil							
293	3.03	2.40	0.08	2.17	0.03	28.7	3006.19
303	3.02	2.40	0.11	2.15	0.04	28.0	3114.13
313	2.99	2.45	0.09	2.14	0.04	23.4	3125.52
323	2.96	2.45	0.09	2.13	0.04	22.2	3211.78
Olive Oil							
293	3.08	2.40	0.07	2.16	0.03	29.0	3012.25
303	3.04	2.42	0.08	2.14	0.04	26.3	3076.44
313	3.03	2.44	0.14	2.12	0.06	24.0	3141.26
323	3.00	2.45	0.12	2.11	0.05	22.3	3214.67
Neem Oil							
293	3.89	2.57	0.11	2.18	0.04	32.3	3074.97
303	3.89	2.62	0.08	2.17	0.03	29.1	3137.32
313	3.86	2.61	0.10	2.15	0.04	29.1	3261.05
323	3.83	2.63	0.08	2.14	0.03	27.3	3344.45

molecule of oils where the presence or absence of any single fatty acid does not make much difference. The dielectric parameters of oils show systematic temperature dependence except for the dielectric permittivity (Є') and loss tangent (tan δ) which show interesting behaviour at particular temperature suggesting some type of molecular resonance/anti resonance occurring between triglyceride molecules of the oil sample used. It is also observed that for detection of adultration the dielectric constants of pure oil and the adultrant oil should be quiet different giving noticeable change in the dielectric constant when mixed.

REFERENCES

Agrawal, S. and Bhatnagar, D. 2005. Dielectric study of binary mixtures of edible unsaturated oils. Indian J. Pure and Appl. Phys. 43:624-629.

Bansal, AK., Singh, PJ. and Sharma, KS. 2001.Dielecrtic properties of different varieties of rapeseed-mustard oil at different temperatures, Indian J. Pure and Appl. Phys. 39:532-540.

Bansal, AK., Singh, PJ. and Sharma, KS. 2001. Dielectric relaxation studies of argemone-mexicana oil in pure form and in dilute solution of benzene at different temperatures. Indian J. Pure and Appl. Phys. 39:329-334.

Frohlich, H. 1958. Theory of Dielectrics. Oxford University Press, London.

Glastone, S., Laider, KJ. and Eyring, H. 1941. The Theory of Rate Processes. McGraw Hill, New York.

Heston, WM.Sr., Franklin, AD., Hannely, EJ. and Smith, CP. 1950. Microwave absorption and Molecular structure in liquids.V.Measurements of Dielectric constant and loss of low loss solutions. Journal Am Chem Soc. 72:3443-3447.

Nelson, SO. 1982. Factors affecting the dielectric properties of grains.Trans ASAE .25(2):1045-1049.

Nelson, SO. 1983[a]. Observations on the density dependence of particulate materials. J. Microwave Power. 18(2):143-152.

Vashisth, VM. 1990. Dielectric relaxation study of some polar molecules and their mixtures at microwave frequencies. Ph.D. Thesis. Gujarat University, Ahmedabad, India.

Venkatesh, MS., St- Denis, E., Raghavan, GSV, Akyel, C. and van de Voort, F.1996. Dielectric properties of some agri-food materials. Asia Pacific Microwave Conference, New Delhi, India. 387-390.

Received: Dec 11, 2008; Revised: June 09, 2009;
Accepted: June 10, 2009

SENRA Academic Publishers, Burnaby, British Columbia
Vol. 3, No. 3, pp. 959-965, 2009
ISSN: 1715-9997

Canadian Journal of pure&applied sciences

ON A CLASS OF COMPUTABLE CONVEX FUNCTIONS

Godwin NO Asemota
Electrical and Electronics Engineering Department
Kigali Institute of Science and Technology, Kigali, Rwanda

ABSTRACT

We shall show in this paper a class of computable convex functions, which have their first two solutions specified, and for which, all the polynomial solutions are uniquely determined. We shall also prove that the class of functions are convex, computable and represents a set of partial functions. Analyses indicate that it is double recursive, which can be composed from its primitive recursive functions. The class of convex functions can be shown to be reducible to Ackermann's functions with some modifications to the algorithm, which lend themselves to computability in the form of Turing machines and λ-calculus, according to Church. Least search operator or minimisation conditions can be imposed on this class of functions, such that, either no solution is returned for a certain term of the function or a term for which, the solution is zero. However, this set of computable convex functions find application in solving optimisation problems in operations research, load and demand side management in electrical power systems engineering, switching operations in computer science and electronics engineering, mathematical logic and several other application areas in industry.

Keywords: computability, optimisation, partial functions, recursive functions, turing machines.

INTRODUCTION

Information theory, electrical load and demand-side management, electronics switching techniques, optimisation, mathematical logic, nonsmooth mechanics (Moreau, 1988) and other application areas in science, engineering and industry consists in determining bounds on certain performance measures (Moon, 2000). Bounds substitute for complicated expressions that are simpler, but not exactly equal and are either larger or smaller than what they replace.

A function $f(x)$ is said to be convex over an interval (a,b) if for every $x_1, x_2 \in (a,b)$ and $0 \le \lambda \le 1$,

$$f(\lambda x_1 + (1-\lambda)x_2)) \le \lambda f(x_1) + (1-\lambda) f(x_2)$$

A function is strictly convex if equality holds only if $\lambda = 0$ or $\lambda = 1$ (Moon, 2000; Potter, 2005). One reason why we are interested in convex functions is that, it is known that over the interval of convexity, there is only one minimum. This fact can strengthen many of the results we might desire (Moon, 2000). The importance of convexity theory derives from that fact that, convex sets occur frequently in many areas of mathematics, science and engineering, and are amenable to rather elementary reasoning. In addition, the concept of convexity serves to unify a wide range of phenomena (Fink and Wood, 1996). Geometrically, every convex combination of points on the graph of the function is either above or on the graph itself. That is, in its epi-graph. This is also equivalent to saying that a function is convex iff its epi-graph is a convex set (Lebanon, 2006). Thus, we can convert a convex function on a convex set A to a convex function on R^n that is equivalent to f in some sense (Lebanon, 2006). In the same vein, a differentiable function f on a convex domain is convex iff $f(y) \ge f(x) + \nabla f(x)^T (y-x)$, that is, the graph is above the second order Taylor approximation plane. A consequence of the foregoing result is that for a convex function f, $\nabla f(x) = 0$ implies that x is a global minimum. For the second order differentiability condition: If f is twice differentiable on a convex domain A, then it is convex iff the Hessian matrix $H(x)$ is positive semi-definite for all $x \in A$.

For a convex function f and a RV X, $f(E(X) \le Ef(X)$.

The following operations preserve convexity of functions:

- A weighted combination with positive weights of convex functions is convex. If $w_i > 0$ and $f_1, ..., f_n$ are convex functions, then $\sum w_i f_i$ is convex (with a similar result for integration rather than summation). This can be seen from the second order

*Corresponding author email: a.osarumwense@kist.ac.rw

condition for convexity.

- The point-wise maximum or supremum of convex functions is convex (this is a consequence of that fact that the intersection of convex epi-graphs is a convex epi-graph).
- If f is convex in (x, y) and C is a convex set, then $\inf_{y \in C} f(x, y)$ is convex in x (Beberian, 1994; Bhatia, 1997; Birge and Louveaux, 1997; Hiriart-Urruty and Lemarechal, 1996[a]; Hiriart-Urruty and Lemarechal, 1996[b]; Lebanon, 2006; Stankova-Frenkel, 2001).

RECURSIVE FUNCTIONS

Recursive functions form a class of computable functions that take their name from the process of recurrence or recursion. In general, the numerical form of recursion consists in defining the value of a function, using other values of the same function (Kasara, 2008). The Ackermann Function is a simple recursive function that produces large values from very simple inputs (Odifredi, 2005).

Proposition 1. A class of computable convex functions, which have their first two solutions specified is that for which, all the polynomial solutions are uniquely determined.

Let the first two initial solutions of the polynomial function be 1 and a.

We can define the function as $A(m, n)$:

$m = 0,\ n = 0 \quad A(0,0) = 1$
$m = 0, n = 1 \quad A(0,1) = 1$
$m = 1, n = 0 \quad A(1,0) = 1$
$m = 1, n = 1 \quad A(1,1) = a$
$m = 1, n = 2 \quad A(1,2) = a^2$
$m = 2, n = 1 \quad A(2,1) = a^2$
$m = 2, n = 2 \quad A(2,2) = a^4$
$m = 2, n = 3 \quad A(2,3) = a^6$
$m = 3, n = 2 \quad A(3,2) = a^6$
$m = 3, n = 3 \quad A(3,3) = a^9$
$m = 3, n = 4 \quad A(3,4) = a^{12}$
$m = 4, n = 3 \quad A(4,3) = a^{12}$
$m = 4, n = 4 \quad A(4,4) = a^{16}$
$m = 4, n = 5 \quad A(4,5) = a^{20}$
$m = 5, n = 4 \quad A(5,4) = a^{20}$
$m = 5, n = 5 \quad A(5,5) = a^{25}$

Therefore, $A(m, n) \equiv A(n, m) = a^{mn}$

We can begin to compute the polynomial and arrange it in an array or matrix form as follows:

		n											
		0	1	2	3	4	5	6	7	8	9	10	n
	0	1	1	1	1	1	1	1	1	1	1	1	1
	1	1	a	a^2	a^3	a^4	a^5	a^6	a^7	a^8	a^9	a^{10}	a^n
	2	1	a^2	a^4	a^6	a^8	a^{10}	a^{12}	a^{14}	a^{16}	a^{18}	a^{20}	a^{2n}
	3	1	a^3	a^6	a^9	a^{12}	a^{15}	a^{18}	a^{21}	a^{24}	a^{27}	a^{30}	a^{3n}
m	4	1	a^4	a^8	a^{12}	a^{16}	a^{20}	a^{24}	a^{28}	a^{32}	a^{36}	a^{40}	a^{4n}
	5	1	a^5	a^{10}	a^{15}	a^{20}	a^{25}	a^{30}	a^{35}	a^{40}	a^{45}	a^{50}	- a^{5n}
	6	1	a^6	a^{12}	a^{18}	a^{24}	a^{30}	a^{36}	a^{42}	a^{48}	a^{54}	a^{60}	- a^{6n}
	7	1	a^7	a^{14}	a^{21}	a^{28}	a^{35}	a^{42}	a^{49}	a^{56}	a^{63}	a^{70}	- - a^{7n}
	8	1	a^8	a^{16}	a^{24}	a^{32}	a^{40}	a^{48}	a^{56}	a^{64}	a^{72}	a^{80}	- - a^{8n}
	9	1	a^9	a^{18}	a^{27}	a^{36}	a^{45}	a^{54}	a^{63}	a^{72}	a^{81}	a^{90}	- - a^{9n}
	10	1	a^{10}	a^{20}	a^{30}	a^{40}	a^{50}	a^{60}	a^{70}	a^{80}	a^{90}	a^{100}	- - a^{10n}
	-												
	-												
	-												
	-												
	m	1	a^m	a^{2m}	a^{3m}	a^{4m}	a^{5m}	a^{6m}	a^{7m}	a^{8m}	a^{9m}	a^{10m}	a^{mn}

Both the first column and the first row can be thought of as initialisation for line 0 of the array. It appears that the function contains hardly any calculations of actual values, but mostly of their indices (Kasara, 2008).

Upon a closer look at the indices, values of each row are proportional to the next. Similarly, values of each column are also proportional to the next. The upper triangle of elements above the diagonal of the matrix is a mirror image of the lower triangle of elements just below the diagonal. The function can be said to be symmetric. The determinant of the matrix above vanishes because two rows or two columns are proportional.

The polynomial can be said to be an alternating function (Uspensky, 1948).

We can also assume the element a to be a complex quantity in order to be able to evaluate its determinant.

The determinant of the above matrix can be determined if it is a square matrix with $m = n$ (that is, $n \times n$ matrix). The value of the determinant of the above matrix is exactly as that of the matrix below:

The determinant above is equivalent to the modified Vandermonde determinant:

$$D = a^{\sum_{1}^{n} n} \begin{vmatrix} 1..a....a^2....a^3.....a^{n-1} \\ 1..a^2...a^4...a^6.....a^{2(n-1)} \\ 1..a^3...a^6....a^9.....a^{3(n-1)} \\ \\ \\ 1..a^m..a^{2m}...a^{3m}.....a^{m(n-1)} \end{vmatrix}$$

This Vandermonde determinant occurs often in practice as monomials of a geometric progression in each row (Wikipedia, 2008).

The simplest way to evaluate the determinant is to replace a_n by a variable a (Uspensky, 1948).

Then, the determinant becomes a polynomial $D_n(a)$ of degree $n-1$ in a. As can be seen, by expanding it by

$$\begin{array}{cccccccccc} a & a^2 & a^3 & a^4 & a^5 & a^6 & a^7 & a^8 & a^9 & a^{10} & a^n \\ a^2 & a^4 & a^6 & a^8 & a^{10} & a^{12} & a^{14} & a^{16} & a^{18} & a^{20} & a^{2n} \\ a^3 & a^6 & a^9 & a^{12} & a^{15} & a^{18} & a^{21} & a^{24} & a^{27} & a^{30} & a^{3n} \\ a^4 & a^8 & a^{12} & a^{16} & a^{20} & a^{24} & a^{28} & a^{32} & a^{36} & a^{40} & a^{4n} \\ a^5 & a^{10} & a^{15} & a^{20} & a^{25} & a^{30} & a^{35} & a^{40} & a^{45} & a^{50} & a^{5n} \\ a^6 & a^{12} & a^{18} & a^{24} & a^{30} & a^{36} & a^{42} & a^{48} & a^{54} & a^{60} & a^{6n} \\ a^7 & a^{14} & a^{21} & a^{28} & a^{35} & a^{42} & a^{49} & a^{56} & a^{63} & a^{70} & a^{7n} \\ a^8 & a^{16} & a^{24} & a^{32} & a^{40} & a^{48} & a^{56} & a^{64} & a^{72} & a^{80} & a^{8n} \\ a^9 & a^{18} & a^{27} & a^{36} & a^{45} & a^{54} & a^{63} & a^{72} & a^{81} & a^{90} & a^{9n} \\ a^{10} & a^{20} & a^{30} & a^{40} & a^{50} & a^{60} & a^{70} & a^{80} & a^{90} & a^{100} & a^{10n} \\ a^m & a^{2m} & a^{3m} & a^{4m} & a^{5m} & a^{6m} & a^{7m} & a^{8m} & a^{9m} & a^{10m} & a^{mn} \end{array}$$

$$\begin{vmatrix} a....a^2...a^3..a^4.....a^5...a^6....a^7...a^8.....a^9.....a^{10}.....a^n \\ a^2..a^4...a^6...a^8....a^{10}..a^{12}..a^{14}..a^{16}.....a^{18}....a^{20}.....a^{2n} \\ a^3..a^6...a^9...a^{12}...a^{15}..a^{18}..a^{21}...a^{24}....a^{27}....a^{30}.....a^{3n} \\ \\ \\ \\ \\ a^m..a^{2m}..a^{3m}..a^{4m}..a^{5m}..a^{6m}..a^{7m}..a^{8m}..a^{9m}..a^{10m}.....a^{mn} \end{vmatrix} = D$$

elements of the last row. For $a = a_1, a_2, ..., a_{n-1}$, this polynomial vanishes since $D(a_\alpha)$ for $\alpha = 1, 2, ..., n-1$ appears as determinant with two identical rows. Hence, $D_n(a) = C(a-a_1)(a-a_2)...(a-a_{n-1})$, where C is the leading coefficient in $D_n(a)$. This coefficient is the minor

$$D_{n-1} = \begin{vmatrix} 1..a_1..a_1^2....a_1^{n-2} \\ 1...a_2....a_2^2.....a_2^{n-2} \\ \\ \\ 1..a_{n-1}...a_{n-1}^2.....a_{n-1}^{n-2} \end{vmatrix}$$

corresponding to a_n^{n-1}, so we have

$$D_n(a_n) = D_n = D_{n-1}(a_n - a_1)(a_n - a_2)...(a_n - a_{n-1}) *$$

The determinant D_{n-1} is of the same type as D_n and can be treated in the same fashion.

But,

$$D_2 = \begin{vmatrix} 1..a_1 \\ 1..a_2 \end{vmatrix} = a_2 - a_1$$

Hence, as follows from (*) for $n = 3$,

$$D_3 = (a_3 - a_1)(a_3 - a_2)(a_2 - a_1)$$

Further,

$D_4 = (a_4 - a_3)(a_4 - a_2)(a_4 - a_1)(a_3 - a_1)(a_3 - a_2)(a_2 - a_1)$, etc

The general expression of Vandermonde determinant is

$$\begin{aligned} D_n = {} & (a_n - a_1)(a_n - a_2)....(a_n - a_{n-1}) \\ & (a_{n-1} - a_1)(a_{n-1} - a_2)....(a_{n-1} - a_{n-2}) \\ & .....\ldots\ldots.. \\ & (a_3 - a_2)(a_2 - a_1) \\ & (a_2 - a_1). \end{aligned}$$

It is a rational integral function of $a_1, a_2, ..., a_n$ that mainly changes sign when two of the variables are transposed and for this reason, it is called an alternating function (Uspensky, 1948). For the exchange of two variables like a_1 and a_2 corresponds to the exchange of the first and second rows, and this causes the change of sign of the Vandermonde determinant.

For an equation with numerical coefficients, the computation of the discriminant can be reduced to the computation of a numerical determinant of the same order as the degree of the equation. If $\alpha_1, \alpha_2, ...\alpha_n$ be the roots of the equation, then the square of Vandermonde determinant becomes (Uspensky, 1948; Wong, 1997).

$$\begin{vmatrix} 1..\alpha_1..\alpha_1^2.....\alpha_1^{n-1} \\ 1..\alpha_2..\alpha_2^2.....\alpha_2^{n-1} \\ \\ \\ 1..\alpha_n..\alpha_n^2.....\alpha_n^{n-1} \end{vmatrix} = (\alpha_n - \alpha_1).....(\alpha_n - \alpha_{n-1})....(\alpha_2 - \alpha_1)$$

differs from D only by the factor a_0^{2n-2}. Now multiplying Vandermonde determinant by itself, column by column, and denoting as usual by

$$s_i = \alpha_1^i + \alpha_2^i + ... + \alpha_n^i$$

The sum of the i th powers of roots, we have

$$\begin{vmatrix} 1..\alpha_1..\alpha_1^2.....\alpha_1^{n-1} \\ 1..\alpha_2..\alpha_2^2.....\alpha_2^{n-1} \\ \\ \\ 1..\alpha_n..\alpha_n^2.....\alpha_n^{n-1} \end{vmatrix} = \begin{vmatrix} s_0..s_1.....s_{n-1} \\ s_1..s_2.....s_n \\ \\ \\ s_{n-1}...s_n.....s_{2n-2} \end{vmatrix},$$

So,

$$D = a_0^{2n-2} \begin{vmatrix} s_0...s_1.....s_{n-1} \\ s_1...s_2.....s_n \\ \\ \\ s_{n-1}..s_n.....s_{2n-2} \end{vmatrix}$$

The sums s_i are readily computed from Newton's formulae (Uspensky, 1948; Wong, 1997).

DOUBLE RECURSION

Primitive recursion can be used to define functions of many variables, but only by keeping all but one of them fixed. Double recursion relaxes this condition. It allows the recursion to happen on two variables instead of only one (Odifredi, 2005).

The Archimedes double recursion is reducible to primitive recursion.

$$h_n(x) = a^{xn}$$

But, the Ackermann's double recursion function is not reducible to primitive functions.

$$a(0,n) = n+1$$
$$a(m+1,0) = a(m,1)$$
$$a(m+1,n+1) = a(m,a(m+1,n))$$

Ackermann's function grows very fast. It can be thought of as defining a function by three arguments, $f(x,y,z)$. Thus. $f(x,y,z) = f_x(y,z)$

In this function, the argument x determines the function in the sequence $f_1, f_2, \ldots$ that needs to be used. z is the recursive parameter and y is idle. By dropping the y parameter, we obtain the Ackermann's function (Odifredi, 2005).

Minimisation (or Least Search)

By introducing minimisation or least search operator μ we are able to define a two place-function $f(x,y)$ by another function $g(x) = \mu y[f(x,y) = 0]$, where $g(x)$ returns the smallest number y, such that $f(x,y) = 0$, provided that any of the two conditions hold:

1. There actually exists at least one z such that $f(x,z) = 0$; and
2. For every $y' \leq y$, the value $f(x,y')$ exists and is positive.

If at least one of the above two conditions fails, then $g(x)$ fails to return a value and is undefined. But, from the introduction of the μ operator, we encounter a partial recursive function that might fail to be defined for some arguments (Odifredi, 2005).

Upon application to partial functions, we need to require that condition (2) above that $f(x,y')$ be defined for every $y' \leq y$. Therefore, μ is thought to try to compute in succession all values $f(x,0), f(x,1), f(x,2), \ldots$ until some m $f(x,m)$, returns 0. In such a case, an m, is returned (Odifredi, 2005).

The two cases where this procedure might fail to give a value are: (a) if no such m exists or if for some of the computations $f(x,0), f(x,1), f(x,2), \ldots$, itself fails to return a value.

We have by this means produced a class of partial functions, which can be obtained from their initial functions through composition, primitive recursion, and least search.

In addition, this class of functions turns out to belong to the class of Turing-computable functions and also to the class of $\lambda-$definable functions of Alonzo Church (Odifredi, 2005; Epstein and Carnielli, 1989).

The μ-Operator

Eliminating the bounds leads to a problem of undefined points. Consider $f(x) =$ the least y such that $y + x = 10$.

For each $x > 10$, $f(x)$ is undefined. Yet f is still computable: for $f(12)$, as an example. We can check each y in turn to see that $y + 12 \neq 10$ (Epstein and Carnielli, 1989).

We can say that there is no such y which makes $f(12)$ defined. We can step outside the system and define a better function that is defined everywhere.

Let us consider the function $h(w) =$ the least $\langle x,y,z \rangle$ such that $x,y,z > 0$ and $x^w + y^w = z^w$

For, $w = 58$, we can constructively check in turn each triple $\langle x,y,z \rangle$ to see if $x^{58} + y^{58} = z^{58}$.

We define the least search operator, also called the $\mu-$operator as:

$\mu y[f(\vec{x},y) = 0] = z$ iff { $f(\vec{x},z) = 0$ and

{for every $y < z$, $f(\vec{x},y)$ is defined and > 0 (Epstein and Carnielli, 1989).

The min-Operator

We denote "$\min_y[f(\vec{x},y) = 0]$", the smallest solution to the equation $f(\vec{x},y) = 0$, if it exists, and is defined otherwise.

However, the min-operator is not the same as the $\mu-$operator. Let us define the primitive recursive function

$$h(x,y) = \begin{cases} x - y \ldots if \ldots y \leq x \\ 1 \ldots\ldots\ldots Otherwise \end{cases}$$

Now we define

$$g(x) = \mu y[2 \dot{-} h(x,y) = 0]$$

$g^*(x) = \min_y [2 \div h(x, y) = 0]$

Then
$g(0), g(1)$ are undefined, $g(2) = 0$
$g^*(0), g^*(1)$ are undefined, $g^*(2) = 0$

But we now define
$f(x) = \mu y[g(y).(x+1) = 0]$
$f^*(x) = \min_y [g^*(y).(x + 1) = 0]$

Then $f(x)$ is undefined for all x. But, for all x, $f^*(x) = 2$ (Epstein and Carnielli, 1989; Robinson, 1947).

The $\mu-$Operator is a Computable Operation

We choose the $\mu-$operator rather than the min-operator, because we may not be able to predict for which x, $f(x, y) = 0$, has a solution.

But with the $\mu-$operator, if $f(x, 0)$ is undefined, then $\mu y[f(x, y) = 0]$ is undefined too. This is so because we may not be able to get at trying $f(x,1) = 0$ (Epstein and Carnielli, 1989). There is, however, a well-defined computable procedure for calculating $g(x)$, although it may not always give a result (Odifredi, 2005; Epstein and Carnielli, 1989; Robinson, 1947).

Partial Recursive Functions

Partial recursive functions are the smallest class containing the zero, successor, and projection functions and closed under composition, primitive recursion and the $\mu-$operator.

We call functions, which may (for all we know) be undefined for some inputs partial functions and may be denoted by the letters $\varphi, \psi, \rho,$ etc. We may write

$\varphi(x)\downarrow$ for "φ applied to x is defined"

$\varphi(x)\not\downarrow$ for "φ applied to x is not defined".

We say that a set A or relation R is recursive if its characteristic function is recursive.

When we use the $\mu-$operator, we need to reverse the roles of 0 and 1 in the characteristic function. So, we define the representing function for a relation R to be $\overline{sg} \circ C_R$ (Odifredi, 2005; Epstein and Carnielli, 1989; Robinson, 1947).

2. It is not as restrictive as it may appear that the $\mu-$operator requires us to search for a y such that $\varphi(\vec{x}, y) = 0$. Given a relation R, we write

$\mu y_{\leq g(\vec{x})}[R(\vec{x}, y)]$

to mean $\mu y[y \leq g(\vec{x}) \wedge R(\vec{x}, y)]$ (Epstein and Carnielli, 1989).

One can, therefore, prove with rigour that a function is convex from any of the following criteria instead of guessing it from the graph.

1. Let $f(x)$ be a continuous function on an interval I. Then $f(x)$ is convex if and only if $(f(a) + f(b))/2 \geq f((a+b)/2)$ holds for all $a, b \in I$. Also, $f(x)$ is strictly convex if and only if $(f(a) + f(b))/2 > f((a+b)/2)$, whenever $a, b \in I$ and $a < b$.
2. Let $f(x)$ be a differentiable function on an interval I. Then $f(x)$ is convex if and only if $f'(x)$ is increasing on I. Also, $f(x)$ is strictly convex if and only if $f'(x)$ is strictly increasing on the interior of I.
3. Let $f(x)$ be a twice differentiable function on an interval I. Then, $f(x)$ is convex if and only if $f''(x) \geq 0$ for all $x \in I$. Also, $f(x)$ is strictly convex if and only if $f''(x) > 0$ for all x in the interior of I (Stankova-Frenkel, 2001).

Concluding Remarks

We have shown that for the class of functions considered in this study that it is both convex and computable. It has also been shown that over the interval of convexity there is only one minimum. This fact strengthens our claim of having the best solution to the application areas of interest in science, technology and industry. Also, a sum of convex functions is convex. Adding a constant or linear function to a convex function does not affect convexity. In addition, a convex function is never above its linear interpolation.

Convex functions represent a class of nonsmooth optimisation algorithms and techniques useful for getting results of very high quality in most application areas.

The importance of convexity theory derives from that fact that convex sets arise frequently in many application areas and often amenable to rather elementary reasoning. Also, the concept of convexity serves to unify a wide range of physical phenomena.

In the financial system, for example, several factors like: (i) equilibrium term structure, (ii) path dependence, and

(iii) convexity, combine to make financial engineering a rigorous discipline that comprise statistics, mathematics, economics and computer science (Kling, 2007). Convexity in the financial system is the curvature that relates value to a random variable, which will determine how the mean and the variance (volatility) of the random variable affect value. In addition, the matrix elements of A and its inverse differ only in the sign in the powers of α. It is possible to use a single computer programme to carry out both types of transformation. This is the same as carrying out a transformation of expressing the value of the coefficients in terms of the input quantities (Wong, 1997).

REFERENCES

Beberian, SK. 1994. A First Course in Real Analysis. Springer-Verlag. New York, USA. pp. 59.

Bhatia, R. 1997. Graduate Texts in Mathematics: Matrix Analysis. Springer-Verlag. New York, USA. 40-281.

Birge, JR. and Louveaux, F. 1997. Introduction to Stochastic Programming. Springer-Verlag. New York, USA. 14-300.

Epstein, RL. and Carnielli, WA. 1989. Computability: Computable Functions, Logic, and The Foundations of Mathematics. Wadsworth & Brooks/Cole Advanced Books & Software. Belmont. 91-127.

Fink, E. and Wood, D. 1996. Fundamentals of Restricted-Orientation Convexity. citeseer.ist.psu.edu/38250.html. (Accessed Oct 18, 2007).

Hiriart-Urruty, J-B. and Lemarechal, C. 1996. Convex Analysis and Minimization Algorithms I. Springer-Verlag. Berlin.

Hiriart-Urruty, J-B. and Lemarechal, C. 1996. Convex Analysis and Minimization Algorithms II. Springer-Verlag. Berlin.

Kasara, R. 2008. The Ackermann Function. http://kosara.net/thoughts/ackermann.html. (Accessed June 10, 2008)

Kling, A. 2007. Convexity. AP Statistics Lectures. http://arnoldkling.com/apstats/convexity.html. (Accessed Oct 18, 2007)

Lebanon, G. 2006. Convex Functions. www.cc.gatech.edu/~lebanon/notes/convexFunctions.pdf. (Accessed 5 December 2007).

Moon, T. 2000. Convexity and Jensen's inequality. http://www.neng.usu.edu/classes/ece/7860/lecture2/node5.html. (Accessed Dec 4, 2007).

Moreau, JJ. 1988. Bounded Variation in Time. In: Topics in Nonsmooth Mechanics. Eds. Moreau, JJ., Panagiotopoulos, PD. and G. Strang. Birkhauser-Verlag, Basel.1-74.

Odifredi, P. 2005. Recursive Functions. Metaphysics Research Lab. CSLI. Stanford University. Stanford Encyclopedia of Philosophy, Stanford.

Potter, L. 2005. Convexity. http://cnx.org/content/m10328/latest/. (Accessed Dec 4, 2007).

Robinson, RM. 1947. Primitive Recursive Functions. Bull. Amer. Math. Soc. 53: 925-942.

Stankova-Frenkel, Z. 2001. Convex Functions. http://mathcircle.berkeley.edu/BMC4/Handouts/inequal/node3.html. (Accessed Dec 5, 2007).

Uspensky, JV. 1948. Theory of Equations. McGraw-Hill Book Company. New York, N.Y. 214-290.

Wikipedia, 2008. Vandermonde Matrix. http://en.wikipedia.org/wiki/Vandermonde_matrix. (Accessed June 13, 2008).

Wong, SSM. 1997. Computational Methods in Physics and Engineering. Second Edition. World Scientific Publishing. Singapore. 63-112.

Received: April 25, 2009; Accepted: Aug 27, 2009

SENRA Academic Publishers, Burnaby, British Columbia
Vol. 3, No. 3, pp. 967-973, 2009
ISSN: 1715-9997

Canadian Journal of pure&applied sciences

EFFECTIVENESS OF LIGNITE COAGULANT FOR REMOVAL OF TEXTILE DYES FROM AQUEOUS SOLUTIONS AND TEXTILE WASTE WATER

*TR Sundararaman[1], V Ramamurthi[2] and N Partha[2]
[1]Department of Chemical Engineering, Adhiparasakthi Engineering College, Melmaruvathur-603 319.
[2]Department of Chemical Engineering, A.C. Tech., Anna University, Chennai-600 025, India.

ABSTRACT

Lignite soil was found to be an effective coagulant aid for color removal of textile dyes from aqueous solutions. A comparative study with conventional coagulant had been done. Results show that lignite soil can effectively remove reactive, vat and disperse dyes from their 50mg/L aqueous solutions. Parameters such as color, settled sludge volume have been evaluated. Results showed an increase of color removal, reduction in settled sludge volume when lignite soil was used as coagulant aid with alum and $MgCl_2$. It was found that color removal for reactive blue, vat blue and disperse red was 93%, 92%, 96% for alum, 100% respectively for all dyes with alum and lignite, 100%, 80%, 92% for $MgCl_2$ and 100% respectively for all dyes with magnesium chloride and lignite. For the textile waste water, the color removal was found to be 85% and 91% for alum and alum with lignite, 84% and 90% for $MgCl_2$ and $MgCl_2$ with lignite. The mechanism for coagulation by lignite was found to be a charge adsorption neutralization process. The optimum pH range for lignite coagulant was from 3 to 6. It was found that the settled sludge volume reduced from 90ml to 55ml, and 150ml to 75ml when lignite was used as coagulant aid for alum and $MgCl_2$, for reactive dyes, 50ml to 10ml and 80ml to 30ml when lignite was used as coagulant aid for alum and $MgCl_2$ for vat dyes, 78ml to 55ml and 92ml to 78ml when lignite was used as coagulant aid for alum and $MgCl_2$ for disperse dyes and 84ml to 55ml and 100ml to 80ml when lignite was used as coagulant aid for alum and $MgCl_2$ for textile waste water.

Keywords: Color removal, lignite, chemical coagulation, dyes.

INTRODUCTION

The wastewater is a major environmental issue of the textile industries. In typical dyeing processes, 50-95% of the dye is fixed on to the fibre, and unfixed dyes from subsequent washing operations are discharged in the spent dye bath or in the waste waters (Jiratananon, 2000). These waters must be treated prior to discharge in order to comply with the environmental protection laws for the receiving waters. Biological treatment processes are frequently used to treat textile effluents. These processes are generally efficient for biochemical oxygen demand (BOD) and suspended solids (SS) removal, but they are largely ineffective for removing color from the wastewater (McKay, 1979) because dyes have slow biodegradation rate (Bennett and Reeser, 1988).

The treatment technologies now recommended to meet color removal requirements are physicochemical treatment operations, including adsorption (Ahmad and Ram, 1992; McKay, 1979), ozonation (Lin, 1993), oxidation (Boon *et al*., 2000), chemical precipitation (Dziubek and Kowal, 1983) etc. Each has its merits and limitations in applied decolorization treatment operations. But coagulation-flocculation is the most common chemical treatment method for decolorization (Bennet and Reeser, 1988; Beulkar and Jekel, 1993; Klimiuk, 1999; Helal Uddin, 2003; Seluk, 2005; Nabi Bidhendi, 2007; Yue, 2008). Coagulation is a process for combining colloidal and suspended particles and/or dissolved organic matter in to large aggregates, thereby facilitating their removal subsequently. Chemical coagulants can destabilize particles by four distinct mechanisms: double layer compression, charge neutralization, enmeshment in a metal hydroxide precipitate and inter-particle bridging.

Aluminium sulphate (alum) is the most widely used coagulant in wastewater treatment industry. Using alum, particle destabilization is believed to be brought about by Alpolymers which are kinetic intermediates in the eventual precipitation of a metal hydroxide. These polymers are adsorbed on colloidal particles. The amount of polymer adsorbed and consequently the dosage of alum coagulant necessary to accomplish destabilization of colloidal particles depend on the concentration of colloids. If pH is below the zero point of charge (z.p.c) of the Al hydroxide, positively charged polymers will prevail and adsorption of these positive polymers can destabilize negatively charged colloids by charge neutralization. At high doses of alum, a sufficient degree

*Corresponding author email: sundararamantr@yahoo.co.in

of oversaturation induces rapid precipitation of a large quantity of aluminum hydroxide to form "sweep floc". $MgCl_2$ is a less commonly used coagulant in the industrial waste water treatment. A number of researchers have revealed that enhanced removal of impurities or pollutants has been observed in the presence of magnesium (Liao and Randtke, 1986; Tan *et al*., 2000). Good coagulation could be achieved if enough Mg^{2+} ion was present in the system of lime treatment (Folkman and Wachs, 1973). Dolomite and bittern, which are enriched in magnesium, are found to be very effective in the removal of turbidity and coloring matters.

Lignite soil is a naturally occurring polyelectrolyte, which is mainly the resultant product of the decayed vegetation over a period of time. It is organic in nature and major components are humic acid, lignin and carbohydrates. The aim of the present investigation was to study the effectiveness of this lignite as coagulant aid to remove, reactive, vat and disperse dyes from their aqueous solution and from textile waste water.

MATERIALS AND METHODS

Lignite soil was collected from Neyveli Lignite Corporation, TamilNadu, India. The alum and $MgCl_2$ of commercial grade were used. Analytical grade HCl and NaOH were used for this study. Textile wastewater was collected from one of the textile industry in Erode, Tamil Nadu, India. Lignite coagulant solution used in this study was 4%(w/v) solution, while for alum and $Mgcl_2$, solution of 1 %(w/v) was used.

Coagulation experiments were carried out with rapid

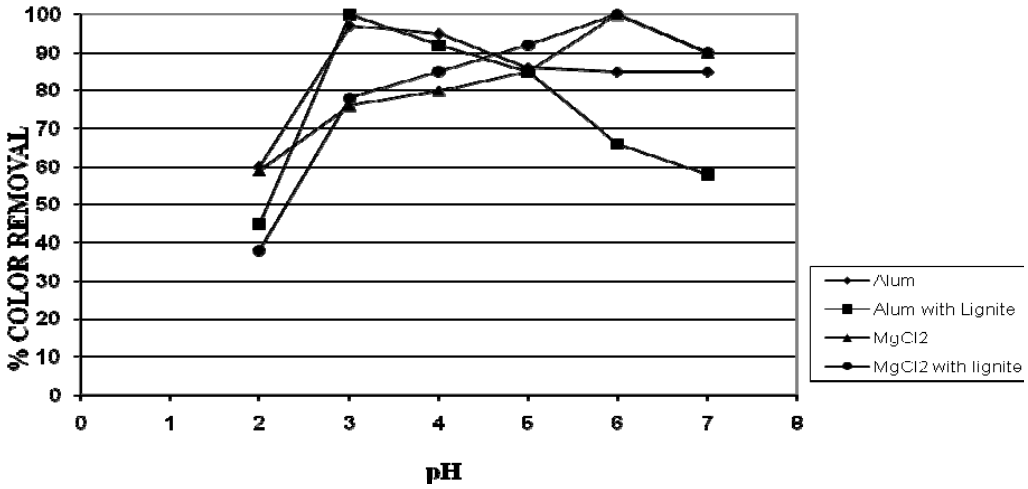

Fig. 1. Effect of pH on color removal of Vat Dyes.

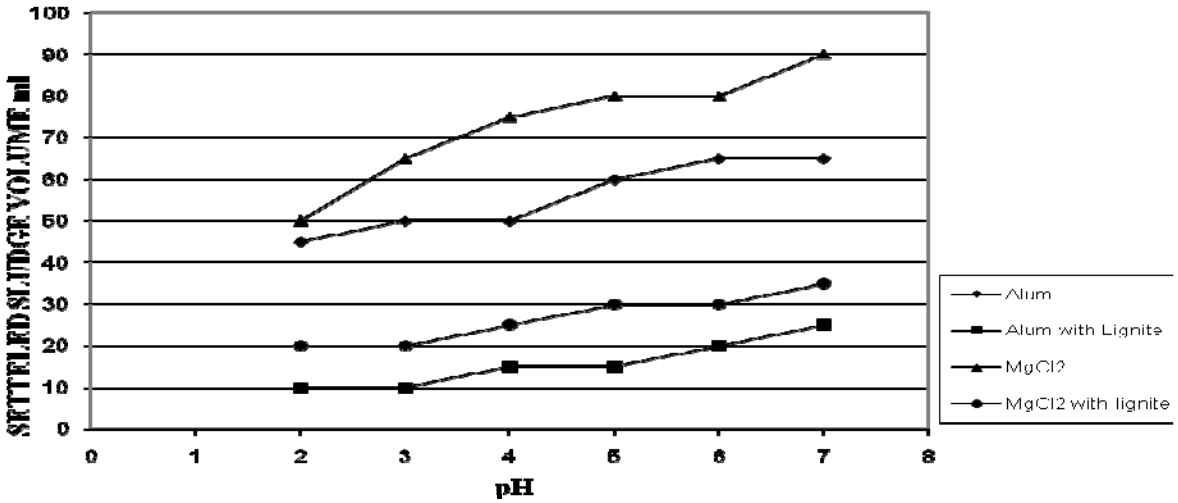

Fig. 2. Settled sludge volume Vs pH for different coagulants for Vat Dyes.

agitation at 500rpm for 2 minutes for thorough mixing, followed by slow mixing at 60rpm for 10 minutes and settling time of 45 minutes. All the experiments were carried out at room temperature. Coagulation studies were conducted in a one litre beaker. Sample volume for dye solution and textile wastewater used was 500ml. After settlement of the sludge, the supernatant was collected for the absorbance measurement and the percentage color removal calculated. Dye Concentration used was 50mg/L for all the dyes. Concentration of the dye samples was measured at the wavelength of the maximum absorbance (λ_{max}), which was determined using a UV-Vis spectrophotometer. The percentage removal of a dye was calculated from the absorbance of the supernatant to the standard curve of each dye obtained from its concentration. For textile wastewater, the λ_{max} was determined by similar method and the percentage removal of the color was calculated considering the original wastewater absorbance value as 0% removal.

RESULTS AND DISCUSSION

In this study, coagulation process was used to decolorize aqueous dye solutions and textile wastewater. The optimum pH and the settled sludge volume were determined by comparing the effectiveness of alum, $MgCl_2$, with Lignite soil for obtaining maximum color removal. At optimum pH and coagulant dose, the effect of coagulant aid has been evaluated. Figures 1,3,5,7 show the percent removal of color at different pH. Figures 2, 4, 6 and 8 show the volume of settled sludge at different pH.

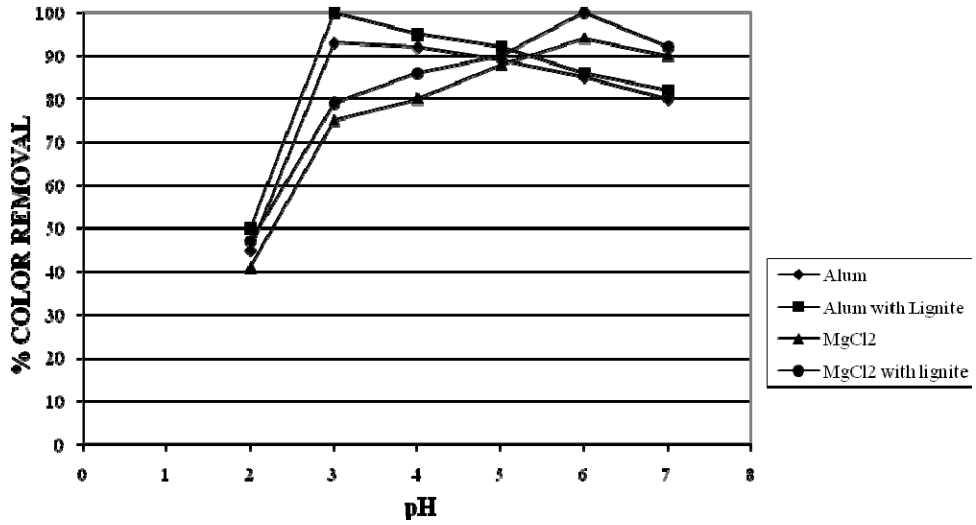

Fig. 3. Effect of pH on color removal of Reactive Dyes.

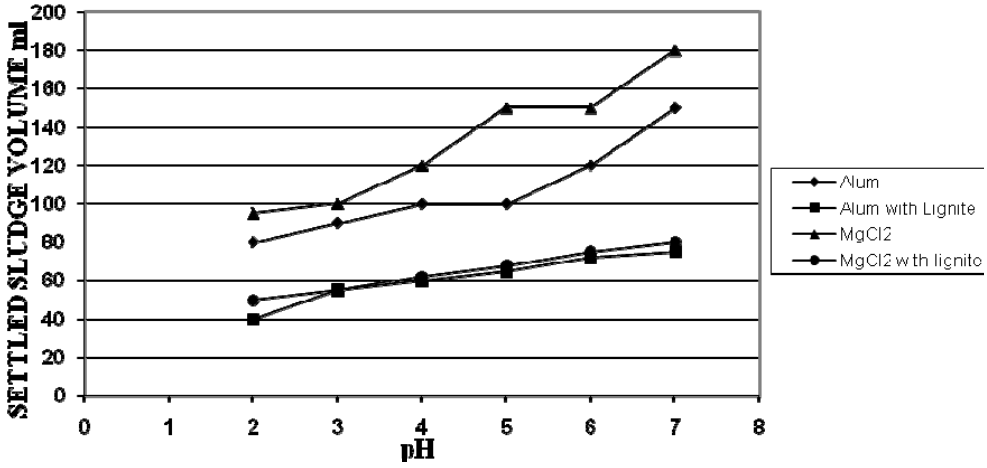

Fig. 4. Settled sludge volume Vs pH for different coagulants for Reactive Dyes.

Alum effect

Vat dyes

Figure 1 shows an increase in color removal from 60% at pH 2 to 97% at pH 3. As the pH was increased from 3 to 7, the percentage color removal decreased from 97 % to 85 %. The settled sludge volume increased from 45 ml to 65 ml as pH was increased from 2 to 7 (Fig. 2). With lignite soil as coagulant aid, there was an increase in color removal from 45 % at pH 2 to 100% at pH 3 (Fig. 1). As the pH was increased from 3 to 7, the color removal decreased from 100% to 58 %. The settled sludge volume increased from 10 ml to 25 ml as pH was increased from 2 to 7 (Fig. 2). At the optimum pH 3, for alum and alum with lignite, the color removal percentage and settled sludge volume were 97%, 100% and 50ml, 10ml respectively.

Reactive dyes.

Figure 3 shows an increase in color removal from 45% at pH 2 to 93 % at pH 3. As the pH was increased from 3 to 7, the percentage color removal decreased from 93% to 80 %. As the pH was increased from 2 to 7, the settled sludge volume increased from 80ml to 150ml (Fig. 4). With lignite soil as coagulant aid, an increase in color removal from 50% at pH 2 to 100 % at pH 3 occurred (Fig. 3). As the pH was increased from 3 to 7, the percentage color removal decreased from 100 % to 82 %. The settled sludge volume increased from 40ml to 75ml as pH was increased from 2 to 7 (Fig. 4). At the optimum pH 3, for alum and alum with lignite, the color removal percentage and settled sludge volume were 93%, 100% and 90ml, 55ml respectively.

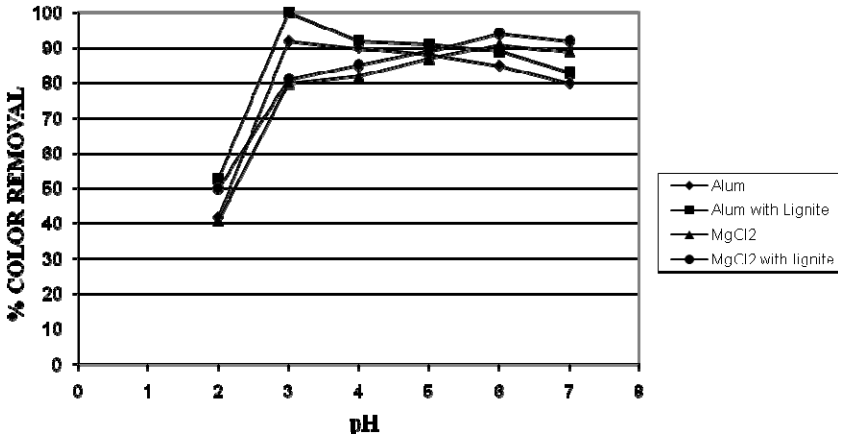

Fig. 5. Effect of pH on color removal of Disperse Dyes.

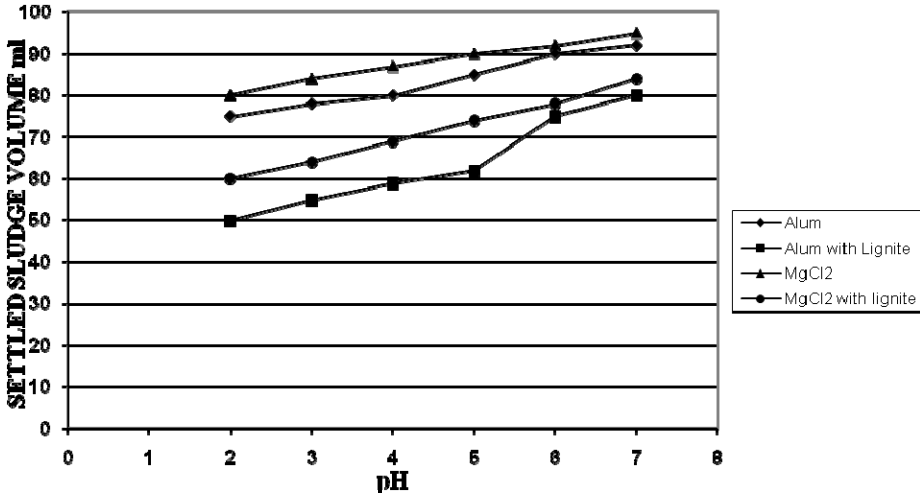

Fig. 6. Settled sludge volume Vs pH for different coagulants for Disperse Dyes.

Disperse dyes

Figure 5 shows an increase in color removal from 42% at pH 2 to 92% at pH 3. As the pH was increased from 3 to 7, the percentage color removal decreased from 92% to 80%. The settled sludge volume increased from 75ml to 92ml as pH was increased from 2 to 7 (Fig. 6). With lignite soil as coagulant aid, an increase in color removal from 53% at pH 2 to 100% at pH 3 was observed (Fig. 5). As the pH was increased from 2 to 7, the percentage color removal decreased from 100% to 83%. The settled sludge volume increased from 50ml to 80ml as P_H was increased from 2 to 7 (Fig. 6). At the optimum pH 3, for alum and alum with lignite, the color removal percentage and settled sludge volume were 92%, 100% and 78ml, 55ml respectively.

Textile dye effluent

Figure 7 shows an increase in color removal from 42% at pH 2 to 85% at pH 3. As the pH was increased from 3 to 7, the percentage color removal decreased from 85 % to 58 %. The settled sludge volume increased from 78ml to 105ml as pH was raised from 2 to 7 (Fig. 8). With lignite soil as coagulant aid, an increase in color removal from 50% at pH 2 to 91% at pH 3 was found (Fig. 7). As the pH was increased from 2 to 7, the percentage color removal was decreased from 91% to 70%. The settled sludge volume increased from 50ml to 80ml as pH was increased from 2 to 7 (Fig. 8). At the optimum pH 3, for alum and alum with lignite, the color removal percentage and settled sludge volume were 85%, 91% and 84ml, 55ml respectively.

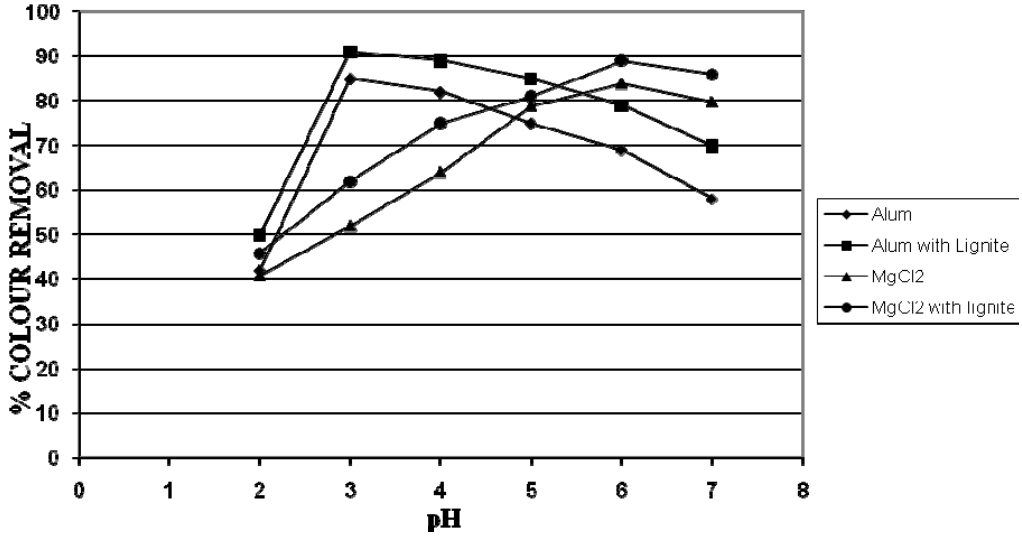

Fig. 7. Effect of pH on color removal of Textile dye effluent.

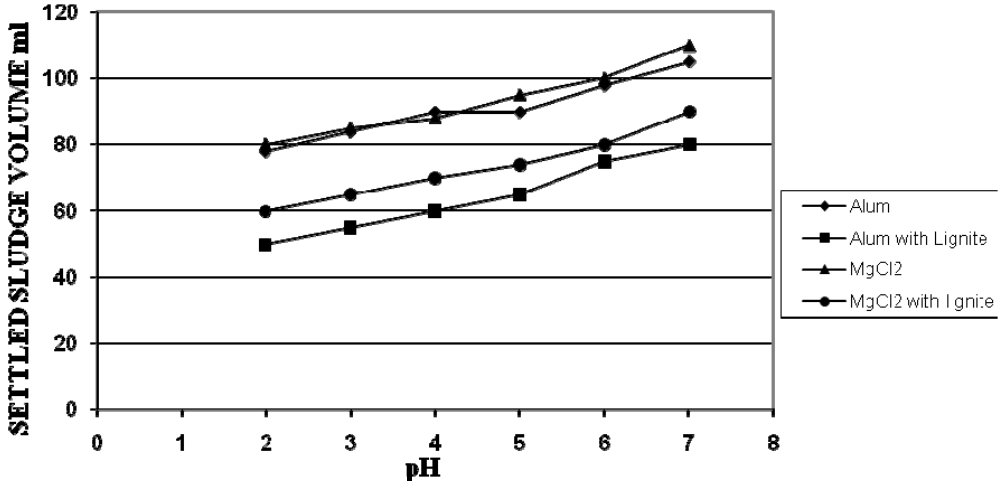

Fig. 8. Settled sludge volume Vs pH for different coagulants for Textile dye effluent.

$MgCl_2$ effect

Vat dyes

Figure 1 shows an increase in color removal from 59% to 100% as the pH was increased from 2 to 6. As the pH was increased from 6 to 7 the color removal decreased from 100% to 90%. The settled sludge volume increased from 50ml to 90ml as pH was increased from 2 to 7 (Fig. 2). With lignite soil as coagulant aid, an increase in color removal from 38 % to 100 % occurred as pH was increased from 2 to 6 (Fig. 1). As the pH was increased from 6 to 7 the percentage color removal decreased from 100 % to 89 %. The settled sludge volume increased from 50 ml to 90 ml as pH was increased from 2 to 7 (Fig. 2). At the optimum pH 6, for $MgCl_2$ and $MgCl_2$ with lignite, the color removal percentage and settled sludge volume were 100%, 100% and 80ml, 30ml respectively.

Reactive dyes

Figure 3 shows an increase in color removal from 41% to 94% as the pH was increased from 2 to 6. As the pH was increased from 6 to 7 the color removal decreased from 94% to 90%. The settled sludge volume increased from 98ml to 180ml as pH was increased from 2 to 7. With lignite soil as coagulant aid, an increase in color removal from 48 % to 97 % occurred as pH was increased from 2 to 6 (Fig. 3). As the pH was increased from 6 to 7, the percentage color removal decreased from 97% to 92%. The settled sludge volume increased from 95ml to 180ml as pH was increased from 2 to 7 (Fig. 4). At the optimum pH 6, for $MgCl_2$ and $MgCl_2$ with lignite, the color removal percentage and settled sludge volume were 94%, 100% and 150ml, 75ml respectively.

Disperse dyes

Figure 5 shows an increase in color removal from 40% to 91% as the pH was increased from 2 to 6. When the pH was increased from 6 to 7 the color removal decreased from 91% to 89%. The settled sludge volume increased from 80ml to 95ml as pH was increased from 2 to 7. With lignite soil as coagulant aid, an increase in color removal from 50 % to 95 % was observed as pH was increased from 2 to 6. When the pH was increased from 6 to 7, the percentage color removal decreased from 95% to 92%. The settled sludge volume increased from 80ml to 95ml as the pH was raised from 2 to 7 (Fig. 6). At the optimum pH 6, for $MgCl_2$ and $MgCl_2$ with lignite, the color removal percentage and settled sludge volume were 91%, 94% and 92ml, 78ml respectively.

Textile dye effluent

Figure 7 shows an increase in color removal from 40% to 91% as the pH was increased from 2 to 6. When the pH was increased from 6 to 7 the color removal decreased from 91% to 89%. The settled sludge volume increased from 80ml to 95ml as the pH was increased from 2 to 7 (Fig. 8). With lignite soil as coagulant aid an increase in color removal from 46 % to 90 % was observed as pH was increased from 2 to 6 (Fig. 1). As the pH was raised from 6 to 7, the percentage color removal decreased from 90 % to 86 %. The settled sludge volume increased from 60 ml to 90 ml as the pH was increased from 2 to 7 (Fig. 8). At the optimum pH 6, for $MgCl_2$ and $MgCl_2$ with lignite, the color removal percentage and settled sludge volume were 84%, 90% and 100ml, 80ml respectively.

CONCLUSIONS

Lignite coagulant is able to remove efficiently 100% of vat and disperse dyes and 96% of reactive dyes from their 50 ppm aqueous solutions. pH plays an important role in coagulation for all the 3 dyes. In the pH range of 3-6, coagulants showed a higher color removal percentage. There was a considerable decrease in settled sludge volume with lignite soil as coagulant aid. The mechanism of coagulation with lignite was found to be charge adsorption neutralization. We can conclude that lignite soil which is freely available can be used as coagulant aid for effective removal of colour and reduction in sludge volume. Lignite also reduces the amount of coagulant used.

REFERENCES

Ahmad, MN. and Ram, RN. 1992. Removal of Basic dye from waste water using silica as adsorbent. Environ. Pollut. 77-99.

Bennett, DH. and Reeser, D. 1988. Pre-treatment of CTMP effluent by lime to reduce sulphite and color. Environmental conference Charleston. 199-207.

Beulker, S. and Jekel, M. 1993. Precipitation and coagulation of organic substances and color from industrial waste water. Water science technology. 28:193-199.

Boon, HT., Tjoon TT. and Mohd Omar. AK. 2000. Removal of dyes and industrial dye wastes by Magnesium Chloride. Water resources. 34:597-601.

Dziubek, AM. and Kowal, AL. 1983. Water treatment by coagulation and adsorption with dolomite. Chemistry for protection of environment In proceedings of an international conference, Toulouse, France. 205.

Folkman, Y. and Wachs, AM. 1973. Removal of algae from stabilization pond effluents by lime treatment. Water Resources.7:419.

Helal uddin, ABM., Ahmad Sujari, AN. and Mohd. Nawi, MA. 2003. Effectiveness of peat coagulant for removal of textile dyes from aqueous solutions and textile waste water. Malaysian journal of chemistry. 5:34-43.

Jiratananon, R., Sungpet, A. and Luangsowan, P. 2000. Performance evaluation of nano filtration membranes for

treatment of effluents containing Reactive Dye and salt. Desalination. 130:177-183.

Klimiuk, E., Filipkowska, U. and Korzeniowska. 1999. Effects of pH and coagulant dosage on effectiveness of coagulation of Reactive dyes from model waste water by polyaluminium chloride. Journal of Environmental studies. 8:73-79.

Liao, MY. and Randtke, SJ. 1986. Predicting the removable of soluble organic contaminants by lime softening. Water Resources. 20:27.

Lin, SH. and Lin, CM. 1993. Treatments of textile waste effluents by ozonation and chemical coagulation. Water resources.27:17-43.

McKay, G. 1979. Waste color removal from textile effluents. J. American Dyestuff Reporter. 68: 29-36.

Nabi Bidhendi, GR., Torabian, A., Ehsani, H. and Razmkhah N. 2007. Evaluation of Industrial dyeing waste water treatment with coagulants and polyelectrolyte as coagulant aid. Journal of Environmental health science Engg. 4:29-36.

Seluk, H. 2005. Decolorization and detoxification of textile waste water by ozonation and coagulation processes. Dyes and Pigments.64:217-222.

Tan, BH., Teng, TT. and Mohd Omar, AK. 2000. Removal of dyes and industrial dye wastes by Magnesium Chloride. Water resources.34:597-601.

Yue, Q.Y., Gao, BY., Wang, Y., Zhang, H., Sun, X., Wang, S.G. and Roy, R. Gu. 2008. Synthesis of polyamine flocculants and their potential use in treating dye waste water. Journal of Hazardous Materials. 152:221-227.

Received: Feb 12, 2009; Revised: July 4, 2009; Accepted: July 7, 2009

SENRA Academic Publishers, Burnaby, British Columbia
Vol. 3, No. 3, pp. 975-981, 2009
ISSN: 1715-9997

Canadian Journal of pure&applied sciences

A THEORETICAL STUDY OF THE THRESHOLD VOLTAGE SENSITIVITY TO PROCESS VARIATION IN SYMMETRIC DOUBLE GATE MOS DEVICES

Ajay Kumar Singh
Faculty of Engineering and Technology, Multimedia University
Jalan Ayer Keroh Lama 75450 Melaka, Malaysia

ABSTRACT

In this paper we have studied the threshold voltage sensitivity to process variation like channel length, silicon film thickness (t_{Si}) and gate oxide thickness (t_{OX}) in undoped symmetric Double gate (SDG) metal oxide semiconductor field effect transistors (MOSFETs) after developing an analytical model of threshold voltage (V_{Th}). In the proposed model we have introduced a parameter α to take care of Drain-induced barrier lowering (DIBL) effect and quantum confinement effect in sub micron SDG metal oxide semiconductor (MOS) devices. To verify the validity of our developed model, we have compared the simulation results of threshold voltage model with two-dimensional MINIMOS simulator results and found a close agreement. These analytical expressions for sensitivity are solved numerically and compared with published results. The analytical expressions of the sensitivity strongly depend on the device parameter combinations. The study suggests that the threshold voltage sensitivity to length imposes a serious constrain on the scaling of SDG MOS devices. The V_{Th} sensitivity to t_{OX} is not a serious issue for longer SDG MOS devices whereas in deep sub-micron regime, its effect can not be ignored which put restriction on the choice of the gate oxide thickness value.

Keywords: Poisson's equation, threshold voltage sensitivity, electrostatic potential, symmetrical double gate MOS devices, mobile charge sheet density**.**

INTRODUCTION

As Complementary metal oxide semiconductor (CMOS) transistor size is approaching the limit imposed by oxide tunneling and voltage non-scaling as discussed by Assad *et al*. (2000), Jurczak *et al*. (2005) and Ishimaru (2008), double gate (DG) MOSFET is becoming a subject of intense VLSI research because of its good control over short channel effects as suggested by Liang and Taur (2004), Reyboz *et al*. (2006), He *et al*. (2007) and Tsormpatzoglou *et al*. (2007). Double gate structure has been the subject of intensive research due to its ideal 60mV/decade subthreshold slope as shown by Jung and Dimitrijev (2006), scaling by silicon film thickness without high doping, and adjusting threshold voltage by gate work functions. The key factors that limit the scaling of DG MOSFETs are threshold voltage roll-off and drain induced barrier lowering (DIBL). The threshold voltage roll-off has been studied extensively by Chen *et al*. (2003), Reyboz *et al*. (2006), Lu and Taur (2006), Ananthan and Roy (2006), Hamid *et al*. (2007), Lime *et al*. (2008), Tsormpatzoglou *et al*. (2008) and Gong *et al*. (2008).

The threshold voltage of DG MOSFETs is a strong function of gate length (L) and silicon film thickness (t_{Si}). An interesting application of the analytical threshold voltage (V_{Th}) model is to study threshold voltage (V_{Th}) sensitivity quantitatively in a more thorough and easier way than the numerical solutions to see the effect of the process variations. Cerderia *et al*. (2008) has performed simulation based study to see V_{Th} sensitivities to L and t_{Si} but they focused only on a single technology node. In this paper authors neither have given any attention on the impact of t_{OX} on V_{Th} variation nor provided a quantitative and systematic analysis. Chen *et al*. (2003) have studied the V_{Th} sensitivities to process parameters in different way and provided the useful information about the scaling limit of DG MOSFETs but their model is lack of DIBL effect. Their model also overestimates the threshold voltage sensitivity parameter to length for thin silicon film.

In the present paper, we have derived the analytical expression for the electrostatic potential in the symmetric double gate (SDG) MOSFETs by solving Poisson's equation under appropriate boundary conditions. The electrostatic potential along the film thickness reduces with increase in film doping concentration as well as source/drain concentration. We have included the DIBL effect and quantum confinement effects in our model and verified the developed model with a close agreement with two-dimensional MINIMOS Simulator results. The analytical models of V_{Th} sensitivities to process variations show a strong dependence on the device parameter combinations. The numerical value of threshold voltage

*Corresponding author email: ajay.singh@mmu.edu.my

sensitivity parameter to length is very close to reported result (~6.8mV/nm) by Takeuchi *et al*. (2001) for very thin silicon film.

Mathematical Formulation

Figure 1 shows the schematic diagram of an undoped symmetric double gate MOSFET (SDG). The channel electrostatic potential under threshold condition is governed by the Poisson's equation with only the inversion charge term included

$$\frac{\partial^2\psi}{\partial x^2} + \frac{\partial^2\psi}{\partial y^2} = \frac{q}{\varepsilon_{si}} n_i e^{\frac{q}{KT}(\psi - \psi_F)} \quad (1)$$

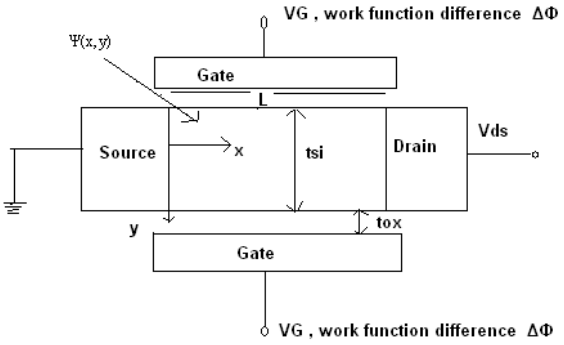

Fig. 1. Schematic diagram of a Symmetric DG MOSFET.

Where Ψ is the electrostatic potential with respect to Fermi level in the source, n_i is the intrinsic electron density and Ψ_F is the non equilibrium quasi-Fermi level with respect to Fermi level in the source and satisfying following boundary conditions; $\Psi_F(0,y)=0$ and $\Psi_F(L,y)=V_{ds}$. According to these two boundary conditions, Ψ_F incurs most of its change near the drain end and stays close to zero in the mid-channel and near source regions. CGA assumes that the Quasi-Fermi potential Ψ_F stays constant along the Y-direction because the current flows along the X-direction i.e. along the channel. Based on these observation $\Psi_F(x,y)$ can be approximated to be zero everywhere except at the end of the channel. Such approximation is implemented by modifying equation (1) as

$$\frac{\partial^2\psi}{\partial x^2} + \frac{\partial^2\psi}{\partial y^2} = \frac{q}{\varepsilon_{si}} n_i e^{\beta\psi} \quad (2)$$

Where β= (q/KT).

In DG MOS, junction depth (X_j) is equal to the silicon body thickness (t_{si}), which is also an important device parameter which is defined by a particular technology. For simplicity of the analysis we have ignored this parameter as well as quantum confinement effect, which dominates for t_{si}<10nm, in the present communication.

Ψ(x,y) in equation (2) can be expressed as

$$\Psi(x,y)=\Psi_0(x)+\Psi_1(x,y) \quad (3)$$

Where $\Psi_0(x)$ is the solution of 1-D Poisson's equation

$$\frac{d^2\psi_0}{dx^2} + \frac{d^2\psi_0}{dy^2} = \frac{q}{\varepsilon_{si}} n_i e^{\beta\psi_0} \quad 4(a)$$

And the solution of equation (4a) is given by Chen *et al*. (2003)

$$\psi_0(x) = \psi_{0m} + \frac{1}{\beta}\ln(\sec^2 B(\frac{x}{L} - \frac{1}{2})) \quad 4(b)$$

Where $\psi_{0m} = V_{bi} - \frac{2}{\beta}\ln\frac{2 + e^{\frac{\beta V_{bi}}{2}}\frac{L}{\lambda_D}}{\pi}$,

represents the minimum potential in the source-channel-drain junction without intervention of the gate bias.

And

$$B = \frac{\pi}{1 + 2e^{\frac{-\beta V_{bi}}{2}}\frac{\lambda_D}{L}}$$

$\lambda_D = \sqrt{\frac{2\varepsilon_{si}}{\beta q n_i}}$ called intrinsic Debye Length

$\Psi_1(x,y)$ is the solution of the remnant 2-D equation

$$\frac{\partial^2\psi_1(x,y)}{\partial x^2} + \frac{\partial^2\psi_1(x,y)}{\partial y^2} = \frac{q}{\varepsilon_{si}} n_i e^{\beta\psi_0}[e^{\beta\psi_1(x,y)} - 1] \quad 4(c)$$

With boundary conditions; $\psi_1(0,y)=0$, $\psi_1(L,y)=0$ and field continuity equation at the interface. We have solved the equation 4(c) by using separation of variable technique and solution is given as,

$$\psi_1(x,y) = [1 + \{1 + 2\ln Sec(\frac{x}{L} - \frac{1}{2}) - \frac{\rho^2 L^2}{2}(\frac{x}{L} - \frac{1}{2})^2 + D\}^{\frac{1}{2}}]\frac{(V_{GS} - \Delta\phi)}{Cosh\rho\gamma} Cosh(\rho y) \quad (5)$$

Where ρ is a separation constant, V_{GS} is gate source voltage, ΔΦ is work function difference of the materials and $D = \frac{\rho^2 L^2}{8} - 2\ln Sec\frac{B}{2}$

After adding equations 4(b) and (5), one can get the potential distribution Ψ(x,y) in the symmetric double gate MOSFET. The minimum electrostatic potential $\Psi_{min}(y)$ (i.e. virtual cathode) in the channel can be found through

$$\frac{\partial \psi(x,y)}{\partial x} = 0 \quad \text{And given as}$$

$$\psi_{\min}(y) = \psi_{0m} + \delta\left(\frac{V_{GS} - \Delta\phi}{Cosh\gamma\rho}\right)Cosh\rho y \qquad 6(a)$$

Where

$$\delta = [1 + \{1 + 2\ln SecB\sqrt{\frac{A(\eta-1)}{2}} - \frac{\rho^2 L^2}{4}A(\eta-1) + D\}^{\frac{1}{2}}]$$

A= (5/2) $(1/B^2)$, $\eta = \sqrt{1 - \frac{4F}{A^2}}$, F=$\frac{15}{2}\frac{1}{B^5}(B-\xi)$

and $\xi = \frac{\rho^2 L^2}{2B}$

The minimum electrostatic potential, along the channel for SDG, occurs at

$$\left(\frac{x_{\min}}{L}\right) = \frac{1}{2} - \sqrt{\frac{A}{2}}\sqrt{\eta - 1} \qquad 6(b)$$

From expression 6(b), it is clear that for η=1, the minimum potential along the channel occurs at the middle of the channel, as in the case of long channel MOS devices. This condition is satisfied,

$$\text{When } \sqrt{1 - \frac{4*F}{A^2}} = 1 \quad \text{or} \quad \frac{4*F}{A^2} = 0 \qquad 6(c)$$

i.e either F=0 or A=∞. A=∞, only when L→0 which is physically not possible.

$$\text{Therefore, F=0 which gives } \rho = \sqrt{2} * \frac{B}{L} \qquad 6(d)$$

To include the DIBL effect in channel potential of the Symmetric Double Gate MOSFET, we have modified the expression 6(d) as

$$\rho = \left(\frac{\alpha B\sqrt{2}}{L} + \frac{V_{ds}}{L}\right) \qquad 6(e)$$

Where, α is a fitting parameter to take care of DIBL effect and expressed in volt. For Vds=0 and α=1, equation 6(e) reduces to ρ=√2 (B/L). Under this condition η=1 and the minimum position will occur at (L/2). As V_{ds} or α increases, the parameter η increases and hence x_{min} moves towards the source end. This is called DIBL effect. The minimum surface potential is obtained by substituting $y=\pm t_{si}$ in equation 6(a) and given as

$$\psi_{s\min} = \psi_{0m} + \delta\left(\frac{V_{GS} - \Delta\phi}{Cosh\gamma\rho}\right)Cosh\left(\frac{t_{si}}{2}\rho\right) \qquad (7)$$

The threshold voltage is that value of gate voltage at which a conducting channel is induced at the surface of the MOSFET. Therefore, the threshold voltage is taken to be that value of gate source voltage for which ψsmin = $2\varphi_f$, where φ_f is difference between the extrinsic Fermi level in the bulk region and intrinsic Fermi level. Thus, substituting $V_{GS}=V_{Th}$ in expression (7) we get;

$$V_{Th} = \Delta\phi + \frac{Cosh\gamma\rho}{Cosh\rho\frac{t_{si}}{2}}\left(\frac{\psi_{s\min} - \psi_{0m}}{\delta}\right) \qquad (8)$$

The equation (8) shows that threshold voltage of undoped symmetric double gate MOSFET dependent on V_{ds} and silicon thickness (t_{si}) whereas the proposed model of Chen *et al.* (2003) is independent of V_{ds}. The threshold voltage dependence on the drain-bias is important for digital applications. The DIBL causes threshold voltage to be a function of the operating voltages. To show the validity of our developed model, we compared the simulation results of equation (8) with MINIMOS simulator and found a close agreement as shown in figure 2.

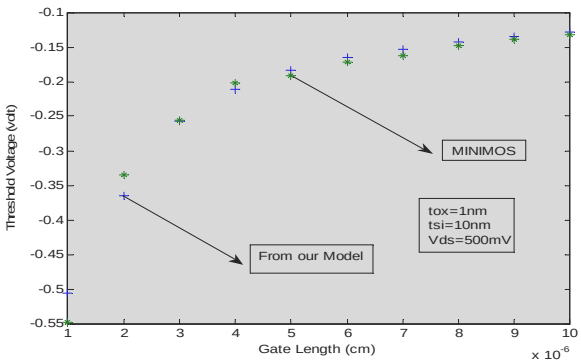

Fig. 2. Comparison of our simulated results with MINIMOS simulator results.

An interesting application of analytical V_{Th} model is to perform quantitative threshold voltage sensitivity analysis of SDG MOSFETS to access the effects of process variation. To demonstrate, V_{Th} sensitivities to process variation, we have derived the analytical models for $(\delta V_{Th}/\delta L)$, $(\delta V_{Th}/\delta t_{OX})$ and $(\delta V_{Th}/\delta t_{Si})$. Using equation (8), the V_{Th} sensitivity to L is given as:

$$\frac{\delta V_{Th}}{\delta L} = \left(\frac{2\phi_B - \psi_{om}}{\delta}\right)\left[\frac{\cosh(\rho\frac{t_{Si}}{2})\gamma\sinh(\gamma\rho) - (\frac{t_{Si}}{2})\cosh(\gamma\rho)\sinh(\rho\frac{t_{Si}}{2})}{\cosh^2(\rho\frac{t_{Si}}{2})}\right]K11$$

$$-\frac{\cosh(\gamma\rho)}{\cosh(\rho\frac{t_{Si}}{2})}\left[\frac{\delta K12 + (2\phi_B - \psi_{om})K13}{\delta^2}\right] \qquad (9)$$

Where

$$K11 = \frac{(L + K\lambda_D)(\frac{-V_{ds} K\lambda_D}{L^2}) - (\pi\sqrt{2} + V_{ds}(1 + K\frac{\lambda_D}{L}))}{(L + K\lambda_D)^2}$$

$$K = 2e^{-\frac{\beta V_{bi}}{2}}, K12 = -(\frac{2}{\beta})\frac{\pi}{(2 + Al\frac{L}{\lambda_D})}(\frac{Al}{\lambda_D}), Al = (\frac{2}{K}), K13 = \frac{d\delta}{dL}$$

Equation (9) shows the dependence of the V_{Th} sensitivity to L on the gate length, silicon film thickness and gate oxide thickness. Our analytical expression clearly shows that as L→0, V_{Th} sensitivity to L approaches to infinity. This reflects that a small change in length causes a large variation in threshold voltage of submicron SDG MOS devices.

Using equation (8) the V_{Th} sensitivity to t_{OX} can be modeled as:

$$\frac{\delta V_{Th}}{\delta t_{OX}} = \frac{m1\rho}{\cosh(\frac{t_{Si}\rho}{2})}\sinh(\gamma\rho) \quad (10)$$

Where $m1 = \frac{(2\phi_B - \psi_{om})}{\delta}$

$$\gamma = (\frac{t_{Si}}{2} + t_{OX})$$

Using $m = \frac{m1}{\cosh(\frac{t_{Si}\rho}{2})}$ and expanding sinh(γρ) by using Taylor's expansion and retaining only first term we get,

$$\frac{\delta V_{Th}}{\delta t_{OX}} = MX + cons\tan t \quad (11)$$

Where $M = m\rho$

And constant=$(M\frac{t_{si}}{2})$ and $X = t_{0x}$

From equation (11) it is clear that the V_{Th} sensitivity to t_{OX} varies linearly with gate oxide thickness for SDG MOS devices of very thin gate with a slope of [$K\rho^2$/cosh ((t_{Si}/2) ρ)]. Therefore, by knowing the slope of the curve, one can also find out the value of the parameter ρ and then α for a given silicon film thickness.

The V_{Th} sensitivity to t_{Si} is

$$\frac{\delta V_{Th}}{\delta t_{Si}} = \frac{-(m1\rho)}{2\cosh^2(\gamma - t_{OX})\rho}[\sinh(t_{OX}\rho)] \quad (12)$$

From relations (9), (10) and (11) it is clear that the analytical models of the threshold voltage sensitivities strongly depend on the device parameter combinations.

The positive and negative signs of the $\frac{\delta V_{Th}}{\delta L}$ and $\frac{\delta V_{Th}}{\delta t_{Si}}$ respectively are dictated by short channel effects (SCEs). From relation (12) it is seen that if ρ→0 i.e. as L→∞ the parameter $\frac{\delta V_{Th}}{\delta t_{Si}} \to 0$. In other words we can say that for very long channel SDG MOS devices the process variation is not a limiting factor.

Expanding the sinh term in equation (12) and retaining only two terms, we have

$$\frac{\delta V_{Th}}{\delta t_{Si}} = \frac{-(m1\rho)}{2\cosh^2(\gamma - t_{OX})\rho}(t_{OX}\rho)[1 + (t_{OX}\rho)^2/6] \quad (13)$$

DISCUSSION

We have compared our model's results with Munteanu *et al*. (2006) model results as shown in figure 3. The two models show a good agreement near the surfaces. The maximum difference of 2% between the two models is reported near the centre due to the negligence of quantum mechanical effect in our proposed model.

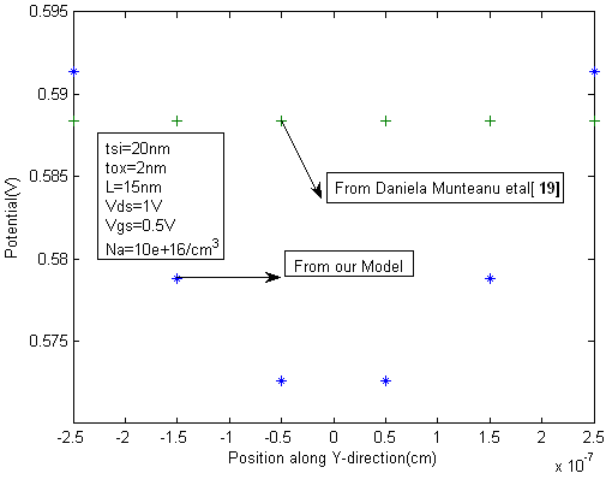

Fig. 3. A comparison of electrostatic potential with two models.

The effect of the silicon film doping on the threshold voltage is less distinct for deep submicron SDG MOS devices as shown in figure 4. It is also observed that threshold voltage takes lower value for any SDG MOS device of lightly doped.

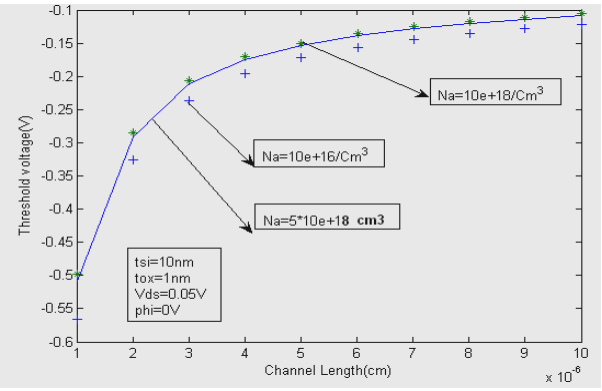

Fig. 4. Variation of threshold voltage with channel length for three different substrate doping concentration.

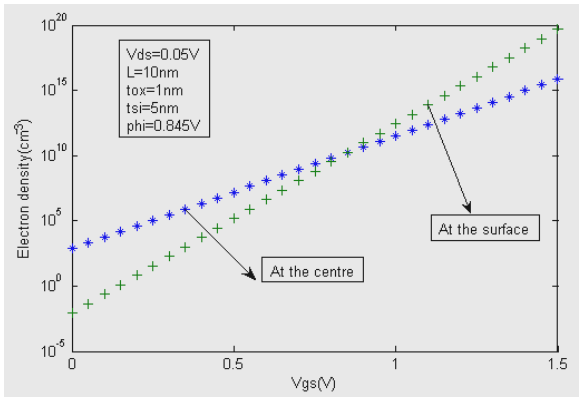

Fig. 5. Variation of electron density with Vgs for surface and Centre.

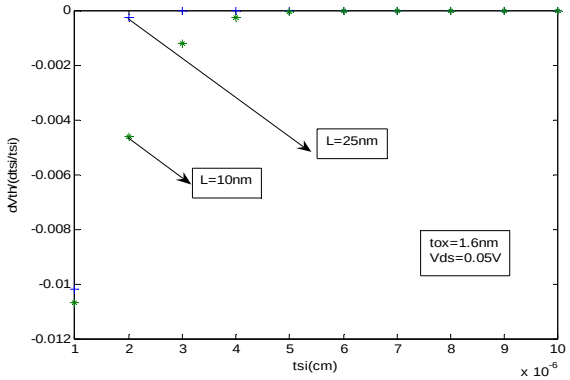

Fig. 6. Variation of threshold voltage sensitivity parameter with silicon film for two channel length.

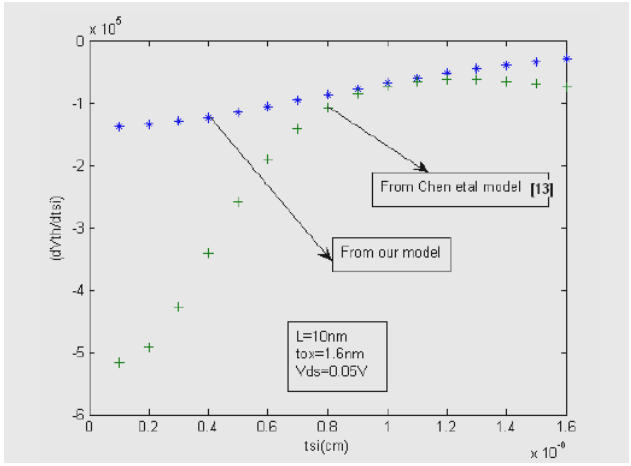

Fig. 7. Threshold voltage sensitivity to tsi parameter with t_{Si}: A comparison.

Figure 5 shows the variation of electron density with gate voltage at the surface and centre. The electron density varies linearly with gate voltage. It is observed that for Vgs<0.9V centre's electron density exceeds the surface electron density whereas for V_{gs}>0.9 V the surface electron density exceeds the centre's electron density and device will enter into the conduction mode. Therefore, we can conclude that there are two distinct regions of operation in the SDG MOS devices, just like in a conventional bulk MOSFETs.

We have plotted the V_{Th} sensitivity to t_{Si} with film thickness for two SDG MOS devices at V_{ds}=0.05V in figure 6. For thicker silicon film (i.e. t_{si}≥40nm), sensitivity parameter remains constant with the thickness irrespective of the channel length. An appreciable change is observed only for t_{si}<40nm. This study clearly shows that threshold voltage variation with silicon film is only a limiting factor for submicron MOS devices and put a stringent requirement for thin silicon film.

We have compared the simulated results of V_{Th} sensitivity to t_{Si} from our model and Chen *et al*. (2003) model as shown in figure 7. These two models show a good agreement for thicker silicon film whereas for thinner film two models deviate very much because of negligence of DIBL effect in Chen *et al*. (2003) model.

In figure 8, we have plotted the results obtained from equations (12) and (13). The two results shows an excellent agreement for thinner film whereas for thicker film (i.e. t_{si}>10nm) both results show disagreement.

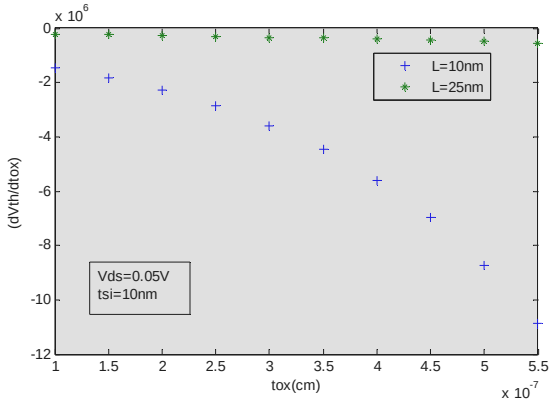

Fig. 9. Variation of threshold voltage sensitivity to tox with gate oxide thickness for two SDG MOS devices.

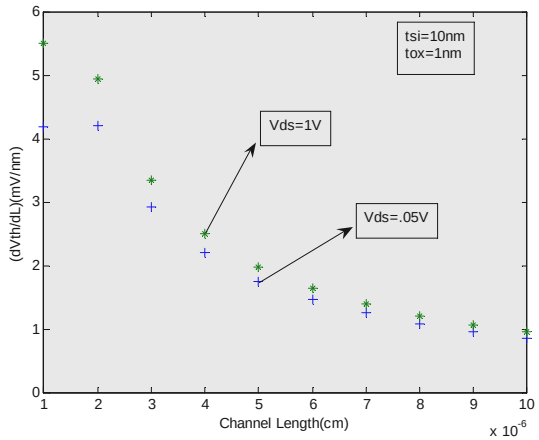

Fig. 10(a). Threshold voltage change versus channel length of SDG MOSFETs for two values of drain voltage.

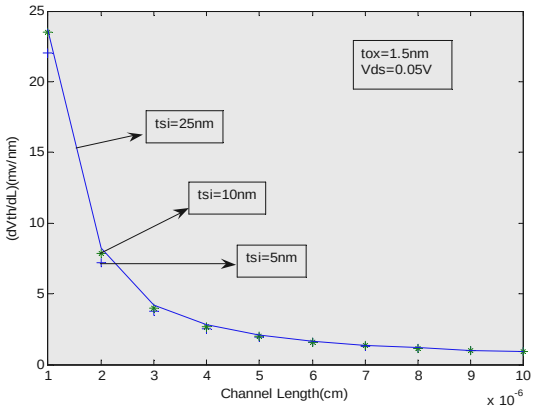

Fig. 10(b). Variation of threshold voltage sensitivity to length with channel length for three different silicon film thicknesses.

The parameter $(\frac{\delta V_{Th}}{\delta t_{OX}})$ is calculated for different values of gate oxide thickness (t_{OX}) by using equation (10) and results are plotted in figure 9. From graph, it is clear that this sensitive parameter shows a slight variation with gate oxide thickness for longer SDG MOS devices after t_{OX}≥2.5nm. An appreciable effect of t_{OX} on $(\frac{\delta V_{Th}}{\delta t_{OX}})$ is observed for sub-micron SDG MOS devices. The sensitive parameter $(\frac{\delta V_{Th}}{\delta t_{OX}})$ falls exponentially with increase in the value of gate oxide thickness. This falls in the parameter put a restriction on the choice of the gate oxide thickness in SDG submicron MOSFETs. This result is contradicting the findings of Chen *et al*. (2003) that the gate oxide thickness causes relatively insignificant threshold voltage variation.

From figure 10(a) it is observed that the sensitivity parameter decreases with channel length irrespective of the value of drain voltage. The sensitivity to L is always higher for higher drain voltage. This result shows that by applying proper drain voltage one can control the change of threshold voltage due to any variation in channel length.

The effect of silicon film thickness (t_{si}) on the threshold voltage (V_{Th}) sensitivity to L is negligible for SDG MOS devices of L≥50nm. The sensitive parameter is only affected by the film thickness for deep submicron MOS devices as shown in figure10 (b). A small V_{Th} sensitivity to L is observed for thinner film thickness. The calculated value of (dV_{Th}/dL) from our model is about 6.3mV/nm for tsi=7nm which is very close to reported result of 6.8mV/nm by Tokeuchi *et al*. (2001) whereas Chen *et al*. (2003) model overestimate this parameter for thinner silicon film. For tighter control over geometric variations, one can use a SDG MOS device of length L≥30nm with thinner silicon film thickness and oxide thickness.

CONCLUSION

In conclusion, the electrostatic potential in SDG MOS devices reduces along the silicon film thickness due to increase in silicon film doping or source/drain concentration. Threshold voltage of the SDG MOS devices can be adjusted at the desired value by choosing proper gate material. For long SDG MOS devices V_{Th} sensitivity to t_{OX} is independent of the gate oxide thickness whereas for submicron SDG MOS devices this parameter can not be ignored. The V_{Th} sensitivity to L decreases exponentially with increase in channel length irrespective of film thickness. The calculated value of the parameter $\frac{\delta V_{Th}}{\delta L}$ is very close to reported result for thin silicon film. The study clearly shows the stringent requirement for thin silicon film.

The limitation of the present study is that the derived model can not be used for a SDG device having film thickness t_{si}<10nm due to non inclusion of quantum mechanical effects.

REFERENCES

Ananthan, Hari. and Roy, Kaushik. 2006. A compact physical model for yield under gate length and body thickness variations in nanoscale double-gate CMOS. IEEE Trans. Electron Devices. 53:2151-2159.

Assad, Farzin., Zhibin, Ren., Vasileska. D., Datta, S. and Lundstorm, M. 2000. On the performance limits for Si MOSFET's: A theoretical study. IEEE Trans on Electron Devices. 47:232-240.

Cerderia, A., Moldovan, O., Iniguez, B. and Estrada, M. 2008. Modeling of potentials and threshold voltage for symmetric doped double-gate MOSFETs. Solid-state Electronics. 52:830-837

Chen, Q., Harrell, M., Evans. and Meindl, DJ. 2003. A Physical short-channel threshold voltage model for undoped symmetric double-gate MOSFETS. IEEE Trans Electron Devices. 50:1631-1637.

Gong, Jing-Feng., Chan, CH., Philip. and Chan, M. 2008. An explicit surface-potential-based model for undoped double-gate MOSFETs. Solid-state Electronics. 52:282-288.

Hamid, Hamdy Abd Ei., Guitart, JR. and Iniguez, B. 2007. Two-dimensional analytical threshold voltage and subthreshold swing models of undoped symmetric Double-gate MOSFETs. IEEE Trans on Electron Devices. 54:1402-1408.

He, Jin., Liu, Feng., Zhang, Jian., Feng, Jie., Hu, Jinhua., Yang, S. and Chan, M. 2007. A Carrier-Based Approach for Compact Modeling of the long-channel undoped Symmetric double-gate MOSFETs. IEEE Trans on Electron Devices. 54:1203-1209.

Ishimaru, K. 2008. 45nm/32nm CMOS –challenge and perspective. Solid-state electronics. 52:1266-1273.

Jung, Hak Kee. and Dimitrijev, S. 2006. Analysis of subthreshold carrier transport for ultimate DGMOSFET. IEEE Trans on Electron Devices. 53:685-691.

Jurczak, Malgorzata., Veloso, Anabela., Rooyackers, Rita., Augendre, Emmanuel., Mertens, Sofie., Rotschild, Aude., Scaekers, Marc., Lindsay, Richard., Lauwers, Anne., Henson, Kirklen., Severi, Simone., Pollentier, Ivan. and Keersgieter, An de. 2005. Challenges in scaling of CMOS devices towards 65nm node. Journal of telecommunications and information technology. 1:3-6.

Liang, Xiaoping. and Taur, Y. 2004. A 2-D Analytical Solution for SCEs in DG MOSFETs. IEEE Trans. On Electron Devices. 51:1385-1391.

Lime, Francois., Iniguez, B. and Moldovan, O. 2008. A Quasi-Two dimensional compact Drain-current model for Undoped Symmetric Double-Gate MOSFETs including Short-channel effects. IEEE Trans on Electron Devices. 55:1441-1448.

Lu, Huxin. and Taur, Y. 2006. An analytical potential model for symmetric and asymmetric DG MOSFETs. IEEE Trans on Electron Devices. 53:1161-1168.

Munteanu, Daniela., Autran, Jean-Luc., Loussier, Xavier., Harrison, Samuel., Cerutti, Robin. and Skotnicki, T. 2006. Quantum short-channel compact modeling of drain-current in double-gate MOSFET. Solid-State Electronics. 50:680-686.

Reyboz, M., Rozeau, O., Poiroux, T., Martin, P, and Jomaah, J. 2006. An explicit analytical charge-based model of undoped independent double-gate MOSFET. Solid State Electronics. 50:1276-1282.

Takeuchi, K., Koh, R. and Mogami, T. 2001. A study of the threshold voltage variation for ultra-small bulk and SOI CMOS. IEEE Trans on Electron Devices. 48:1995-2001.

Tsormpatzoglou, Andreas., Dimitriadis, A. Charalabos., Clerc, Raphael., Rafhay, Quentin., Pananakakis, G. and Ghibaudo, Gerard. 2007. Semi-Analytical Modeling of Short-Channel effects in Si and Ge symmetrical Double-Gate MOSFETs. IEEE Trans on Electron Devices. 54:1943-1952.

Tsormpatzoglou , Andreas., Dimitriadis, CA., Clerc, R., Pananakakis, G. and Ghibaudo, G. 2008. Threshold voltage model for short-channel undoped symmetrical double-gate MOSFETs. IEEE Trans on Electron Devices. 55:2512-2516.

Received: May 6, 2009; Revised: July 29, 2009; Accepted: August 4, 2009

SENRA Academic Publishers, Burnaby, British Columbia
Vol. 3, No. 3, pp. 983-992, 2009
ISSN: 1715-9997

Canadian Journal of pure&applied sciences

SYNTHESIS AND EVALUATION OF ANTIMICROBIAL ACTIVITY OF PHENYL AND FURAN-2-YL[1,2,4] TRIAZOLO[4,3-a]QUINOXALIN-4(5*H*)-ONE AND THEIR HYDRAZONE PRECURSORS

*Olayinka O Ajani[1] and Obinna C Nwinyi[2]
[1]Chemistry Department, College of Science and Technology, Covenant University
Canaanland, Km 10, Idiroko Road, PMB. 1023, Ota, Ogun State, Nigeria.
[2] Department of Biological Sciences, College of Science and Technology, Covenant University Canaanland,
Km 10, Idiroko Road, PMB. 1023, Ota, Ogun State, Nigeria.

ABSTRACT

A variety of 1-(s-phenyl)-[1,2,4]triazolo[4,3-a]quinoxalin-4(5*H*)-one **(3a-3h)** and 1-(s-furan-2-yl)-[1,2,4]triazolo[4,3-a]quinoxalin-4(5*H*)-one **(5a-d)** were synthesized from thermal annelation of corresponding hydrazones **(2a-h)** and **(4a-d)** respectively in the presence of ethylene glycol which is a high boiling solvent. The structures of the compounds prepared were confirmed by analytical and spectral data. Also, the newly synthesized compounds were evaluated for possible antimicrobial activity. 3-(2-(4-hydroxylbenzylidene)hydrazinyl)quinoxalin-2(1*H*)-one **(2e)** was the most active antibacterial agent while 1-(5-Chlorofuran-2-yl)-[1,2,4]triazolo[4,3-a]quinoxalin-4(5*H*)-one **(5c)** stood out as the most potent antifungal agent.

Keywords: 3-Hydrazinoquinoxalin-2(1*H*)-one, benzodiazine, antifungal agent, uv-visible, spectroscopy, benzaldehyde.

INTRODUCTION

For more than a century, heterocycles have constituted one of the largest areas of research in organic chemistry. In the recent years, there has been considerable attention on the preparation of useful heterocyclic compounds in organic synthesis. The motivation for this present study was the known widespread application of benzo-fused N-heterocycles, especially quinoxalines (Alleca *et al.,* 2003) which was reported to have anti-cancer (Solano *et al*., 2007; Zarranz *et al*., 2004), anti-inflammatory (Olayiwola *et al*., 2007) anti-malarial (Zarranz *et al*., 2005), antimycobacterial (Seitz *et al*., 2002) activities, among others.

Quinoxaline belongs to the family of benzodiazine with its nitrogen heteroatoms situated at 1 and 4-positions. The most common way to construct quinoxaline ring is by simple condensation reaction between ortho-phenylenediamine and oxalic acid or its derivatives. In a nutshell, quinoxalines are relatively easy to prepare and various derivatives have been synthesized (Obafemi and Akinpelu, 2005; Refaat *et al*., 2004; Kim and Kim, 2003; Nasr *et al*., 2002; Ali *et al.,* 2000) in order to obtain biologically active materials (Heravi *et al.,* 2007; Stasweszka *et al*., 2005). Quinoxaline nucleus is a common substructure of many biologically (Catarzi *et al*., 2008; El-Hawash *et al*., 2006) and pharmacologically (Colotta *et al*., 2008; Catarzi *et al*., 2005; Holschbach *et al*., 2005) active compounds. Furthermore, quinoxaline moiety is found as the skeletal structure in various antibiotics such as echinomycin (Hasaninejad *et al*., 2008), levomycin (Ammar *et al*., 2009) and actinoleutin (Islami *et al*., 2008; Aggarwal *et al*., 2006) that are known to inhibit growth of gram-positive bacteria and are active against various transplantable tumors. Quinoxalines are useful precursors for the synthesis of some fused ring derivatives such as thieno- (Zaleska *et al.,* 2001), pyrrolo (Kollenz *et al*., 2001), pyrimido (Charushin *et al*., 2001) and more especially, triazoloquinoxaline.

Triazoloquinoxaline and their hydrazones derivatives are classes of heterocycles that are of considerable interest because of the diverse range of their biological properties. Therefore, large efforts have been directed towards the synthetic manipulation of quinoxaline derivatives in order to discover more useful compounds. For instance, a number of methods have been developed for the synthesis of substituted quinoxalines (Kumar *et al*., 2008; Vicente *et al*., 2008; Zhenjiang *et al*., 2008; Harrak *et al*., 2007; Hazarika *et al.,* 2007; Szekelyhidi *et al.,* 2005; Vidaillac *et al*., 2005) as well as hydrazone frameworks (Sridharan *et al*., 2007; Abd-Elhafez *et al*., 2003; Vicini *et al*., 2003). However, incorporation of hydrazone into quinoxaline and subsequent generation of triazolo moieties may lead to increase in potency of such library.

Multi-drug resistance is one of the major immediate threats to human health today (Masunari and Tavares, 2007; Kaatz *et al*., 2005; Dyatkina *et al*., 2002). Also,

*Corresponding author email: wajanfresh@yahoo.com

epidemiological studies have also revealed that emergence of new diseases is at the alarming rates in the recent time (Nayak *et al*., 2007). Based on the various challenges aforementioned among others, there is a continuous need for the synthesis of new organic compounds as potential antimicrobial agents. Thus, it is conceivable in this present work, to develop a series of hydrazinylquinoxalines and triazoloquinoxalines with the aim of investigating its antimicrobial properties.

MATERIALS AND METHODS

Chemistry

Melting points were determined with open capillary tube on a Gallenkamp (variable heater) melting point apparatus and were uncorrected. Infra red spectra were recorded as KBr pellets on a Buck Spectrometer while uv-visible spectra were recorded on a Heλioseα ν2.02 Unicam Spectrophotometer using methanol solvent. ^{1}H- and ^{13}C-NMR were run on a Bruker-AC 400-MHz and JEOL-JNM-GX 50-MHz spectrometer (δ in ppm relative to Me_4Si) respectively using deuteriated methanol. Mass spectra were run on Finnigan MAT 312 machine. All compounds were routinely checked by TLC on silical gel G plates using $CHCl_3$:CH_3OH (9:1, v/v) solvent system and the developed plates were visualized by UV light. The elemental analysis (C, H, N) of compounds were performed using a Carlo Erba-1108 elemental analyzer. Solvents used were of analytical grade and, when necessary, were purified and dried by standard methods. All furfural derivatives, orthophenylenediamine, ethanol and ethylene glycol were obtained from Aldrich Chemical, Germany while benzaldehyde derivatives as well as hydrazine hydrate and oxalic acid dihydrate were obtained from BDH Chemical Limited. Other solvents were obtained from May and Baker Limited.

Synthesis of 3-Hydrazinoquinoxalin-2(1*H*)-one (1). To a solution of pure 1,2,3,4-tetrahydroquinoxaline-2,3-dione (20.1 g, 124.0 mmol) in hydrazine hydrate (100.0 ml, 2.2 mol), was added water (50 mL) drop wise with constant stirring at 100^{o}C. The resulting mixture was refluxed under continuous stirring for 3h. The mixture was allowed to cool and the formed precipitate was filtered, recrystallized from ethanol to give **1.** ^{1}H-NMR (400 MHz, CH_3OH-d_4): δ 5.81(s-br, 2H, NH_2; D_2O exchangeable), 7.49-7.96(m, 4H, Ar-H), 8.14(s, 1H, NH; D_2O exchangeable), 12.55(s, 1H, NH; D_2O exchangeable). ^{13}C-NMR (50 MHz, CH_3OH-d_4): δ 190.5(C=O), 141.9, 134.2, 125.7, 119.6, 117.0, 115.4, 110.4 ppm. IR (KBr, cm^{-1}): ν_{max} 3412(N-H), 3280(N-H), 3175(N-H), 1679(C=O), 1620(C=C). λ_{max} in nm (log ε_{max}): 216(4.34), 247(3.75s), 327(3.61s). MS: in m/z[rel. %]: 176[M^{+}, 55.5 %], 161[92.3 %], 146[85.5 %], 118[100 %], 106[80.1 %].

General procedure for synthesis of 3-(2-s-benzylidene)hydrazinyl)quinoxalin-2(1*H*)-one (2a-h). To a ground mixture of 3-hydrazinoquinoxalin-2(1*H*)-one **1** (1.0g, 5.7 mmol) and corresponding benzaldehyde (5.7 mmol), was added ethanol (20mL) with a continuous stirring until homogeneity was achieved. The resulting mixture was refluxed at a controlled temperature of 95^{o}C for 3h. The solution was allowed to cool and the formed precipitate was filtered, recrystallized from ethanol to give **(2a-h)**.

Synthesis of 3-(2-benzylidene)hydrazinyl)quinoxalin-2(1*H*)-one (2a). ^{1}H-NMR (400 MHz, CH_3OH-d_4): δ 7.01 (s, 1H, NH; D_2O exchangeable), 5.35 (s, 1H, OH; D_2O exchangeable), 6.85-7.78 (m, 4H, Ar-H), 7.09-8.27(m, 4H, Q-Ar), 8.00 (s, 1H, NH; D_2O exchangeable), 8.54 (s, 1H, N=CH). ^{13}C-NMR (50 MHz, CH_3OH-d_4): δ 160.8(C=O), 158.0(C-OH), 157.6, 146.8(N=CH), 142.7, 131.7, 130.6, 130.6, 129.1, 126.3, 125.9, 123.5, 116.0, 116.0, 115.2 ppm. IR (KBr, cm^{-1}): ν_{max} 3241(N-H), 1685(C=O), 1612(C=C), 1563(C=N). λ_{max} in nm (log ε_{max}): 212(4.58), 276(4.03), 308(4.02s), 352(4.48), 376(4.60), 394(3.84s).

Synthesis of 3-(2-(2-nitrobenzylidene)hydrazinyl) quinoxalin-2(1*H*)-one (2b). ^{1}H-NMR (400 MHz, CH_3OH-d_4): δ 7.03 (s, 1H, NH; D_2O exchangeable), 7.09-8.29 (m, 4H, Q-Ar), 7.59-8.09(m, 4H, Ar-H), 8.00 (s, 1H, NH; D_2O exchangeable), 8.54(s, 1H, N=CH). ^{13}C-NMR (50 MHz, CH_3OH-d_4): δ 158.0(C=O), 157.5, 147.8, 143.3, 142.7, 134.9, 131.9, 131.7, 130.1, 129.1, 128.4, 125.9, 124.0, 123.5, 115.3 ppm. IR (KBr, cm^{-1}): ν_{max} 1685 (C=O), 1606(C=C), 1563(C=N), 979(NO_2). λ_{max} in nm (log ε_{max}): 220(4.29), 328(3.72), 368(3.97), 383(3.94).

Synthesis of 3-(2-(2-chlorobenzylidene)hydrazinyl) quinoxalin-2(1*H*)-one (2c). ^{1}H-NMR (400 MHz, CH_3OH-d_4): δ 7.01(s, 1H, NH; D_2O exchangeable), 7.09-8.28(m, 4H, Q-Ar), 7.40-7.77(m, 4H, Ar-H), 8.00(s, 1H, NH; D_2O exchangeable), 8.99(s, 1H, N=CH). ^{13}C-NMR (50 MHz, CH_3OH-d_4): δ 158.0(C=O), 157.6, 142.7, 138.7, 134.7, 133.9, 132.4, 131.7, 130.1, 129.1, 127.2, 126.9, 125.9, 123.5, 115.2 ppm. IR (KBr, cm^{-1}): ν_{max} 3214(N-H), 1685(C=O), 1606(C=C), 1565(C=N). λ_{max} in nm (log ε_{max}): 216(3.85), 372(3.56).

Synthesis of 3-(2-(4-(N,N-dimethylaminobenzylidene) hydrazinyl)quinoxalin-2(1*H*)-one (2d). ^{1}H-NMR (400 MHz, CH_3OH-d_4): δ 7.02(s, 1H, NH; D_2O exchangeable), 3.06(s, 6H, *J* = 7Hz, 2x CH_3), 6.81-7.50(m, 4H, Ar-H), 7.07-8.25(m, 4H, ArH), 8.00 (s, 1H, NH; D_2O exchangeable), 8.52(s, 1H, N=CH). ^{13}C-NMR (50 MHz, CH_3OH-d_4): δ 158.0(C=O), 157.6, 153.4, 146.8, 142.7, 131.7, 129.1, 128.3, 128.3, 125.9, 123.5, 123.2, 111.9, 111.9, 115.2, 41.6, 41.6(-N(CH_3)$_2$) ppm. IR (KBr, cm^{-1}): ν_{max} 3351(N-H), 2925(CH aliphatic), 1685(C=O), 1606(C=C), 1563(C=N). λ_{max} in nm (log ε_{max}): 224 (4.71), 332 (4.50), 396(4.81).

Synthesis of 3-(2-(4-hydroxylbenzylidene) hydrazinyl) quinoxalin-2(1*H*)-one (2e). ^{1}H-NMR (400 MHz, CH_3OH-d_4): δ 5.35(s, 1H, OH; D_2O exchangeable), 6.85-7.78(m, 4H, Ar-H), 7.00(s, 1H, NH; D_2O exchangeable), 7.09-8.27(m, 4H, Q-Ar), 8.00(s, 1H, NH; D_2O exchangeable), 8.54(s, 1H, N=CH). ^{13}C-NMR (50 MHz, CH_3OH-d_4): δ 160.8(C-OH), 158.0(C=O), 157.6, 146.8(N=CH), 142.7, 131.7, 130.6, 130.6, 129.1, 126.3, 125.9, 123.5, 116.0, 116.0, 115.2 ppm. IR (KBr, cm^{-1}): ν_{max} 3241(N-H), 1685(C=O), 1612(C=C), 1563(C=N). λ_{max} in nm (log ε_{max}): 212(4.58), 276(4.03), 308(4.02s), 352(4.48), 376 (4.60), 394 (5.84s). MS: in m/z[rel. %]: 280 [M^+, 47 %], 263[M-OH, 79 %], 187[88 %], 118[100 %].

Synthesis of 3-(2-(4-hydroxyl-3-methoxybenzylidene) hydrazinyl)quinoxalin-2(1*H*)-one (2f). ^{1}H-NMR (400 MHz, CH_3OH-d_4): δ 7.01(s, 1H, NH; D_2O exchangeable), 3.83(s, 3H, *J* = 8.5Hz, OCH_3), 5.35(s, 1H, OH; D_2O exchangeable), 6.91-7.52(m, 3H, Ar-H), 7.09-8.27(m, 4H, Q-Ar), 8.00(s, 1H, NH; D_2O exchangeable), 8.36(s, 1H, N=CH). ^{13}C-NMR (50 MHz, CH_3OH-d_4): δ 158.0(C=O), 157.6, 151.0(C-OH), 149.3, 146.8, 142.7, 131.7, 130.9, 129.1, 125.9, 123.5, 122.9, 117.0, 115.2, 112.1, 56.1(OCH_3) ppm. IR (KBr, cm^{-1}): ν_{max} 3241(N-H), 1685(C=O), 1620(C=C), 1510(C=N), 1278(C-O). λ_{max} in nm (log ε_{max}): 220(4.32), 348(3.37), 376(3.42).

Synthesis of 3-(2-(3-hydroxylbenzylidene)hydrazinyl) quinoxalin-2(1*H*)-one (2g). ^{1}H-NMR (400 MHz, CH_3OH-d_4): δ 7.01(s, 1H, NH; D_2O exchangeable), 5.35(s, 1H, OH; D_2O exchangeable), 7.02-7.46(m, 4H, Ar-H), 7.09-8.28(m, 4H, Q-Ar), 8.00(s, 1H, NH; D_2O exchangeable), 8.36(s, 1H, N=CH). ^{13}C-NMR (50 MHz, CH_3OH-d_4): δ 158.6(C-OH), 158.0(C=O), 157.6, 146.8, 142.7, 138.7, 131.7, 130.2, 129.1, 125.9, 123.5, 121.8, 118.2, 115.2, 114.9 ppm. IR (KBr, cm^{-1}): ν_{max} 3240(N-H), 1685(C=O), 1612(C=C), 1575(C=N). λ_{max} in nm (log ε_{max}): 220(4.13), 368(4.19), 388(3.89).

Synthesis of 3-(2-(2-hydroxylbenzylidene)hydrazinyl) quinoxalin-2(1*H*)-one (2h). ^{1}H-NMR (400 MHz, CH_3OH-d_4): δ 7.01(s, 1H, NH; D_2O exchangeable), 5.35(s, 1H, OH; D_2O exchangeable), 7.01-7.66(m, 4H, Ar-H), 7.09-8.27(m, 4H, Ar-H), 8.00(s, 1H, NH; D_2O exchangeable), 8.78(s, 1H, N=CH). ^{13}C-NMR (50 MHz, CH_3OH-d_4): δ 158.0(C=O), 157.6, 157.2(C-OH), 146.0, 142.7, 132.4, 131.7, 129.1, 127.5, 125.9, 123.5, 121.4, 118.5, 117.8, 115.2 ppm. IR (KBr, cm^{-1}): ν_{max} 3240(N-H), 1686(C=O), 1618(C=C), 1575(C=N). λ_{max} in nm (log ε_{max}): 212(3.68), 356(3.46), 372(3.51), 392(3.40).

General procedure for the synthesis of 1-(s-phenyl)-[1,2,4]triazolo[4,3-a]quinoxalin-4(5*H*)-one (3a-3h). To a dried pure corresponding hydrazone **2** (10mmol) was added ethylene glycol (5 mL) and the reacting mixture was heated at 200^{o}C under reflux for 5 h. The solution was allowed to stand at room temperature after which it was poured into crushed ice (5g). The product was filtered off, dried and crystallized from ethanol.

Synthesis of 1-phenyl-[1,2,4]triazolo[4,3-a]quinoxalin-4(5*H*)-one (3a). ^{1}H-NMR (400 MHz, CH_3OH-d_4): δ 7.32-7.81(m, 4H, Ar-H), 7.41-8.28(m, 4H, Ar-H), 8.00(s, 1H, NH; D_2O exchangeable). ^{13}C-NMR (50 MHz, CH_3OH-d_4): δ 165.2(C=O), 162.3, 158.9, 144.9, 137.2, 134.4, 132.6, 131.1, 129.2, 129.2, 129.2, 127.5, 127.5, 127.3, 126.6 ppm. IR (KBr, cm^{-1}): ν_{max} 1685(C=O), 1610(C=C), 1560(C=N). λ_{max} in nm (log ε_{max}): 216(3.67), 360(4.00), 389(3.62).

Synthesis of 1-(2-nitrophenyl)-[1,2,4]triazolo[4,3-a]quinoxalin-4(5*H*)-one (3b). ^{1}H-NMR (400 MHz, CH_3OH-d_4): δ 7.30-7.81(m, 4H, Q-Ar-H), 7.67-8.05(m, 4H, Ar-H), 8.00(s, 1H, NH; D_2O exchangeable). ^{13}C-NMR (50 MHz, CH_3OH-d_4): δ 165.2(C=O), 162.3, 158.9, 150.1, 144.9, 137.2, 135.3, 133.0, 132.6, 129.6, 129.2, 127.3, 126.6, 126.2, 124.4 ppm. IR (KBr, cm^{-1}): ν_{max} 1685(C=O), 1605(C=C), 1565(C=N), 979(NO_2). λ_{max} in nm (log ε_{max}): 220(3.69), 325(3.98), 361(3.47). MS: in m/z[rel. %]: 307[M^+, 61 %], 261[M^+- NO_2, 82 %], 185[91 %], 118[100 %].

Synthesis of 1-(2-chlorophenyl)-[1,2,4]triazolo[4,3-a]quinoxalin-4(5*H*)-one (3c). ^{1}H-NMR (400 MHz, CH_3OH-d_4): δ 7.30-7.82(m, 4H, Q-Ar-H), 7.36-7.73(m, 4H, Ar-H), 8.00(s, 1H, NH; D_2O exchangeable). ^{13}C-NMR (50 MHz, CH_3OH-d_4): δ 165.2(C=O), 162.3, 158.9, 144.9, 138.5, 137.2, 132.6, 132.2, 130.1, 129.3, 129.2, 128.9, 127.3, 127.3, 126.6 ppm. IR (KBr, cm^{-1}): ν_{max} 3214(N-H), 1685(C=O), 1606(C=C), 1560(C=N). λ_{max} in nm (log ε_{max}): 216(4.19), 374(3.91).

Synthesis of 1-(4-(N,N-dimethylamino)phenyl)-[1,2,4]triazolo[4,3-a]quinoxalin-4(5*H*)-one (3d). ^{1}H-NMR (400 MHz, CH_3OH-d_4): δ 3.06(s, 6H, *J* = 7.1Hz, 2x CH_3), 6.82(dd, 2H, *J* = 3, 10Hz, Ar-H), 7.97(dd, 2H, *J* = 3.5, 11Hz, Ar-H), 7.37-7.86(m, 4H, Q-Ar-H), 8.02(s, 1H, NH; D_2O exchangeable). ^{13}C-NMR (50 MHz, CH_3OH-d_4): δ 165.2(C=O), 162.3, 158.9, 155.3, 144.9, 137.2, 132.6, 129.2, 128.4, 128.4, 127.3, 126.6, 123.9, 112.7, 112.7, 41.3, 41.3 ppm. IR (KBr, cm^{-1}): ν_{max} 2925 (CH aliphatic), 1685(C=O), 1606(C=C), 1563(C=N). λ_{max} in nm(log ε_{max}):220(3.82), 345(3.44).

Synthesis of 1-(4-hydroxyphenyl)-[1,2,4]triazolo[4,3-a]quinoxalin-4(5*H*)-one (3e). ^{1}H-NMR (400 MHz, CH_3OH-d_4): δ 5.34(s, 1H, OH; D_2O exchangeable), 6.86(dd, 2H, *J* = 3, 10Hz, Ar-H), 7.32-7.83(m, 4H, Q-Ar-H), 7.91(dd, 2H, *J* = 3.6, 11.2Hz, Ar-H), 8.00(s, 1H, NH; D_2O exchangeable). ^{13}C-NMR (50 MHz, CH_3OH-d_4): δ 165.2 (C=O), 162.3, 158.9, 158.5 (C-OH), 144.9, 137.2, 132.6, 130.7, 130.7, 129.2, 127.3, 127.0, 126.6, 116.7, 116.7 ppm. IR (KBr, cm^{-1}): ν_{max} 3239(N-H), 1685 (C=O),

1612(C=C), 1563(C=N). λ_{max} in nm (log ε_{max}): 212(4.38), 276(4.07), 352(4.48), 379(4.32).

Synthesis of 1-(4-hydroxyl-3-methoxyphenyl)-[1,2,4] triazolo[4,3-a]quinoxalin-4(5*H*)-one (3f). ^{1}H-NMR (400 MHz, CH_3OH-d_4): δ 3.83(s, 3H, OCH_3), 5.35(s, 1H, OH; D_2O exchangeable), 6.90-7.48(m, 3H, Ar-H), 7.35-7.85(m, 4H, Ar-H), 8.01(s, 1H, NH; D_2O exchangeable). ^{13}C-NMR (50 MHz, CH_3OH-d_4): δ 162.3, 158.9, 155.3, 148.7(C-OH), 148.0, 144.9, 137.2, 132.6, 129.2, 127.3, 126.6, 124.2, 123.0, 115.8, 112.7, 51.6 ppm. IR (KBr, cm^{-1}): ν_{max} 3161(N-H), 1685(C=O), 1615 (C=C), 1514(C=N), 1278(C-O). λ_{max} in nm (log ε_{max}): 220(3.75), 348(3.99), 371(3.55).

Synthesis of 1-(3-hydroxyphenyl)-[1,2,4]triazolo[4,3-a]quinoxalin-4(5*H*)-one (3g). ^{1}H-NMR (400 MHz, CH_3OH-d_4): δ 5.35(s, 1H, OH; D_2O exchangeable), 6.91-7.84(m, 4H, Ar-H), 7.30-7.84(m, 4H, Q-Ar), 8.01(s, 1H, NH; D_2O exchangeable). ^{13}C-NMR (50 MHz, CH_3OH-d_4): δ 165.2(C=O), 162.3, 158.9, 157.5(C-OH), 144.9, 137.2, 132.6, 132.0, 130.6, 129.2, 127.3, 126.6, 120.1, 115.9, 112.9 ppm. IR (KBr, cm^{-1}): ν_{max} 3240(N-H), 1685(C=O), 1620(C=C), 1575(C=N). λ_{max} in nm (log ε_{max}): 220 (3.84), 350(3.41), 379(3.33).

Synthesis of 1-(2-hydroxyphenyl)-[1,2,4]triazolo[4,3-a]quinoxalin-4(5*H*)-one (3h). ^{1}H-NMR (400 MHz, CH_3OH-d_4): δ 5.35(s, 1H, OH; D_2O exchangeable), 7.01-7.63(m, 4H, Ar-H), 7.32-7.82(m, 4H, Q-Ar-H), 8.00 (s, 1H, NH; D_2O exchangeable). ^{13}C-NMR (50 MHz, CH_3OH-d_4): δ 165.2(C=O), 162.3, 158.9, 154.1(C-OH), 144.9, 137.2, 132.6, 131.9, 130.1, 129.2, 127.3, 126.6, 121.8, 118.3, 117.8 ppm. IR (KBr, cm^{-1}): ν_{max} 3240(N-H), 1687(C=O), 1616(C=C), 1575(C=N). λ_{max} in nm (log ε_{max}): 215(4.29), 354(3.81), 395(4.02).

General procedure for the synthesis of 3-(2-(s-furan-2-yl)methylene)hydrazinyl)quinoxalin-2(1*H*)-one (4a-4d). To a homogeneous mixture of 3-hydrazino-quinoxalin-2(1*H*)-one **1** (1.0 g, 5.7 mmol) and corresponding furfural (5.7 mmol), was added ethanol (20 mL) with a continuous stirring until homogeneity was achieved. The resulting mixture was refluxed at a controlled temperature of 95^{o}C for 4h. The solution was allowed to cool and the formed precipitate was filtered, recrystallized from ethanol to give **(4a-4d)**.

3-(2-(furan-2-yl)methylidene)hydrazinyl)quinoxalin-2(1*H*)-one (4a). ^{1}H-NMR (400 MHz, CH_3OH-d_4): δ 6.52-7.75(m, 3H, Fr-H), 7.00 (s, 1H, NH; D_2O exchangeable), 7.09-8.28(m, 4H, Ar-H), 8.00(s, 1H, NH; D_2O exchangeable), 8.45(s, 1H, N=CH). ^{13}C-NMR (50 MHz, CH_3OH-d_4): δ 158.0(C=O), 157.6, 149.1, 144.4, 142.7, 134.6(N=CH), 131.7, 129.1, 125.9, 123.6, 118.9, 115.2, 112.6 ppm. IR (KBr, cm^{-1}): ν_{max} 3140(N-H), 1690(C=O), 1620(C=C). λ_{max} in nm (log ε_{max}): 220 (4.02), 265(4.13), 310(3.95).

3-(2-(5-nitrofuran-2-yl)methylidene)hydrazinyl) quinoxalin-2(1*H*)-one (4b). ^{1}H-NMR (400 MHz, CH_3OH-d_4): δ 7.00(s, 1H, NH; D_2O exchangeable), 7.09-7.59(dd, 2H, *J* = 2.5, 8.5Hz, Fr-H), 7.09-8.27(m, 4H, Ar-H), 8.01(s, 1H, NH; D_2O exchangeable), 8.45(s, 1H, N=CH). ^{13}C-NMR (50 MHz, CH_3OH-d_4): δ 158.0(C=O), 157.6, 152.0, 151.8, 142.7, 134.7(N=CH), 131.7, 129.1, 125.9, 123.5, 115.2, 114.4, 114.3 ppm. IR (KBr, cm^{-1}): ν_{max} 3140(N-H), 1685(C=O), 1612(C=C), 1575(C=N). λ_{max} in nm (log ε_{max}): 220(4.02), 244(4.11), 270(3.93), 290 (3.84).

3-(2-(5-chlorofuran-2-yl)methylidene)hydrazinyl) quinoxalin-2(1*H*)-one (4c). ^{1}H-NMR (400 MHz, CH_3OH-d_4): δ 6.54(s, 2H, Fr-H), 7.00(s, 1H, NH; D_2O exchangeable), 7.09-8.27(m, 4H, Ar-H), 8.00(s, 1H, NH; D_2O exchangeable), 8.45(s, 1H, N=CH). ^{13}C-NMR (50 MHz, CH_3OH-d_4): δ 158.0(C=O), 157.6, 149.5, 142.7, 134.6(N=CH), 133.4, 131.7, 129.1, 125.9, 123.5, 115.2, 112.5, 107.1 ppm. IR (KBr, cm^{-1}): ν_{max} 3140(N-H), 1685(C=O), 1618(C=C), 1575(C=N). λ_{max} in nm (log ε_{max}): 220(3.99), 273(3.72), 305(3.61).

3-(2-(5-methylfuran-2-yl)methylidene)hydrazinyl) quinoxalin-2(1*H*)-one (4d). ^{1}H-NMR (400 MHz, CH_3OH-d_4): δ 2.30(s, 3H, *J* = 8Hz -CH_3), 6.08-6.85(dd, 2H, *J* = 3.5, 9.2Hz, Fr-H), 7.00 (s, 1H, NH; D_2O exchangeable), 7.09-8.27(m, 4H, Ar-H), 8.00(s, 1H, NH; D_2O exchangeable), 8.45(s, 1H, N=CH). ^{13}C-NMR (50 MHz, CH_3OH-d_4): δ 158.0(C=O), 157.6, 155.6, 147.3, 142.7, 134.6(N=CH), 131.7, 129.1, 125.9, 123.5, 115.2, 110.1, 106.7, 13.4(CH_3). IR (KBr, cm^{-1}): ν_{max} 3412 (N-H), 2929(CH aliphatic), 1706(C=O), 1606(C=C), 1515(C=N), 1266(C-O furan). λ_{max} in nm (log ε_{max}): 220(4.01), 274(3.79), 310(3.66), 325(4.11).

General procedure for the synthesis of 1-(5-s-furan-2-yl)-[1,2,4]triazolo[4,3-a]quinoxalin-4(5*H*)-one (5a-5d). To a dried pure corresponding hydrazone **4** (10mmol) was added ethylene glycol (5 mL) and the reacting mixture was heated at 200^{o}C under reflux for 7 h. The solution was allowed to stand at room temperature after which it was poured into crushed ice (5g). The product was filtered off, dried and crystallized from ethanol.

1-(Furan-2-yl)-[1,2,4]triazolo[4,3-a]quinoxalin-4(5*H*)-one (5a). ^{1}H-NMR (400 MHz, CH_3OH-d_4): δ 6.68(t, 1H, *J* = 7.5Hz, Fr-H), 7.21(d, 1H, *J* = 7.5Hz Fr-H), 7.34-7.81(m, 4H, Ar-H), 8.00(s, 1H, NH; D_2O exchangeable), 8.15(d, 1H, *J* = 7.5Hz, Fr-H). ^{13}C-NMR (50 MHz, CH_3OH-d_4): δ 165.2(C=O), 160.9, 158.9, 154.0, 144.9, 142.9, 137.2, 132.6, 129.2, 127.3, 126.6, 112.0, 107.1 ppm. IR (KBr, cm^{-1}): ν_{max} 3140(N-H), 1690(C=O),

1620(C=C), 1525(C=N). λ_{max} in nm (log ε_{max}): 220(4.02), 260(3.91), 300(3.46).

1-(5-Nitrofuran-2-yl)-[1,2,4]triazolo[4,3-a]quinoxalin-4(5*H*)-one (5b). ^{1}H-NMR (400 MHz, CH_3OH-d_4): δ 7.32-7.81(m, 6H, Ar-H & Fr-H), 8.00(s, 1H, NH; D_2O exchangeable). ^{13}C-NMR (50 MHz, CH_3OH-d_4): δ 165.2(C=O), 160.9, 158.9, 157.9, 150.8, 144.9, 137.2, 132.6, 129.2, 127.3, 126.6, 109.8, 109.5 ppm. IR (KBr, cm^{-1}): ν_{max} 3304(N-H), 1686(C=O), 1620(C=C). λ_{max} in nm (log ε_{max}): 210(4.01), 244(3.86), 273(4.11).

1-(5-Chlorofuran-2-yl)-[1,2,4]triazolo[4,3-a] quinoxalin-4(5*H*)-one (5c). ^{1}H-NMR (400 MHz, CH_3OH-d_4): δ 6.54-7.07(dd, 2H, *J* = 3.4, 8.5Hz, Fr-H), 7.32-7.81(m, 4H, Ar-H), 8.00(s, 1H, NH; D_2O exchangeable). ^{13}C-NMR (50 MHz, CH_3OH-d_4): δ 165.2(C=O), 160.9, 158.9, 154.4, 144.9, 137.2, 135.7, 132.6, 129.2, 127.3, 126.6, 110.2, 102.1 ppm. IR (KBr, cm^{-1}): ν_{max} 3140(N-H), 1690 (C=O), 1620(C=C). λ_{max} in nm (log ε_{max}): 220(4.01), 275(3.88), 298(3.65).

1-(5-Methylfuran-2-yl)-[1,2,4]triazolo[4,3-a] quinoxalin-4(5*H*)-one (5d). ^{1}H-NMR (400 MHz, CH_3OH-d_4): δ 2.30(s, 3H, CH_3), 6.08-6.95 (dd, 2H, *J* = 3.5, 8.5Hz, Fr-H), 7.32-7.82 (m, 4H, Ar-H), 8.00 (s, 1H, NH; D_2O exchangeable). ^{13}C-NMR (50 MHz, CH_3OH-d_4): δ 165.2(C=O), 160.9, 158.9, 152.2, 151.4, 144.9, 137.2, 132.6, 129.2, 127.3, 126.6, 107.8, 107.6, 13.7(CH_3) ppm. IR (KBr, cm^{-1}): ν_{max} 3140 (N-H), 1685 (C=O), 1612 (C=C). λ_{max} in nm (log ε_{max}): 220(3.97), 277(4.12), 315(4.00).

RESULTS AND DISCUSSION

3-Hydrazino-2-quinoxalinone **1** which was acting as the building block for the synthesis of all the hydrazones and triazoloquinoxalines, was itself prepared by hydrazinolysis of quinoxalin-2,3-dione using the method earlier described by Ajani *et al*. (2009). To a solution of quinoxalin-2,3-dione in hydrazine hydrate was added 50 ml of water and the resulting solution was reflux for 3 h. The mixture was allowed to cool and the formed precipitate was recrystallized from ethanol to afford 89% yield of **1**. The result of percentage yields and other physical parameters as well as elemental analysis is as shown in table 1. The condensation of **1** with benzaldehyde derivatives in the presence of ethanol gave the hydrazones **2a-h** which was subsequently thermally annelated at 200°C in the presence of ethylene glycol, a high boiling inert solvent, to afford crystalline products whose elemental analyses were consistent with the triazolo derivatives **3a-h** (Scheme 1). Part of the motivation for the conversion of hydrazones to triazolo products herein was based on the earlier findings by Rashed *et al*. (1990). In a like manner, exchanging of the aromatic aldehyde starting material with furfural led to the formation of hydrazones **4a-d** as the candidates for cyclization in order to obtain **5a-d** as the triazoloquinoxalinone, in good to excellent yields. The result of the reaction may be explained according to the mechanism illustrated in Schemes 1 and 2.

Compound **2e**, which was considered to be the typical representative of the hydrazones **2**, showed an infrared

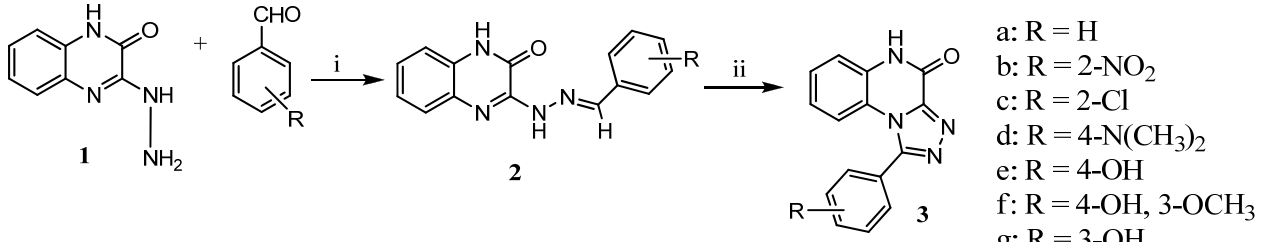

Scheme 1: i = ethanol, 95°C, 3h reflux; ii = ethylene glycol, 200°C, 5h reflux

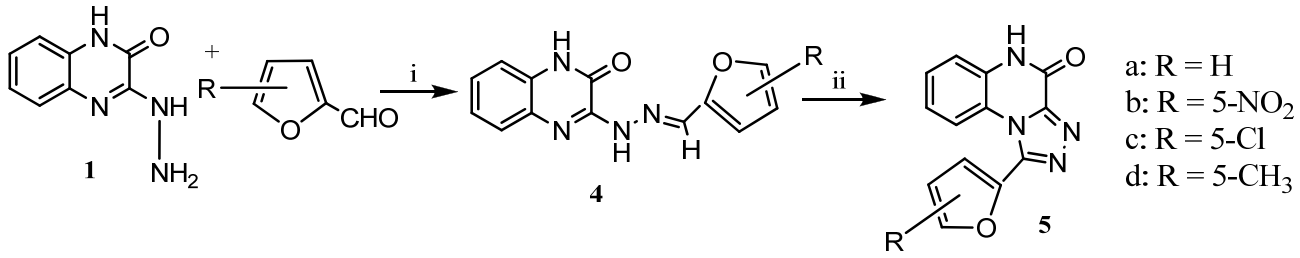

Scheme 2: i = ethanol, 95°C, 4h reflux; ii = ethylene glycol, 200°C, 5-7h reflux

Table 1. The Result of Physical Data and Elemental Analysis of the Synthesized Compounds 1-5d.

No	M.P. (°C)	Yield	R_f[a] Value	Mol. Formula (Mol. Weight)	Elem. Analy.% Calcd. (% Found) C	H	N
1	>360	89	0.63	$C_8H_8N_4O$ (176)	54.55(54.52)	4.55(4.57)	31.82(31.83)
2a	245-247	97	0.67	$C_{15}H_{12}N_4O$ (264)	68.18(68.25)	4.55(4.83)	21.21(21.09)
2b	260-261	91	0.64	$C_{15}H_{11}N_5O_3$ (309)	58.25(58.15)	3.56(3.61)	22.65(22.60)
2c	317-321	96	0.64	$C_{15}H_{11}N_4OCl$(298.5)	60.30(60.38)	3.69(3.62)	18.76(18.69)
2d	279-280	95	0.78	$C_{17}H_{17}N_5O$(307)	66.45(66.49)	5.54(5.48)	22.80(22.77)
2e	285(dec)	96	0.79	$C_{15}H_{12}N_4O_2$(280)	64.29(64.21)	4.29(4.38)	20.00(20.11)
2f	320(dec)	98	0.75	$C_{16}H_{14}N_4O_3$(310)	61.94(61.90)	4.52(4.59)	18.06(18.12)
2g	280-281	92	0.74	$C_{15}H_{12}N_4O_2$(280)	64.29(64.33)	4.29(4.17)	20.00(19.98)
2h	275-279	94	0.78	$C_{15}H_{12}N_4O_2$(280)	64.29(64.23)	4.29(4.34)	20.00(20.09)
3a	322-324	87	0.58	$C_{15}H_{10}N_4O$ (262)	68.70(68.85)	3.82(3.80)	21.37(21.44)
3b	329-330	87	0.77	$C_{15}H_9N_5O_3$ (307)	58.63(58.54)	2.93(2.69)	22.80(22.71)
3c	>360	81	0.81	$C_{15}H_9N_4OCl$(296.5)	60.71(60.54)	3.04(3.11)	18.89(18.68)
3d	347-349	79	0.66	$C_{17}H_{15}N_5O$(305)	66.89(66.97)	4.92(4.88)	22.95(22.90)
3e	355-357	80	0.59	$C_{15}H_{10}N_4O_2$(278)	64.75(64.67)	3.60(3.69)	20.14(20.29)
3f	>360	86	0.71	$C_{16}H_{12}N_4O_3$(308)	62.34(62.27)	3.90(3.14)	18.18(18.22)
3g	>360	81	0.64	$C_{15}H_{10}N_4O_2$(278)	64.75(64.79)	3.60(3.67)	20.14(20.11)
3h	315-317	74	0.59	$C_{15}H_{10}N_4O_2$(278)	64.75(64.70)	3.60(3.56)	20.14(20.09)
4a	216-219	77	0.61	$C_{13}H_{10}N_4O_2$(254)	61.42(61.38)	3.94(3.90)	22.05(21.99)
4b	282-284	95	0.50	$C_{13}H_9N_5O_4$(299)	52.17(52.22)	3.01(3.08)	23.41(23.39)
4c	301-303	90	0.66	$C_{13}H_9N_4O_2Cl$(288.5)	54.07(53.96)	3.12(3.01)	19.41(19.20)
4d	315-318	89	0.51	$C_{14}H_{11}N_4O_2$(267)	62.92(63.00)	4.12(4.19)	20.97(21.00)
5a	>360	88	0.54	$C_{13}H_8N_4O_2$(252)	61.90(61.98)	3.17(3.13)	22.22(22.16)
5b	>360	94	0.70	$C_{13}H_7N_5O_4$(297)	52.53(52.49)	2.36(2.41)	23.57(23.49)
5c	>360	97	0.63	$C_{13}H_7N_4O_2Cl$(286.5)	54.45(54.56)	2.44(2.35)	19.55(19.51)
5d	>360	72	0.44	$C_{14}H_9N_4O_2$(265)	63.40(63.44)	3.40(3.42)	21.13(21.18)

[a] Solvent System. $CHCl_3$:CH_3OH (9:1, v/v)

absorption band at ν 1685 cm^{-1} as a result of the presence of C=O of amide while the one observed at ν 1612 cm^{-1} and 1563 cm^{-1}depicted the presence of C=C of aromatic and C=N of hydrazone respectively. The highest frequency band noticed at ν 3241 cm^{-1} confirmed the presence of N-H of amide. The uv-visible absorption spectrum of **2e**, showed peaks at λ_{max} 212, 276, 352 and 376 nm and two noticeable shoulders at λ_{max} 308 and 394 nm respectively. The peak at 212nm is as a result of π→π* transition of C=C aromatic. ^{1}H-NMR spectrum of **2e** showed one –OH singlet at δ 5.35 ppm which disappeared upon D_2O shaking. The four aromatic protons of phenyl side chain gave rise to a multiplet at δ 6.85-7.78 ppm while four aromatic protons of benzofused quinoxaline was observed as a multiplet at 7.09-8.27. Also, the exchangeable protons of NH of hydrazone and that of amide both appeared down field of TMS scale at exactly δ 7.0 and 8.0 ppm respectively. Azomethine proton that confirmed the presence of hydrazone in **2e** was observed as a singlet at δ 8.54 ppm down field. Furthermore, ^{13}C-NMR spectrum of **2e** showed the presence of fifteen carbon atoms with carbon of hydrazone resonating at δ 146.8 ppm. All other signals were for the aromatic carbon atoms with sp^2 hybridization except δ 160.8 and 158.0 ppm which corresponded with carbonyl of amide and phenolic carbon atoms respectively.

Antimicrobial Screening

All the prepared compounds **1-5d** were screened for their antimicrobial activity against nine gram positive and five gram negative bacteria (Table 2) as well as one fungus *Candida albican* (Fig. 1). For comparison, the compounds were screened in vitro along side with streptomycin and fluconazole as the standard antibacterial and antifungal drugs respectively. The general sensitivity testing was carried out in DMSO at 1000µg/mL using agar well diffusion method while minimum inhibitory concentration (MIC) was determined using two-fold dilution method (Russell and Furr, 1977). From the result of the antibacterial screening (Table 2), it was observed that some of the compounds exhibited significant activity. For instance, **2e, 2f, 3f, 4b** were active on five gram positive and five gram negative bacteria; **1, 4b, 5c** were active on five gram positive and four gram negative bacteria. In a like fashion, **2g, 3b, 3e, 3g** inhibited the growth of five gram positive and three gram negative bacterial strains while **2c, 2d, 3d, 3h, 4d, 5b** inhibited growth of four gram positive and two gram negative bacteria. Although, **2h, 3a, 4c** had low activity on gram negative bacteria,

Table 2. Result of antibacterial Screening (Sensitivity testing) with zones of inhibition in (mm).

Bacteria → / Comp. No↓	*B.a*	*B.c*	*B.p*	*B.s*	*B.su*	*C.s*	*C.p*	*S.a*	*S.f*	*E.c*	*K.p*	*P.a*	*P.f*	*S.d*
1	10	10	10	11	15	R	R	R	R	14	12	10	9	R
2a	R	R	R	16	R	R	R	R	R	14	10	R	11	11
2b	R	15	R	18	20	R	R	R	R	25	8	10	R	12
2c	12	R	R	16	21	R	R	14	R	10	16	R	R	R
2d	15	25	R	31	30	R	R	R	R	18	R	11	R	R
2e	24	26	R	25	28	R	R	12	R	30	22	28	15	20
2f	22	12	R	18	R	7	9	R	R	12	15	R	R	R
2g	24	20	7	20	11	R	R	R	R	28	12	15	R	R
2h	18	18	14	15	11	5	R	R	R	16	14	R	R	R
3a	18	15	R	15	15	5	8	R	8	R	12	17	R	R
3b	13	20	R	13	16	R	R	8	R	9	16	14	R	R
3c	R	R	R	14	10	R	R	R	R	22	17	R	R	R
3d	11	8	R	10	11	R	R	R	R	19	19	R	R	R
3e	R	16	R	15	19	R	10	R	7	28	18	15	R	R
3f	13	13	R	12	18	R	R	R	7	17	23	15	13	11
3g	15	22	R	20	14	R	R	R	10	13	22	17	R	R
3h	18	20	15	21	R	R	R	R	R	14	12	R	R	R
4a	12	18	R	17	13	R	R	R	R	8	20	12	R	R
4b	18	R	R	12	15	4	8	R	R	21	13	13	R	19
4c	15	13	9	16	14	11	R	R	R	14	19	R	R	R
4d	17	23	8	28	R	R	R	R	R	13	R	11	R	R
5a	14	15	11	10	24	R	11	R	R	22	17	15	R	17
5b	21	18	R	12	19	R	R	R	R	19	15	R	R	R
5c	11	22	R	12	29	R	R	15	R	24	20	15	11	R
5d	13	20	R	17	20	R	R	R	R	20	11	14	R	R
str	24	20	18	15	19	21	13	27	30	R	R	13	14	13

B.a = Bacillus anthracis (LIO)$^{G+}$, *B.c = Bacillus cereus* (NCIB 6349)$^{G+}$, *B.p = Bacillus polymyxa* (LIO)$^{G+}$, *B.s = Bacillus stearothermophilus* (NCIB 8222)$^{G+}$, *B.su = Bacillus subtilis* (NCIB 3610)$^{G+}$, *C.s = Clostridium sporogenes* (LIO)$^{G+}$, *C.p = Corynebacterium pyogene* (LIO)$^{G+}$, *S.a = Staphylococcus aureus* (NCIB 8588)$^{G+}$, *S.f = Streptococcus faecalis* (NCIB775)$^{G+}$, *E.c = Escherichia coli* (NCIB 86)$^{G-}$, *K.p = Klebsiella pneumonia* (NCIB 418)$^{G-}$, *P.a = Pseudomonas aeruginosa* (NCIB 950)$^{G-}$, *P.f = Pseudomonas fluorescence* (NCIB 3756)$^{G-}$, *S.d = Shigella dysenteriae* (LIO)$^{G-}$; Str = Streptomycin, $^{G+}$ Gram positive, $^{G-}$ Gram negative, R = Bacteria are resistant to the compounds at 1000 µg/mL.

however, they inhibited the growth of six gram positive bacterial isolates. Streptomycin had broad activity spectrum on all gram positive and three gram negative organisms. Nevertheless, *E. coli* and *Klebsiella pneumonia* developed resistance against streptomycin while all the synthesized compounds were active on the two organisms. Due to variation in sensitivity testing result, minimum inhibitory concentration (MIC) test, which is defined as the lowest concentration of drug that completely inhibited the growth of the organism, was selectively carried out on four gram positive and two gram negative bacteria (Table 3). The MICs value for all the compounds varied between 7.8µg/mL and 125µg/mL while that of streptomycin standard was between 7.8 µg/mL and 15.6µg/mL. Compounds **3e, 3f, 3h**, had the same MIC range with streptomycin while **2e** was observed to be the only compound that had MIC value of 7.8µg/mL throughout. The results indicated that **2e** has a higher activity than streptomycin against most of the tested bacterial isolates.

The result of the antifungal activity was as shown in figure 1. It was noticed that **5c** competed favourable with fluconazole at 32 mm while all other compounds were not as active as fluconazole standard because their zones of inhibition varied between 19mm and 28mm.

CONCLUSION

As envisaged from literature review, the thermal annelation of various hydrazones **2a-h** and **4a-4d** to give the corresponding [1,2,4]triazolo[4,3-a]quinoxalin-4(5*H*)-one **3a-3h** and **5a-d** respectively, was successful. Compounds **2e** and **5c** emerged as the most active antibacterial and antifungal agents respectively.

Table 3. Result of Minimum Inhibitory Concentration (MIC) test on some selected bacteria in µg/mL.

Bacteria → Comp. No↓	*Bacillus anthracis*	*Bacillus cereus*	*Bacillus Stearotherm.*	*Bacillus subtilis*	*Escherichia coli*	*Klebsiella pneumonia*
1	62.5	31.3	62.5	62.5	15.6	15.6
2a	R	R	15.6	R	7.8	31.3
2b	R	15.6	15.6	7.8	7.8	125.0
2c	31.3	R	31.3	15.6	31.3	31.3
2d	62.5	15.6	7.8	7.8	15.6	R
2e	7.8	7.8	7.8	7.8	7.8	7.8
2f	15.6	31.3	15.6	R	31.3	31.3
2g	7.8	15.6	15.6	62.5	7.8	31.3
2h	15.6	15.6	15.6	31.3	15.6	31.3
3a	7.8	15.6	15.6	15.6	R	31.3
3b	31.3	7.8	31.3	15.6	31.3	15.6
3c	R	R	15.6	31.3	7.8	7.8
3d	31.3	31.3	15.6	15.6	7.8	7.8
3e	R	7.8	15.6	15.6	7.8	15.6
3f	15.6	15.6	15.6	7.8	7.8	7.8
3g	31.3	7.8	31.3	7.8	31.3	7.8
3h	15.6	7.8	7.8	R	15.6	15.6
4a	31.3	15.6	15.6	31.3	62.5	7.8
4b	7.8	R	31.3	15.6	7.8	15.6
4c	15.6	31.3	7.8	15.6	15.6	7.8
4d	15.6	7.8	7.8	R	31.3	R
5a	15.6	15.6	31.3	7.8	7.8	7.8
5b	7.8	7.8	31.3	15.6	15.6	15.6
5c	31.3	15.6	15.6	7.8	7.8	7.8
5d	31.3	7.8	15.6	7.8	7.8	62.5
str	7.8	7.8	15.6	7.8	R	R

Str = Streptomycin, R = Bacteria are resistant to the compounds at 1000µg/mL.

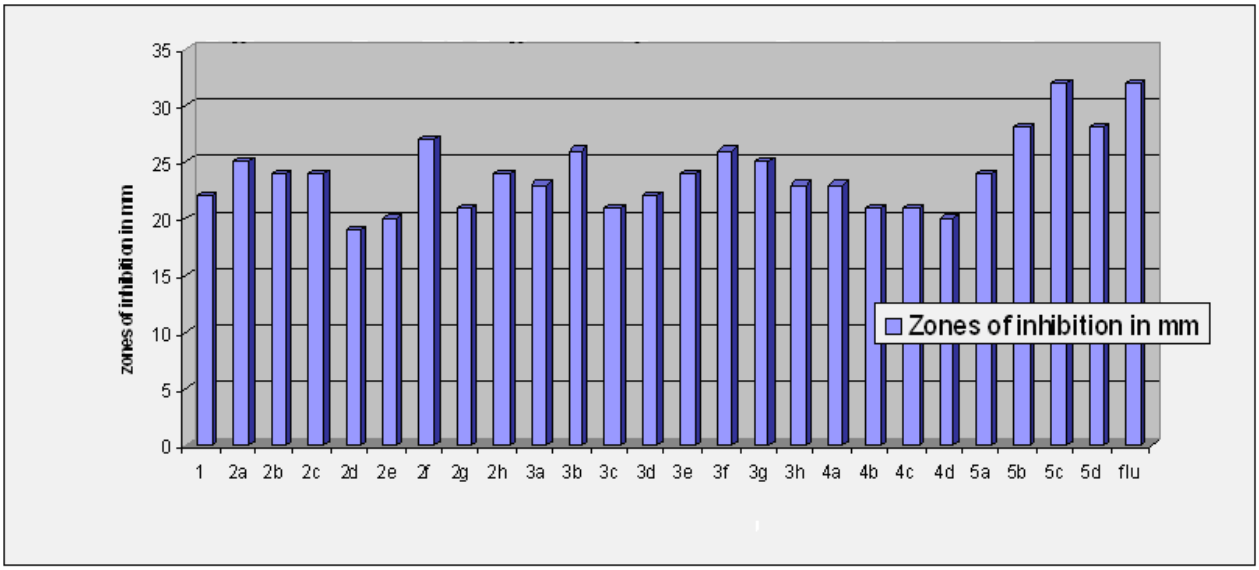

Synthesized compounds (1-5d) and Fluconazole

Fig. 1. Result of antifungal activity with zones of inhibition in mm

REFERENCES

Abd-Elhafez, OM., El-khrisy, ED., Badria, F. and Fathy, AD. 2003. Synthesis and biological investigations of new thiazolidinone and oxadiazoline coumarin derivatives. Arch. Pharm. Res. 26(9):686-696.

Aggarwal, R., Sumran, G., Saini, A. and Singh, SP. 2006. Hypervalent iodine oxidation of benzyl-α-arylimino oximes: an efficient synthesis of 2,3-diphenylquinoxaline-1-oxides. Tetrahedron Lett. 47(28):4969-4971.

Ajani, OO., Obafemi, CA., Ikpo, CO., Ajanaku, KO., Ogunniran, KO. and James, OO. 2009. Comparative study of microwave assisted and conventional synthesis of novel 2-quinoxalinone-3-hydrazone derivatives and its spectroscopic properties. Int. J. Physical Sciences. 4(4):156-164.

Ali, MM., Ismail, MMF., El-Gaby, MSA., Zahran, MA. and Ammar, YA. 2000. Synthesis and anti-microbial activities of some novel quinoxalinone derivatives. Molecules 5:864-873.

Alleca, S., Corona, P., Loriga, M., Paglietti, G., Loddo, R., Mascia, V., Busonera, B. and La Cola, P. 2003. Quinoxaline chemistry. Part 16. 4-Substituted anilino and 4-substituted phenoxymethyl pyrrolo[1,2-a]quinoxalines and N-[4-(pyrrolo[1,2-a]quinoxalin-4-yl)amino and hydroxylmethyl] benzoyl glutamates. Synthesis and evaluation of in vitro biological activity. II Farmaco 58(9):639-650.

Ammar, YA., Al-Sehemi, AG., El-Sharief, AMS. and El-Gaby, MSA. 2009. Chemistry of 2,3-dichloroquinoxaline. Phosphorus, Sulfur and Silicon and the Related Elements. 184(3):660-698.

Catarzi, D., Colotta, V., Varano, F., Filacchioni, G., Gratteri, P., Sgrignani, J., Galli, A. and Costagli, C. 2008. Synthesis and biological evaluation of novel 9-heteroaryl substituted 7-chloro-4,5-dihydro-4-oxo-1,2,4-triazolo[1,5-a]quinoxaline-2-carboxylates (TQX) as (R,S)-2-amino-3-(3-hydroxy-5-methylisoxazol-4-yl)propionicacid (AMPA) receptor antagonists. Chem. Pharm. Bull. (Tokyo) 56(8):1085-1091.

Catarzi, D., Colotta, V., Varano, F., Lenzi, O., Filacchioni, G., Trincavelli L., Martini, C., Montopoli, C. and Moro, S. 2005. 1,2,4-Triazolo[1,5-a]quinoxaline as a versatile tool for the design of selective human A3 adenosine receptor antagonists: synthesis, biological evaluation, and molecular modeling studies of 2-(hetero)aryl- and 2-carboxy-substituted derivatives. J. Med. Chem. 48(25):7932-7945.

Charushin, VN., Kotovskaya, SK., Perova, NM. and Chupakhin, ON. 2001. Pyrido[2,3-b] and pyrimido[4,5-b] quinoxaline: the first fluorine-containing derivatives. Mendeleev Commun. 11(2): 54-55.

Colotta V., Catarzi D., Varano F., Lenzi O., Filacchioni G., Martini C., Trincavelli L., Ciampi O., Traini C., Pugliese A.M., Pedata F., Morizzo E. and Moro, S. 2008. Synthesis, ligand-receptor modeling studies and pharmacological evaluation of novel 4-modified-2-aryl-1,2,4 triazolo[4,3-a]quinoxalin-1-one derivatives as potent and selective human A(3) adenosine receptor antagonists. Bioorg. Med. Chem. 16(11):6086-6102.

Dyatkina, NB., Roberts, CD., Keicher, JD., Dai, Y., Nadherny, JP., Zhang, W., Schmitz, U., Kongpachith, A., Fung, K., Novikov, AA., Lou, LI., Velligan, M., Khorlin, AA. and Chen, MS. 2002. Minor grove DNA binders as antimicrobial agents. 1 pyrazoles tetraamides are potential antibacterial against vancomycin resistant *Enterococci* [corrected] and methicillin-resistant *S. aureus*. J. Med. Chem. 45:805-817.

El-Hawash, SAM., Habib NS. and Kassem, MA. 2006. Synthesis of some new quinoxalines and 1,2,4 triazolo[4,3-a]-quinoxalines for evaluation of in vitro antitumor and antimicrobial activities. Arch. Pharm. 339(10):564-571.

Harrak, Y., Weber, S., Gómez, AB., Rosell, G. and Pujol MD. 2007. Two alternatives for the synthesis of pyrrolo[1,2-a]quinoxaline derivatives. Arkivoc. 4:251-259.

Hasaninejad, A., Zare, A., Mohammadizadeh, MR. and Shekouhy, M. 2008. Oxalic acid as an efficient, cheap, and reused catalyst for the preparation of quinoxaline via condensation of 1,2-diamines with α-diketone at room temperature. Arkivoc. 13:28-35.

Hazarika, P., Gogoi, P. and Konwar, D. 2007. Efficient and green method for the synthesis of 1,5-benzodiazepine and quinoxaline derivatives in water. Synth. Commun. 37(1):3447-3454.

Heravi, MM., Bakhtiari, K., Bamoharram, FF. and Tehrani, MH. 2007. Wells-Dawson type heteropolyacid catalyzed synthesis of quinoxaline derivatives at room temperature. Monatsh. Chem. 138(5):465-467.

Holschbach, MA., Bier D., Wutz, W., Sihver W., Schuller M. and Olsson, RA. 2005. Derivatives of 4,6-diamino-1,2-dihydro-2-phenyl-1,2,4-triazolo[4,3-a]quinoxalin-2*H*-1-one: potential antagonist ligands for imaging the A_{2A} adenosine receptor by position emission tomography (PET). Eur. J. Med. Chem. 40(5):421-437.

Islami, MR. and Hassani, Z. 2008. One pot and efficient protocol for synthesis of quinoxaline derivatives. Arkivoc. 15:280-287.

Kaatz, GW., McAleese, F. and Seo, SM. 2005. Multidrug resistance in *Staphylococcus aureus* due to overexpression of a novel Multidrug and Toxin Extrusion (MATE) transport protein. Antimicrob. Agent Chemother. 49(5):1857-1864.

Kim, SH. and Kim, JH. 2003. Synthesis and tautomerism of novel quinoxalines (part i). J. Korean Chem. Soc. 47(3):241-243.

Kollenz, G., Theuer, R., Peters, K. and Peters, E-M. 2001. Reactions of cyclic oxalyl compounds, 43: synthesis and thermolysis of fused 1-arylaminopyrrolones. J. Heterocycl. Chem. 38(5):1055-1064.

Kumar, A., Kumar, S., Saxena, A., De, A. and Mozumdar, S. 2008. Ni-Nanoparticle: an efficient catalyst for the synthesis of quinoxalines. Catal. Commun. 9(5):778-784.

Masunari, A. and Tavares, LC. 2007. A new class of nifuroxazide analogues: synthesis of 5-nitrophene derivatives with antimicrobial activity against multidrug-resistant *Staphylococcus aureus.* Bioorg. Med. Chem. 15:4229-4236.

Nasr, MNA. 2002. Synthesis and antibacterial activity of fused 1,2,4-triazolo[4,3-a]quinoxaline and oxopyrimido[2,1:5,1]-1,2,4-triazolo[4,3-a]quinoxaline derivatives. Arch. Pharm. 335(8):389-394.

Nayak, N., Nag, TC., Satpathy, G. and Ray, SB. 2007. Ultrastructural analysis of slime positive and slime negative *Staphylococcus epidermidis* isolates in infectious keratitis. Indian J. Med. Res. 125:767-771**.**

Obafemi, CA. and Akinpelu, DA. 2005. Synthesis and antimicrobial activity of some 2(1*H*) quinoxalinone-6-sulfonyl derivatives. Phosphorus, Sulfur, Silicon Relat. Elem. 180:1795-1807.

Olayiwola, G., Obafemi, CA. and Taiwo, FO. 2007. Synthesis and neuropharmacological activity of some quinoxalinone derivatives. African J. Biotech. 6(6):777-786.

Rashed N, El Massry AM., El Ashry E-SH., Amer A., and Zimmer, H. 1990. A facile synthesis of novel triazoloquinoxalinones and triazinoquinoxalinones. J. Heterocycl. Chem. 27: 691-694.

Refaat, HM., Moneer, AA. and Khalil, OM. 2004. Synthesis and anti-microbial activity of certain novel quinoxalines. Arch. Pharm. Res. 27:1093-1098.

Russel, AD. and Furr, JR. 1977. Antibacterial activity of a new chloroxylenol preparation containing ethylenediamine tetraacetic acid. J. Appl. Bacteriol. 43:253-260.

Seitz, LE. Suling, WJ. and Reynolds, RC. 2002. Synthesis and antimycobacterial activity of pyrazine and quinoxaline derivatives. J. Med. Chem. 45:5604-5606.

Solano, B., Junnotula, V., Marín, A., Villar, R., Burguete, A., Vicente, E., Pérez-Silanes, S., Aldana, I., Monge, A., Dutta, S., Sarkar, U. and Gates, KS. 2007. Synthesis and biological evaluation of new 2-arylcarbonyl-3-trifluoromethylquinoxaline 1,4-di-*N*-oxide derivatives and their reduced analogs. J. Med. Chem. 50:5485-5492.

Sridharan, V., Perumal, PT., Avendaño, C. and Menéndez, CJ. 2007. The first aza Diel-Alder reaction involving an α,β-unsaturated hydrazone as the dienophile: stereoselective synthesis of C-4 functionalized 1,2,3,4-tetrahydroquinolines containing a quaternary stereocenter. Org. Biomol. Chem. 5:1351-1353.

Staszewska A., Stefanowicz, P. and Szewczuk Z. 2005. Direct solid-phase synthesis of quinoxaline-containing peptides. Tetrahedron Lett. 46(33):5525-5528.

Szekélyhidi, Z., Pató, J., Wáczek, F., Bánhegyi, P., Hegymegi-Barakonyi, B., Erós D., Mészáros, G., Hollósy, F., Hafenbradl, D., Obert, S., Klebl, B., Kéri, G. and Orfi, L. 2005. Synthesis of selective SRPK-1 inhibitors: novel tricyclic quinoxaline derivatives. Biorg. Med. Chem. Lett. 15:3241-3246.

Vicente, E., Villa, R., Burguete, A., Solano, B., Ancizu, S., Perez-Silanes, S., Aldana, I. and Monge, A. 2008. Substitution of fluorine atoms and phenoxy groups in the synthesis of quinoxaline 1,4-di-N-oxide derivatives. Molecules 13:86-95.

Vicini, P., Zani, F., Cozzini, P. and Doytchinova, I. 2002. Hydrazones of 1.2-benzisothiazole hydrazide: synthesis, antimicrobial activities and QSAR investigation. Eur. J. Med. Chem. 37(7): 553-564.

Vidaillac, CA., Guillon, JA., Arpin, CB., Moreau, SA., Lagardere, AA., Larrouture, SA., Dallemagne, P., Quentin, CB. and Jarry, CA. 2005. New 4-[2-(alkylamino)ethylthio]pyrrolo[l,2-a]quinoxalines, as potential bacterial multidrug resistance pump inhibitors: synthesis, pharmacomodulation and biological activity evaluation: O9. Fundam. Clinical Pharmacol. 19(2):196.

Zaleska, B., Ciez, D. and Lech, J. 2001. Efficient synthesis of pyrrolo[3,4-b]hexahydro-1*H*-1,5-benzo diazepine derivatives. Synlett 12:1953-1955.

Zarranz, B., Jaso, A., Aldana, I., Monge, A., Maurel, S., Deharo, E., Jullian, V. and Sauvain, M. 2005. Synthesis and antimalarial activity of new 3-arylquinoxaline-2-carbonitrile derivatives. Arzneim.-Forsch. 55:754-761.

Zarranz, B., Jaso, A., Aldana, I. and Monge, A. 2004. Synthesis and anticancer activity evaluation of new 2-alkylcarbonyl and 2-benzoyl-3-trifluoromethyl-quinoxaline 1,4-di-*N*-oxide derivatives. Bioorg. Med. Chem. 12:3711-3721.

Zhenjiang, L., Weisi, L., Yingjie, S., He, H. and Pingkai, O. 2008. Facile synthesis of quinoxaline catalyzed by amidosulfonic acid. J. Heterocycl. Chem. 45:285-288.

Received: May 4, 2009; Revised: June 30, 2009; Accepted: July 2, 2009

SENRA Academic Publishers, Burnaby, British Columbia
Vol. 3, No. 3, pp. 993-1000, 2009
ISSN: 1715-9997

Canadian Journal of pure&applied sciences

EFFECT OF TOP LAYER'S MATERIAL AND FLOW DIRECTION ON MASS TRANSFER THROUGH MULTI-LAYER CERAMIC MEMBRANES

*+A Hussain[1], A Seidel-Morgenstern[2,3] and E Tsotsas[2]
[1] Centre for Chemical Engineering & Material Sciences, (CCE&MS)
National University of Science & Technology (NUST), Islamabad, Pakistan
[2] Institute of Process Engineering, Otto-von-Guericke-University Magdeburg, Germany
[3] Max-Planck-Institut für Dynamik komplexer technischer Systeme Magdeburg, Germany

ABSTRACT

The influence of top layer's material of membrane and flow direction on gas transport has been investigated. A simulation analysis has been done to study the influence of the material of permselective layer (top membrane layer), temperature and the direction of gas flow on the mass transfer through a composite membrane. Dusty gas model for single gas permeation has been used to study these effects. It is obvious from analysis that apart from top layer's material, flow direction have also an influnce on the mass transfer though composite membrane.

Keywords: Gas permeation, permselective layer, mass transfer, dusty gas model, membrane reactor.

INTRODUCTION

The influence of composite nature of the membrane on the gas transport has been investigated, though mostly focused on polymeric composite membranes (Henis and Tripodi, 1981; Fouda *et al*., 1991; Mulder, 1991), to explain the membrane performance and selectivity. The asymmetry of the membrane can be used to facilitate the diffusion of one of the reactants while hindering the other one. Successive layers of different thicknesses and materials can also contribute to carrying out different consecutive reactions in different regions of the membrane (Coronas and Santamaria, 1999). The permeability of the membrane may also not be uniform along the entire length. The formation of top layer of different thickness on the support layer is a complicated process, which demands a perfect interaction between the materials of top and intermediate/support layers to produce a good composite membrane. But in practice it has been found that the structure of top layer is far from being homogenous throughout its thickness. Some regions adjoining the top layer to the support/intermediate layer can be abrupted. This shortcoming can be attributed to the phenomena of deformation-orientational order that occur during the formation of selective, thin layer on a porous support (Drechsel *et al*., 1953). Hence, the nature of material and interaction between the material of top layer and the support profoundly affects the structure and properties of the composite membrane (Polotsky and Polotskaya, 1998). It has also been revealed from a simulation analysis that the direction of gas flow has also an influence on the mass transfer through composite membrane

Membrane characterization

Much effort has been devoted to the problem of predicting the parameters of a porous membrane. Dusty Gas Model (DGM) (Tuchlenski *et al*., 1998; Thomas *et al*., 2001; Thomas, 2003) is widely used to characterize the porous membranes. From the practical point of view, it is still better to determine these parameters directly by mass transfer experiments. To test a theory whose mathematical formulation is based on adjustable parameters, a comprehensive set of experiments is required to determine the model parameters. Mass transfer experiments enable the identification and validation of all mass transport parameters of the membrane. Single gas permeation experiments (Fig. 1) have been performed mainly for the identification of structural parameters of every membrane layer by using air, N_2 and He for different temperatures (20-500°C) and pressures (1-3 bar).

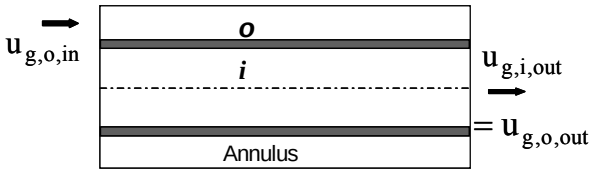

Fig. 1. Experimental set-up for the single gas permeation experiment.

Single gas permeation experiments

The principle of steady state, single gas permeation measurements is depicted in figure1, see also Tuchlenski

*Corresponding author email: arshad-ccems@nust.edu.pk
+Present address: Department of Chemical Engineering, Sem Saelands vei 4, NO-7491 Trondheim, Norway

et al. (1998), Thomas *et al*. (2001), Thomas (2003), Capek and Seidel-Morgenstern (2001) and Uchytil *et al*. (2000). As the sketch shows, gas is introduced in the annulus, flows through the membrane due to the pressure difference ΔP, and leaves the cell at the end of the tube.
In this case, and for a homogeneous membrane, the general DGM equation (Tuchlenski *et al*., 1998; Thomas *et al*., 2001; Thomas, 2003; Capek and Seidel-Morgenstern, 2001; Uchytil *et al*., 2000; Fernández-Pineda *et al*., 2002) for species j in a mixture of N components is expressed by the relationship

$$\sum_{k=1,k\neq j}^{N}\frac{\tilde{x}_k\dot{n}_j-\tilde{x}_j\dot{n}_k}{D^e_{jk}}+\frac{\dot{n}_j}{D_{K,j}}=-\frac{P}{\tilde{R}T}\nabla\tilde{x}_j-\frac{\tilde{x}_j}{\tilde{R}T}\left(1+\frac{B_0}{\eta_j D_{K,j}}\bar{P}\right)\nabla P \quad (1)$$

where j = 1 to N.

The driving forces are included in the right-hand part of eq. (1) in terms of total pressure and molar fraction (partial pressure) gradients, while the resulting fluxes, $\dot{n}_j$, appear at the left-hand side of the equation. For single gas permeation the DGM eq. (1) reduces to:

$$\dot{n}_j=-\frac{1}{\tilde{R}T}\left(\frac{4}{3}K_0\sqrt{\frac{8\tilde{R}T}{\pi\tilde{M}_j}}+\frac{B_0}{\eta_j}\bar{P}\right)\nabla P. \quad (2)$$

For cylindrical coordinates and a relatively moderate membrane thickness the expression

$$\frac{\dot{N}_j}{\Delta P}=-\frac{2\pi L}{\tilde{R}T\ln\left(\frac{r_{m,o}}{r_{m,i}}\right)}\left(\frac{4}{3}K_0\sqrt{\frac{8\tilde{R}T}{\pi\tilde{M}_j}}+\frac{B_0}{\eta_j}\bar{P}\right) \quad (3)$$

is obtained by integration of eq. (2).

With the additional assumption of tortuous, monodispersed capillaries, which are neither interconnected, nor change their cross-sectional area with their length, the three parameters of the dusty gas model can be expressed as

$$B_0=F_0\frac{d_P^2}{32}, \quad (4)$$

$$K_0=F_0\frac{d_P}{4}, \quad (5)$$

$$F_0=\frac{\varepsilon}{\tau}, \quad (6)$$

and are, thus, reduced to a set of only two morphological parameters, namely the diameter of the assumed cappilaries

$$d_p=\frac{8B_0}{K_0}, \quad (7)$$

and

$$\frac{\varepsilon}{\tau}=\frac{(K_0)^2}{2B_0}, \quad (8)$$

In eq. (3), $\bar{P}$ is the mean pressure in the membrane, $\bar{P}=(P_o+P_i)/2$, ΔP is the pressure drop, $\Delta P=P_o-P_i$. In experiments with a homogeneous membrane the pressure level, i.e. $\bar{P}$, is varied, while the pressure difference, ΔP, and P_i, P_o, or both are measured. Additionally, the gas flow rate, which permeates through the membrane, is determined, and converted to the gas molar flow rate, $\dot{N}_j$. With known geometry of the membrane (L, $r_{m,o}$, $r_{m,i}$) and gas properties, the parameters of the dusty gas model, K_0 and B_0, can then be specified, compare also with Fernández-Pineda *et al*. (2002). Specifically, and due to the linearity of eq. (3), the Knudsen coefficient, K_0, is derived from the intercept, and the permeability constant, B_0, from the slope of a plot of the ratio $\dot{N}_j/\Delta P$ (termed as permeability coefficient) versus $\bar{P}$.

In case of any additional homogeneous layer on the original membrane, the described series of permeation experiments are repeated and eq. (3) can be applied to calculate the pressure at the interface between the first and the second layer of the composite. In this manner, pressures and flux are known for the second layer, so that the derivation of K_0 and B_0 can be specified also for this layer, in exactly the previously discussed way. Recursively, the parameters of every layer of any composite membrane can be derived individually, provided that all intermediate membranes, starting from the support and ending with the final composite, are available. The features of investigated membrane and results of this derivation are summarized in tables 1and 2.

Though the identification of K_0 and B_0 can be done with only one gas at only one temperature, a large amount of experiments have been conducted in the present work for different gases at various temperatures.

Influence of top layer

The role of top layer (permselective layer) in an asymmetric membrane is to enhance the separation properties of the composite membrane. It should also be noticed that a composite membrane may exhibit asymmetry dependent fluxes due to non-isommetric pressure profiles (Thomas, 2003). As the top layer thickness is very small (~ 2 μm) so it can not sustain alone the pressure differences required to achieve reasonable fluxes. Hence it is deposited on support/intermediate membrane layers to provide the

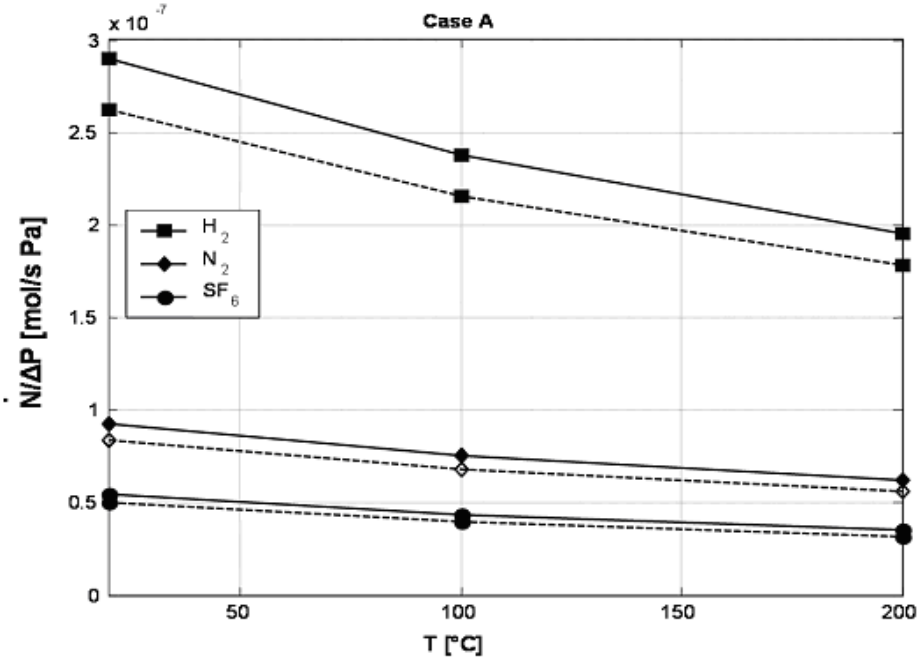

Fig. 2. Ratio of molar flow rate to pressure drop versus temperature for three different gases (solid lines: gas entering first the support layer, broken lines: gas entering first the permselective layer).

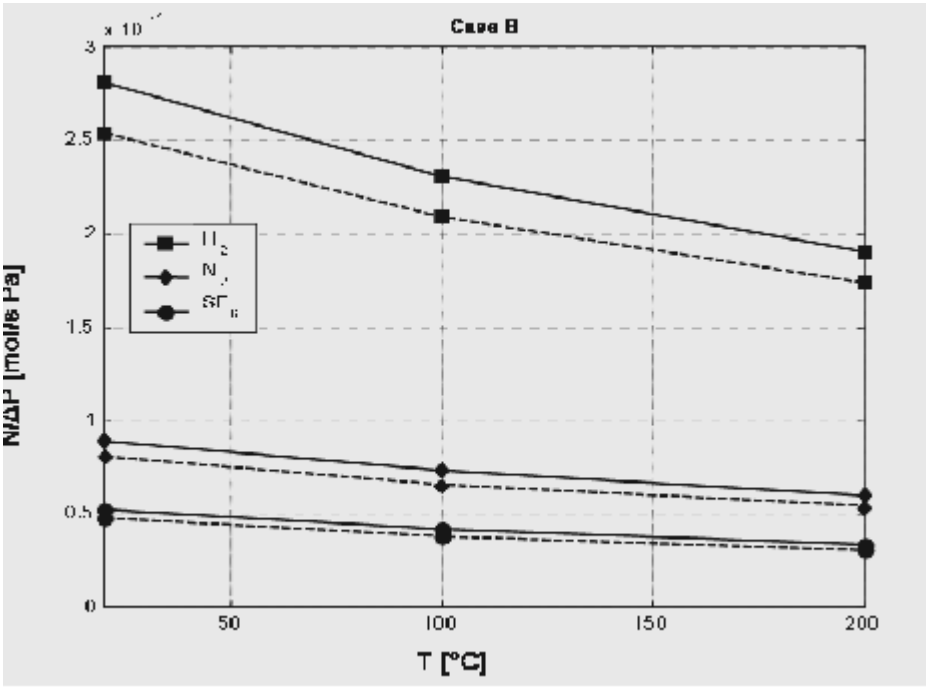

Fig. 3. As in Fig. 2, however for case B membrane.

required mechanical strength. A simulation analysis for three different gases was done to study the influence of temperature, flow direction and the top layer's material on the gas flow rates and pressure profiles in the composite membrane. Simulation study has been done for two cases which correspond to two different top layer materials. Two constant pressures (1 and 2 bar) on the two sides of the membrane and three different temperatures have been taken for the calculations. The membrane structural parameters used were identified by Uchytil *et al*. (2000). However, a shorter membrane length was considered in these simulations. Membrane structural parameters and the geometrical information for both cases are given in tables 1 and 2. All parameters of the membrane layers are

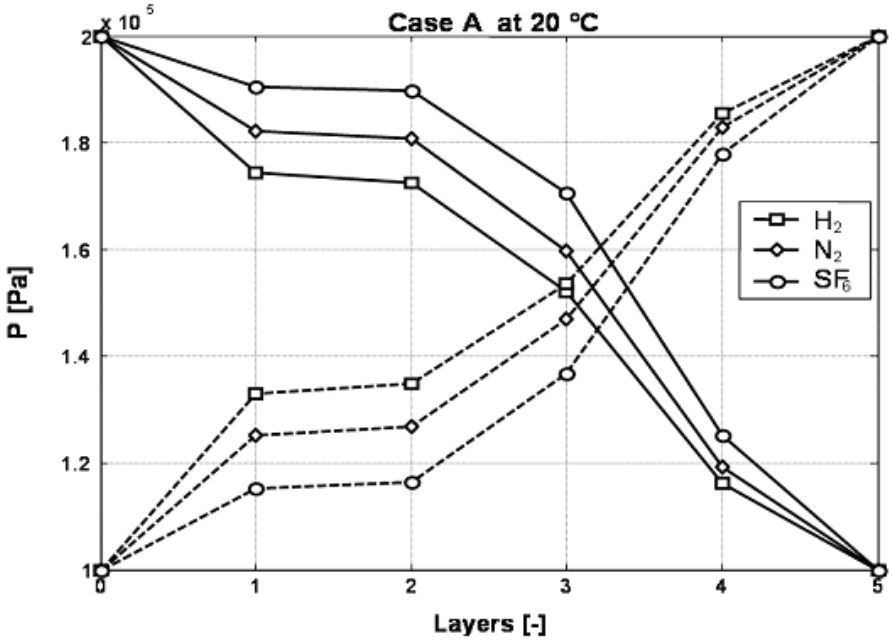

Fig. 4. Pressure profiles in the composite membrane at 20°C for three different gases at the pressure level of 1 & 2 bars.

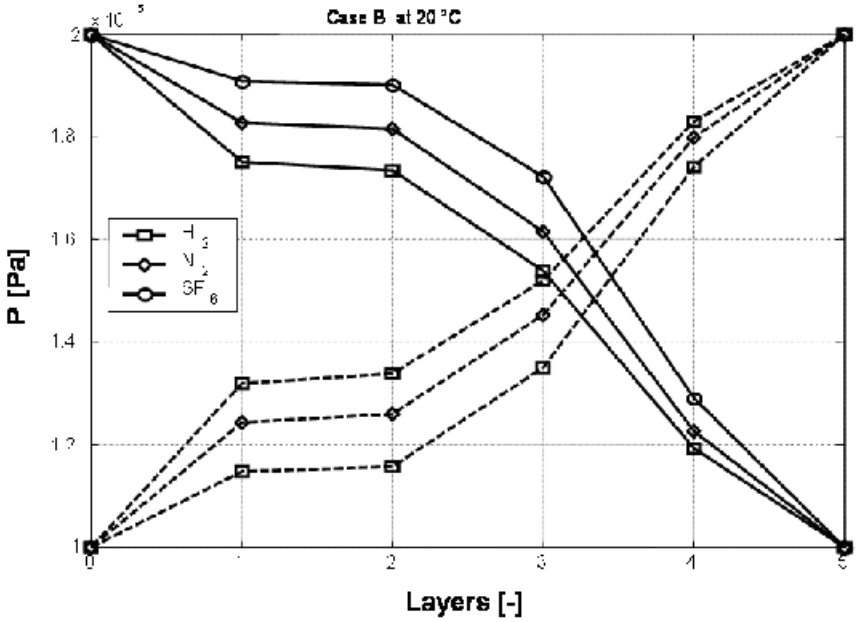

Fig. 5. Pressure profiles in the composite membrane at 20°C for three different gases at the pressure level of 1 & 2 bars.

same in both cases excluding the parameters of the top layer (permselective layer). In case A, the top layer is made of γ-Al_2O_3 while in case B, the top layer is made of TiO_2.

The simulations have been completed using the dusty gas model equation eq. (3) for the permeation of three different gases (H_2, N_2, SF_6) at three different temperatures (20°C, 100 °C, 200°C) for both types of composite membrane (case A & Case B). The influence of flow direction was quantified by alternatively setting two different pressures on the membrane sides (differentiating that the gas first enters the membrane support or the permselective layer). Simulation results are presented in figures 2 and 3.

Figure 2 shows for the calculated values of the ratio of molar flow rate to pressure drop (permeability coefficient)

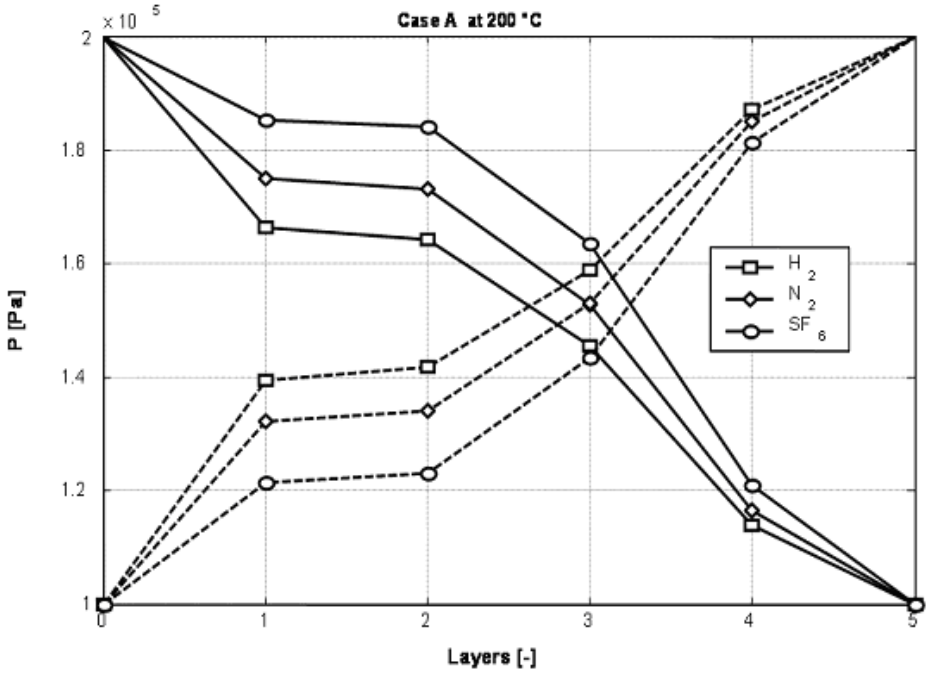

Fig. 6. Pressure profiles in the composite membrane at 200°C for three different gases at the pressure level of 1 & 2 bars.

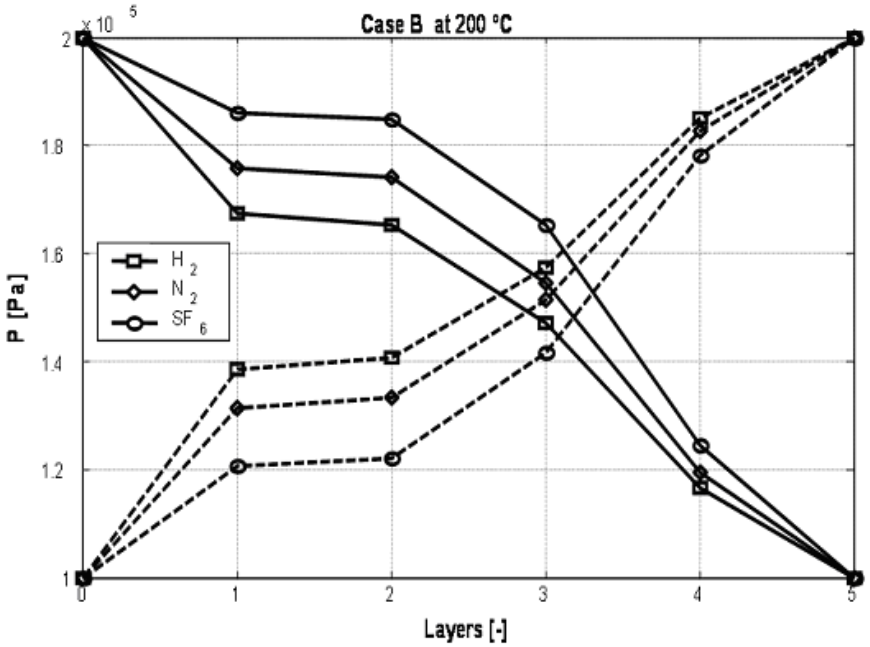

Fig.7. As Fig. 6, though for case B membrane.

plotted against the temperature for Case A for all gases. It can be seen that the ratio of molar flow rate to pressure drop decreases as the molar mass of the gas increases. The ratio of molar flow rate to pressure drop decreases also by increasing the temperature as the gas viscosity increases by the temperature. The major effect to show in these figures is the influence of flow direction on the ratio of molar flow rate to pressure drop (permeability coefficient). In both figures, full lines correspond to the gas entering first the support membrane and the broken lines correspond to the gas entering first the permselective layer. It can be seen that in both cases (A & B), the ratio of molar flow rate to pressure drop is higher when the gas first enters the support membrane.

Case A: L = 150 mm $d_{m,o}$ = 10 mm $d_{m,i}$ = 7 mm (approx.)

Table 1. Parameters of all membrane's layers for case A.

Layer	Composition	Nom. pore diameter [m]	Thickness [m]	K_0 [m]	B_0 [m^2]	d_p [m]	$\frac{\varepsilon}{\tau}$
Support	α-Al_2O_3	3.0×10^{-6}	1.5×10^{-3}	9.34×10^{-8}	3.58×10^{-14}	3.07×10^{-6}	0.122
1st layer	α-Al_2O_3	1.0×10^{-6}	25×10^{-6}	4.11×10^{-8}	9.47×10^{-15}	1.84×10^{-6}	0.089
2nd layer	α-Al_2O_3	0.2×10^{-6}	25×10^{-6}	9.40×10^{-9}	2.24×10^{-16}	0.19×10^{-6}	0.197
3rd layer	α-Al_2O_3	60×10^{-9}	25×10^{-6}	5.97×10^{-9}	5.69×10^{-17}	76×10^{-9}	0.313
4th layer	γ-Al_2O_3	6.0×10^{-9}	2×10^{-6}	1.11×10^{-9}	2.18×10^{-18}	16×10^{-9}	0.283

Case B: L = 150 mm $d_{m,o}$ = 10 mm $d_{m,i}$ = 7 mm (approx.)

Table 2. Parameters of all membrane's layers for case B.

Layer	Composition	Nom. pore diameter [m]	Thickness [m]	K_0 [m]	B_0 [m^2]	d_p [m]	$\frac{\varepsilon}{\tau}$
Support	α-Al_2O_3	3.0×10^{-6}	1.5×10^{-3}	9.34×10^{-8}	3.58×10^{-14}	3.07×10^{-6}	0.122
1st layer	α-Al_2O_3	1.0×10^{-6}	25×10^{-6}	4.11×10^{-8}	9.47×10^{-15}	1.84×10^{-6}	0.089
2nd layer	α-Al_2O_3	0.2×10^{-6}	25×10^{-6}	9.40×10^{-9}	2.24×10^{-16}	0.19×10^{-6}	0.197
3rd layer	α-Al_2O_3	60×10^{-9}	25×10^{-6}	5.97×10^{-9}	5.69×10^{-17}	76×10^{-9}	0.313
4th layer	TiO_2	5.0×10^{-9}	2×10^{-6}	9.17×10^{-10}	1.51×10^{-18}	13.2×10^{-9}	0.278

This behaviour of the composite membrane can be attributed to the local distribution of resistances in the membrane (Thomas, 2003; Capek and Seidel-Morgenstern, 2001). The differences in ratios of molar flow rate to pressure drop (permeability coefficients) are upto 9% for case A and about 8% for the case B (Fig. 3).

This deviation can be critical when employing the porous membrane for selective dosing of educts (Beuscher and Gooding, 1999; Tuchlenski and Schramm, 1997). If both diagrams are compared, it can be further seen that the ratio of molar flow rate to pressure drop is higher in Case A and Case B. This is due to the fact that the permselective layer made of TiO_2 (case B) has smaller pores than the permselective layer made of γ-Al_2O_3 (case A). It is also to notice here that the rise in molar mass of the gas reduces the above mentioned deviation in both cases.

Figures 4 to 7 show the calculated pressure profiles in all membrane layers for different temperatures and gases. Again, the analysis has been done for two alternative situations, gas entering the support membrane first and gas entering the permselective layer first. In all figures, zero corresponds to support side of the membrane while 5 corresponds to the permselective side of the composite membrane and 1 to 4 are the interfaces of intermediate layers in the composite membrane. Consequently, the full lines correspond to the pressure profiles when gas enters the support layer first and broken lines correspond to the pressure profiles when gas enters the permselective layer first.

In a catalytic membrane reactor, pressure effects can contribute to a better accessibility of reactants to catalyst, which can improve the conversion rate in some reactions (Iojoiu *et al*., 2005). The analysis of pressure profiles shown in figures 4 to 7 reveals that the pressure drop in case B (TiO_2 layer as a permselective layer), for all gases and temperatures, is comparatively higher than in case A (γ-Al_2O_3 as a permeselective layer). The permselective layer influences the local distribution of pressure drop in every individual layer of the composite membrane. In spite of this, the pressure drop is higher in the 3rd layer of the membrane for all gases and temperatures in both cases. Moreover, it has been found in the analysis that the pressure drop in the permselective layer rises as the molar mass of the gas increases.

CONCLUSION

The single gas permeation experiments have been carried out for every membrane layer. In this way, the identification of mass transfer parameters could be

conducted separately for every individual layer of the composite. Doing so, the influences of temperature, pressure and molar mass of the gas can be precisely understood and accurately predicted by means of the dusty gas model, which successfully combines the mechanisms of Knudsen diffusion, viscous flow and molecular diffusion. The simulation analysis shows the influence of flow direction and top layer on the mass transfer through the membrane. The analysis reveals that the choice of flow direction may be significant, especially when employing the membrane for the selective dosing of educts in a catalytic reactor. It has also been shown that the fluxes may depend on the flow direction in a composite membrane. Also the choice of the material of permselective layer is substantial in terms of pressure drop and fluxes. It is evident from the simulation analysis that different permselective layers can considerably shift the pressure profile in the composite membrane.

ACKNOWLEDGEMENT

The financial support of the German Research Foundation (research group "Membrane supported reaction engineering", FOR 447/1-1) is gratefully acknowledged.

Nomenclature

B_0	m^2	Permeability constant in dusty gas model
d	m	Diameter
D	$m^2 s^{-1}$	Diffusion coefficient
F_0	-	Ratio of effective to molecular diffusion coefficient
K_0	m	Knudsen coefficient in dusty gas model
L	m	Length
$\tilde{M}$	$kg\ mol^{-1}$	Molar mass
$\dot{n}$	$mol\ m^{-2} s^{-1}$	Molar flux
$\dot{N}$	$mol\ s^{-1}$	Molar flow rate
P	Pa	Pressure
$\bar{r}$	m	Mean membrane radius
$\tilde{R}$	$J\ mol^{-1} K^{-1}$	Universal gas constant
$\tilde{x}$	-	Mole fraction

Indices

e	Effective
j,k	Species in the mixture
K	Knudsen
m	Membrane
o	Outer, annulus side
p	Pore

Greek symbols

ε	-	Porosity
η	$Pa\ s^{-1}$	Viscosity
τ	-	Tortuosity

REFERENCES

Beuscher, U. and Gooding, C.H. 1999. The influence of the porous support layer of composite membranes on the separation of binary gas mixtures. Journal of Membrane Science. 152 (1):99-116.

Capek, P. and Seidel-Morgenstern, A. 2001. Multicomponent mass transport in porous solids and estimation of transport parameters. Applied Catalysis A. General. 211 (2): 227-237

Coronas, J. and Santamaria, J. 1999. Catalytic reactors based on porous membranes. Catalysis Today. 51:377-389.

Drechsel, P., Hoard, JL. and Long, FA. 1953. Diffusion of acetone into cellulose nitrate films and study of the accompanying orientation. Journal of Polymer Science. 10:241-252.

Fernández-Pineda, C., Izquierdo-Gil, MA. and Garćia Payo, MC. 2002. Gas permeation and direct contact membrane distillation experiments and their analysis using different models. Journal of Membrane Science. 198 (1):33-49.

Fouda, A., Chen, Y., Bai, J. and Matsuura, T. 1991. Wheatstone bridge model for the laminated polydimethylsiloxane/polyethersulfone membrane for gas separation. Journal of Membrane Science. 64:263-271.

Henis, JMS. and Tripodi, MK. 1981. Composite membranes for gas separation: The resistance model approach. Journal of Membrane Science. 8:233-246.

Iojoiu, EE., Walmsley, JC., Raeder, H., Miachon, S. and Dalmon, JA. 2005. Catalytic membrane structure influence on the pressure effects in an interfacial contactor catalytic membrane reactor applied to wet air oxidation. Catalysis Today. 104 (2-4):329-335.

Mulder, M. 1991. Basic Principles of Membrane Technology. Kluwer Academic Press, Boston.

Polotsky, AE. and Polotskaya, GA. 1998. Study on the top layer structure of the composite membranes. Journal of Membrane Science. 140:97-102.

Thomas, S., Schäfer, R., Caro, J. and Seidel-Morgenstern, A. 2001. Investigation of mass transfer through inorganic membranes with several layers. Catalysis Today. 67 (1-3):205-216.

Thomas, S. 2003. Kontrollierte Eduktzufuhr in Membranreaktoren zur Optimierung der Ausbeute gewünschter Produkte in Parallel- und Folgereaktionen, PhD. thesis, Otto-von-Guericke-Universität Magdeburg, Germany.

Tuchlenski, A., Uchytil, P. and Seidel-Morgenstern, A. 1998. An experimental study of combined gas phase and surface diffusion in porous glass. Journal of Membrane Science. 140 (2):165-184.

Tuchlenski, A., Schramm, O. And Seidel-Morgenstern, A. 1997. Steady state and dynamic mass transfer of gases in porous materials. Collection of Czechoslovak Chemical Communications. 62 (7):1043-1056.

Uchytil, P., Schramm, O. and Seidel-Morgenstern, A. 2000. Influence of the transport direction on gas permeation in two-layer ceramic membranes. Journal of Membrane Science. 170 (2):215-224.

Received: April 14, 2009; Accepted: August 29, 2009

SENRA Academic Publishers, Burnaby, British Columbia
Vol. 3, No. 3, pp. 1001-1002, 2009
ISSN: 1715-9997

Canadian Journal of pure&applied sciences

A NEW PROOF FOR THE EULER THEOREM IN THE COMPLEX NUMBERS THEORY

S Askari
Mechanical Engineering Department, Iran University of Science and Technology
Tehran 16844, Iran

ABSTRACT

In this paper, a new proof for the Euler equation ($exp(ix) = \cos x + i \sin x$) has been presented. At first, a new and general formula has been proved from which the Euler equation has been derived.

2000 Mathematics Subject Classification: 30A99, 30B40

Keywords: Euler theorem, complex numbers, analytic function.

INTRODUCTION

Euler equation in the theory of the complex numbers is usually proved by expansion of sin(x), cos(x) and exp(x) into power series. A general proof of this equation based on direct mathematical analysis does not exist. In this paper, at first a new formula has been proved from which the Euler equation has been derived as a special result.

Analysis

Let f be an analytic function with the following characteristics

$$f(z) = u(x, y) + iv(x, y),\ f(z) \neq \pm iz_0, z_0 = a + ib \neq 0, z = x + iy, i = \sqrt{-1} \quad (1)$$

Since f is an analytic function [1]

$$\frac{\partial u}{\partial x} = \frac{\partial v}{\partial y}, \frac{\partial u}{\partial y} = -\frac{\partial v}{\partial x} \quad (2)$$

U and V are defined as follows

$$U(\phi,\varphi) = \frac{\phi}{\phi^2 + \varphi^2}, V(\phi,\varphi) = -\frac{\varphi}{\phi^2 + \varphi^2},$$

$$\phi = \phi(x, y), \varphi = \varphi(x, y) \Rightarrow$$

$$\frac{\partial U}{\partial x} = \frac{(\varphi^2 - \phi^2)\frac{\partial \phi}{\partial x} - 2\phi\varphi\frac{\partial \varphi}{\partial x}}{(\phi^2 + \varphi^2)^2}, \frac{\partial U}{\partial y} = \frac{(\varphi^2 - \phi^2)\frac{\partial \phi}{\partial y} - 2\phi\varphi\frac{\partial \varphi}{\partial y}}{(\phi^2 + \varphi^2)^2} \quad (3)$$

$$\frac{\partial V}{\partial x} = -\frac{(\phi^2 - \varphi^2)\frac{\partial \varphi}{\partial x} - 2\phi\varphi\frac{\partial \phi}{\partial x}}{(\phi^2 + \varphi^2)^2}, \frac{\partial V}{\partial y} = -\frac{(\phi^2 - \varphi^2)\frac{\partial \varphi}{\partial y} - 2\phi\varphi\frac{\partial \phi}{\partial y}}{(\phi^2 + \varphi^2)^2} \quad (3)$$

Let define g as

$$g(z) = \frac{1}{f^2(z) + z_0^2} = \frac{1}{\phi_1 + i\varphi_1} = U(\phi_1, \varphi_1) + iV(\phi_1, \varphi_1), \phi_1 = u^2 - v^2 + a^2 - b^2, \varphi_1 = 2(uv + ab)$$

Using Eq. 2

$$\frac{\partial \phi_1}{\partial x} = 2u\frac{\partial u}{\partial x} - 2v\frac{\partial v}{\partial x}, \frac{\partial \phi_1}{\partial y} = -2u\frac{\partial v}{\partial x} - 2v\frac{\partial u}{\partial x}, \frac{\partial \varphi_1}{\partial x} = 2u\frac{\partial v}{\partial x} + 2v\frac{\partial u}{\partial x}, \frac{\partial \varphi_1}{\partial y} = 2u\frac{\partial u}{\partial x} - 2v\frac{\partial v}{\partial x} \quad (4)$$

From Eqs. 3 and 4

$$\frac{\partial U}{\partial x} = \frac{\partial V}{\partial y} = 2\frac{(\varphi_1^2 u - \phi_1^2 u - 2\phi_1\varphi_1 v)\frac{\partial u}{\partial x} + (-\varphi_1^2 v + \phi_1^2 v - 2\phi_1\varphi_1 u)\frac{\partial v}{\partial x}}{(\phi_1^2 + \varphi_1^2)^2}$$

$$\frac{\partial U}{\partial y} = -\frac{\partial V}{\partial x} = 2\frac{-(\varphi_1^2 u - \phi_1^2 u - 2\phi_1\varphi_1 v)\frac{\partial v}{\partial x} + (-\varphi_1^2 v + \phi_1^2 v - 2\phi_1\varphi_1 u)\frac{\partial u}{\partial x}}{(\phi_1^2 + \varphi_1^2)^2}$$

Therefore, g is an analytic function. Let define h as follows

$$h(z) = \frac{1}{f(z) + iz_0} = \frac{1}{\phi_2 + i\varphi_2} = U(\phi_2, \varphi_2) + iV(\phi_2, \varphi_2), \phi_2 = u - b, \varphi_2 = v + a$$

*Corresponding author email: bas_salaraskari@yahoo.com

Using Eq. 2

$$\frac{\partial \phi_2}{\partial x}=\frac{\partial u}{\partial x},\frac{\partial \phi_2}{\partial y}=-\frac{\partial v}{\partial x},\frac{\partial \varphi_2}{\partial x}=\frac{\partial v}{\partial x},\frac{\partial \varphi_2}{\partial y}=\frac{\partial u}{\partial x} \qquad (5)$$

From Eqs. 3 and 5

$$\frac{\partial U}{\partial x}=\frac{\partial V}{\partial y}=\frac{(\varphi_2^2-\phi_2^2)\frac{\partial u}{\partial x}-2\phi_2\varphi_2\frac{\partial v}{\partial x}}{(\phi_2^2+\varphi_2^2)^2},\frac{\partial U}{\partial y}$$

$$=-\frac{\partial V}{\partial x}=\frac{-(\varphi_2^2-\phi_2^2)\frac{\partial v}{\partial x}-2\phi_2\varphi_2\frac{\partial u}{\partial x}}{(\phi_2^2+\varphi_2^2)^2}$$

Therefore, h is an analytic function. Let define s as

$$s(z)=\frac{1}{f(z)-iz_0}=\frac{1}{\phi_3+i\varphi_3}$$

$$=U(\phi_3,\varphi_3)+iV(\phi_3,\varphi_3),\phi_3=u+b,\varphi_3=v-a$$

Like the procedure was used for h(z), it can be shown similarly that s(z) is also an analytic function.
Since f(z) is an analytic function, for any continuous curve C from z_0 to z (Kreyszig, 1999).

$$\int_C f(z)dz=\int_{Z_0}^{Z} f(z)dz=F(z)-F(z_0)=F(z)+c_0,F'(z)=f(z)$$

$$g(z)f'(z)=h(z)s(z)f'(z)=\frac{1}{2iz_0}(s(z)-h(z))f'(z)\Rightarrow$$

$$\int_C\frac{f'(z)dz}{f^2(z)+z_0^2}=\frac{1}{2iz_0}\int_C\left(\frac{f'(z)}{f(z)-iz_0}-\frac{f'(z)}{f(z)+iz_0}\right)dz+c_0$$

$$\Rightarrow\frac{1}{z_0}\tan^{-1}\frac{f(z)}{z_0}+c_0=\frac{1}{2iz_0}\ln\frac{f(z)-iz_0}{f(z)+iz_0}\Rightarrow\frac{f(z)-iz_0}{f(z)+iz_0}$$

$$=e^{2i\tan^{-1}\frac{f(z)}{z_0}+2ic_0z_0},\ for\ f(z)=0\Rightarrow -1=e^{2ic_0z_0}\Rightarrow$$

$$\frac{f(z)-iz_0}{f(z)+iz_0}=-e^{2i\tan^{-1}\frac{f(z)}{z_0}},\ f(z)\neq\pm iz_0 \qquad (6)$$

The function f(z) can be defined as

$$f(z)=z_0\tan(p(z)/2)\Rightarrow\frac{f(z)-iz_0}{f(z)+iz_0}$$

$$=-\cos p(z)-i\sin p(z)\quad and\quad -e^{2i\tan^{-1}\frac{f(z)}{z_0}}=-e^{ip(z)}\Rightarrow$$

$$e^{ip(z)}=\cos p(z)+i\sin p(z) \qquad (7)$$

For $p(z) = z$, the Laurent expansion of e^{iz} is [z]

$$e^{iz}\,[=cos(z)+i\,sin(z)]=\sum_{n=0}^{\infty}\frac{z^n}{n!}=$$

$$\sum_{n=0}^{\infty}\frac{(-1)^n}{(2n)!}z^{2n}+i\sum_{n=0}^{\infty}\frac{(-1)^n}{(2n+1)!}z^{2n+1}$$

This equation shows that

$$cos(z)=\sum_{n=0}^{\infty}\frac{(-1)^n}{(2n)!}z^{2n}\quad and$$

$$sin(z)=\sum_{n=0}^{\infty}\frac{(-1)^n}{(2n+1)!}z^{2n+1}$$

Therefore, power series expansion of *cos(z)* and *sin(z)* have been obtained without direct expansion of these functions. In contrary to the traditional procedure of proving the Euler equation, in this paper, it has been proved directly and then power series expansion of *cos(z)* and *sin(z)* has been derived from it.

REFERENCE

Kreyszig, E. 1999. Advanced Engineering Mathematics. John Wily & Sons. 669 and 717.

Received: July 13, 2009; accepted: Sept 21, 2009